

**SPIN ECHO & MULTIPLE PULSE NUCLEAR QUADRUPOLE RESONANCE  
(NQR) INVESTIGATIONS ON SPIN  $I = 3/2$  SYSTEMS USING A  
MICROPROCESSOR - CONTROLLED PULSED SPECTROMETER**

A Thesis Submitted  
In Partial Fulfilment of the Requirements  
for the Degree of

**DOCTOR OF PHILOSOPHY**

*by*

**NARSIMHA REDDY**

*to the*

**DEPARTMENT OF CHEMISTRY**

**INDIAN INSTITUTE OF TECHNOLOGY KANPUR**

**JANUARY, 1987**

DEDICATED  
TO  
MY PARENTS



CHM-1987-D-RED-SP

8 NOV 1989

CENTRAL LIBRARY  
U.S. AIR FORCE

Acc. No. AI 06235...

106235

DEPARTMENT OF CHEMISTRY  
INDIAN INSTITUTE OF TECHNOLOGY KANPUR, INDIA

CERTIFICATE OF COURSE WORK

This is to certify that Mr. Narsimhan Reddy has satisfactorily completed all the courses required for the Ph.D. degree programme. These courses include:

Chm 501 Advanced Organic Chemistry I  
Chm 521 Chemical Binding  
Chm 524 Modern Physical Methods in Chemistry  
Chm 534 Electronics for Chemists  
Chm 541 Advanced Inorganic Chemistry I  
Chm 600 Mathematics for Chemists II  
Chm 622 Chemical Kinetics  
Chm 634 Symmetry and Molecular Structure  
Chm 800 General Seminar  
Chm 801 Special Seminar  
Chm 900 Ph.D. Thesis

Mr. Narsimha Reddy was admitted to the candidacy of the Ph.D. degree in January 1982 after he successfully completed the written and oral qualifying examinations.



(P. S. Goel)

Head,

Department of Chemistry,  
I.I.T., KANPUR-16



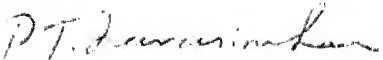
(S. Sarkar)

Convener,

Departmental Post-Graduate  
Committee, Deptt. of Chemistry,  
I.I.T., KANPUR-16

CERTIFICATE II

Certified that the work contained in this thesis entitled:  
"Spin Echo & Multiple Pulse Nuclear Quadrupole Resonance (NQR)  
Investigations on Spin  $I = 3/2$  Systems Using A Microprocessor-  
Controlled Pulsed Spectrometer" has been carried out by  
Mr. Narsimha Reddy under my supervision and the same has not  
been submitted elsewhere for a degree.

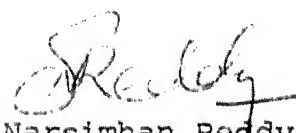
  
(P.T. Narasimhan)  
Professor of Chemistry,  
I.I.T., Kanpur  
Thesis Supervisor

Kanpur  
January 1987.

STATEMENT

I hereby declare that the matter embodied in this thesis is the result of investigations carried out by me in the Department of Chemistry, Indian Institute of Technology, Kanpur, India, under the supervision of Professor P.T. Narasimhan.

In keeping with the general practice of reporting scientific observations, due acknowledgements have been made wherever the work described is based on the findings of other investigators.

  
Narsimhan Reddy

Kanpur  
January 1987.

### ACKNOWLEDGEMENTS

I am happy to place on record my indebtedness to Professor P.T. Narasimhan who introduced me to the exciting area of magnetic Resonance in general and Nuclear Quadrupole Resonance in particular. His guidance and encouragement throughout the period of my work has lead to the successful completion of this thesis.

I thank my colleagues Drs. S. Aravamudhan, V. Harihara Subramanian, F.P. Thankachan, S. Shankar, R. Ramachandran, Amrita Tripathi and Messrs Ravinder Reddy, A.K. Dubey and A. Ramamoorthy for their valuable help and cooperation.

I thank Mr. Arun Bhavsar for his help in designing electronic circuits and microprocessor programming.

I wish to express my sincere thanks to my uncle Sri H. Hanumantha Reddy and his family for their encouragement particularly during my higher education.

I thank my friends D. Ramaiah, C.S. Sivasubramanian, Siddharth Shankar Ray, Sujit Roy, Govindaraju, Raghu, Sabastian, and Manoharan for helping me in processing the manuscript of the thesis, and K. Ashok and Antony for taking the photographs of the spectrometer.

It is a pleasure to express my thanks to Prof. P. Raghunathan and his family, Prof. S. Chandrasekaran and his family, Professor N. Sathyamurthy and his family, Dr. R.F.N. Ashok and his family

## SYNOPSIS

This thesis deals with the Zeeman perturbed spin echo envelope modulation (ZSEEM) and multiple pulse Nuclear Quadrupole Resonance (NQR) investigations on spin  $I = 3/2$  powder specimens using a microprocessor-controlled pulsed NQR spectrometer.

Zeeman perturbed quadrupole energy levels are dependent on the asymmetry parameter ( $\eta$ ) of the electric field gradient (efg) tensor. For  $I = 3/2$  systems much work on  $\eta$  has been reported earlier in the literature from Zeeman studies using continuous wave (c.w.) spectrometers both with single crystals and powder specimens. In the case of powders the method of Morino and Toyama has been extensively used for the determination of  $\eta$ . However, the use of c.w. spectrometers for this purpose has been shown to lead to erroneous results on account of modulation broadening effects and generally poor Zeeman NQR signals. Pulsed methods do not suffer from this drawback and coherent signal averaging can be readily performed to obtain better signal-to-noise ratio. ZSEEM studies on powders with  $I = 3/2$  spins have been performed earlier in our laboratory and the preliminary work showed that an analysis of these ZSEEM patterns can lead to a determination of  $\eta$ . However, the point-by-point acquisition of spin echo amplitude data as a function of pulse separation in a two-pulse experiment made this approach

tedious and time consuming. In the present thesis we have designed and constructed a microprocessor-controlled pulsed NQR spectrometer capable of automatically acquiring the ZSEEM data under software control.

The response of NMR ( $I = 1/2$ ) systems to multiple pulses has been extensively studied in the literature and it has been shown that the dipolar broadening could be eliminated and high resolution NMR spectra of solids obtained. Similar studies on pure NQR ( $I \geq 1$ ) spectroscopy have not, however, been pursued with vigour. Further we noticed that very little work has been carried out on  $I = 3/2$  systems in this regard. We have, therefore, undertaken experimental investigations of responses of NQR systems containing  $I = 3/2$  nuclei to multiple pulses using our microprocessor-controlled pulsed NQR spectrometer.

The thesis consists of four chapters. Chapter I describes principles of NQR, theoretical description of the transient phenomena in NQR spectroscopy and a brief survey of methods of NQR detection and instrumentation. A description of line-splitting and broadening mechanisms is included in this chapter keeping in view the material on line narrowing phenomena presented in Chapter IV. A brief survey of some applications of NQR spectroscopy is also presented in Chapter I which concludes with an outline of the scope of the present thesis.

The microprocessor-controlled pulsed NQR spectrometer used in this work has been designed and developed by the author and

his collaborators at the Indian Institute of Technology, Kanpur. Chapter II describes the automation and control of our pulsed NQR spectrometer which uses an Intel 8085-based microprocessor system and a signal analyzer equipped with signal averaging, processing and computational capabilities. Details of the software for the generation of several simple and multiple pulse sequences are given in this chapter. The high flexibility that can be achieved by the use of a microprocessor in pulsed NQR instrumentation has been demonstrated. Several simple and complex pulsed NQR experiments namely, (i) single-pulse FID FT-NQR experiments, (ii) two-pulse experiments such as Lee-Goldburg experiment and ZSEEM experiments, and (iii) multiple-pulse experiments have been automated with our present spectrometer system. Chapter II also gives details concerning the performance of the spectrometer system. Typical recordings obtained in various experiments are presented to demonstrate the capabilities of the set up./

Chapter III describes our experimental ZSEEM investigations on spin  $I = 3/2$  powder specimens. This study has been undertaken with a view to further assess the possibility of evaluating the asymmetry parameter  $\eta$  of the efg tensor from ZSEEM patterns. Experimental ZSEEM patterns obtained from a series of two-pulse experiments have been compared with theoretically simulated pattern to estimate  $\eta$  values. We have carried out ZSEEM investigations at  $^{35}\text{Cl}$  sites in the following compounds



at room temperature: (i)  $\text{KClO}_3$  ( $\nu_0 = 28.0896$  MHz), (ii) two sites of  $\text{HgCl}_2$  ( $\nu_0 = 22.0599$  MHz; and  $\nu_0 = 22.2389$  MHz), and (iii) two sites of  $\text{SbCl}_3$  ( $\nu_0 = 20.4015$  MHz; and  $\nu_0 = 19.1713$  MHz). Our present results on  $\eta$  are in good agreement with those obtained earlier by Pamachandran and Narasimhan from our laboratory using an unautomated spectrometer system. With the present spectrometer system a single ZSEEM experiment could be done in a few minutes (10-12 mins.) as compared to several hours that were required with the earlier unautomated system.

With the usual two-pulse method of obtaining ZSEEM patterns, one has to perform point-by-point measurements of echo amplitude as a function of the pulse separation in a series of two-pulse experiments. Ernst and coworkers have recently (1985) developed a new technique in electron spin resonance (ESR) spectroscopy for obtaining SEEM patterns by a single experiment. In this method the spin system is prepared for an extended period of time using a weak radio-frequency perturbation followed by a strong refocussing  $\pi$ -pulse to map the interactions within the spin system. We have successfully adopted this technique for the first time in NQR spectroscopy using soft pulse excitation for the extended time preparation and obtained ZSEEM patterns from spin  $I = 3/2$  powder specimens and these results are also presented in Chapter III. The dependence of the ZSEEM patterns on the power of the soft pulse has also been studied.

Chapter IV of the thesis begins with a survey of the earlier work on multiple-pulse experiments in NQR. Details of our experimental investigations on the response of spin  $I = 3/2$  powder specimens to several multiple-pulse sequences are then presented. All the pulse sequences employed by us can be categorized into two general sequences, namely, (i)  $90_x - (\tau - \theta_{(x+\emptyset)} - \tau)_n$ ; hereafter we refer to this sequence as the spin-locking sequence, and (ii)  $90_x - (\tau - \theta_{-x} - 2\tau - \theta_x - \tau)_n$ , the phase alternated multiple-pulse sequence. Some of the well-known pulse sequences studied by us include: (a) Carr-Purcell (CP), (b) Carr-Purcell-Meiboom-Gill (CPMG) and (c) Ostroff-Waugh, sequences. Under the influence of these multiple-pulse sequences the transverse magnetization has been shown to remain in the X-Y plane for times much larger than the spin-spin relaxation time ( $T_2$ ). The effective echo decay time constant ( $T_{2\text{eff}}$ ) has been evaluated and its dependence on the pulse sequence parameters, namely, (i) the flip angle ( $\theta$ ), (ii) the pulse separation, and (iii) phase ( $\emptyset$ ) has been studied and the results are presented in this chapter. The effect of resonance off-set on the equilibrium magnetization and  $T_{2\text{eff}}$  has also been investigated here. All these results are examined in the context of currently available theories of multiple-pulse response from NQR systems. In contrast to the theoretical predictions of Ainsbinder and Furman who claim that spin-locking is obtained only if the phase  $\emptyset$  in sequence (i) mentioned above satisfies the condition  $\emptyset = (2k + 1)\pi/2$  (where  $k = 0, 1, 2$ ), we have observed

spin-locking in powder samples containing spin  $3/2$  nuclei without satisfying this condition.

The thesis concludes with an outline of the scope for future experimental and theoretical work in the context of the present thesis.

|  |          |
|--|----------|
|  | xiv      |
| <u>CONTENTS</u>  |          |
|  | Page     |
| CERTIFICATE OF COURSE WORK   | ... iii  |
| CERTIFICATE II   | ... iv   |
| STATEMENT  | ... v    |
| ACKNOWLEDGEMENTS   | ... vi   |
| SYNOPSIS   | ... viii |
| CHAPTER  |          |
| I - INTRODUCTION   | ... 1    |
| I.A THEORY OF NQR  | ... 2    |
| I.B TRANSIENT PHENOMENON IN NQR  | ... 10   |
| I.B(1) Classical Picture   | ... 10   |
| I.B(2) Quantum Mechanical Treatment of<br>the Formation of Transient Signals<br>in NQR | ... 16   |
| I.C A BRIEF SURVEY OF METHODS OF NQR<br>DETECTION AND INSTRUMENTATION                  | ... 31   |
| I.C(1) Continuous Wave (c.w.) Techniques   | ... 31   |
| I.C(2) Pulse and Double Resonance Tech-<br>niques                                      | ... 34   |
| I.D LINE SPLITTING AND BROADENING<br>MECHANISMS IN NQR                                 | ... 45   |
| I.D(1) Splitting and Broadening of NQR<br>Spectra due to Magnetic Inter-<br>actions    | ... 45   |
| I.D(2) Electrical Sources of Broadening  | ... 48   |
| I.D(3) Line Broadening due to Dynamic<br>Effects                                       | ... 48   |
| I.E SOME APPLICATIONS OF NQR SPECTROSCOPY  | ... 49   |
| I.F SCOPE OF THE PRESENT THESIS  | ... 63   |
| Summary  | ... 64   |
| II - AUTOMATION AND CONTROL OF A PULSED NQR<br>SPECTROMETER USING A MICROPROCESSOR     | ... 79   |
| II.A AUTOMATION AND CONTROL OF PULSED NQR<br>SPECTROMETERS: GENERAL BACKGROUND         | ... 80   |

|   |     |     |
|---|-----|-----|
| II.A(1) Introduction  | ... | 80  |
| II.A(2) Pulse Programmers   | ... | 84  |
| II.A(3) P.F. Transmitter  | ... | 92  |
| II.A(4) Receiver  | ... | 95  |
| II.A(5) Data Acquisition and Spectrometer Automation                      | ... | 95  |
| II.B DETAILS OF THE PRESENT MICROPROCESSOR CONTROLLED SPECTROMETER SYSTEM | ... | 98  |
| II.B(1) Introduction  | ... | 98  |
| II.B(2) Description of the Spectrometer System                            | ... | 100 |
| II.C HARDWARE DETAILS OF THE MICROPROCESSOR SYSTEM                        | ... | 105 |
| II.D PULSE SEQUENCE GENERATION  | ... | 109 |
| II.D(1) Single-Pulse Sequence   | ... | 113 |
| II.D(2) Two-Pulse Sequence  | ... | 118 |
| II.D(3) Multiple-Pulse Sequences  | ... | 122 |
| II.D(4) WAHUNA Four-Pulse & MREV 8-Pulse Cycles                           | ... | 130 |
| II.E AUTOMATION OF VARIOUS PULSED NQR EXPERIMENTS                         | ... | 135 |
| II.E(1) Automation of FT-NQR Experiment                                   | ... | 136 |
| II.E(2) Automation of Modified Lee-Goldburg Experiment                    | ... | 138 |
| II.E(3) Automation of ZSEEM Experiment                                    | ... | 139 |
| II.E(4) Automation of STEEN Experiment                                    | ... | 148 |
| II.F CAPABILITIES AND PERFORMANCE EVALUATION OF THE SPECTROMETER          | ... | 153 |
| II.F(1) Typical FT-NQR Recordings   | ... | 154 |
| II.F(2) Spin-Echo and ZSEEM Experiments                                   | ... | 159 |
| II.F(3) Response of Lee-Goldburg Experiment                               | ... | 159 |
| II.F(4) Multiple-Pulse Response   | ... | 162 |
| Summary   | ... | 163 |

## CHAPTER

## Page

|          |  |     |     |
|----------|--|-----|-----|
| III -    | ZEEMAN PERTURBED NUCLEAR QUADRUPOLE SPIN-ECHO ENVELOPE MODULATION (ZSEEM) STUDIES ON SPIN $I = 3/2$ NUCLEI IN POWDER SPECIMENS | ... | 169 |
| III.A    | EVALUATION OF $\eta$ FOR $I = 3/2$ SPIN SYSTEMS FROM POWDER NQR  | ... | 170 |
| III.B    | GENERAL BACKGROUND ON SPIN ECHO ENVELOPE MODULATION  | ... | 174 |
| III.C    | THEORETICAL ANALYSIS OF ZSEEM FOR SPIN- $3/2$ NQR SYSTEMS  | ... | 178 |
| III.C(1) | Response of Spin $I = 3/2$ Systems to a Two-Pulse Sequence in the Absence of Zeeman Field                                      | ... | 179 |
| III.C(2) | Response of Spin $I = 3/2$ Systems to a Two-Pulse Sequence in the Presence of Perturbing Zeeman Field                          | ... | 182 |
| III.D    | EXPERIMENTAL STUDY OF ZSEEM FROM SPIN- $3/2$ POWDER SAMPLES USING TWO PULSE ECHO METHOD  | ... | 186 |
| III.E    | EXTENDED TIME EXCITATION TECHNIQUE FOR OBTAINING ECHO ENVELOPE MODULATION  | ... | 205 |
| III.E(1) | Introduction   | ... | 205 |
| III.E(2) | Experimental Study on Extended Time Excitation in NQR of Spin $I = 3/2$ Powder Samples to Obtain ZSEEM                         | ... | 209 |
| III.E(3) | A Comparative Study of the two Methods of Obtaining ZSEEM from Powder Samples  | ... | 225 |
| III.E(4) | Conclusion   | ... | 233 |
|          | Summary  | ... | 234 |
| IV -     | MULTIPLE-PULSE RESPONSES IN NQR SPECTROSCOPY: AN EXPERIMENTAL STUDY ON POWDER SAMPLES CONTAINING SPIN $I = 3/2$ NUCLEI         | ... | 239 |
| IV.A     | MULTIPLE PULSE STUDIES IN NQR: A SURVEY  | ... | 240 |

|             |   |     |     |
|-------------|---|-----|-----|
| IV.B        | RESPONSE OF $^{35}\text{Cl}$ CONTAINING POLYCRYSTALLINE SAMPLES TO MULTIPLE-PULSE SEQUENCES: EXPERIMENTAL RESULTS | ... | 254 |
| IV.B(1)     | Experimental Details  | ... | 254 |
| IV.B(2)     | Results from Various Multiple-Pulse Sequences   | ... | 256 |
| IV.B(2.i)   | Investigations with the spin-locking sequence:<br>[ $90_x - (\tau - \theta_{(x+\phi)} - \tau)_n$ ]                | ... | 257 |
| IV.B(2.i.a) | Study of $\theta$ -dependence   | ... | 259 |
| IV.B(2.i.b) | Study of $\phi$ -dependence   | ... | 266 |
| IV.B(2.i.c) | Study of off-set dependence   | ... | 276 |
| IV.B(2.i.d) | Study of $\tau$ -dependence   | ... | 280 |
| IV.B(2.ii)  | Investigations using phase alternated multiple-pulse sequence (PAPS)  | ... | 283 |
| IV.B(2.iii) | Conclusions   | ... | 287 |
|             | Summary   | ... | 290 |
|             | SCOPE FOR FUTURE WORK   | ... | 295 |

## CHAPTER I

### INTRODUCTION



This chapter gives a brief outline of the theory of nuclear quadrupole interaction, principles of nuclear quadrupole resonance (NQR) and a description of transient phenomena in NQR. Methods of detection of NQR signals are also reviewed. This chapter also highlights some applications of NQR spectroscopy.

Section I.A presents general principles of NQR while Section I.B contains a brief description of classical and quantum mechanical picture of transient phenomena in NQR. Methods of detection and instrumentation in NQR are briefly outlined in Section I.C. A brief discussion on NQR line broadening mechanisms is presented in Section I.D, while section I.E. presents some applications of NQR. The chapter concludes with an outline of the scope of the present thesis.

## I.A THEORY OF NQR

In nuclear quadrupole resonance (NQR) spectroscopy the energy levels between which, transitions observed are established by the interaction between the electric quadrupole moment of a nucleus (with spin  $I \geq 1$ ) and the electric field gradient (efg) arising from the surrounding non-uniform electric charge distribution [1].\* A nucleus with  $I \geq 1$  possesses non-spherical charge distribution and hence an electric quadrupole moment [2]. According to the classical picture, the efg produced by the external

---

\*References appear at the end of each chapter.

charge distribution exerts a torque on the quadrupolar nucleus tending to align it along the direction of the maximum efg [3]. The torque is proportional to both ' $eQ$ ' and ' $e q$ ', where ' $eQ$ ' is the scalar electric quadrupole moment and ' $e q$ ' is the maximum component of the efg tensor. Since the nucleus possesses an angular momentum too, this torque generates a precessional motion. The nuclear quadrupole precesses about the direction of the maximum efg with a frequency  $\nu_Q$  proportional to the product of ' $eQ$ ' and ' $e q$ '. According to the quantum mechanical picture the energy of a quadrupolar nucleus in a non-zero efg depends on the orientation of the nucleus and thus one gets a set of doubly degenerate quadrupolar energy levels. Observation of transitions between these quadrupole energy levels by the application of an oscillating radio frequency (r.f.) field is often referred to as 'pure NQR'. These transitions are magnetic dipole transitions between quadrupolar energy levels. After the first direct observation of NQR by Dehmelt and Krüger [4] in 1950, nuclear quadrupole interaction became readily accessible to many experimentalists for the study of structure, bonding and dynamics in the solid state. The observation of transient signals in 1954 by Bloom and Norberg [5] and Hahn and Herzog [6] has led to a considerable development which is attributable to the many advantages and possibilities of pulse methods.

The interaction energy between the nuclear electric charge distribution  $\rho_n(x)$  and its neighbouring electric charge distribution can be expressed [3] as a Taylor series

$$\begin{aligned}
E = & V(0) \int \rho_n(x) \, d\tau_n + \sum_i \left( \frac{\partial V}{\partial x_i} \right)_0 \int x_i \rho_n(x) \, d\tau_n \\
& + \frac{1}{2!} \sum_i \sum_j \left( \frac{\partial^2 V}{\partial x_i \partial x_j} \right)_0 \int x_i x_j \rho_n(x) \, d\tau_n \\
& + \frac{1}{3!} \sum_i \sum_j \sum_k \left( \frac{\partial^3 V}{\partial x_i \partial x_j \partial x_k} \right)_0 \int x_i x_j x_k \rho_n(x) \, d\tau_n \\
& + \frac{1}{4!} \sum_i \sum_j \sum_k \sum_l \left( \frac{\partial^4 V}{\partial x_i \partial x_j \partial x_k \partial x_l} \right)_0 \int x_i x_j x_k x_l \rho_n(x) \, d\tau_n \\
& + \text{other higher order terms} \quad \dots (I.1)
\end{aligned}$$

where  $V(x)$  is the electric potential produced by the charge distribution external to the nucleus. The first term on the right hand side of equation (I.1) is the Coulomb energy and is of no interest here. The second and fourth terms are the dipole and the octupole terms and they vanish [2] due to the symmetry of the nuclear charge distribution (i.e.,  $\rho_n(x) = \rho_n(-x)$ ). The third term is the quadrupole term and is the one of main interest in this thesis. This term describes the interaction of nuclear electric quadrupole moment ( $Q$ ) with the electric field gradient ( $\nabla E$ ) at its position due to surrounding charges.

$$H_Q = Q \cdot \nabla E \quad \dots (I.2)$$

where  $H_Q$  is the quadrupole Hamiltonian,  $Q$  and  $\nabla E$  are second rank tensors. The nine components ( $V_{ij}$ ) defining the field gradient tensor ( $\nabla E$ ) in Cartesian coordinate system are,

$$V_{ij} = \frac{\partial^2 V}{\partial x_i \partial x_j} \quad (x_i, x_j = x, y, z) \quad \dots (I.3)$$

Here  $V$  is the electrostatic potential at the nucleus due to the surrounding charges. Since, the electric field at the nucleus is produced entirely by charges external to the nucleus, Laplace equation is valid, i.e.,

$$V_{XX} + V_{YY} + V_{ZZ} = 0 \quad \dots (I.4)$$

Also the efg tensor is symmetric and hence we can represent the tensor by its five irreducible components in the principal axes system [7]. The asymmetry parameter  $\eta$  of the field gradient tensor is defined by the relation

$$\eta = \left| \frac{V_{XX} - V_{YY}}{V_{ZZ}} \right| \quad \dots (I.5)$$

The principal components  $V_{XX}$ ,  $V_{YY}$  and  $V_{ZZ}$  are chosen such that,  $|V_{XX}| < |V_{YY}| < |V_{ZZ}|$ .  $\eta$  values can thus range from zero to unity.

One can obtain a quantum mechanical expression for the quadrupolar Hamiltonian from the classical energy expression (I.2). In the principal co-ordinate system we thus have [7-9]

$$\mathcal{H}_Q = \frac{e^2 q Q}{4I(2I-1)} [3\hat{I}_Z^2 - \hat{I}^2 + \eta(\hat{I}_X^2 - \hat{I}_Y^2)] \quad \dots (I.6)$$

which can also be written as

$$\mathcal{H}_Q = \frac{e^2 q Q}{4I(2I-1)} [3\hat{I}_Z^2 - \hat{I}^2 + \eta/2 (\hat{I}_+^2 + \hat{I}_-^2)] \quad \dots (I.6a)$$

where the spin operators  $I_+$  and  $I_-$  correspond to raising and lowering operators and are defined as

$$\hat{I}_{\pm} = \hat{I}_X \pm i\hat{I}_Y \quad \dots (I.6b)$$

The quantity  $e^2qQ$  in the right hand side of the equation (I.6) is often referred to as the quadrupole coupling constant and is expressed in frequency units as  $e^2qQ/h$ .

To calculate the quadrupolar energy levels, from the above Hamiltonian we need to evaluate the matrix elements  $\mathcal{H}_Q^{mm'} = \langle I, m | \mathcal{H}_Q | I, m' \rangle$ . Due to the presence of  $\hat{I}_X^2$  and  $\hat{I}_Y^2$  when  $\eta \neq 0$ , this Hamiltonian matrix is not diagonal in the 'm' representation. The normal approach to solve this problem is to construct linear combinations of spin functions  $|I, m\rangle$ ,  $|I, m'\rangle$  having  $\Delta m = \pm 2$  (where  $\Delta m = m' - m$ ) and calculate the coefficients in these linear combinations from the energies obtained as the eigenvalues of the  $\mathcal{H}_Q$  matrix. For various values of nuclear spin  $I$ , the secular equations (roots of these equations are eigen values) have been tabulated in the book by Das and Hahn [7]. There have been two basic approaches for obtaining the eigenvalues of the  $\mathcal{H}_Q$  matrix for nuclei with spin  $I > 3/2$ . In the first approach due to Bersohn [10] perturbation theory is employed and the eigenvalues are expressed as a power series in  $\eta$ . This approach is satisfactory for  $\eta < 0.25$ . In the other approach due to Cohen [11] the secular equation is solved numerically for various values of  $\eta$  and the solutions are tabulated.

Although analytical solutions for  $I = 1$  and  $3/2$  were available earlier in the literature, only recently methods have been developed for obtaining exact analytical solutions of the secular equations for spins  $I = 5/2, 7/2$  and  $9/2$  [12]. The energy levels are derived as a function of the interaction parameters. It should be noted here that such a general procedure for  $I = 7/2$  pure quadrupole interaction is also applicable for spin  $I = 3/2$  case with Zeeman interaction [12-14] because the secular equations for both of these cases are quartic equations. Recently, Krishnan and Sanctuary [15] have used multipole operator technique for the pure quadrupole Hamiltonian with arbitrary asymmetry parameter. Using this technique, they have obtained secular equations for spins  $I = 1, 3/2$  &  $5/2$ , and solved exactly in terms of quadrupole interaction parameters.

In the case of  $I = 3/2$  nuclei ( $^{35}\text{Cl}$  nucleus studied in this thesis has  $I = 3/2$ ), we get two sets of doubly degenerate energy levels (the secular equation for  $I = 3/2$  pure quadrupole interaction is quadratic) and are given as [7]

$$E_{A_2, B_2} = \frac{3e^2qQ}{12} \left(1 + \frac{\eta^2}{3}\right)^{1/2} \quad \dots (I.7)$$

$$E_{A_1, B_1} = - \frac{3e^2qQ}{12} \left(1 + \frac{\eta^2}{3}\right)^{1/2} \quad \dots (I.8)$$

where  $A_1, B_1, A_2, B_2$  are linear combinations of the pure  $|m\rangle$  functions and are given below:

$$A_1 = \cos (\alpha/2) |1/2\rangle - \sin (\alpha/2) |-3/2\rangle \quad \dots (I.9)$$

$$A_2 = \sin (\alpha/2) |1/2\rangle + \cos (\alpha/2) |-3/2\rangle \quad \dots (I.10)$$

$$B_1 = \cos (\alpha/2) |-1/2\rangle - \sin (\alpha/2) |3/2\rangle \quad \dots (I.11)$$

$$B_2 = \sin (\alpha/2) |-1/2\rangle + \cos (\alpha/2) |3/2\rangle \quad \dots (I.12)$$

where  $\sin \alpha = \eta \sqrt{3\rho}$ ,  $\cos \alpha = \rho$   
and  $\rho = (1 + \frac{\eta^2}{3})^{1/2}$ .

Since there are only two sets of doubly degenerate energy levels and hence only one transition, one cannot obtain both  $\frac{e^2 q Q}{h}$ , the quadrupole coupling constant (QCC) and  $\eta$ , the asymmetry parameter, from a study of pure NQR of spin 3/2 nuclei. Zeemann field has to be applied to lift  $\pm m$  degeneracy which then makes it possible to obtain both these parameters characterizing quadrupolar interaction. One such procedure for experimentally obtaining the asymmetry parameter for  $I = 3/2$  case is described in Chapter III of this thesis. The  $\eta$  value so obtained can be substituted into the pure quadrupole resonance frequency expression,

$$\nu_Q = 1/2 \left( \frac{e^2 q Q}{h} \right) \left[ 1 + \frac{\eta^2}{3} \right]^{1/2}$$

to obtain quadrupole coupling constant  $\left( \frac{e^2 q Q}{h} \right)$ . However, it should be noted that the sign of the quadrupole coupling constant cannot be determined from NQR studies unless an additional interaction of known sign, such as dipolar coupling, perturbs

the system. Mössbauer spectroscopic studies on single crystals on the other hand, can yield the sign of quadrupolar coupling constant [16].

As was mentioned earlier, NQR transitions are magnetic dipole transitions just as in the case of NMR, though the energy levels originate from an electric interaction. The main difference between NQR and NMR arises due to the  $\pm m$  degeneracy of the NQR levels. Because of this degeneracy, if a linearly polarized r.f. field of frequency  $\nu_0$  is applied in a direction perpendicular to the axis of quantization (Z-axis), both the rotating components of r.f. field, namely, the one rotating clockwise and the other rotating counter-clockwise in the XY-plane can cause transitions. Hence, in the presence of the r.f. field, a linearly pulsating magnetization is obtained in the direction of the r.f. field. (In NMR, since only one rotating component is effective in causing transitions, a rotating magnetization is induced in the XY plane.) The presence of a linearly pulsating magnetization in the direction of the applied r.f. field implies that 'Crossed Coil' arrangement will not work in a 'pure NQR' study, when neither static Zeeman field nor dynamic Zeeman modulation field is employed. The presence of these magnetic fields lifts the degeneracy of the  $\pm m$  states and a rotating magnetization would be then induced in the XY-plane and the crossed coil arrangement can then be used. A few NQR studies have been conducted with crossed coil arrangement with Zeeman modulation [17-19].



The present thesis is concerned with the spin echo and multiple pulse investigations on spin  $I = 3/2$  NQR systems. We shall therefore consider in some detail how transient signals (free induction signals and spin echo signals) arise in NQR.

## I.B TRANSIENT PHENOMENA IN NQR

### I.B(1) Classical Picture

Bloom and Norberg [5], and Hahn and Herzog [6] were the first to observe experimentally pulse responses in pure nuclear quadrupole resonance. The theoretical explanation of these observations can be done either classically or quantum mechanically. Before considering a quantum mechanical description of the evolution of the spin system following resonant r.f. pulses, it is helpful to visualize the macroscopic magnetization vector  $\vec{M}$  during the various stages of a pulsed NQR experiment [20]. Such pictures are classical in nature and, therefore, have limited value. They are, however, very useful for developing an intuitive feeling for pulsed resonance experiments [21].

Consider a single crystal sample oriented in an r.f. coil with its efg  $V_{ZZ}$ -axis perpendicular to the coil axis. At thermal equilibrium and in the absence of a static magnetic field, the magnetization vector has a magnitude of zero. Therefore, the system may be thought of as having a positive  $\vec{M}_Z$  component  $\vec{M}_+$  and an equal negative component  $\vec{M}_-$ . The effect of an r.f. field, applied along the X-axis, on the magnetization vectors  $\vec{M}_+$  and  $\vec{M}_-$

is shown in Fig. I.1. The magnetic field  $H_x = 2H \cos \omega t$  is viewed as being composed of two rotating parts, each having a magnitude of  $H_1$ . At the beginning of an r.f. pulse each magnetic field component is perpendicular to each magnetization vector component,  $\vec{M}_+$  and  $\vec{M}_-$ , as is shown in Fig. I.1(a). The initial torque on  $\vec{M}_+$  is in the +Y direction and in the -Y direction for  $\vec{M}_-$ . However, the quadrupole interaction causes  $\vec{M}_+$  to precess about the Z-axis in a counter-clockwise direction looking along the +Z-axis. The M-component will precess in a clockwise direction. Thus, one component of  $H_x$  will remain perpendicular to  $\vec{M}_+$ , provided the applied r.f. field has a frequency equal to the resonance frequency  $\nu_Q$ . The other component of  $H_x$  follows  $\vec{M}_-$ , and remains perpendicular even though  $\vec{M}_-$  spirals away from the Z-axis. This situation is depicted in Fig. I.1(b) and 1(c).

If the pulse is terminated after the  $\vec{M}_+$  and  $\vec{M}_-$  vectors have been rotated into the XY-plane, it is called a 90 degree pulse. As Fig. I.1(d) shows, this results in  $\vec{M}_+$  and  $\vec{M}_-$  adding together along the X-axis and a net linearly polarized macroscopic magnetization is produced along the X-direction. The magnitude of  $\vec{M}_+$  and  $\vec{M}_-$  can be deduced from the expressions which we shall derive later in this section.

Let us now consider the more realistic situation where a distribution of resonant frequencies occurs. The situation is depicted in Figs. I.2(a) to I.2(d) by considering formation of a spin echo signal. It is advantageous for us to visualize the

Fig. I.1. The effect of an r.f. field on the macroscopic magnetization.

- a) At the beginning of an r.f. pulse both  $\vec{M}_+$  and  $\vec{M}_-$  are parallel to the Z-axis. The applied r.f. magnetic field is viewed as two components rotating in opposite directions with angular velocity  $\omega_Q = \hbar \nu_Q$ .
- b & c) During the pulse the vectors  $\vec{M}_+$  and  $\vec{M}_-$  spiral away from the Z-axis, remaining perpendicular to their respective rotating  $H_1$  component.
- d) At the end of a  $90^\circ$  pulse, both  $\vec{M}_+$  and  $\vec{M}_-$  have moved into the X-Y plane. This produces a linearly polarized magnetization in the X-direction.

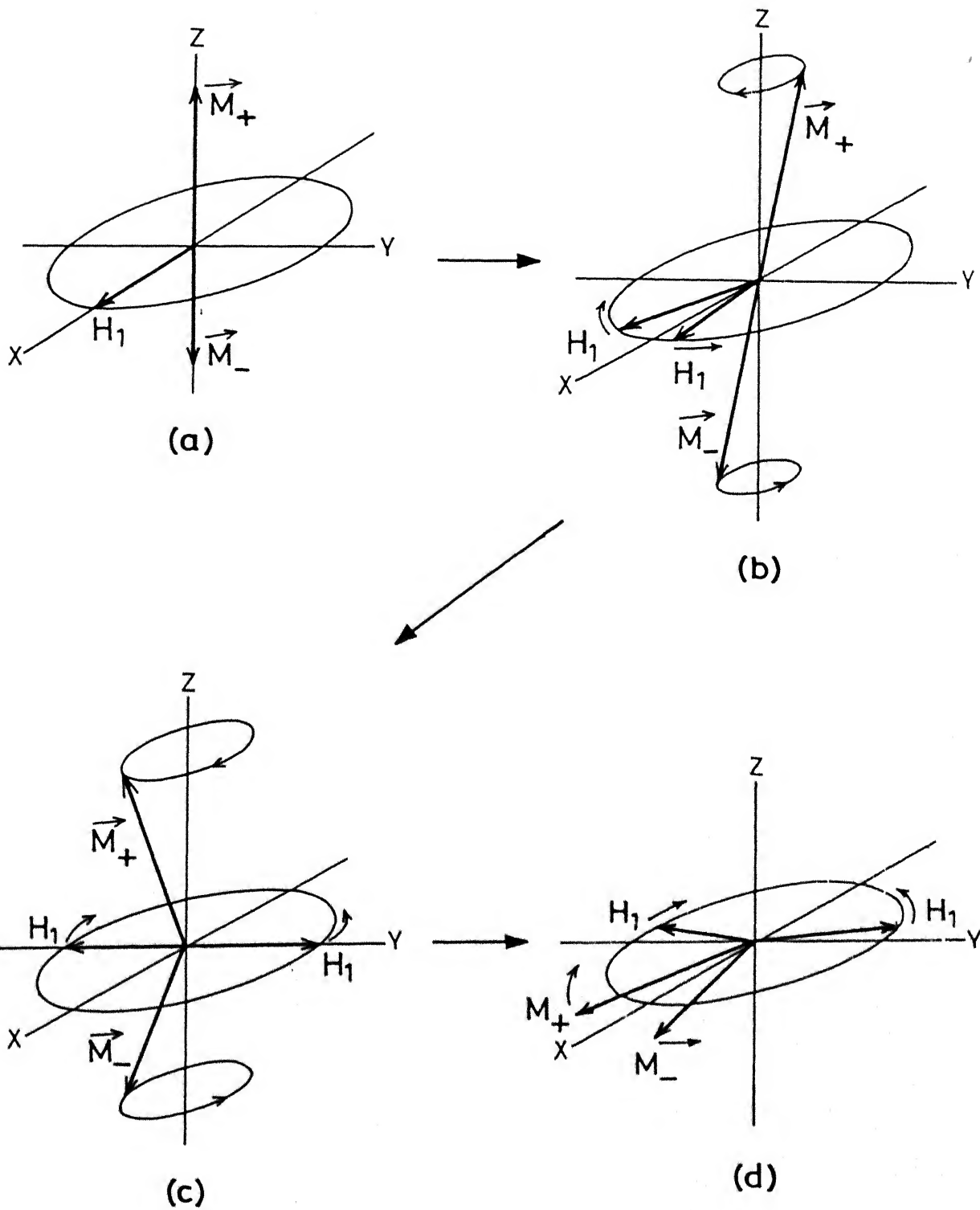
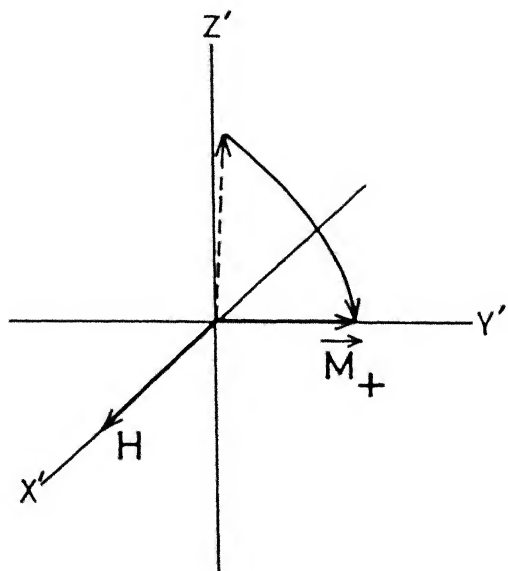


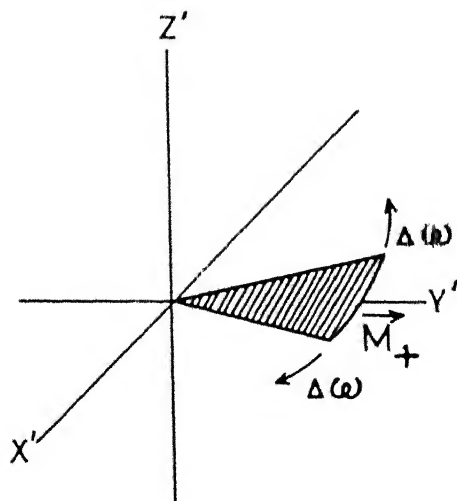
Fig. 1.2. The formation of a spin echo following a  $90^\circ - \tau - 180^\circ$  pulse sequence as viewed from the rotating frame of  $\vec{M}_+$ .

- a) After a  $90^\circ$  pulse is applied.
- b) Dephasing of the spins at the end of time  $\tau$ .
- c) A  $180^\circ$  pulse is applied at the end of time  $\tau$ .
- d) The process following the  $180^\circ$  pulse brought the spins in phase and an echo is formed at time  $2\tau$ .

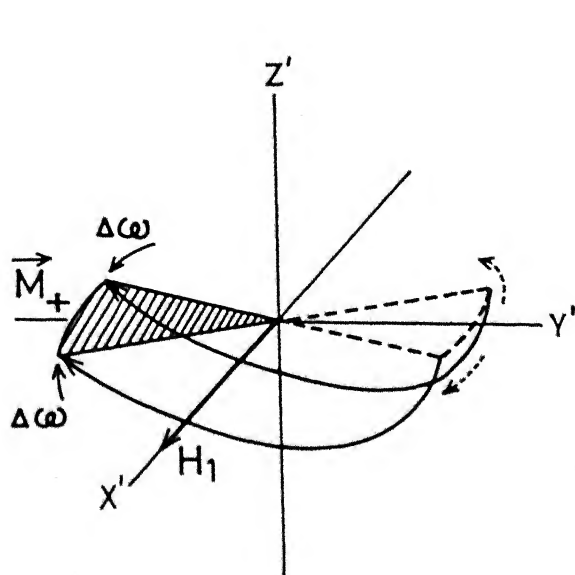
Since  $\vec{M}_+$  is rotating in the laboratory frame opposite in direction to  $\vec{M}_-$ , a linearly polarized  $\vec{M}_x$  is formed.



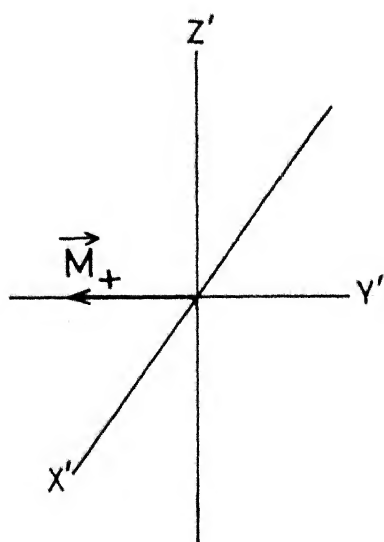
(a)



(b)



(c)



(d)

situation in a frame of reference whose  $Z'$  coincides with  $Z$ , and  $X'$  and  $Y'$  rotate counter clockwise about  $Z$ -axis with an angular velocity  $\omega_Q$ . When a distribution of resonant frequencies occurs after a  $90^\circ$  pulse the  $\vec{M}_+$  and  $\vec{M}_-$  components do not remain constant in amplitude as a function of time, but decay with a time constant  $T_2^*$ . This can be visualized graphically by considering  $\vec{M}_+$  as the sum of many vectors spread out like a fan (see Fig. I.2(b)). As time increases after a 90 degree pulse, this fan spreads out and the sum,  $\vec{M}_+$ , goes to zero. If after a time second 180 degree refocussing pulse is applied, the situation may be visualized as in Fig. I.2(c). Notice that the vectors with the highest precessional rates are behind those with the slow rates at the end of 180 degree pulse. After another time  $\tau$ , the fast vectors will catch up with the average, the slow ones will also coincide with all others, and an echo will be formed as in Fig. I.2(d). A similar situation can be visualized for the other component ( $\vec{M}_-$ ) by considering the rotating frame for  $\vec{M}_-$ .

## I.B(2) Quantum Mechanical Treatment of the Formation of Transient Signals in NQR

The expected NQR signals following resonant r.f. pulses can be calculated by a quantum mechanical treatment of evolution of the spin system. Several approaches have been used in the literature for this purpose [22-24]. Density matrix formalism [24,25]

in the interaction representation provides a convenient method of calculating the transient response of an ensemble of quadrupolar nuclei.

The wavefunction  $\Psi$  of a system can be expanded in terms of a set of orthonormal functions  $U_n$  which are independent of time

$$\Psi = \sum_n C_n(t) U_n \quad \dots (I.13)$$

The time dependence is carried by the coefficients  $C_n(t)$ . The expectation value of an operator such as  $I_x$  can be written as:

$$\langle I_x \rangle = \sum_{nk} C_k^* C_n \langle k | I_x | n \rangle \quad \dots (I.14)$$

The matrix  $C_n C_k^*$  is the representation of the matrix elements of an operator  $\sigma$ , i.e.,

$$\sigma_{nk} = \langle n | \sigma | k \rangle = C_n C_k^* \quad \dots (I.15)$$

The matrix formed by these elements is called the density matrix and the details of its usefulness are discussed in standard text books [26,27].

In order to calculate the response of a quadrupolar spin system following the r.f. pulse one proceeds as follows:



Before the application of r.f. pulse the system is assumed to be at thermal equilibrium under the influence of  $\mathcal{H}_Q$ . In the high temperature approximation [28] the thermal equilibrium density matrix is denoted by  $\sigma(t < 0)$  and is given by

$$\sigma(t < 0) \approx \exp[-(\mathcal{H}_Q/kT)] / \text{Tr}[\exp(-\mathcal{H}_Q/kT)] \\ \approx \text{Tr}(\mathbb{1})^{-1} [\mathbb{1} - \mathcal{H}_Q/kT] \quad \dots (I.16)$$

where  $\mathbb{1}$  is the unit matrix. In order to follow the time development of the system we need to consider only  $\rho$  which is related to  $\sigma$  by the equation

$$\sigma = \text{Tr}(\mathbb{1})^{-1} [\mathbb{1} - (1/kT) \rho] \quad \dots (I.16a)$$

$\rho$  is referred to as the reduced density matrix.

The equation of motion for the reduced density matrix can be written as

$$\frac{d\rho}{dt} = i/\hbar [\rho, \mathcal{H}] \quad \dots (I.17)$$

The expectation value of  $I_x$ , for example, is then given by

$$\langle I_x \rangle = \text{Tr}(\rho I_x) \quad \dots (I.18)$$

The quadrupolar Hamiltonian in an axially symmetric field gradient ( $\eta=0$ ) in the principal axes system is given by

$$\mathcal{H}_Q = \frac{e^2 q Q}{4I(2I-1)} [3 I_z^2 - I^2] \quad \dots (I.19)$$

In the presence of time-dependent r.f. interaction, the total Hamiltonian becomes

$$\mathcal{H}(t) = \mathcal{H}_0 + \mathcal{H}_1(t) \quad \dots (I.20)$$

$$\text{where } \mathcal{H}_1(t) = -\gamma \hbar (2 H_1 \cos(\omega t)) \hat{I}_x \quad \dots (I.20a)$$

Here, it is assumed that r.f. field is applied along X-direction, at right angles to the efg symmetry axis (Z), with amplitude  $H_1$  and frequency  $\omega$ . In the above equation (I.20a)  $\gamma$  is the gyromagnetic ratio of the nucleus under consideration.

If we express energy in frequency units (radians/sec), and set  $\hbar = 1$ , equation (I.20) becomes for the  $I = 3/2$  case,

$$\mathcal{H}(t) = \omega_0/2 \mathcal{H}_Q' + 2 \omega_1 \cos(\omega t) \hat{I}_x \quad \dots (I.21)$$

$$\text{where } \mathcal{H}_Q' = (\hat{I}_Z^2 - 1/3 \hat{I}^2)$$

$$\text{with } \omega_1 = \gamma H_1 \text{ and } \omega_0 = \frac{e^2 q Q}{2}.$$

We note that the Hamiltonian (I.21) consists of a large time-independent interaction (first term) and a much smaller time-dependent term (second term). In this kind of situations the time dependence of the Hamiltonian is effectively removed, by studying the dynamics of the spin system in the interaction representation, defined by the transformation operator

$$U = \exp \left[ -i \frac{\omega}{2} \mathcal{H}_Q' t \right] \quad \dots (I.22)$$

Although in the NMR literature this transformation is referred to as effecting a transformation to rotating frame it does not have any simple geometrical interpretation in the quadrupolar case.

The transformed Hamiltonian in this representation is given by [24]

$$\tilde{\mathcal{H}}(t) = U^{-1} \mathcal{H}(t) U = \frac{1}{2} (\omega_0 - \omega) \mathcal{H}_Q' + \tilde{\mathcal{H}}_1(t) \quad \dots (I.23)$$

The first and second terms of (I.23) are obtained respectively by the unitary transformation of the first and second terms of equation (I.21), the transformation operator being that defined in equation (I.22).

The terms with coherent time dependence  $e^{i\omega_0 t}$  and  $e^{2i\omega_0 t}$  in the transformed Hamiltonian  $\tilde{\mathcal{H}}(t)$ , are dropped as non-secular high frequency oscillations and the spin system is considered to evolve, to a good approximation, only by the time independent effective Hamiltonian  $\mathcal{H}^*$  (defined below). The evaluation of  $\tilde{\mathcal{H}}(t)$  is simplified by using the matrix representation for the different operators. With this the time independent effective Hamiltonian, in the interaction representation reduces to

$$[\mathcal{H}^*] = \left( \frac{\sqrt{3}}{2} \right) \omega_1 [A] + \frac{1}{2} (\Delta\omega) [\mathcal{H}_Q'] \quad \dots (I.24)$$

where  $\Delta\omega = (\omega_0 - \omega)$  and

$[A]$  is a matrix defined as [24]:

$$[A] = \begin{bmatrix} 0 & 0 & 0 & 1 \\ 0 & 0 & 1 & 0 \\ 0 & 1 & 0 & 0 \\ 1 & 0 & 0 & 0 \end{bmatrix} \quad \dots (I.24a)$$

The effective Hamiltonian given above in equation (I.24) is essentially governed by the strength of the applied r.f. field for ' $\omega$ ' very close to  $\omega_0$ .

The response of the spin system to r.f. pulse excitation can now be calculated by considering the density matrix equation of motion. Before the application of r.f. pulses, the spin system is assumed to be at thermal equilibrium under the influence of the pure quadrupolar Hamiltonian.

In the high temperature approximation, the thermal equilibrium density matrix of the spin system for the  $I = 3/2$  case is given by

$$\begin{aligned} \sigma(t < 0) &= \text{Tr} \left[ \exp \left( - \frac{\omega_0}{2} \frac{\mathcal{H}'_Q}{kT} \right) \right]^{-1} \cdot \exp \left[ - \frac{\omega_0}{2} \frac{\mathcal{H}'_Q}{kT} \right] \\ &\approx [\text{Tr}(\underline{1})]^{-1} \cdot \left[ 1 - \left( \frac{\omega_0}{2} \right) \frac{\mathcal{H}'_Q}{kT} \right] \quad \dots (I.25) \end{aligned}$$

The evolution of the system is not affected by the first term. We therefore need to follow the evolution of the thermal equilibrium reduced density matrix  $\rho(0)$  alone which we define

here as

$$\rho(0) = \mathcal{H}_Q' \quad \dots (I.26)$$

Transforming into the interaction representation, we have

$$\tilde{\rho}(0) = \tilde{\mathcal{H}}_Q' = \mathcal{H}_Q' \quad \dots (I.27)$$

because  $\mathcal{H}_Q'$  is invariant going into the interaction representation.

The equation of motion that is satisfied by the reduced density matrix is

$$\frac{d\tilde{\rho}(t)}{dt} = i [\tilde{\rho}(t), \mathcal{H}^*] \quad \dots (I.28)$$

the solution of which is

$$\tilde{\rho}(t) = \exp [-i\mathcal{H}^* t] \cdot \tilde{\rho}(0) \cdot \exp [i\mathcal{H}^* t] \quad \dots (I.29)$$

$\tilde{\rho}(t)$  is calculated using some of the properties of exponential operators [28] and one obtains for  $\tilde{\rho}(t_w)$ , at the end of the first pulse written with a width =  $t_w$ , the expression

$$\tilde{\rho}(t_w) = \mathcal{H}_Q' \cos(\sqrt{3} \omega_1 t_w) - [B] \sin(\sqrt{3} \omega_1 t_w) \quad \dots (I.30)$$

where  $[B]$  is a matrix defined as [24]:

$$[B] = \begin{bmatrix} 0 & 0 & 0 & -i \\ 0 & 0 & -i & 0 \\ 0 & i & 0 & 0 \\ i & 0 & 0 & 0 \end{bmatrix}$$

After the pulse is removed the spin system evolves according to

$$\tilde{\rho}(t') = \exp \left[ -\frac{i}{2}(\Delta\omega) \mathcal{H}'_Q t' \right] \cdot \tilde{\rho}(t_w) \cdot \exp \left[ \frac{i}{2}(\Delta\omega) \mathcal{H}'_Q t' \right] \quad \dots (I.31)$$

where  $t' = t - t_w$  with  $t \geq t_w$ . This equation simplifies to give

$$\begin{aligned} \tilde{\rho}(t') &= \mathcal{H}'_Q \cos(\sqrt{3} \omega_1 t_w) - \sin(\sqrt{3} \omega_1 t_w) \\ &\{ [B] \cos(\Delta\omega t') - [A] \sin(\Delta\omega t') \} \quad \dots (I.32) \end{aligned}$$

Now, with the density matrix describing the evolution of the spin system after the pulse (equation I.32) in hand, we have for the Laboratory frame expectation value of the X-component of the magnetization [24,29]

$$\langle I_X(t') \rangle = \text{Tr}[\tilde{\rho}(t') \tilde{I}_X] \quad \dots (I.33)$$

which leads to

$$\begin{aligned} \langle I_X(t') \rangle &= -\frac{1}{4} \left( \frac{\omega_0}{2kT} \right) \sin(\sqrt{3} \omega_1 t_w) \\ &\{ 2\sqrt{3} \cos(\Delta\omega t') \sin(\omega t') - 2\sqrt{3} \sin(\Delta\omega t') \sin(\omega t') \} \\ &\dots (I.34) \end{aligned}$$

The above equation has been derived assuming a single resonance frequency ( $\omega_0$ ) but in reality there will be a distribution of resonance frequencies about a mean value. This arises from a distribution in efg's associated with strains and imperfections in a crystal and from dipolar couplings with neighbours. Assuming a Gaussian distribution for  $g(\Delta\omega)$ , we have

$$g(\Delta\omega) = (2\pi)^{-1/2} \delta^{-1} \exp \left[ -\frac{\Delta\omega^2}{2\delta^2} \right] \quad \dots (I.35)$$

which can be written as,

$$g(\Delta\omega) = (2\pi)^{-1/2} T_2^* \exp \left[ -\frac{(\Delta\omega T_2^*)^2}{2} \right] \quad \dots (I.36)$$

$$\text{where } \delta = \frac{1}{T_2^*} = \frac{(\Delta\omega)_{1/2}}{(2 \ln 2)^{1/2}} \quad \dots (I.37)$$

is the root mean square deviation in  $\Delta\omega$  and  $(\Delta\omega)_{1/2}$  is the half width at half intensity.

The average over the distribution is given by

$$\begin{aligned} \overline{\langle I_x(t') \rangle} &= \frac{(2\pi)^{-1/2}}{T_2^*} \int_{-\infty}^{+\infty} \langle I_x \rangle \cdot \exp \left[ -\frac{\Delta\omega^2 T_2^{*2}}{2} \right] d\omega \\ &= \left( \frac{\omega_0}{2kT} \right) \left( \frac{\sqrt{3}}{2} \right) \cdot \sin(\sqrt{3}\gamma H_1 t_w) \cdot \exp \left[ -\frac{t'^2}{2T_2^{*2}} \right] \sin(\omega_0 t') \\ &\quad \dots (I.38) \end{aligned}$$

The voltage induced in the coil is obtained by taking the time derivative of  $\overline{\langle I_x(t') \rangle}$ . Hence, we have, for the induced voltage in a coil along the x-axis of the crystal (efg x-axis),

$$\Delta V_x = K \sqrt{3} \left( \frac{\omega_0^2}{4kT} \right) \sin(\sqrt{3} \gamma H_1 t_w) \exp\left(-\frac{t_w^2}{2T_2^*}\right) \cos(\omega_0 t') \quad \dots (I.39)$$

where  $K$  is a constant depending on the number of nuclei and coil geometry. Due to the exponential damping term, the induced voltage decays at a rate determined by  $T_2^*$ . This voltage represents the free induction decay (FID) signal following a single pulse and has a maximum value for a pulse width  $t_w = \pi/2\sqrt{3}\gamma H_1$  usually called the  $\pi/2$  pulse.

We can show by substituting  $\tilde{I}_Y$  and  $\tilde{I}_Z$  for  $\tilde{I}_X$  into the equation (I.33) that  $\langle \tilde{I}_Y \rangle$  and  $\langle \tilde{I}_Z \rangle$  are both zero. Hence the r.f. voltage induced in a coil perpendicular to the r.f. field is zero, again confirming the fact that a crossed coil experiment is not possible in pure NQR.

By extending the above analysis, we can obtain the response to a two-pulse sequence. Such a response can be related to echo envelope modulation function  $\mathcal{E}(2\tau)$ . We shall postpone a discussion of this to Chapter III where we present the details of our study on echo envelope modulation in NQR for  $I = 3/2$  case.

The above treatment is applicable only to the case of a single crystal oriented such that the efg  $V_{ZZ}$  axis is perpendicular to the axis of the r.f. coil. In a powdered crystalline sample the effective r.f. field seen by a crystallite is  $H_1 \cos\theta$ , where  $\theta$  is the angle between  $H_1$  direction and the X axis of the efg tensor of the crystallite. The component of



$I_x$  along the coil axis is therefore  $I_x \cos \theta$ .

Let us now consider the meaning of  $90^\circ$  and  $180^\circ$  pulses for the case of powder samples. For this purpose we can consider the equation (I.39) without including the exponential damping factor.

$$\Delta V_x = K\sqrt{3} \left( \frac{\omega_o^2}{4kT} \right) \sin(\sqrt{3}\gamma H_1 t_w) \cos(\omega_o t) \quad \dots (I.40)$$

When powder specimen are studied, this result has to be modified by taking all possible orientations of the crystallites in a powder into consideration.

If a crystallite is oriented with its efg X-axis making an angle  $\theta$  with the coil axis, the effective rf. field along the efg X-axis of the crystallite will be

$$H_1^{(eff)} = H_1 \cos \theta$$

Also the signal induced in the coil will no longer be proportional to the  $\langle I_x(t) \rangle$  since it is linearly polarized at an angle  $\theta$  with the coil axis. The component along the axis of the coil is responsible for the signal and is given by

$$(\Delta V)_{coil} = K\sqrt{3} \left( \frac{\omega_o^2}{4kT} \right) \cos \theta \sin(\sqrt{3}\gamma H_1 t_w \cos \theta) \cos(\omega_o t) \quad \dots (I.41)$$

Since all the crystallites are randomly oriented, the fraction with their X-axis pointing at an angle between  $\theta$  and

$\theta + d\theta$  with respect to  $H_1$  direction is given by

$$\frac{2\pi \sin\theta \cdot d\theta}{4\pi} = \frac{\sin\theta \cdot d\theta}{2}$$

$(\Delta V)_{\text{coil}}$  may now be averaged over all possible orientations

$$\begin{aligned} (\overline{\Delta V})_{\text{coil}} = K\sqrt{3} \left( \frac{\omega_0^2}{4kT} \right) \cdot \cos(\omega_0 t) \int_{\theta=0}^{\theta=\pi} \cos\theta \cdot \sin(\sqrt{3} \gamma H_1 \cos\theta t_w) \\ \cdot \frac{\sin\theta \cdot d\theta}{2} \quad \dots (I.42) \end{aligned}$$

This integral can be easily evaluated by changing the independent variable  $\theta$  to  $x$  (with a substitution of  $\cos\theta = x$ ) and the result is

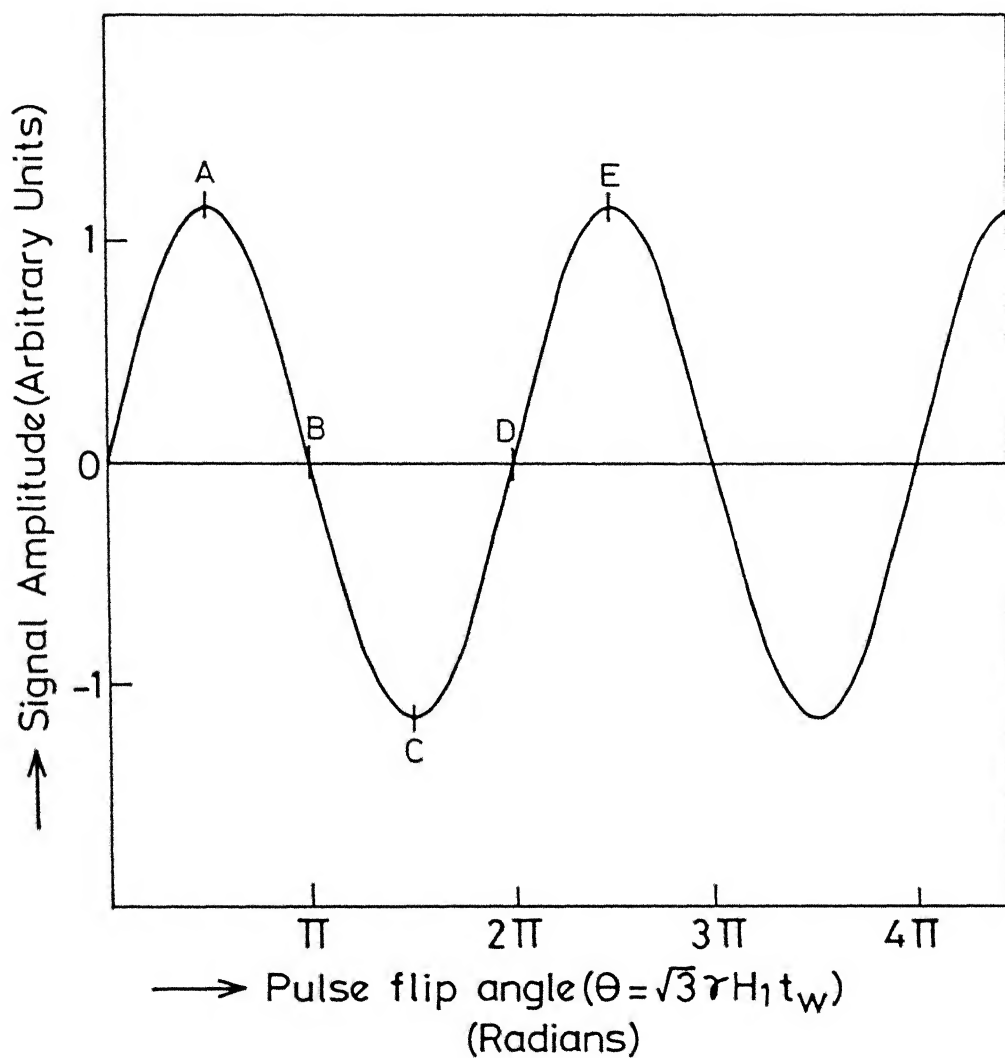
$$(\overline{\Delta V})_{\text{coil}} = K\sqrt{3} \left( \frac{\omega_0^2}{4kT} \right) \cos\omega_0 t \cdot \frac{1}{\xi} [\sin\xi - \xi \cos\xi] \quad \dots (I.43)$$

where  $\xi = \sqrt{3} \gamma H_1 t_w$ . This equation can be written as

$$(\overline{\Delta V})_{\text{coil}} = K\sqrt{3} \left( \frac{\omega_0^2}{4kT} \right) \cos\omega_0 t \cdot J_1(\xi) \quad \dots (I.43a)$$

where  $J_1(\xi)$  is the spherical Bessel function with an argument  $\xi$ .

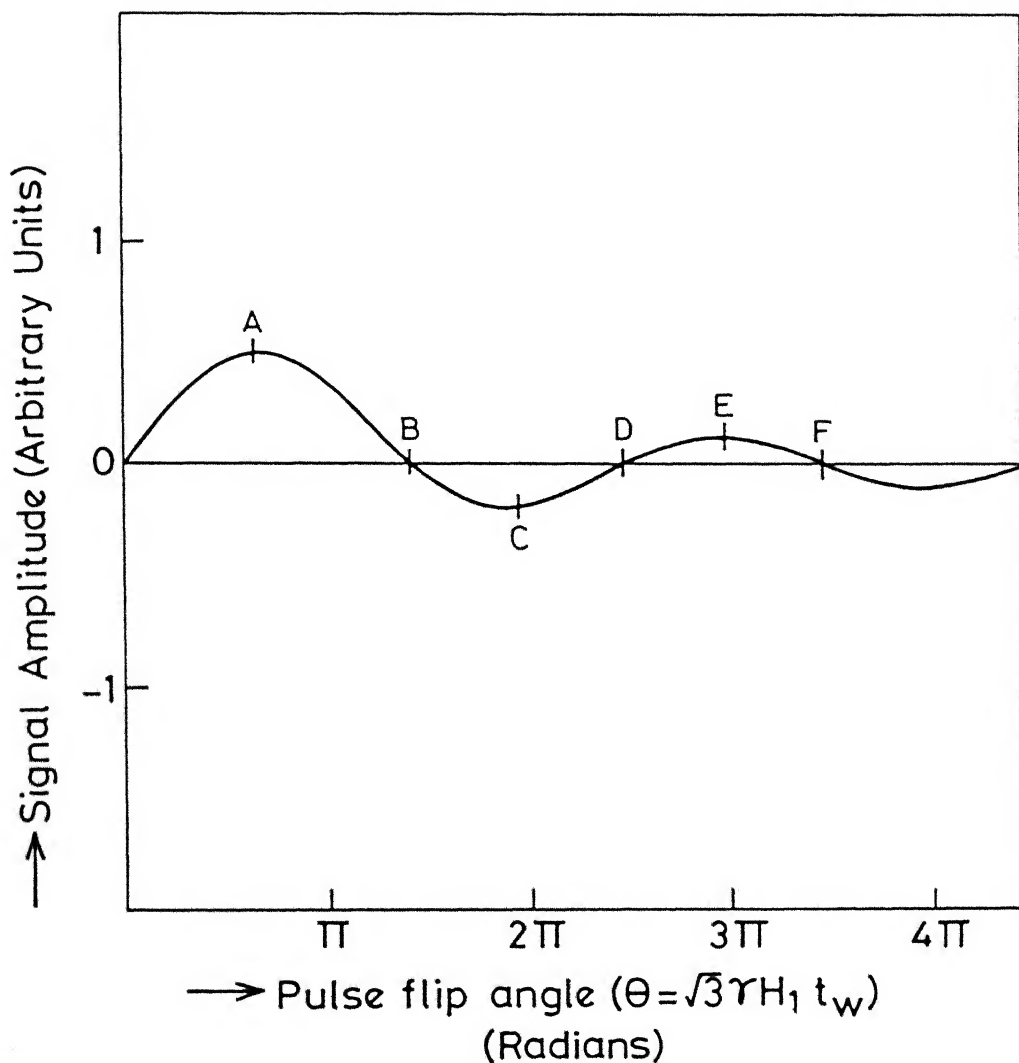
It is interesting to plot  $(\overline{\Delta V})_{\text{coil}}$  as a function of  $\sqrt{3} \gamma H_1 t_w$  since this quantity represents the rotational angle of the pulse for spins  $I = 3/2$  and the plot determines the signal following a resonant pulse as a function of pulse width (pulse flip angle). This plot is shown in Fig. I.3(b). It can be seen from the plot the signal does not equal zero when  $\sqrt{3} \gamma H_1 t_w$



Various points A,B,C etc. on the curve correspond to the following ' $\theta$ ' values:

A :  $\pi/2$  ( $90^\circ$ );    B :  $\pi$  ( $180^\circ$ );  
 C :  $3\pi/2$  ( $270^\circ$ );    D :  $2\pi$  ( $360^\circ$ ).

Fig.I-3(a) A plot showing response to a single resonant pulse of a single crystal NQR sample ( $I=3/2$ ) as a function of pulse flip angle ( $\theta = \sqrt{3} \gamma H_1 t_w$ ).



Various points A,B,C etc. on the curve correspond to the following ' $\theta$ ' values

A:  $0.66\pi$  ( $119^\circ$ ); B:  $1.42\pi$  ( $257^\circ$ );

C:  $1.88\pi$  ( $340^\circ$ ); D:  $2.46\pi$  ( $443^\circ$ ).

Fig.I-3(b) Same as in Fig.I-3(a), but the response is from polycrystalline sample.

equals  $\pi$  as it does with a single crystal (Fig. I.3(a)). Thus, a so-called " $180^\circ$ " pulse is longer for a powder sample than for a single crystal. Fig. I.3(b) also indicates that successive maxima will decrease as the pulse width is increased. This does not occur in a single crystal. Similarly a longer pulse width must be used to maximize the FID in powders than in single crystals. The required width for a so called " $90^\circ$  pulse" for powders is found from first maxima at point A (Fig. I.3(b)) which corresponds to  $0.66\pi$  rather than  $0.5\pi$  for single crystals. It is also interesting to note from Fig. I.3(b) that the width of the  $180^\circ$  refocussing pulse (first maximum) following the  $90^\circ$  pulse (in a  $90^\circ$ - $\tau$ - $180^\circ$  sequence) is different from width of a  $180^\circ$  pulse which gives zero FID signal. The  $180^\circ$  refocussing pulse width corresponds to the difference between the first maximum (point A) and the first minimum (point C) for which  $\sqrt{3}\gamma H_1 t_w$  must equal  $1.22\pi$  ( $1.88\pi - 0.66\pi$ ). In the latter case (where we get zero FID) the  $180^\circ$  pulse corresponds to a value of  $1.43\pi$  (point B). Both of these values are different from the value  $\pi$  for single crystals. All these trends have been observed in our experiment on  $^{35}\text{Cl}$  studies on powder samples.

An expression similar to that of equation (I.43(a)) has been obtained by Peterson [20] for  $I = 1$  case. Das and Saha [23] have obtained an expression for the pulse response applicable for quadrupolar nuclei of any general spin in single crystals with axial symmetry. Powder averaging of this result yields an

expression with the same functional form as that of equation (I.43(a)). Hence it is expected that the pure NQR pulse responses from powders containing nuclei with arbitrary spin and  $\eta = 0$  follow the same trend as far as the pulse width requirements of so-called "90 degree" and "180 degree" pulses are concerned.

## I.C A BRIEF SURVEY OF METHODS OF NQR DETECTION AND INSTRUMENTATION

### I.C(1) Continuous Wave (c.w.) Techniques

There are several techniques available for the detection of nuclear quadrupole interaction. Some of these techniques have been reviewed recently by Smith [30,31]. In this section we are concerned only with NQR methods of detecting this interaction.

The detection of NQR signals requires an r.f. transmitter (an oscillator) operating at the appropriate frequency and a receiver working at the same frequency. In the continuous wave (c.w.) NQR spectrometers separate transmitter and detector are not usually employed; rather an oscillator detector combination is used, i.e., one which detects the change in the oscillation level of an oscillator in the presence of NQR absorption by a sample placed in the coil forming part of the tank circuit. Three types of oscillators have been employed in NQR viz., the marginal oscillator [32-34], the regenerative oscillator [35]

and the super-regenerative oscillator (SRO) [36-40]. Though there have been several versions of all these oscillators only a few of the typical versions of them are being cited here.

[Marginal oscillators have been extensively used for the study of NQR especially in the lower frequency range primarily to study  $^{14}\text{N}$  NQR [41-43].] Significant improvement in sensitivity has been achieved by the use of field-effect Transistors (FET's) in the marginal oscillators [44,45] FET-based marginal oscillators working at higher frequencies (30-40 MHz) have also been described in the literature [46,47]. Marginal oscillators are favoured for line shape studies since they are capable of reproducing accurate line shape. These oscillators are well suited for the NQR study of saturable nuclei with long spin-lattice relaxation time because of their operation at low r.f. levels.]

Regenerative oscillators, as a rule, have poor sensitivity though they do possess good line shape response [48]. Regenerative oscillator circuits for operation at very high frequencies have been constructed and used for NQR studies [48,49]. Livingston and Zeldas [49] have constructed a regenerative oscillator using triodes (6C4) and employing transmission line-tuned circuit operating at frequencies in the range 150-350 MHz. Another regenerative oscillator circuit based on co-axial bridge has been developed by Kesserling and Gautshi [50] for observing high-frequency NQR signals. An important advantage of the regenerative oscillator is its response only to the absorption line shape. A spectrometer based on regenerative oscillator

with feedback control [51] has been constructed earlier in our laboratory [52] for the measurement of accurate line widths. Pure absorption signals are readily obtained using regenerative oscillators as they respond only to absorption line shape. However, searching for unknown signals is very difficult using these oscillators because of their poor sensitivity.

SRO's have the highest sensitivity among these three types of oscillators and are very simple in their design. Hence these oscillators have been extensively used for NQR studies. However, it is not easy to get pure absorption line shapes using simple SRO's. Yet, SRO's are ideally suited for the detection of NQR signals over wide frequency ranges because of their sensitivity. However, because of the presence of quench side bands exact frequency measurement is difficult. Dean and Pollak [39] have described a spectrometer with side band suppression so that only the main band of the SRO induces NQR signals. An improved version of SRO based NQR spectrometer which incorporates automatic gain control and side-band suppression has been described by Smith and Tong [40]. Oscillators to be used at higher frequencies require specialized circuits. Variable frequency SRO's employing 'butterfly' capacitors have been constructed and used in the frequency range 200 to 650 MHz [53]. Various aspects of SRO based spectrometers and their utility for the detection of NQR signals have been reviewed by Smith [54] in a series of articles. A recent review article by Porte [43] gives relevant



literature references to various SRO circuits. Injection- and Phase-locking of an SRO to a stable external crystal oscillator can improve its frequency stability and line shape response [55-58]. Hence, signal averaging can be undertaken in such spectrometers to increase the signal-to-noise ratio of weak NQR signals [58]. It should be added here that yet another important class of oscillators, namely, limited oscillators have recently been described by Robinson [59]. These oscillators are characterized by high sensitivity and relatively large frequency range of operation.

#### I.C(2) Pulse and Double Resonance Techniques

Pulse techniques are much more advantageous in the detection of NQR because of their higher sensitivity. In these techniques, the pulsed r.f. power is applied to the sample and the signals are detected by the receiver in the 'off' period of the transmitter. The advantages of pulsed NQR spectrometers are manifold, namely they, (i) overcome the saturation and modulation problems that are associated with c.w. spectrometers, (ii) improve the sensitivity to wide lines, (iii) in addition to the detection of NQR signals and corresponding interaction parameters, pulse methods allow the measurement of various relaxation time constants, namely,  $T_1$ ,  $T_2$  and  $T_2^*$ , (iv) the fast signal averaging possibilities in pulsed spectrometers help improve signal-to-noise ratio in relatively shorter time periods,

small splittings in a NQR spectrum caused by dipolar or indirect spin-spin interactions can also be detected by pulsed spin-echo technique as modulations on the echo envelope [7,60].

It is pertinent to mention at this point that the c.w. methods of detection generally suffer from spurious signals and instabilities which are annoying and time-consuming to the experimenter. [Producing a false echo is impossible with a pulsed NQR spectrometer. Thus, if a spin echo is detected, it is surely due to a nuclear signal.] Also, since pulse NQR techniques are more sensitive and do not suffer from the observation of false resonances, a properly designed pulsed NQR spectrometer can be conveniently used to search for new resonances with faster rates [61]. A point worth mentioning here is the effect of a small magnetic field on NQR signals. With c.w. spectrometers, i.e., in the frequency domain one notices a line broadening while with pulsed spectrometer, i.e., in time domain the echo signals appear sharper.

Time-domain response in a pulsed experiment is related to frequency-domain response by the Fourier Transform (FT). Fourier transform techniques have been applied in the area of NQR spectroscopy [62-64]. [Details of Pulsed and FT-NQR spectrometers are available in the literature [7,20,60-68].] FT-NQR method has been employed for the detection of fine structure of NQR lines arising out of direct [63] and indirect spin-spin interactions [64,67]. Mention may be made here of a recently developed

technique, namely, the time domain zero field NQR technique based on field cycling methods [69]. This method is characterized by high sensitivity and resolution at low frequencies.

Detection of rare nuclei whose resonances are very weak due to low natural abundance and/or low quadrupole coupling constant, is not possible by the conventional NQR methods described above. Application, of double resonance methods for the detection of such quadrupolar nuclei, greatly enhances the sensitivity. All the nuclear double resonance techniques depend on there being present in the same substance a nuclear species 'p' (observe nucleus) with a large nuclear resonance signal and strongly coupled to the rare nuclear species 'Q' of interest for the detection. A variety of nuclear quadrupole double resonance techniques have been developed and implemented in the literature [70-78]. Several reviews describing these techniques have been published [79-83]. The principles involved in various double resonance techniques will now be described. These can broadly be divided into two categories, namely, (1) pure quadrupole double resonance (PQDR) where the observe nucleus 'p' and the nucleus to be detected 'Q' are both quadrupolar. The detection of NQR signal of 'Q'-spins is done by monitoring the pure quadrupole resonance signal of 'p'-spins, and (2) NMR-based quadrupole double resonance where the observe nuclear 'p' resonance is monitored in high magnetic fields (NMR signal) while the 'Q'-spin irradiation is done in the absence of magnetic field or a

small Zeeman field where necessary. There are several PQDR schemes that are employed in the literature which can be classified into four types, namely,

i) spin-echo double resonance (SEDOR)

ii) double resonance in the rotating frame (DRRF)

iii) steady-state double resonance (SSDR)

and iv) double resonance following adiabatic demagnetization in the rotating frame (DR/ADRF).

(i) The spin-echo double resonance (SEDOR) technique [70,71] employs a  $\pi/2$ - $\tau$ - $\pi$  pulse sequence for the 'p'-spins to produce a spin-echo signal. The spin-echo signal is monitored while applying a resonant perturbation to the 'Q'-spins. 'Q'-spin perturbation can either be resonant c.w. irradiation [70] or a resonant  $\pi$ -pulse in the 'Q'-spin channel coincident with the  $\pi$ -pulse in the 'p'-spin channel [71]. Change in the echo signal amplitude of 'p'-spins as a function of 'Q'-spin irradiation frequency gives the quadrupole resonance spectrum of 'Q'-spins.

(ii) In the method of double resonance in the rotating frame (DRRF) [72] the 'p'-spins that are initially at the lattice temperature are brought to a state of low spin-temperature in their rotating frame by the application of a resonant  $\pi/2$  pulse followed by a  $90^\circ$  phase-shifted spin-locking pulse. When the 'p'-spins are in the spin-locked condition thermal contact is established between the 'p'-spins and the 'Q'-spins by irradiating the latter at their laboratory frame resonance frequency

and satisfying the Hartmann-Hahn condition [72]  $\omega_p = \omega_Q$ , where  $\omega_p$  and  $\omega_Q$  are the resonance frequencies of 'p' and 'Q'-spin systems in their respective rotating frames. The double resonance effect is monitored by observing the reduction in amplitude of spin-locked free induction decay of 'p'-spins as a function of 'Q'-spin irradiation frequency.

(iii) In the steady-state double resonance method (SSDR) [74] the 'p'-spins are subjected to a train of coherent near-resonant r.f. pulses of a few microseconds width and a pulse separation 't' which is small compared to  $T_2^*$ . This results in the 'p'-spins reaching a steady-state, definable by a spin-temperature. The 'p'-spin magnetization is monitored only when the r.f. field is off and the double resonance detection of the 'Q'-spins of interest is effected by applying suitable c.w. irradiation at the 'Q'-spin resonance frequency.

(iv) In the DR/ADRF method, i.e. double resonance following ADRF (adiabatic demagnetization in the rotating frame) one prepares the quadrupole 'P'-spin system in the spin-locked state along  $H_{1p}$  (after a  $90^\circ$  pulse) and then adiabatically demagnetizes by reducing the spin-locking field ( $H_{1p}$ ) to zero. The internal order and energy will then reside in the 'P' system [72]. This ordered energy of 'P' spins can be transferred to P-Q energy sink by a burst of saturating r.f. field at 'Q' spins ( $H_{1Q}$ ) at the laboratory resonance condition. After  $H_{1Q}$  is applied for a

time  $t$  (in the demagnetized state of 'P'-spins), it is turned off. The cumulative reduction in 'P'-spin energy (for  $n$  saturating pulses in the 'Q' spin channel) will be reflected in a reduction of 'P'-spin magnetization which is recovered and observed after  $H_{1P}$  is adiabatically turned on, and then abruptly turned off.

So far we have outlined the principles involved in various methods of PQDR. We now consider briefly some of the NMR-based quadrupole double resonance techniques, namely,

i) double resonance by level crossing (DRLC) in a low magnetic field,

ii) double resonance with spin mixing by continuous coupling (DRCC), and double resonance with coupled multiplets (DRCM),

and iii) double resonance in the laboratory frame via the solid effect.

These three methods are described below:

(i) The double resonance by level crossing (DRLC) in the laboratory frame [73,75] can be used in cases where the nucleus to be detected 'Q' has non-zero electric quadrupole interaction and the 'P'-spin is NMR active ( $I = 1/2$  usually) with a large gyromagnetic ratio. In the absence of Zeeman magnetic field the 'P'-spin levels are degenerate (without any splitting), while the 'Q'-spin quadrupole levels are split in the local electric field gradient. On the other hand, in a high enough magnetic

field, the Zeeman splitting of 'P' will be larger than the quadrupole splittings of 'Q' levels. Somewhere between these two extremes, the Zeeman splittings of the 'P'-spins and the Zeeman-perturbed electric quadrupole splittings of the 'Q'-spins will be the same. At this value of the magnetic field, resonance energy transfer between the two spin species is possible, and if the spin-temperatures of the two systems differ, they soon equalize. The effect of the radiofrequency perturbation of the 'Q' system can now be transferred to the 'P' system via the P-Q dipole-dipole coupling and the double resonance effect can be detected as a change in the NMR signal of the 'P'-spins. The high and low field regions may be physically separated with the sample shuttling between these two regions [73] or the fields may be switched between high and low values without sample shuttling [84].

(iii) There are two other double resonance methods which are similar to DRLC in principle but the sensitivity in these two methods is more because of continuous thermal coupling of 'Q'-spin states with the 'P'-spin reservoir. These methods are double resonance with spin mixing by continuous coupling (DRCC) [77] and double resonance with coupled multiplets (DRCM) [78]. The limitation on the sensitivity of DRLC for small numbers of 'Q'-spins may be removed by arranging that the 'P' and 'Q'-spin systems remain in good thermal contact during the irradiation phase. In these circumstances a small number of 'Q'-spins may continuously

absorb power and pass it to the 'P'-spins without saturation occurring until the total polarization of abundant 'P'-spins has been destroyed. This is the principle underlying the DRCC method. In DRCM, during the irradiation phase the multiplets of 'Q'-spins are continuously coupled thermally to the 'P'-spin reservoir.

(iii) Double resonance in the laboratory from via the 'solid-effect' (DRSE): Dipolar coupling between the integer nuclear spins (Q-spin systems) in an asymmetric electric field gradient and other spins ('P'-spin system) is reduced to a great extent in zero magnetic field [85]. This effect is usually called spin quenching. However, it should be noted that the two spin systems ('P' and 'Q') can be coupled by the application of a strong r.f. magnetic field to the sample with a frequency either (a) near one of the quadrupole transitions frequencies of the 'Q' nuclei when the sample is in zero magnetic field and the 'P'-spins exhibit no quadrupole coupling, or (b) equal to  $\omega_P \pm \omega_Q$  when the Zeeman or quadrupole coupling of the 'P' and 'Q' nuclei is non-zero. Here  $\omega_P$  is one of the transition frequencies between the energy levels of the 'P' nuclei, and  $\omega_Q$  is that of the 'Q' nuclei. This effect is one of the forms of the 'solid effect' [86]. Nuclear double resonance detection can now be done via the coupling due to solid effect (DRSE). The 'P'- and 'Q'-spins are left in contact until thermal equilibrium of both spin systems with the lattice is reached. At this



moment, a strong r.f. field pulse at frequency  $\omega$  close to  $\omega_0$  is applied to the sample. At the end of this pulse, a  $90^\circ$  pulse is applied to the 'P'-spin system at one of the 'P'-spin resonance frequency  $\omega_p$  and the 'P'-spin free induction decay amplitude is measured. Now, the same process is repeated without the strong r.f. field pulse at  $\omega$ , and the 'P'-spin free induction decay amplitude at a frequency  $\omega_p$  is again measured. The difference between the two free induction decays recorded as a function of  $\omega$  gives the double resonance signal.

All these double resonance techniques have been used to detect the resonances of rare nuclei such as  $^2\text{H}$ ,  $^{10,11}\text{B}$ ,  $^{14}\text{N}$ ,  $^{23}\text{Na}$ ,  $^{39}\text{K}$ ,  $^{85,87}\text{Rb}$ ,  $^{133}\text{Cs}$ ,  $^{17}\text{O}$ ,  $^{27}\text{Al}$  etc., with relative ease in several chemically interesting compounds. Thus, Jones and Hartmann [74] have used SSDR technique to detect  $^{40,41}\text{K}$  in their natural abundance from  $\text{KClO}_3$ . Ireland and Brown [76] have used SEDOR technique to detect  $^2\text{D}$  nuclear quadrupole resonance in  $\text{DMn}(\text{CO})_5$ . Weiden et al. [87] have used SEDOR method to detect the nuclear quadrupole resonances of  $^{23}\text{Na}$ ,  $^{39}\text{K}$ ,  $^{85,87}\text{Rb}$  and  $^{133}\text{Cs}$  nuclei in natural abundance and  $^{17}\text{O}$  in enriched samples of the corresponding chlorates and bromates. They have also investigated the  $^{27}\text{Al}$  resonances in  $\text{KAl}_2\text{Br}_7$  [88,89] and in  $(3,5\text{-ClC}_6\text{H}_3\text{O-AlBr}_2)_2$  [89] using SEDOR technique. Recently a new DRRF technique based on off-resonant pulse methods has been developed and implemented by Ramachandran and Narasimhan [90] to detect  $^{23}\text{Na}$  in  $\text{NaClO}_3$ . This method is highly sensitive and works with low transmitter power in the observe channel.

Following the work of Hahn and co-workers [91] who have showed, for the first time, that  $^{17}\text{O}$  NQR signals could be detected in natural abundance by the use of double resonance techniques involving sample transfer, there has been a wealth of literature on this subject. Thus, Poplett and Smith [92] have used DRSE technique for the detection of  $^{39}\text{K}$  in several potassium salts. Poplett et al., have also used highly sensitive double resonance techniques such as DRSE [93], DRCM [94-96] and DRLC [95] to detect nuclear quadrupole resonances of  $^{17}\text{O}$  and  $^2\text{H}$  in their natural abundance from several compounds. They have also used DRLC technique [97] to detect  $^{23}\text{Na}$  and  $^2\text{H}$  NQR signals in some hydroxide compounds. These authors have detected  $^{23}\text{Na}$  quadrupole resonances by a special variation of the usual level-crossing technique and pointed out that the modification is particularly useful in the study of half integral spin nuclei with long  $T_1$ . Budak et al., [98] have also used DRLC technique to detect  $^2\text{H}$  and  $^{14}\text{N}$  NQR signals in cytosine and cytosine hydrobromide. Apart from obtaining the quadrupole interaction parameters these double resonance techniques have been employed by them to detect the dipolar structure in many compounds containing  $^2\text{H}$ ,  $^{10,11}\text{B}$  and  $^{17}\text{O}$  [99]. An interesting example of the usefulness of these double resonance methods has recently been demonstrated by Smith and co-workers [100] who investigated proton disorder in hydrogen bonded carboxylic acid dimers. Edmonds and Mailer [101] have earlier studied  $^{23}\text{Na}$  by DRLC method in  $\text{NaOH}$ . Brosnan and

Edmonds [102] have used DRCM technique to study  $^{17}\text{O}$  in ice. Cheng and Brown [103] have successfully used DRLC technique to detect  $^{17}\text{O}$  NQR signals in several organic compounds. Avignon and Brown [104] have used this technique (DRLC) to study  $^{14}\text{N}$  NQR spectra of several metal complexes involving metal-nitrogen interactions. Lotz and Voitlander [105] have also used DRLC technique to study  $^{10,11}\text{B}$  and  $^{14}\text{N}$  resonances in  $\text{H}_3\text{BNH}_3$ . Kado et al. [106, 107] have used a sensitive nuclear triple resonance method to detect naturally abundant  $^{17}\text{O}$  NQR signals in some organic solids. This method is closely related in its principle to that described by Hahn and coworkers [91]. Recently Lotz et al. have studied  $^{10,11}\text{B}$  and  $^{14}\text{N}$  resonances in several ring compounds with transannular boron-nitrogen bonds [108], and  $^{14}\text{N}$  NQR in borazine [109]. Spectrometers for pulsed NQR double resonance have been described in the literature [68, 73, 80, 84, 98, 103, 110-114].

In recent years computer/microprocessor-controlled pulsed NQR spectrometers have been described in the literature [60, 115-117]. These systems have much more flexibility than the hard wired pulse programmer-based spectrometers and are capable of automatic acquisition, averaging and processing of NQR signal data. Chapter II of the present thesis gives the details of a microprocessor-controlled pulsed NQR spectrometer [117] designed and developed in our laboratory.

## I.D LINE SPLITTING AND BROADENING MECHANISMS IN NQR

In many cases the fine structure of NQR lines cannot be revealed because of line broadening effects. In such situations the use of suitable line narrowing methods similar to those used in solid state NMR [118] might remove the interactions which normally broaden NQR lines and yield valuable information on the fine structure. Chapter IV of this thesis is concerned with line narrowing studies using multiple pulse sequences. It is, therefore, felt appropriate to include here a brief description of various sources of line broadening and splitting in NQR spectroscopy.

In general, width, shape and structure of NQR signals can have contributions from both static and dynamic effects [7]. For example, magnetic dipole-dipole interactions, indirect spin-spin interactions, perturbations due to lattice impurities, dislocations, and vibrational and rotational motions of the molecules modify the line shapes, width and structure of NQR lines. In this section we consider these factors that could contribute to line width and line splitting in NQR spectra.

### I.D(1) Splitting and Broadening of NQR Spectra due to Magnetic Interactions

There are two types of magnetic interactions possible between the resonant nucleus and other surrounding nuclei of the same or different species (non-resonant nuclei).

- i) A direct magnetic dipole-dipole interaction between neighbouring nuclei [119],  
and ii) indirect spin-spin interaction between two nuclei (J-interaction).

(i) When the resonant nucleus has a very close neighbor, the magnetic dipole-dipole interaction with it predominates over that of distant neighbors, and a fine splitting of the quadrupole spectra is produced, which is analogous to the 'Pake splitting' in NMR [119, 120]. An example of this kind of splitting occurs in  $\text{HIO}_3$  (iodic acid) where the splitting is due to interaction between the proton and the  $^{127}\text{I}$  nucleus [48]. In recent years, with the development of sensitive nuclear quadrupole double resonance techniques, dipolar structure has been detected in many compounds containing  $^2\text{H}$  and  $^{10,11}\text{B}$  [92, 99-102, 121]. In all these cases the quadrupolar nuclei are directly bonded to hydrogen or fluorine atoms which have a large magnetic moment. The magnetic dipole-dipole interaction between the resonant nucleus and other distant neighboring nuclei, other than the very close neighbour, broadens the NQR lines and the fine components produced by the action of the close neighbour will not be seen. When there is no particular close neighbor, only a broadening of the NQR spectra occurs.

(ii) Indirect spin-spin interaction between two nuclei (J-interaction) originates from the magnetic interactions of two nuclei with the electrons that form the chemical bond between

them [122-124]. Ainsbinder and Shaposhnikov [124] have given a theoretical analysis of indirect spin-spin interaction in NQR spectroscopy. The J-interaction can lead to an appreciable fine splitting of the quadrupole spectra as its short range effect is sufficiently strong to overcome the direct dipole-dipole interaction. J-interaction can also occur between nuclei in atoms which are not directly bonded to one another but through other atoms. In such cases, however, it will be weak [122], hence its effects on the quadrupole spectra (broadened by dipolar and other interactions) may not be revealed by the usual methods. Some of the examples where J-interactions have been observed by conventional c.w. methods are between the  $^{127}\text{I}$  nuclei in  $\text{I}_2$ , between  $^{79}\text{Br}$  nuclei in  $\text{Br}_2$ , and between  $^{127}\text{I}$  and  $^{35}\text{Cl}$  nuclei in  $\text{ICl}$  in the solid state. Kojima et al. [125] have observed a five-line pattern for the  $3/2 \rightleftharpoons 1/2$  transition in solid iodine arising out of J-interaction between the two iodine atoms. Other authors have subsequently studied the splittings due to J-interactions [51, 126-128]. Indirect spin-spin interactions would be expected to be stronger in the case of bonds between heavier atoms. Thus we may expect fairly large spin-spin interactions in As, Sb and Bi halides, particularly in bromides and iodides.

It should be mentioned here that, in NMR spectroscopy, line narrowing techniques which selectively average certain broadening interactions have been developed and implemented to obtain high resolution NMR spectra in solids [118]. Designing of

appropriate multiple pulse sequences and implementing them in NQR spectroscopy to achieve suppression of the dipolar and other broadening interactions and obtaining high resolution is of enormous interest since the J-interaction can then be well-studied.

### I.D(2) Electrical Sources of Broadening

Dislocations and strains in the crystal or powder grains [51, 126, 129] are known to broaden the quadrupole spectra. The broadening due to strains and dislocations arises from random distribution of field gradients at nuclear sites. Similarly, a distribution in field gradients is produced by the disorder in the crystal lattice [130]. Presence of impurities in the crystal lattice also causes a random distribution of environment around different nuclei, and hence leads to a broadening of the pure quadrupole lines [131, 132].

### I.D(3) Line Broadening due to Dynamic Effects

In NQR, torsional motions contribute most to the spin lattice relaxation. Since spin-lattice relaxation limits the life time of the excited state, it contributes to a line broadening mechanism known as "life-time broadening". Hence, the contribution to line widths from dynamic effects are related to  $T_1$  and are generally estimated to be of the order of tens of Hertz.

Torsional motions in the solid state cause a time dependence in the efg parameters  $q$  and  $\eta$ . Since these motions are

interrupted by interaction with vibrational and rotational degrees of freedom of the molecules. Thus, random fluctuations in the field gradient arise at the site of the nucleus. If these fluctuations have a Fourier frequency component in the neighborhood of a quadrupole resonance frequency of the nucleus, it will induce transitions between the corresponding quadrupole energy levels and produce relaxation effects. The component in the vicinity of  $\nu_Q$  causes  $\Delta m = \pm 1$  transitions and that in the vicinity of  $2\nu_Q$  causes  $\Delta m = \pm 2$  transitions. Bayer [133] has calculated these transition probabilities  $W_{\pm 1}^T$  and  $W_{\pm 2}^T$  for  $\Delta m = \pm 1$  and  $\Delta m = \pm 2$ , respectively. Considering the molecules as oscillating in a nearly parabolic potential well. With this picture, the energy levels of the torsional motion resemble those of a harmonic oscillator. Woessner and Gutowsky [134] have calculated  $W_{\pm 1}^T$  and  $W_{\pm 2}^T$  for spin 3/2 nuclei following the basic approach of Bayer but using more detailed harmonic oscillator dynamics. The experimental studies of Weber [135] on p-dichlorobenzene lend support to theories based on Bayer's approach.

## I.E SOME APPLICATIONS OF NQR SPECTROSCOPY

A considerable amount of information regarding the electronic environment around a quadrupolar nucleus can be obtained from NQR spectroscopy [7, 54, 136, 137]. NQR spectroscopic studies yield information on efg parameters  $\frac{e^2 q Q}{h}$ , the quadrupole coupling constant (QCC) and  $\eta$ , the asymmetry parameter. These



parameters reveal the electronic distribution leading to a better understanding of the chemical bond and other related properties of the molecule or ion in which the nucleus is involved in the solid state. A large amount of studies on chemical applications of NQR have been carried out in the literature and have been reviewed extensively [31, 43, 54, 136-140]. In this section we shall highlight some of the typical applications.

In cases where more than one NQR frequency exists, the information on both the interaction parameters, namely, QCC and  $\eta$  can be obtained from NQR spectroscopy. In case of  $I = 3/2$ , Zeeman NQR studies are required to obtain information on both these parameters. From single crystal studies it is also possible to determine the orientation of principal axes of the efg tensor with respect to the crystal axes. These data are quite useful in elucidating the nature of the chemical bond and the charge distribution in the solid state where the molecules are no longer free but under the influence of neighboring molecules.

The small difference in quadrupole interaction parameters in gaseous and solid state may be interpreted in terms of intermolecular interactions in the solid state. An understanding of the nuclear quadrupole interaction in free molecules and in the molecules in solid state, in terms of their electron distribution can therefore lead to an insight into the intermolecular interactions present in the solid state [7].

QCC involves a nuclear property  $Q$  and a molecular property  $q$ . Hence, a knowledge of one can determine the other through the experimental coupling constants. The quantity  $q$  is related to the charge distribution over the molecule and an exact description of the charge distribution in turn requires a knowledge of wave functions of very high quality (Hartree-Fock SCF quality with a basis set containing core as well as valence shell atomic orbitals). One can resort to one of the several choices for the molecular wavefunctions, typically, valence-bond or molecular orbital wavefunctions. Also whenever necessary the configuration interaction, and variations in geometry should be taken into consideration. An exact calculation of efg components requires rigorous evaluation of a number of molecular one-electron integrals of one-, two-, or three-centre kind. Results of ab initio level efg calculations for free molecules have been reviewed by Lucken [136], Moccia and Zandomeneghi [141], Snyder and Bosch [142] and Palmer [143]. High sensitivity of the theoretically calculated efg values towards the changes in molecular geometry necessitates the "frozen nucleus" calculations to be supplemented by vibrational averaging [144-146] over the molecular motion in order to obtain good agreement with experimental results. Such sophisticated calculations at the ab initio level are expected to yield accurate efg's and from these one can obtain precise values for the nuclear quadrupole moment using experimental QCC's of free molecules as obtained from sources such as microwave spectroscopy [136].

CENTRAL LIBRARY  
I. I. T. KANPUR

Acc. No. A. 106235

Ab initio calculations of efg's on large molecules is rather cumbersome and requires large computer time. The problem becomes more serious if the molecules contain polar bonds and a CI-based calculation is required. In such situations and also in the cases where limited computer time is available, the use of empirical and semi-empirical methods would be appropriate. The pioneering work in this direction was that of Townes and Dailey [147]. Expressions for  $q$ 's at the nucleus of interest based on the Townes-Dailey approach are available [7, 136]. The efg's are expressed in terms of electron populations on the p-orbitals. The contributions from the inner core of atoms are completely neglected. Thus the Sternheimer [148, 149] effects are not considered. These effects play an important role in the evaluation of efg's when deformations of electron core takes place either by electric field gradient due to outer orbitals or by nuclear quadrupole moment. Cotton and Harris [150], Sichel and Whitehead [151], and White and Drago [152] have attempted to remove some of the deficiencies of the Townes-Dailey approach. Some authors [136, 153] have employed p-orbital populations obtained from semi-empirical as well as ab initio MO calculations with a view to correlate the efg's of first and second row atoms, especially using the Townes-Dailey type approach and have obtained varying success. Dewar et al. [154] have used MINDO/3 method to calculate efg's at N-site in some molecules. Two other groups of workers [155, 156] have made semi-empirical SCF MO level calculations in several molecules at

deuterium site. Recently Thankachan and Narasimhan [157] have calculated efg's in several molecules at D, Li, N and O sites using four different semi-empirical SCF MO methods. Since the efg operator is a one electron operator and samples the region of space close to the nucleus, the behaviour of the semi-empirical wavefunctions in this region can be properly assessed by these calculations. All the above referred calculations of  $q$  values pertain to isolated 'free' molecules. No satisfactory method is as yet available for the calculation of wavefunctions of molecules in the solid state. Accordingly one can use the data on free molecules only as a guide line for the interpretation of quadrupole couplings obtained from the solid state as in NQR spectroscopy.

Bray et al., [158] have analyzed the results of  $^{14}\text{N}$  NQR data in solids using Townes-Dailey approach. They have also used NQR data to correlate biological activity of certain biologically important molecules. For planar molecules the asymmetry parameter ( $\eta$ ) for halogen nuclei can be related to the double bond character of the bond in which the halogen atom takes part [7, 159]. The interpretation of quadrupole interaction parameters can also give an insight into the hybridization of molecules and ionic character of the chemical bonds in them [7, 136, 160]. NQR spectral parameters can also be correlated with several other chemical- and physico-chemical constants, such as i) Hammet-Taft  $\sigma$  parameters which give substituent effects on a particular

reaction series, (ii) electronegativities, and (iii) dissociation constants [136, 160]. NQR technique is also useful for studying nature of bonding in addition compounds [161].

Efg's are quite insensitive to isotopic substitution and hence the ratio of quadrupole moments of different isotopes can be obtained from the ratio of QCC's from a NQR study of the same compound with different isotopes. This is one of the most accurate methods of obtaining nuclear quadrupole moment ratios for different isotopes [162-164].

NQR spectroscopy can also be used to distinguish between "chemically inequivalent" and "physically inequivalent" sites of the same quadrupolar nucleus in a crystal [7]. "Chemical inequivalence" implies that the magnitudes of the components of efg tensor are different between the two sites whereas "physical inequivalence" implies the orientations of the efg principal axes are different though the magnitudes of the components of efg tensor are same for the two sites. Hence, "chemically inequivalent" sites would have different NQR frequencies and it is a straightforward matter to distinguish between them using NQR. "physically inequivalent sites would have same NQR frequencies at lower temperatures. However, the NQR frequencies of two different "physically inequivalent" sites are expected to have different temperature dependences. Hence, at high enough temperatures when the torsional motions play an important role, even "physically inequivalent" sites could have different NQR

frequencies. This situation is illustrated by the  $^{35}\text{Cl}$  NQR frequencies in chloroform [165]. "Chemical inequivalence" also arises from the stereochemistry of the atoms in molecules and hence NQR frequencies can be used to study stereochemistry in the solid state [54, 137]. Apart from crystal structure, it is also possible to identify crystal modifications in favourable cases. A recent study of  $^{35}\text{Cl}$  in  $\text{Sr}(\text{ClO}_3)_2$  at room temperature by V. Ramakrishna et al. [166] has revealed the presence of three physically inequivalent  $^{35}\text{Cl}$  sites. These authors have concluded that the crystal belongs to the monoclinic class and the additional site may be due to the twinning (crystal modification) present in the crystal.

NQR frequencies ( $\nu_Q$ ) are quite sensitive to temperature changes. Useful information regarding molecular motions in solids can be obtained from a systematic study of the temperature dependence of the NQR frequency. Normally, the temperature coefficient of the NQR frequency,  $d\nu_Q/dT$ , is negative. Bayer [133] has pointed out that this type of behaviour can be explained by an averaging of efg's to lower values by the increased amplitudes of torsional motions at high temperatures. However, Bayer's theory does not predict the presence of positive temperature coefficients. Kushida, Benedek and Bloembergen (KBB) [167] have shown on the basis of lattice dynamic arguments that Bayer's theory predicts only  $(\partial\nu_Q/\partial T)_V$  whereas the experimental measurements are done under constant pressure conditions and the

have given a simple theory for pressure dependences of  $\nu_Q$  through a description of pressure dependence of the efg. In crystals where intermolecular binding is weak, a large positive pressure coefficient is observed and as binding becomes stronger the pressure coefficient decreases, goes to zero and finally becomes negative for very strong intermolecular binding. Mackowiak et al. [185] have recently performed a high pressure NQR study of the phase transition in anilinium iodide in the temperature range 77 K to 290 K. Their study revealed a negative pressure coefficient for the NQR frequency. They have also evaluated QCC and  $\eta$  at various pressures. Their results confirm the close connection between the mechanism of the phase transition and the dynamics of the  $\text{N-H}^+ \cdots \text{I}^-$  hydrogen bonds.

In the past several years pulsed NQR methods have been widely employed to obtain information concerning structural and dynamical aspects of molecules in solids. A survey of applications of pulse methods in NQR has been made by Guibe [42]. Information about the molecular dynamics in the solid state can be obtained by using pulsed NQR techniques [134, 135, 178] by studying the relaxation behavior of the nuclear spins following the application of resonant r.f. pulses. In quadrupolar spin systems the spin lattice relaxation can be quantitatively related to the nature and frequency of the molecular and lattice motions [133-135, 186]. Spin-spin and spin-lattice relaxation processes are temperature and pressure dependent. An accurate measurement of these NQR spectral parameters as a function of temperature

and pressure therefore leads to valuable information on lattice dynamics.

Unlike c.w. methods, pulsed-Fourier transforms (FT) techniques do not suffer from modulation broadening effects. This fact has advantageously been used for resolution enhancement of NQR lines. Gibson et al. [64] have employed FT-NQR method for studying fine structure in solid chlorine. Mackowiak et al. [67] have employed this technique for the study of spin-spin interactions in the ferroelectric phase of solid HCl. Lucken and coworkers [62, 187-193] have employed FT technique for obtaining fine structure [62, 190] and also for Zeeman NQR investigations in single crystals [187, 193]. The doublet splitting observed by them in the  $^{35}\text{Cl}$  FT-NQR spectrum of  $\text{PCl}_3$  [190] has been ascribed to the effect of  $^{31}\text{P}$ - $^{35}\text{Cl}$  dipole-dipole coupling. Apart from obtaining quadrupole interaction parameters of NQR lines in several organic molecules, their FT-NQR studies have also shed considerable light on conformations and symmetries [187, 191-193] of the molecules in crystals. Ambrosetti et al. [194] have studied  $^{14}\text{N}$  FT-NQR at the ferroelectric transition in  $\text{NaNO}_2$ .

It is pertinent to mention here that FT-NQR technique together with appropriate line-narrowing techniques could further resolve the fine structure generally masked in broad NQR lines. Thus, line-narrowing techniques assume a special significance in NQR spectroscopy. Some of our attempts in the direction of



line narrowing in NQR are described in Chapter IV of the present thesis.

New possibilities have been introduced with the development of pulsed double resonance techniques which allow measurement of very weak quadrupole interactions from less sensitive and/or low natural abundant quadrupolar nuclei. Double resonance techniques have been utilized to resolve the structure due to  $^{17}\text{O}$ --- $^1\text{H}$  dipolar splitting [31, 99]. This splitting pattern has been utilized to deduce the sign of  $^{17}\text{O}$  quadrupole coupling constant and the orientation of the principal axes with respect to the O-H bond direction. The elements hydrogen, nitrogen and oxygen have important role in the compounds of chemical and biochemical importance. Prior to the development of double resonance techniques, only  $^{14}\text{N}$  out of the above mentioned elements was investigated. Even in the case of  $^{14}\text{N}$ , the experimental difficulties associated with instrumentation made it very difficult to undertake systematic investigations of nitrogen quadrupole couplings. Now, with the advent of double resonance techniques it has become possible to obtain NQR data on these important elements, namely,  $^2\text{H}$ ,  $^{14}\text{N}$ , and  $^{17}\text{O}$  in natural abundance in a fashion which may be described as routine in comparison to the earlier era. Review articles by Blinc [79], Ragle and Minott [81] and Poplett [82] gives a detailed survey of double resonance techniques in NQR spectroscopy and their applications. It must be emphasized here that the above presentation has been made with a view to illustrate some of the typical applications of NQR and no attempt

has been made to present an extensive survey of the literature.

Amongst the potential applications of NQR spectroscopy mention may be made of the possibility of observing a weak interaction, namely, hexadecapole interaction which is an interaction between a nuclear electric hexadecapole moment and its surrounding charge distribution. The interaction Hamiltonian,  $\mathcal{H}_{\text{Hex}}$  is given as (fifth term in the equation I.1):

$$\mathcal{H}_{\text{Hex}} = M_{16} \cdot V_4 \quad \dots \text{(I.44)}$$

$M_{16}$  and  $V_4$  are fourth rank tensors describing nuclear electric hexadecapole moment ( $M_{16}$ ) and the fourth derivative of the potential ( $V_4$ ) at the nuclear site due to charges external to it.  $M_{16}$  exists for a nucleus only if its spin  $I \geq 2$ .

Nuclear hexadecapole interaction (HDI) perturbs quadrupolar energy levels and the expressions for NQR frequencies in terms of HDI are given in the literature [51]. It should however, be mentioned that nuclear hexadecapole coupling constants are expected to be extremely small (of the order of a few kHz) and hence a precise experimental determination of quadrupole resonance frequencies is required for its detection through NQR. Wang [51] has measured the three NQR transition frequencies of  $^{123}\text{Sb}$  ( $I = 7/2$ ) nucleus in  $\text{SbBr}_3$ , with the accuracy that was possible with his experimental set up, and reported for the first time the existence of measurable hexadecapole coupling in  $^{123}\text{Sb}$ . Later some more workers [195-199] have investigated the

possibility of detecting HDI through NQR spectroscopy. Some of them [196, 198] support the existence of hexadecapole interaction, while others [195, 197] do not. Recently, Doering and Waugh [200] have attempted to observe the splitting pattern in the NMR signal of  $^{181}\text{Ta}$  in  $\text{KTaO}_3$  due to electric hexadecapole coupling. On account of cubic symmetry around  $^{181}\text{Ta}$  the electric quadrupole interaction in this compound should vanish. However, the absence of perfect cubic symmetry could lead to a residual quadrupolar interaction. This and the magnetic dipole-dipole couplings can in principle be suppressed by using multiple-pulse line narrowing methods. Infact, Doering and Waugh attempted the use of multiple pulse line narrowing method for this purpose. Experimental difficulties prevented the observation of signal response to WAHUHA 4-pulse sequence on  $^{181}\text{Ta}$  and hence it was not possible for them to observe splittings due to HDI. However, they have observed NMR signal of  $^{181}\text{Ta}$  at two different magnetic fields and the  $\gamma_{\text{Ta}}$  evaluated from the two corresponding resonance frequencies is constant. This means that the observed NMR line-width (12 kHz) is not due to magnetic field inhomogeneities. Also the magnetic dipole-dipole broadening in this compound has been estimated to be very small. The only cause for this broadening could therefore be either due to quadrupolar-broadening or due to hexadecapole-broadening. If the former is the cause the expected quadrupole coupling constant (QCC) would be 30 kHz for this line-width of 12 kHz and if the latter is responsible for the broadening the expected hexadecapole coupling

constant (HCC) would be 400 kHz. In fact, their theoretical estimate for QCC considering maximum expected imperfections gave a value of 30 kHz and an estimate of HCC considering maximum anti-shielding factor and other induced charge effects gave a value for the splitting due to HCC be of the order of a hundred Hz. Hence, the authors have favoured the cause for the broadening to be the quadrupole coupling arising from imperfections in cubic crystals rather than the hexadecapole coupling. They have also been able to fit Gotou's [198] NQR experimental data without invoking the HDI and thus have concluded that Gotou's data do not support the claim that he has observed hexadecapole interaction.

It should be mentioned here that, as the NQR frequencies are very sensitive to temperature variations an exact measurement of all the three quadrupole resonance frequencies in the case of  $I = 7/2$  system should be made at precisely the same temperature in order to help verify the existence of HDI by means of the NQR spectroscopic method.

From the above discussion, it is clear that NQR is a valuable tool for the investigation of structure, bonding and dynamics in solid state.

The research activity in this area is reflected in the eight bi-annual "International Symposia" that were held in the recent past. Proceedings of the first two symposia have been published in the form of books [201, 202] while papers presented in the subsequent symposia have appeared in Scientific Journals,

namely, "Journal of Magnetic Resonance" and "Journal of Molecular Structure". The papers of a recent symposium (1985) have been published in Part 'A' of "Zeitschrift für Naturforschung".

## I.E SCOPE OF THE PRESENT THESIS

Spin echo techniques in NQR facilitate an accurate study of weaker interactions as the inhomogeneous contributions to the resonance linewidth, which often cause problems in the steady-state techniques will be removed in the formation of spin echo. Echo envelope modulation studies in the presence of small Zeeman interaction facilitate the evaluation of the asymmetry parameter  $\eta$ , of the efg tensor for spin  $I = 3/2$  nuclei in polycrystalline specimens. Earlier workers from this laboratory have utilized Zeeman-perturbed spin echo envelope modulation (ZSEEM) studies to examine the possibility of evaluation of  $\eta$  [203]. They utilized a home-built spectrometer system [90] whose operation was completely manual and hence performing ZSEEM experiments with that instrument was tedious and time consuming. For this purpose and also for the purpose of performing many other complex experiments based on multiple pulse sequences we have automated this pulsed NQR spectrometer using a microprocessor and a signal analyzer.

Chapter II of this thesis deals with the generation of pulse sequences using a microprocessor and gives the details of automation and control of several pulsed NQR experiments. This chapter concludes with the evaluation of performance of the new

spectrometer system by a presentation of typical results of various experiments.

In Chapter III, the results of ZSEEM studies on  $I = 3/2$  polycrystalline samples using the automated spectrometer system have been presented. Apart from two pulse echo envelope modulation studies, Chapter III also presents the results of our studies on the use of extended excitation for obtaining ZSEEM in NQR.

Our microprocessor controlled pulse NQR spectrometer system is capable of generating several multiple pulse sequences. We have studied the effect of various multiple-pulse sequences on spin  $3/2$  polycrystalline samples and the results are presented in Chapter IV. Experimental results on effects of pulse sequence parameters and resonance off-set are presented and discussed in this chapter.

The thesis concludes with an outline of the scope for future work.

### Summary

In this chapter a discussion of the basic theory and applications of NQR has been presented which has been followed by a brief survey of various methods of NQR detection and instrumentation. Classical picture of formation of transient signals in NQR and their quantum mechanical description based on density matrix formalism has been outlined in this chapter. A description

of line splitting and broadening mechanisms in NQR has been included. The scope of the present thesis has also been outlined here.

In the next chapter, the details of control of the spectrometer and automation of data acquisition using a microprocessor and a signal analyzer will be presented.

REFERENCES

- [1] H.B.G. Casimir, *Physica*, 2, 719 (1935).
- [2] N.F. Ramsey, "Nuclear Moments," Wiley, New York (1953).
- [3] H.G. Dehmelt, *Amer. J. Phys.*, 22, 110 (1954).
- [4] H.G. Dehmelt and H. Krüger, *Naturwiss.*, 37, 111 (1950).
- [5] M. Bloom and R.E. Norberg, *Phys. Rev.*, 93, 638 (1954).
- [6] E.L. Hahn and B. Herzog, *Phys. Rev.*, 93, 639 (1954).
- [7] T.P. Das and E.L. Hahn, "Nuclear Quadrupole Resonance Spectroscopy," *Solid State Physics, Supplement 1*, Academic Press, New York (1958).
- [8] R.V. Pound, *Phys. Rev.*, 79, 685 (1950).
- [9] M.H. Cohen and F. Reif in "Solid State Physics," *Advances in Research and Applications*, Vol. 5, Ed. F. Seitz and D. Turnbull Academic Press, New York (1957) p. 321.
- [10] R. Bersohn, *J. Chem. Phys.*, 20, 1505 (1952).
- [11] M.H. Cohen, *Phys. Rev.*, 96, 1278 (1954).
- [12] (a) R.B. Creel, H.R. Brooker and R.G. Barnes, *J. Mag. Reson.*, 41, 146 (1980).  
(b) R.B. Creel, *J. Magn. Reson.*, 52, 515 (1983).
- [13] G.M. Muha, *J. Magn. Reson.*, 53, 85 (1983).
- [14] R.B. Creel and D.A. Drabold, *J. Molec. Struct.*, 111, 85 (1983).
- [15] M.S. Krishnan and B.C. Sanctuary, *Z. Naturforsch.*, 41a, 353 (1986).
- [16] T.C. Gibb and N. Greenwood, "Mössbauer Spectroscopy," Chapman and Hall Press, London (1971).
- [17] L.B. Robinson, *Can. J. Phys.*, 35, 1344 (1957); 36, 1295 (1958).



- [18] H. Hartmann and H. Silles, *Theor. Chim. Act.*, 2, 63 (1964); 2, 371 (1964).
- [19] W.G. Proctor and K. Lu, *Varian Technical Information Bulletin* (1965).
- [20] G.L. Petersen, Ph.D. Thesis, Brown University (1975).
- [21] E.L. Hahn, *Phys. Rev.*, 80, 580 (1950).
- [22] M. Bloom, E.L. Hahn and B. Herzog, *Phys. Rev.*, 97, 1699 (1955).
- [23] T.P. Das and A.K. Saha, *Phys. Rev.*, 98, 516 (1955).
- [24] J.C. Pratt, *Molec. Phys.*, 34, 539 (1977).
- [25] S. Alexander and A. Tzalmona, *Phys. Rev.*, 138A, 845 (1965).
- [26] A. Abragam, "The Principles of Nuclear Magnetism," Clarendon Press, Oxford (1961).
- [27] C.P. Slichter, "Principles of Magnetic Resonance," Solid State Science, Springer-Verlag, Berlin (1980).
- [28] R.S. Cantor and J.S. Waugh, *J. Chem. Phys.*, 73, 1054 (1980).
- [29] U. Haeberlen in "High Resolution NMR in Solids: Selective Averaging," Supplement 1 to *Advances in Magnetic Resonance*, Ed. J.S. Waugh, Academic Press, New York (1976), p. 50.
- [30] J.A.S. Smith, *Z. Naturforsch.*, 41a, 453 (1986).
- [31] J.A.S. Smith, *Chem. Soc. Rev.*, 15, 225 (1986).
- [32] R.V. Pound and W.D. Knight, *Rev. Sci. Instrum.*, 21, 219 (1950).
- [33] G.D. Watkins and R.V. Pound, *Phys. Rev.*, 85, 1062 (1951).
- [34] F.N.H. Robinson, *J. Sci. Instrum.*, 36, 481 (1959); *Rev. Sci. Instrum.*, 34, 1260 (1963).
- [35] R. Livingston, *Annals of New York Academy of Science*, 55, 800 (1952).

- [36] H.C. Torrey, Phys. Rev., 75, 1326 (1949).
- [37] D. Williams, Physica, 17, 454 (1951).
- [38] C. Dean, Phys. Rev., 96, 1053 (1954).
- [39] C. Dean and M. Pollak, Rev. Sci. Instrum., 29, 630 (1958).
- [40] J.A.S. Smith and D.A. Tong, J. Phys. E: Sci. Instrum., 1, 8 (1968).
- [41] L. Guibe, Topics in Current Chemistry, Springer Verlag, Heidelberg, 30, 77 (1972).
- [42] L. Guibe in "Advances in NQR," Vol. 1, Ed. J.A.S. Smith, Heyden and Son, London (1975), p. 375.
- [43] A.L. Porte in "Annual Reports on the Progress of Chemistry," Section C (Physical Chemistry), Vol. 80, Royal Society of Chemistry, Burlington House, London (1983), p. 162.
- [44] T.L. Viswanathan, T.R. Viswanathan and K.V. Sane, Rev. Sci. Instrum., 41, 477 (1970).
- [45] R. Labrie, M. Infantes and J. Vanier, Rev. Sci. Instrum., 42, 26 (1971).
- [46] J.D. Idoine, Jr. and J.R. Brandenberger, Rev. Sci. Instrum., 42, 715 (1971).
- [47] J. Lee and S.H. Choh, Rev. Sci. Instrum., 53, 232 (1982).
- [48] N.J. Hopkins, Rev. Sci. Instrum., 20, 401 (1949).
- [49] R. Livingston and H. Zeldas, J. Chem. Phys., 26, 351 (1957).
- [50] P. Kesserling and M. Gautshi, J. Sci. Instrum., 44, 911 (1967).
- [51] T.C. Wang, Phys. Rev., 99, 566 (1955).
- [52] Dinesh, Ph.D. Thesis, Indian Institute of Technology, Kanpur, India (1967).

- [53] P. Butcher, J.A.S. Smith and C.J. Turner, J. Phys. E: Sci. Instrum., 12, 484 (1979).
- [54] J.A.S. Smith, J. Chem. Education, 48, 39 (1971); 48, A77 (1971); 48, A149 (1971); 48, A243 (1971).
- [55] J.G. Graybeal and C.D. Cornwell, J. Phys. Chem., 62, 483 (1958).
- [56] D.A. Tong, J. Phys. E: Sci. Instrum., 1, 1153 (1968).
- [57] M. Read, in "Advances in NQR," Vol. 1, Ed. J.A. S. Smith, Heyden & Son, London (1974), p. 203.
- [58] V. Harihara Subramanian, P.T. Narasimhan and K.R. Srivatsan, J. Phys. E: Sci. Instrum., 14, 870 (1981).
- [59] F.N.H. Robinson, J. Phys. E: Sci. Instrum., 15, 814 (1982); 15, 1093 (1982).
- [60] D. Geizendanner, R. Lenk and G. Litzistorf, J. Phys. E: Sci. Instrum., 8, 8 (1975).
- [61] G.L. Petersen and T. Oja, in "Advances in Nuclear Quadrupole Resonance," Vol. 1, Ed. J.A.S. Smith, Heyden and Son, London (1974), p. 179.
- [62] R. Lenk and E.A.C. Lucken, Chem. Phys. Lett., 21, 552 (1973).
- [63] R. Lenk and E.A.C. Lucken, Pure and Appl. Chem., 40, 199 (1974).
- [64] A.A.V. Gibson, J.R. Brookeman and T.A. Scott, Phys. Lett., 50A, 31 (1974).
- [65] A. Colligiani and G. Ambrosetti, Gazz. Chim. Ital., 106, 439 (1976); J. Magn. Reson., 32, 93 (1978).
- [66] U. Henriksson, L. Ödberg, J.C. Eriksson and L. Westman, J. Phys. Chem., 81, 76 (1977).

- [67] M. Mackowiak and J.R. Brookeman, *Acta Phys. Polonica*, 52A, 281 (1977).
- [68] R. Ramachandran and P.T.Narasimhan, *J. Phys. E: Sci. Instrum.*, 16, 643 (1983).
- [69] A. Bielecki, D.B. Zax, A.M. Thayer, J.M. Miller and A. Pines, *Z. Naturforsch.*, 41a, 440 (1986) and references cited therein.
- [70] B. Herzog and E.L. Hahn, *Phys. Rev.*, 103, 148 (1956).
- [71] M. Emshwiller, E.L. Hahn and D. Kaplan, *Phys. Rev.*, 118, 414 (1960).
- [72] S.R. Hartmann and E.L. Hahn, *Phys. Rev.*, 128, 2042 (1962).
- [73] R.E. Slusher and E.L. Hahn, *Phys. Rev.*, 166, 332 (1968).
- [74] E.R. Jones and S.R. Hartmann, *Phys. Rev. Lett.*, 22, 867 (1969); *Phys. Rev.*, 6B, 757 (1972).
- [75] D.T. Edmonds, M.J. Hunt, A.L. Mackay and C.P. Summers, in "Advances in Nuclear Quadrupole Resonance," Vol. 1, Ed. J.A.S. Smith, Heyden and Son, London (1974), p. 145.
- [76] P.S. Ireland and T.L. Brown, *J. Magn. Reson.*, 20, 300 (1975).
- [77] D.T. Edmonds and J.P.G. Mailer, *J. Magn. Reson.*, 26, 93 (1977).
- [78] S.G.P. Brosnan and D.T. Edmonds, *J. Magn. Reson.*, 38, 47 (1980); 45, 490 (1981).
- [79] R. Blinc, in "Advances in Nuclear Quadrupole Resonance," Vol. 2, Ed. J.A.S. Smith, Heyden and Son, London (1975), p. 71.
- [80] D.T. Edmonds, *Phys. Rep.*, 29C, 234 (1977).
- [81] J.L. Ragle and G.L. Minott III, in "Advances in Nuclear Quadrupole Resonance," Vol. 3, Ed. J.A.S. Smith, Heyden and Son, London (1978), p. 205.

- [82] I.J.F. Poplett, in "Advances in Nuclear Quadrupole Resonance," Vol. 4, Ed. J.A.S. Smith, Heyden and Son, London (1980), p. 115.
- [83] D.T. Edmonds, Bull. Magn. Reson., 3, 53 (1981).
- [84] A.G. Redfield, W. Fite and H.E. Bleich, Rev. Sci. Instrum., 39, 710 (1968).
- [85] G.W. Leppelmeier and E.L. Hahn, Phys. Rev., 141, 724 (1966).
- [86] M. Goldman, "Spin Temperature and Nuclear Magnetic Resonance in Solids," Chapter 7, Oxford University Press, London (1970).
- [87] N. Weiden, J.J. Breit and A. Weiss, J. Molec. Struct., 58, 43 (1980).
- [88] N. Weiden and A. Weiss, J. Magn. Reson., 30, 403 (1978).
- [89] N. Weiden and A. Weiss, Faraday Symp., 13, 93 (1979).
- [90] R. Ramachandran and P.T. Narasimhan, J. Magn. Reson., 51, 67 (1983).
- [91] Y. Hsieh, J.C. Koo and E.L. Hahn, Chem. Phys. Lett., 13, 563 (1972).
- [92] I.J.F. Poplett and J.A.S. Smith, J. Chem. Soc., Faraday Trans. II, 77, 1155 (1981).
- [93] I.J.F. Poplett and J.A.S. Smith, J. Chem. Soc., Faraday Trans. II, 75, 1703 (1979).
- [94] I.J.F. Poplett, J. Magn. Reson., 44, 488 (1981).
- [95] I.J.F. Poplett, J. Magn. Reson., 50, 382 (1982).
- [96] I.J.F. Poplett, J. Magn. Reson., 50, 397 (1982).
- [97] I.J.F. Poplett and J.A.S. Smith, J. Chem. Soc., Faraday Trans. II, 77, 235 (1981).

- [98] H. Budak, M.L.S. Garcia, I.C. Ewart, I.J.F. Poplett and J.A.S. Smith, *J. Magn. Reson.*, 35, 309 (1979).
- [99] See reference no. 82 and the references cited therein.
- [100] A. Gough, M.M.I. Haq and J.A.S. Smith, *Chem. Phys. Lett.*, 117, 389 (1985).
- [101] D.T. Edmonds and J.P.G. Mailer, *J. Magn. Reson.*, 36, 411 (1979).
- [102] S.G.P. Brosnan and D.T. Edmonds, *J. Molec. Struct.*, 58, 23 (1980).
- [103] C.P. Cheng and T.L. Brown, *J. Amer. Chem. Soc.*, 101, 2327 (1979); *Symp. Faraday Soc.*, 13, 75 (1979); *J. Amer. Chem. Soc.*, 102, 6418 (1980).
- [104] D.A. Avignon and T.L. Brown, *Inorg. Chem.*, 21, 3041 (1982) and references therein.
- [105] A. Lötzt and J. Voightländer, *J. Magn. Reson.*, 48, 1 (1982).
- [106] R. Kado, Y. Takarada and H. Hatanaka, *Phys. Lett.*, 47A, 49 (1974).
- [107] R. Kado and Y. Takarada, *J. Magn. Reson.*, 32, 89 (1978).
- [108] A. Lötzt, J. Voightländer, D. Stephenson and J.A.S. Smith, *Z. Naturforsch.*, 41a, 200 (1986) and references therein.
- [109] A. Lötzt, J. Voightländer and J.A.S. Smith, *Z. Naturforsch.*, 41a, 206 (1986).
- [110] N. Weiden and Al. Weiss, *J. Magn. Reson.*, 20, 334 (1975).
- [111] P.S. Ireland and T.L. Brown, *J. Magn. Reson.*, 20, 300 (1975).
- [112] O. Lumpkin, *J. Chem. Phys.*, 62, 3281 (1975).
- [113] A. Lötzt and J. Voightländer, *J. Phys. E: Sci. Instrum.*, 11, 1179 (1978).
- [114] A. Ader and M. Shporer, *J. Magn. Reson.*, 47, 483 (1982).

- [115] D. Giesendanner, S. Sengupta and G. Litzistorf, *J. Molec. Struct.*, 58, 519 (1980).
- [116] M. Gourdji and A. Peneau, *J. Molec. Struct.*, 83, 361 (1982).
- [117] Narsimha Reddy, Arun Bhavsar and P.T. Narasimhan, *Z. Naturforsch.*, 41a, 449 (1986).
- [118] U. Haeberlen, "High Resolution NMR in Solids: Selective Averaging" Supplement 1 to *Advances in Magnetic Resonance*, Ed. J.S. Waugh, Academic Press, New York (1976).
- [119] G.E. Pake, in "Solid State Physics," Vol. 2, Ed. R. Seitz and D. Turnbull, Academic Press, New York (1956), p. 24.
- [120] G.E. Pake, *J. Chem. Phys.*, 16, 327 (1948).
- [121] D.T. Edmonds, M.J. Hunt and A.L. Mackay, *J. Magn. Reson.*, 9, 66 (1973).
- [122] N.F. Ramsey, *Phys. Rev.*, 91, 303 (1953).
- [123] H.M. McConnell, *J. Chem. Phys.*, 24, 460 (1956).
- [124] N.E. Ainbinder and I.G. Shaposhnikov, in "Advances in Nuclear Quadrupole Resonance," Vol. 3, Ed. J.A.S. Smith, Heyden and Son, London (1978), p. 101.
- [125] S. Kojima and K. Tsukada, *J. Phys. Soc. Japan*, 10, 591 (1955).
- [126] R. Livingston, *J. Phys. Chem.*, 57, 496 (1953).
- [127] G.D. Watkins and R.M. Walkev, *Bull. Am. Phys. Soc.*, 1, 11 (1956).
- [128] T. Itoh and K. Kembe, *J. Phys. Soc. Japan*, 12, 763 (1957).
- [129] G.D. Watkins and R.V. Pound, *Phys. Rev.*, 85, 1062 (1952).
- [130] H.C. Meal and H. Allen Jr., *Phys. Rev.*, 90, 348 (1953).
- [131] C. Dean, *J. Chem. Phys.*, 23, 1734 (1955).

- [132] Y. Imaeda, J. Sci. Hiroshima Univ., 24, 239 (1960).
- [133] H. Bayer, Z. Physik, 130, 227 (1951).
- [134] D.E. Woessner and H.S. Gutowsky, J. Chem. Phys., 39, 440 (1963).
- [135] M.J. Weber, J. Phys. Chem. Solids, 17, 267 (1961).
- [136] E.A.C. Lucken, "Nuclear Quadrupole Coupling Constants," Academic Press, New York (1969).
- [137] E.A.C. Lucken in "Advances in Nuclear Quadrupole Resonance," Vol. 1, Ed. J.A.S. Smith, Heyden and Son, London (1974), p. 235.
- [138] Al. Weiss in "Advances in Nuclear Quadrupole Resonance," Ed. J.A.S. Smith, Heyden and Son, London (1974), p. 1.
- [139] L. Ramakrishna, S. Soundararajan, V.S.S. Sastry and J. Ramakrishna, Coord. Chem. Rev., 22, 123 (1977).
- [140] K.V.S. Rama Rao and S. Rama Prabhu, Phys. Stat. Sol(a), 93, 17 (1986).
- [141] R. Moccia and M. Zandomeneghi, "Advances in Nuclear Quadrupole Resonance," Vol. 2, Ed. J.A.S. Smith, Heyden and Son, London (1975), p. 135, and references therein.
- [142] L.C. Snyder and H. Basch, "Molecular Wave Functions and Properties," Wiley-Interscience (1972) and references therein.
- [143] M.H. Palmer, Z. Naturforsch., 41a, 147 (1986) and references therein.
- [144] J.C. Browne and F.A. Matsen, Phys. Rev., 135, 1227 (1964).
- [145] P. Grigolini and R. Maccia, J. Chem. Phys., 57, 1369 (1972).
- [146] M.H. Palmer, D. Stephenson and J.A.S. Smith, Chem. Phys., 97, 103 (1985).



- [147] C.H. Townes and B.P. Dailey, J. Chem. Phys., 17, 1782 (1949).
- [148] R.M. Sternheimer, Phys. Rev., 80, 102 (1950); 95, 736 (1954) and references therein.
- [149] K.D. Sen and P.T. Narasimhan, in "Advances in Nuclear Quadrupole Resonance," Vol. 1, Ed. J.A.S. Smith, Heyden and Son, London (1974), p. 277.
- [150] F.A. Cotton and C.B. Harris, Proc. Natl. Acad. Sci. USA, 56, 21 (1966).
- [151] J.M. Sichel and M.A. Whitehead, Theor. Chim. Acta, 11, 220 (1968).
- [152] W.D. White and R.S. Drago, J. Chem. Phys., 52, 4717 (1970).
- [153] E.A.C. Lucken, "Topics in Current Chemistry," Vol. 30, Springer Verlag, Berlin (1972), p. 155.
- [154] M.J.S. Dewar, H.W. Kollman and H.O. Suck, J. Amer. Chem. Soc., 97, 5590 (1975).
- [155] J.E. Bloor and Z.B. Maksic, in "Proceedings of the Second International Symposium on NQR Spectroscopy," Ed. A. Colligiani, A. Vallerini Publishers, Pisa, Italy (1975), p. 1.
- [156] M. Barfield, H.P.W. Gottlieb and D.M. Doddrell, J. Chem. Phys., 69, 4504 (1978).
- [157] P.P. Thankachan and P.T. Narasimhan, J. Molec. Struct., 83, 289 (1982).
- [158] P.J. Bray and S.G. Greenbaum, J. Molec. Struct., 83, 35 (1982) and references therein.
- [159] R. Bersohn, J. Chem. Phys., 22, 2078 (1954).
- [160] G.K. Semin, T.A. Babushkina, and G.G. Yakobson, in "Nuclear Quadrupole Resonance in Chemistry," translated from Russian by A. Barauch, Ed. A.J. Pick, John Wiley and Sons, New York (1975).

- [161] W. Fichtner and Al. Weiss, Z. Naturforsch., 31b, 1626 (1976).
- [162] R. Livingston, Phys. Rev., A82, 289 (1951).
- [163] R. Livingston and H. Zeldas, Phys. Rev., 90, 609 (1953).
- [164] M. Bloom, Phys. Rev., 94, 1996 (1954).
- [165] H.S. Gutowsky and D.W. McCall, J. Chem. Phys., 32, 548 (1960).
- [166] V. Ramakrishna, D. Krishna Rao, G. Satyanandam and C.R.K. Murthy, Acta Phys. Polon., A63, 833 (1983).
- [167] T. Kushida, G.B. Benedek and N. Bloembergen, Phys. Rev., 104, 364 (1956).
- [168] Sasane, D. Nakamura and M. Kubo, J. Magn. Reson., 8, 179 (1972).
- [169] T.L. Brown and L.G. Kent, J. Phys. Chem., 74, 3572 (1970).
- [170] R.L. Armstrong and G.L. Baker, Can. J. Phys., 48, 2411 (1970).
- [171] T.B. Brill and G.C. Long, J. Phys. Chem., 75, 1898 (1971).
- [172] R.L. Armstrong and H.M. Van Driel, in "Advances in Nuclear Quadrupole Resonance," Vol. 2, Ed. J.A.S. Smith, Heyden and Son, London (1975), p. 179.
- [173] D. Rupp and E.A.C. Lucken, Z. Naturforsch., 41a, 208 (1986).
- [174] D. Nakamura, R. Ikeda and M. Kubo, Coord. Chem. Rev., 17, 281 (1975).
- [175] D.B. Utton and J.B. Vannier, Instrum. Technol., 23, 47 (1976).
- [176] A. Ohte and H. Iwakawa, IEEE Trans. Instrum. Meas., 1M25, 357 (1976).

- [177] V.P. Anferov, O.N. Bryuchanov, V.S. Grechishkin and T.N. Rudakov, J. Molec. Struct., 83, 365 (1982) and references therein.
- [178] G.C. Gillies and R.J.C. Brown, Can. J. Chem., 54, 2266 (1976).
- [179] R.L. Armstrong, G.L. Baker and H.M. Van Driel, Phys. Rev., B3, 3072 (1971).
- [180] G.C. Gillies and R.J.C. Brown, Can. J. Chem., 50, 2586 (1972).
- [181] T.B. Brill, J. Chem. Phys., 61, 424 (1974).
- [182] J.A.S. Smith in "Proceedings of the Second International Symposium on NQR Spectroscopy (1973)," Ed. A. Colligiani, A. Vallerini Publisher, Pisa, Italy (1975), p. 293.
- [183] R.J.C. Brown and S. Segal, J. Phys. F, 5, 1073 (1975).
- [184] R.J.C. Brown, J.G. Smeltzer and R.D. Heyding, J. Magn. Reson., 24, 269 (1976).
- [185] M. Mackowiak, M.Z. Fraczek, P. Koziol, J. Stankowski and Al. Weiss, Z. Naturforsch., 41a, 290 (1986).
- [186] G.W. Leppelmeier and E.L. Hahn, Phys. Rev., 142, 179 (1966).
- [187] K. Mano, D. Giezendanner, S. Sengupta and E.A.C. Lucken, J. Molec. Struct., 58, 221 (1980).
- [188] D. Giezendanner, S. Sengupta and E.A.C. Lucken, J. Molec. Struct., 58, 229 (1980).
- [189] S. Sengupta, G. Litzistorf and E.A.C. Lucken, J. Magn. Reson., 42, 45 (1981).
- [190] G. Litzistorf, S. Sengupta and E.A.C. Lucken, J. Molec. Struct., 83, 285 (1982).
- [191] K. Mano, S. Sengupta, E.A.C. Lucken and G. Litzistorf, J. Molec. Struct., 96, 173 (1982).

- [192] K. Mano, S. Sengupta, G. Litzistorf and E.A.C. Lucken, J. Molec. Struct., 98, 89 (1983).
- [193] K. Mano, S. Sengupta, G. Litzistorf and E.A.C. Lucken, J. Molec. Struct., 111, 287 (1983).
- [194] R. Ambrosetti, R. Angelone and A. Colligiani, Phys. Rev., B15, 4318 (1977).
- [195] R.R. Hewitt and B.F. Williams, Phys. Rev., 129, 1188 (1963).
- [196] Dinesh and J.A.S. Smith, "Proceedings of the Second International Symposium on NQR Spectroscopy," (1973), Ed. A. Colligiani, A. Vallerini Publisher, Pisa, Italy (1975).
- [197] S.L. Segal, J. Chem. Phys., 69, 2434 (1978).
- [198] H. Gotcu, J. Magn. Reson., 54, 36 (1983).
- [199] T.J. (T.C.) Wang, J. Magn. Reson., 64, 194 (1985).
- [200] E.B. Doering and J.S. Waugh, J. Chem. Phys., 85, 1753 (1986).
- [201] "Advances in Nuclear Quadrupole Resonance," Vol. 1, Ed. J.A.S. Smith, Heyden and Son, London (1974).
- [202] "Proceedings of the Second International Symposium on NQR Spectroscopy (1973)," Ed. A. Colligiani, A. Vallerini Publisher, Pisa, Italy (1975).
- [203] R. Ramachandran and P.T. Narasimhan, Molec. Phys., 48, 267 (1983).

## CHAPTER II

### AUTOMATION AND CONTROL OF A PULSED NQR SPECTROMETER USING A MICROPROCESSOR

This chapter deals with, (i) automation and control of a pulsed NQR spectrometer using a microprocessor, (ii) generation of various pulse sequences by the microprocessor, and (iii) incorporation of signal averaging, processing and Fourier transform facilities using a signal analyzer.

Section II.A is devoted to a review on performance requirements, automation and control of pulsed NQR spectrometers. Details of the present microprocessor-controlled pulsed NQR spectrometer are outlined in section II.B and section II.C gives the hardware details of the microprocessor system. Software developed for the generation of various pulse sequences is described in section II.D, while section II.E deals with the automation of various pulsed NQR experiments. The chapter concludes with section II.F which presents capabilities and performance evaluation of the present spectrometer system.

## II.A AUTOMATION AND CONTROL OF PULSED NQR SPECTROMETERS: GENERAL BACKGROUND

### II.A(1) Introduction

The aim of this section is to survey briefly the literature related to automation and control of pulsed NQR spectrometers and to indicate the specific requirements for each subsystem of the spectrometer.

NQR signals are often very weak and broad. Their observation requires pulse techniques where signal-to-noise ratio can

be conveniently improved by coherently averaging the transient signals. The spin echo method of Hahn [1] has been successfully adapted to NQR spectroscopy [2,3]. There have been a large number of modifications on the original spin echo experiment and these involve variations in the amplitude, phase, duration, separation and number of the r.f. pulses employed. Multiple pulse and double resonance investigations are amongst some of these experiments. The task of performing all these varieties of experiments with ease and also employing signal averaging techniques, Fourier transforming of time domain signals to frequency domain etc, are some of the many reasons for automating pulsed NQR spectrometers.

It is common practice that a researcher working in NQR designs and constructs his own spectrometer depending upon the frequency range of interest. Such home-built systems generally suffer from a dependence on manual operation which is not only tedious but also lacks precision and reproducibility. Interfacing these instruments to mini-computers/microprocessors can greatly enhance their performance and reduce the time required for carrying out the experiments.

The main functions demanded of such an automated system are:

- i) Generation of simple as well as complex pulse sequences.
- ii) Control and automatic adjustment of parameters like pulse width, pulse separation, frequency, phase, probe damping etc.

- iii) Acquisition, time averaging and processing of signals.
- iv) Automatic processing of data in various complex experiments.

We may point out at this juncture that the main components of a pulsed NQR spectrometer are essentially same as that of a high-power variable frequency solid-state pulsed NMR spectrometer, except for the magnet.

Block diagram of a typical pulsed NQR spectrometer system is shown in Fig. II.1. The main functions of various components of the system can be described as follows:

R.f. from a stable oscillator is fed to a phase shifting device to obtain r.f. of desired phases. These are gated in the gating scheme with the help of logic pulses from the pulse generator. It should be noted here that the pulse generator may be a hard-wired one or one which is controlled by a Computer. Computer interface to the spectrometer is shown with dashed lines in the block diagram of Fig. II.1. The r.f. pulse sequence with desired relative phases from the gate system is amplified and coupled to the sample coil of the probe assembly. The NQR signal induced in the sample coil as a response to the applied pulse sequence is received and detected by the receiver system. The detected NQR signals can either be displayed on an oscilloscope for the visual observation or be recorded through a boxcar integrator. In the case of spectrometers with signal averager/computer interfaced to it the NQR signals can be averaged, stored and processed further.



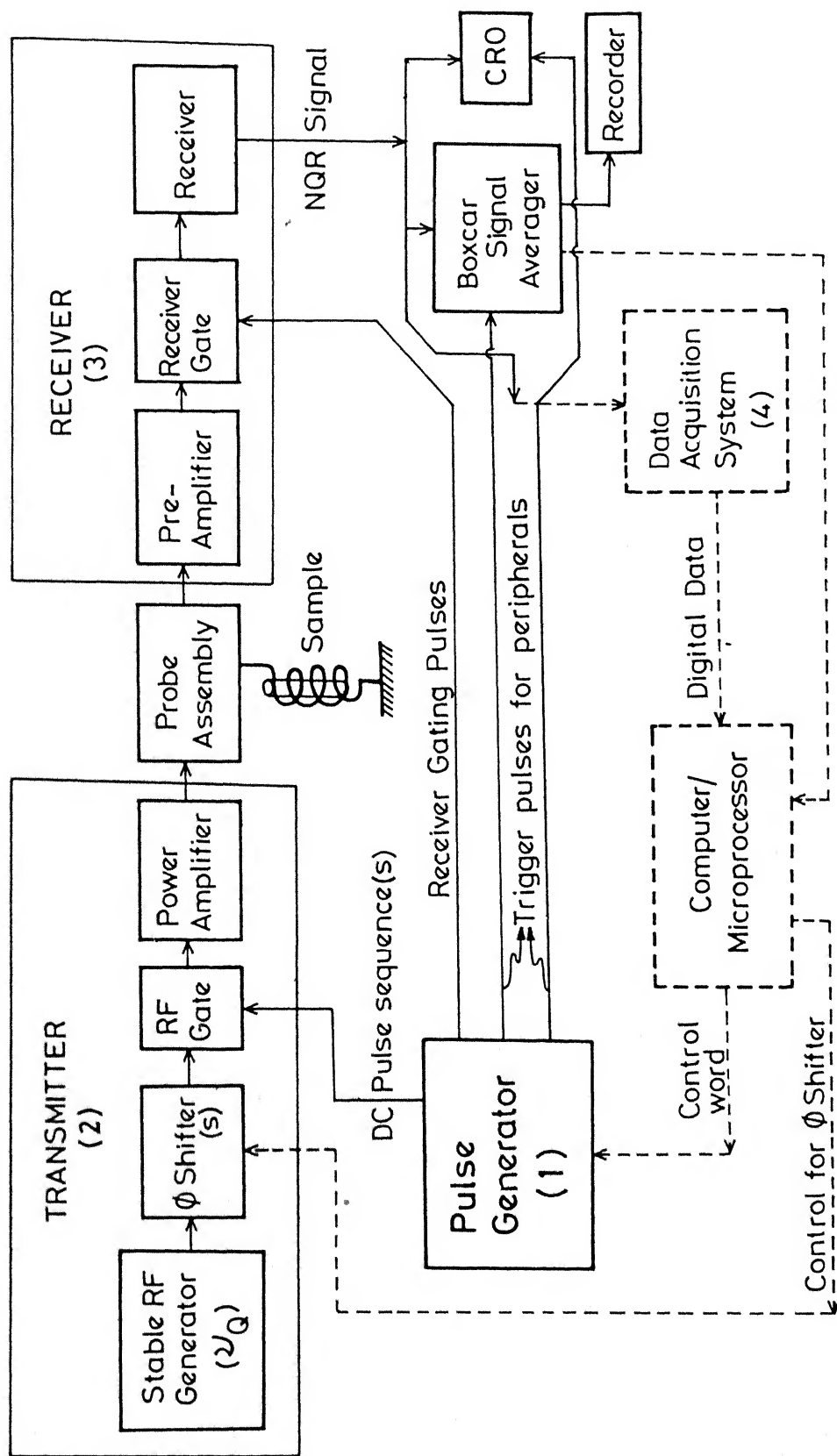


Fig. 11.1 Block Diagram of a pulsed NQR Spectrometer System (The computer interfacing is shown in dashed lines)

In what follows, we shall review some features of the main units that form part of an automated NQR system, keeping in mind that some of these are also common for NMR systems. For the generation of the pulse sequences one needs a pulse programmer which gates the transmitter and receiver. The pulse programmer is also used to control data acquisition and trigger various other peripherals. After a review of the various types of pulse programmers described in the literature, we shall deal with transmitter and receiver details. This will be followed by a discussion of the methodology of data acquisition and spectrometer automation.

#### II.A(2) Pulse Programmers

The central control unit of a pulsed spectrometer is the pulse programmer (pulse generator). A versatile pulse programmer greatly enhances the range of experiments which can be performed by the spectrometer. The pulse programmer should therefore be capable of generating a large variety of pulse sequences, ranging from single pulse to complicated multiple pulse sequences used in line narrowing experiments. The pulse programmer should also be flexible enough to quickly change the pulse sequence and to incorporate new pulse sequences. An ideal way of achieving such a flexibility is to use computer/microprocessor to control pulse sequence generator.

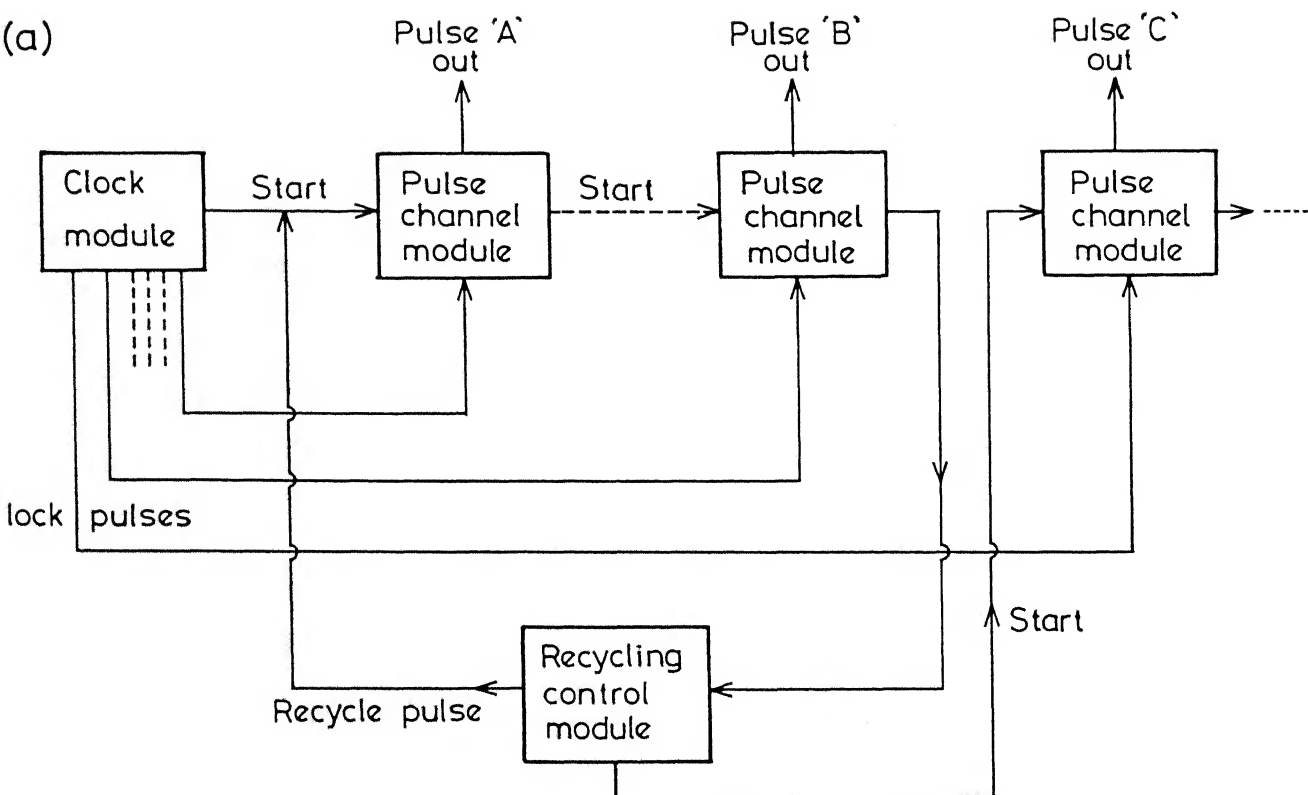
There have been a large number of publications describing pulse programmers of varying levels of sophistication. A review

article by Geiger and Holz [4] gives a detailed account of pulse programmers and their control. Different types of pulse programmers may be divided broadly into

- i) hardware pulse programmers,
- ii) hardware pulse programmers with software control,
- iii) pure software pulse programmers.

In the hardware pulse programmers we have again two types, namely, (a) single purpose rigid hardware pulse programmers, and (b) flexible hardware pulse programmers with hardware control. As we are concerned with automation of spectrometer systems, single purpose hardware pulse generators are not of much interest to us here. However, the ideas involved in some of the flexible hardware pulse programmers with hardware control will be considered, because these ideas help in understanding the concepts involved in software controlled pulse programmers. Three types of basic modules are used in flexible hardware pulse generators (Fig. II.2(a)). These are (i) clock module, (ii) single pulse channel modules (or counter modules) and (iii) recycling control modules. The clock module provides clock pulses to various pulse channel modules and starts pulse sequences. Each pulse channel module generates a gating pulse for the transmitter, then a start pulse is sent to the next module after a required amount of delay. The gating pulse width may be controlled by using monostable multi-vibrator or digitally by using high frequency counters. These modules can therefore be thought of as consisting of two simple counter modules, one counting the pulse width, the other

(a)



(b)

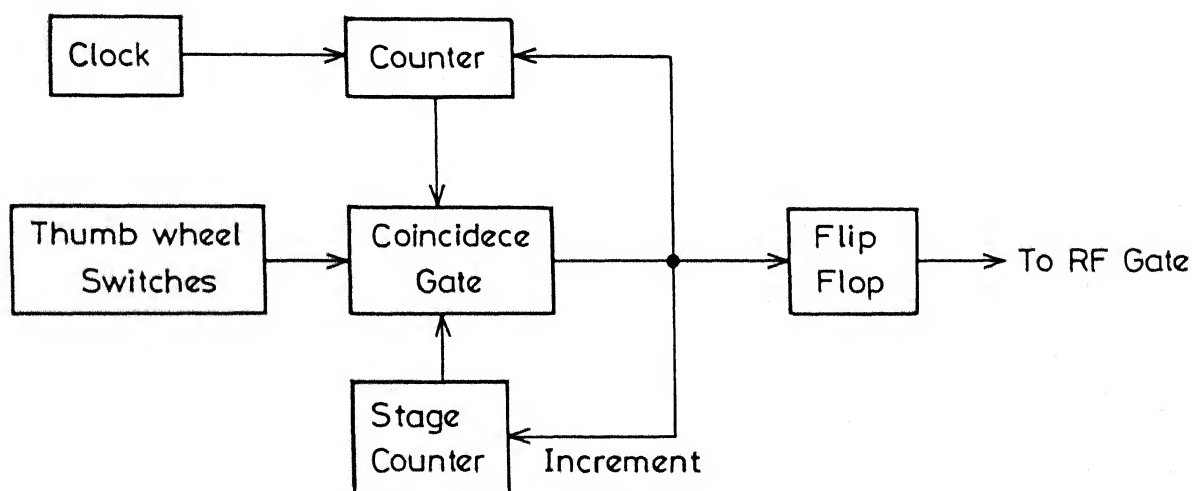


Fig. II.2 Block diagrams of flexible hardware pulse generators: (a) Using a cascade of pulse channel modules, (b) Using hardware control circuitry.

the delay time. This concept was pursued for the first time by Lalanne and Eletr [5], and later modified by Lind [6] and Adduci et al. [7]. The recycling control module recycles the output of any channel to trigger the previous channel a preselected number of times. Thus, repetitive pulse sub-groups may be generated.

Another way of designing a flexible hardware pulse generator was described by Ellett et al [8] and Shenoy et al. [9]. Shenoy et al. have used only one counter to produce all delays and pulse widths. Five sets of thumbwheel switches allow the preselection of three pulse widths and two delay times. The setting of these thumbwheel switches is compared with the actual counter reading by a coincidence circuit. The selection of the actual thumbwheel switch is done by a 'stage counter' according to the desired pulse program (Fig. II.2(b)). Different pulse sequences are produced by using different 'logic circuits' which are selected by the thumbwheel switch reading. The pulse programmer described by Ellett et al. [8] was different from this in one aspect that these authors have used plug-in cards to select different pulse sequences.

The hardware pulse programmers with software control can now be understood as follows:

The thumbwheel switch setting is replaced by data stored in a memory or an internal register of a microprocessor/mini-computer. The selection logic under 'stage counter' and control is transformed

to program instructions read under program counter control. The realization of new pulse sequences is thus essentially reduced to a software problem. This kind of pulse programmer is organized like a central processor of a computer. There will be essentially three main components: the memory unit, the control logic circuitry and the address counter. In the memory, data and instructions are stored, which are needed to produce pulse sequences. The control logic circuitry decodes bit patterns read from the memory and accordingly selects pulse and trigger channels, produces pulse widths and delay times etc. The address circuitry provides the address of the next memory word to be treated. Programmable pulse programmers are described by Ellett et al. [8] and Matson [10]. In these designs pulse widths and also partly delay times are produced using manually set monoflops for continuous pulse width adjustment. In recent designs pulse widths are produced digitally using very high frequency counters enabling fine adjustment. In this case the control words in the memory specify the logic levels of the output channels and the time during which this state will remain unchanged, before the next control word to be executed, which specifies the new state of the output channels. This concept is also realized in commercially available [11] timing simulators (TS). Karlicek and Lowe [12] described the use of this device (TS) in a broad band pulsed NMR spectrometer. Bruker Spectrospin AG [13] also used this method in CXP-spectrometer series. Whereas the TS used by Karlicek et al., allows only sequential execution of the memory

contents, the CXP pulse generator allows address modification to execute programmed jumps. There are other software controlled hardware pulse generators such as that described by Lapray et al. [14] where only the timing data is stored in the memory and a hard wired program logic selects the required pulse sequence. In contrast to this Toms [15] stores only level and address jump information in a shift register memory that circulates constantly and established in this way the time intervals. Caron and Herzog [16] described a programmable timer which works in a similar way to the TS mentioned above, but also allows sub-burst generation by looping.

So far we have considered hardware pulse generators controlled by computer software; coming to the pure software pulse generators Wright and Rogers [17] and Huang and Rogers [18] described systems where pulse sequences are totally produced by the computer without any hardware circuit. In these designs the basis of the timing clock is the definite execution time of the software instructions and thus the time intervals are produced by software counters. In pure software pulse generators some of the output lines of the computer are used to output logic levels whose duration can be changed by appropriate software program (software counters). In some of the applications where continuous variation of pulses is required, the logic levels produced by the computer are used to trigger monostable multivibrators. The length of each monostable pulse is varied manually to form

$90^\circ$  or  $180^\circ$  pulses. This method (pure software pulse generation) is relatively easier to implement but puts a considerable load on the CPU. Software pulse generators are also used in the systems described by Geiger and Hertz [19] where the time base to produce proper intervals between gating pulses is given by hardware interrupts of the programmable computer clock rather than by the execution time of software instructions. Pulse width is controlled directly through the computer by using a digital counter with multiplexed output. Pure software pulse generators can be implemented at a low cost using microprocessors with sufficient number of I/O lines [20].

Finally, it should be noted that in the field of pulse sequence generation the most promising line of development is the use of flexible hardware pulse generators operating under software control. In such designs controlling the pulse sequence generator is only part of the main functions of the computer and the computer will be available for other purposes as well. However, in the case of pure software pulse generators the computer is completely occupied with the job of pulse sequence generation. For example, in the systems described by Ellett et al. [8] and in the Bruker CXP-series spectrometers the computer controls the whole spectrometer apart from controlling the pulse generator. Here again, we mention that a convenient and inexpensive version is the use of microprocessor [12] to control the time interval settings (via latched BCD lines) in a commercial multipulse generator. Ader et al. [21] have used the microprocessor which



supervises a programmable clock and the data acquisition module. Thus microprocessor provides a relatively inexpensive alternative to the dedicated computer approach and at the same time provides all the computing power necessary to implement a stand alone computer-based system. Extended pulse programmer functions such as autoincrementation of pulse spacings [20,22] can be easily performed using the microprocessor software. A multitude of commonly used pulse sequence programs can be stored in read-only memory (ROM) of the microprocessor for instant access or alternately, any desired new pulse sequence can be quickly created at the console key-board.

It is pertinent to mention at this point that a versatile pulse programmer based on two LSI timer chips [Advanced Micro-Devices, Am 9513 System Timing Controller (STC)] controlled by a 16-bit microcomputer is described by H.S. Jalmes et al. [23]. Am 9513 timer has 5 independent programmable counters which can be programmed to count either in binary or in BCD and can be reloaded automatically from a load or hold register. It also allows dynamic reconfiguration and has a maximum counting frequency of 7 MHz. These properties of the timer makes the pulse programmer flexible with good pulse width resolution. Mohr et al. [24] demonstrated an elegant way of controlling a versatile pulse sequence generator (PSG) using an Apple II computer. The Apple II computer available with them was engaged in controlling the whole experimental apparatus. Therefore, the important requirement for their pulse sequence generator was that it operates with a

minimum of computer supervision. They have used Am 9513 counter/timer chips and high speed TTL counters (74F190) as fast timers, and have come up with a design where all the operating parameters input to the pulse sequence generator from the computer are latched for later use. This minimized the dependence of the pulse sequence generator upon the computer. In their system, the computer can even be turned off once the pulse sequence generator is programmed and is operating. Use of the Am 9513 counter/timer chips in their design gave the pulse sequence generator, the ability to generate any complex pulse sequence. Also they have achieved a pulse duration resolution of 20 ns by the use of high speed counters.

Finally we mention that the use of a 16-bit microprocessor [25] with good computing facility in this kind of a design makes the system more simple and cost-effective.

## II.A(3) Transmitter

In this sub-section we consider r.f. source, phase shifters for producing different relative phases, r.f. gates and power amplifier.

Nuclear quadrupole resonance frequencies of a given nucleus (for example  $^{35}\text{Cl}$ ) vary over a broad frequency range. Radio frequency source used in NQR spectrometers must therefore be a crystal oscillator or a synthesizer with a wide frequency coverage. The r.f. gating schemes should also be able to give

good on off ratio. Even a small continuous wave signal leak through the gate is not desirable, because this signal will get amplified in the power amplifier and reach the receiver which might get saturated. The power amplifier must be capable of delivering high-power r.f. pulses with very short rise and fall times with a minimum power droop in the r.f. pulse.

Instabilities of the transmitter during multiple-pulse sequences consisting of many pulses with relative phase differences is quite well known. This problem could be reduced by synchronization of pulse programmer clock and transmitter r.f. In fixed frequency spectrometers synchronization of pulse programmer clock and the r.f. source can be done by using a quartz controlled oscillator both as clock source for the pulse programmer as well as the r.f. source [26].

Variable frequency spectrometers with a synthesizer as r.f. source can be completely synchronized to a master quartz oscillator which can also serve as the computer/microprocessor clock [12]. The main advantage of the coherent spectrometer operation is phase stability and stability of the effective r.f. pulse length [27].

A sophisticated pulsed spectrometer should be able to deliver transmitter r.f. pulses with  $0^\circ$ ,  $90^\circ$ ,  $180^\circ$  and  $270^\circ$  phase difference. Commercially available variable delay lines can be used to produce these phases. This method is not convenient for variable frequency operation. The automatic generation of the

## IIA(4) Receiver

A receiver with high gain and fast recovery after an intense r.f. pulse is very much essential for high power solid state NMR and NQR spectrometers. Therefore, besides the probe damping, automatic receiver blocking schemes have been developed to minimize the recovery time following the overload by the r.f. pulse [12, 35-38]. Karlicek and Lowe[12] have modified HP-model 10534A double balanced mixers [39] using 1N914B diodes, and used them as blocking gates which gave a good isolation of the transmitter from the receiver and achieved a recovery time as low as  $0.5 \mu\text{s}$  at 60 MHz. The blocking signal for the receiver is provided by the pulse programmer. They have carefully matched the diodes used in the construction of the gates in order to avoid gating pedestals and large switching transients.

Adduci et al.[40] have described a fast-recovery receiver using commercially available amplifier stages having nonsaturating overload characteristics and achieved a recovery time of 250 nsec for short transmitter pulses which increases to  $2 \mu\text{sec}$  for relatively long ( $75 \mu\text{sec}$ ) transmitter pulses. Stoll [41] has constructed a receiver based on commercially available units but with passive voltage limiters placed before each stage and achieved a  $2.35 \mu\text{sec}$  with a high Q resonant sample probe. The recovery time of this receiver did not depend on the length of transmitter pulse and has been measured to be same for 100 msec long pulses.

## II.A(5) Data Acquisition and Spectrometer Automation

In digital data acquisition it is required to satisfy the sampling theorem known as Nyquist theorem [42]. According to

this theorem recording of a spectrum unambiguously with frequencies as high as  $\nu$  is possible only if the transient signal is sampled at a rate of at least  $2\nu$ . High sampling rates are required in NQR as the resonance lines are generally wide. Dynamic range which is determined by resolution of the digitizer must be large. In other words, the digitizer resolution must be adequate to accommodate the most intense signal of the transient and also be able to resolve the smallest signal present (The word "resolution" here means resolution in amplitude not frequency).

Digital data acquisition is a general task in laboratory automation. Problems concerning the choice of appropriate sampling rates and the required resolution of analog to digital conversion are treated in monographs and periodicals [42-44]. For the purpose of data acquisition time averagers were used extensively for a long time. These are hard-wired special purpose minicomputers available in various commercial designs which include an ADC, an arithmetic unit to add successive signals for signal-to-noise ratio improvement, a memory to store these signals in a digital form and output capabilities. Another device which is useful when very fast signals have to be digitized and which is appropriate in connection with the use of a minicomputer, is the 'transient recorder'. Very fast conversion rates of upto 500 MHz are realized. These transient recorders do not have the possibility of signal accumulation. Usually the fast transient signal is stored in a shift register, from where it can be read out,

during the delay time between the pulses, into the minicomputer to accumulate and average the signals. Simple and inexpensive systems have been described in the literature [45, 46]. Rhodes et al. [47] have described a computer interface, which includes an ADC. The computer starts the pulse programmer of the spectrometer, which in turn delivers a suitably timed trigger pulse to start a computer routine that operates the ADC under software control. The ADC is thus initialized and the process of analog to digital conversion begins. The computer waits until the conversion is over. After that the obtained value is read, added and stored in the computer memory. Finally the computer displays the digitized and accumulated signals on an oscilloscope via a digital-to-analog converter.

A pulsed NQR spectrometer system with complete automation and control built around the Bruker pulse-spectrometer coupled with Nicolet model 1074 signal averager and a PDP 8/E mini-computer has been described by Geisendanner et al. [48]. Another NQR spectrometer system with computer control using biomation model 805 fast transient recorder and 16-bit HP-2100A computer has been described by Gourdjji et al. [49]. We have utilized a minicomputer-based signal analyzer (Model SM-2100B, from Iwatsu Electric Company Limited, Japan) with signal acquisition and processing capabilities and developed a spectrometer system [20] which operates under the supervision of Intel 8085A based-microprocessor system (Microfriend-I, from Dinalog Micro-Systems, India). Automation of several pulsed NQR experiments has been achieved with this

system (one such experiment is described in reference [20]). Complete details of this spectrometer are presented in the following sections. Spectrometers for automation of certain complex pulsed NQR experiments [20, 48, 50] have been described earlier in the literature.

It is pertinent to mention here that, the computational capabilities of the computer interfaced to an NQR spectrometer can be advantageously used for purposes such as, (i) digital filtering of the signals accumulated and stored in the digital memory of the computer [51,52], (ii) correction of phase errors in a multiline FT-NQR spectrum [48], (iii) the exponential fitting of data in relaxation time measurements. We describe in section II.E, the utilization of computational features of the signal analyzer to automate certain complex pulsed NQR experiments.

## II.B DETAILS OF THE PRESENT MICROPROCESSOR-CONTROLLED SPECTROMETER SYSTEM

### II.B(1) Introduction

Prior to the present work we had available in our laboratory a pulsed NQR spectrometer [38] with single point boxcar averaging facility. This spectrometer was based on hardware pulse programmer capable of generating pulse sequences having a maximum of three pulses. Like any other unautomated system (section II.A) this hardware pulse programmer based spectrometer system suffered from, (i) not having the flexibility of

performing various experiments involving complex pulse sequences, (ii) lack of time averaging and signal processing facilities, and (iii) complete dependence on manual operation. To illustrate one of the problems encountered in pulsed NQR experimentation with unautomated systems, we can consider the problems associated with Zeeman perturbed spin-echo envelope modulation (ZSEEM) experiment, where a two pulse ( $90-\tau-180$ ) sequence is used and the echo maximum is plotted as a function of separation  $\tau$ , between the two pulses. Obtaining ZSEEM [53] patterns using the unautomated spectrometer was quite tedious and time consuming, because the variation of  $\tau$  in the  $90-\tau-180$  sequence (spin-echo sequence) was done manually for each data point and also the delay between the boxcar trigger pulse and the echo maximum at 2 had to be adjusted manually for each increment of  $\tau$ . Such problems are encountered in several other pulsed NQR experiments. To avoid these difficulties and also to reduce the experiment time we thought it worthwhile to automate our pulsed NQR spectrometer system using a microprocessor. Compared to minicomputer-based systems microprocessor-based systems are relatively inexpensive. We therefore automated our pulsed NQR spectrometer using a microprocessor. As will be seen in the following sections of this chapter the use of microprocessor offers complete flexibility of generating several complex pulse sequences and automation of various pulsed experiments by appropriate software.



## II.B(2) Description of the Spectrometer System

The block diagram of the present spectrometer system underlining the role of microprocessor and the signal analyzer is shown in Fig. II.3(a) (a photograph of the spectrometer system is given in Fig. II.3(b)). The desired pulse sequence is generated by the microprocessor system. Software required for generating various pulse sequences has been developed (details of these are discussed in section II.D) and stored in the on-board EPROM. When necessary, the appropriate software program can be called from EPROM to the on-board user RAM and can be executed to generate the required pulse sequence. The pulse sequence is output through one of the I/O ports of the microprocessor system. The sequences are passed through 2N-2369 transistor-based current drivers before passing to the r.f. gating scheme. These pulses are made available at the BNC-connectors mounted on the side panel of the card cage of the microprocessor system (a photograph of the microprocessor system along with the card cage is shown in Fig. II.3(c)). The pulses available at these BNC-connectors are routed to appropriate ports depending on the required gating scheme. The r.f. signal to be gated is generated from a signal generator (Model 8640B from Hewlett-Packard, USA). Some of the gating schemes used in the present spectrometer system are similar to those described earlier [38]. The gating schemes required for certain special experiments involving phase alternant pulse sequence, WAHUHA-4 pulse cycle, MREV-8 pulse cycle etc. are discussed later in this chapter.

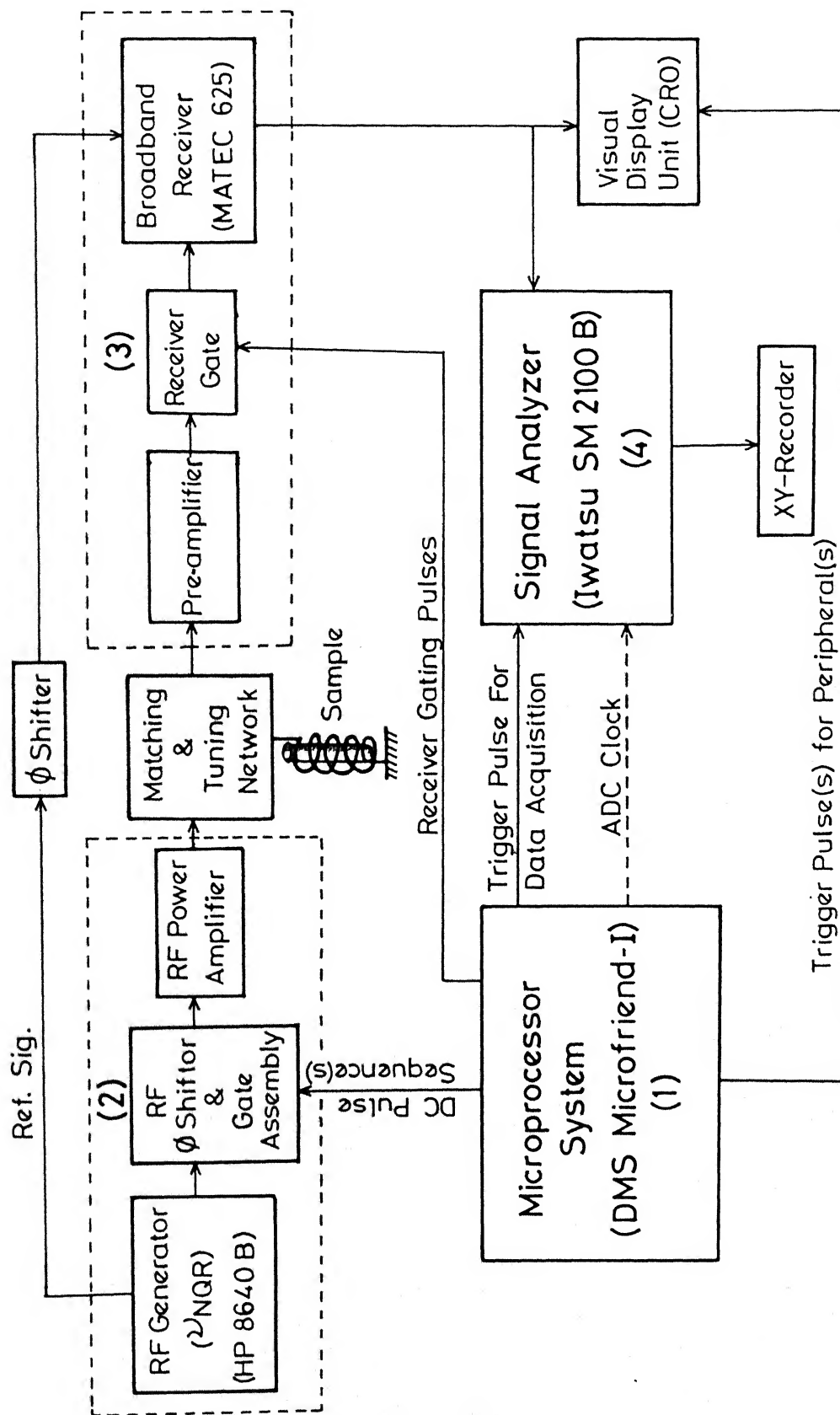
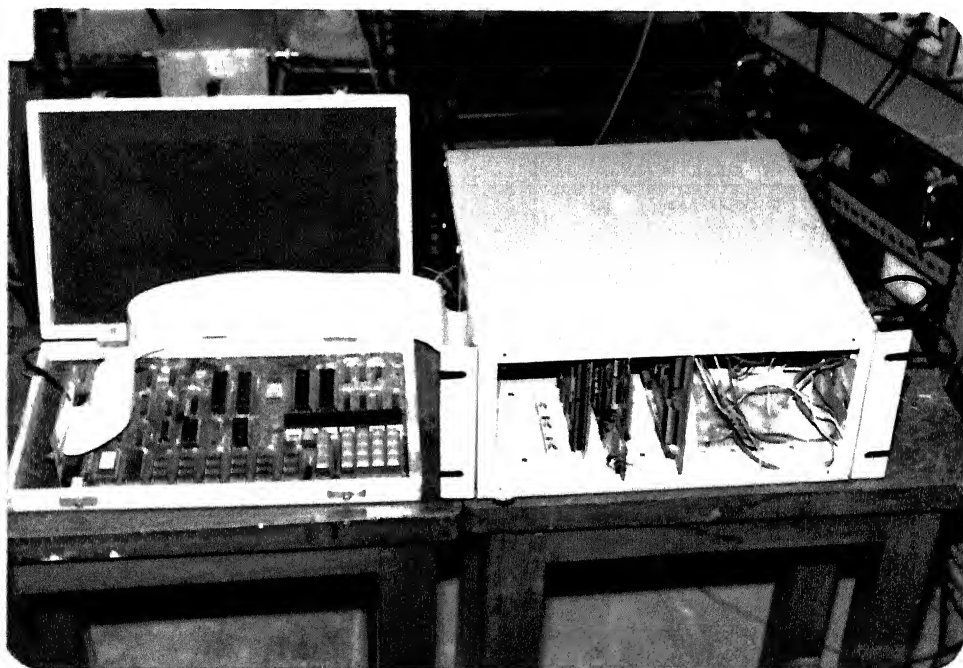


Fig.II.3(a) Block Diagram of the Microprocessor-Controlled Pulsed NQR Spectrometer.



(b)



(c)

Fig. II.3(b) Photograph of the Microprocessor-Controlled Pulsed NQR Spectrometer.

(c) Photograph of the Microprocessor System.

The gated r.f. pulses are amplified using a home-made low-noise tuned power amplifier [38] and coupled to the sample coil through an impedance matching and tuning network. This home-made amplifier has considerable power droop and it was observed that it has poor long-time power stability when carrying out multiple pulse experiments where a large average power is drawn. For these experiments we have used an ENI (Electronic Navigation Industries, Inc., New York, USA) power amplifier (Model A-300) to drive the final tuned stage of the home-made power amplifier. This combination gives long time stability of pulse power and also reduces power droop considerably.

The NQR signal induced in the sample coil (as a response to the r.f. pulse) is first amplified using a 3N-200 FET based low noise tuned preamplifier which is protected from high power r.f. pulses by the use of cross diodes at its input. The output of the preamplifier is further amplified and detected by a broadband (2-200 MHz) receiver (Model 625, from Matec, USA). All the r.f. amplification stages of the Matec receiver are internally protected by cross diodes and the overall recovery time of the pre-amplifier and receiver combination is 10-15  $\mu$ sec after a short intense  $\pi/2$  pulse. It has been observed that the recovery time of the receiver increases in multiple pulse experiments and experiments involving the application of long r.f. pulses.

The NQR signal information available at the output of the receiver can either be presented on an oscilloscope or be

acquired and processed further using a signal analyzer (Model SM 2100B, from Iwatsu Electric Co. Ltd., Tokyo, Japan).

The signal analyzer has two channels to acquire time domain signals with a 12-bit ADC. The ADC has a maximum clock frequency of 400 kHz. The signal analyzer has the facility of coherent averaging of transient signals to increase S/N ratio. The averaged signals can be stored in any of its eight blocks of memory. Each one of these blocks has a maximum capacity of 4K (it can be set to 0.5, 1, 2 or 4K). The time domain signals acquired into the signal analyzer can be processed using inbuilt system routines. These include average, FFT, IFFT, auto power spectrum, cross power spectrum, auto correlation, cross correlation etc. These routines can be executed with the help of front panel "Function keys" of the signal analyzer. The signal analyser has BASIC language option and is provided with a BASIC key board for programming. The processing of the time domain signals can also be done in the BASIC mode. With this facility any kind of mathematical processing of the signal can be done. In the BASIC mode the inbuilt system routines can also be used wherever necessary. The signal analyzer also has a 6-inch CRT display which is useful for displaying signals and also for BASIC programming. The inbuilt mini-floppy disk drive enables one to store the processed signals into the floppy disk. These signals can be brought back to the block memory when desired and can be recorded on to an X-Y recorder through "pen-out" of the signal analyzer. The GPIB interface facility of the signal analyzer enables one

to connect any instrument with this interface facility to enhance its capabilities.

In the case of experiments requiring single point averaging a boxcar averager (Model CW-1, from Princeton Applied Research, USA) is used.

Apart from generating pulses to the r.f. gates, the microprocessor also generates trigger pulses for the oscilloscope and for the initiation of data acquisition etc. It also generates appropriate clock pulses to the ADC of the signal analyzer in the experiments where synchronization between the microprocessor and the data acquisition by the signal analyzer is required.

## II.C HARDWARE DETAILS OF THE MICROPROCESSOR SYSTEM

A low cost Intel 8085A-based eight-bit microprocessor system (Microfriend-I) manufactured by M/s Dynalog Microsystems, Bombay (India), is the control system in the present spectrometer. The 8085A microprocessor chip contains six general purpose eight-bit registers (namely, B, C, D, E, H and L) for data storage and data transfer, and an eight-bit accumulator (Register A) for performing arithmetic and logic operations. The functional block diagram of the microprocessor system is shown in Fig. II.4. The processor of this system utilizes a 6.144 MHz crystal and hence the CPU operates at 3.072 MHz and has 1.3  $\mu$ sec instruction cycle. The system has a 2K RAM which is useful for developing software programs and also it can be utilized during

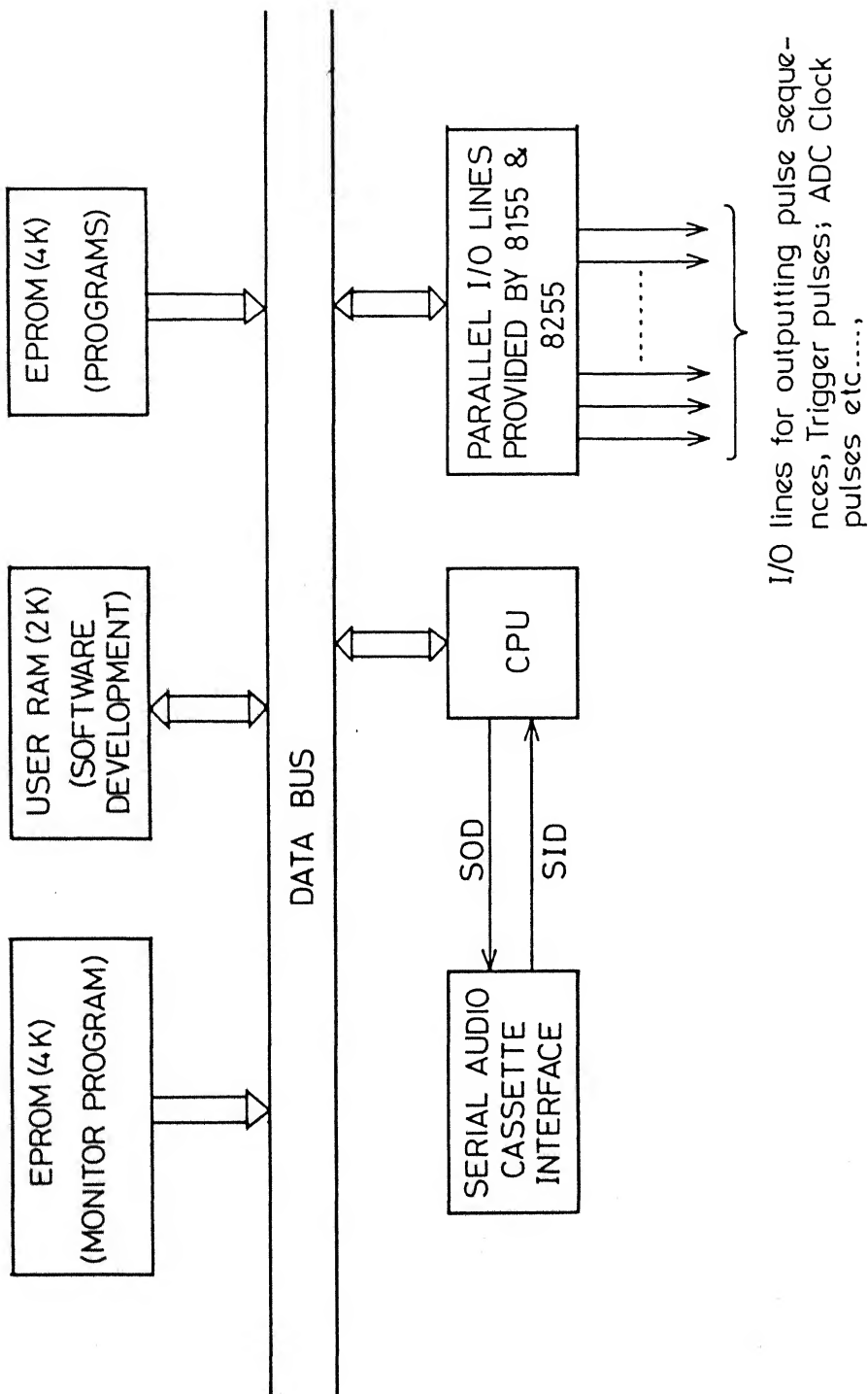


Fig. II.4 Functional block diagram of the microprocessor system (Microfriend-1) showing the common communication path between various components through the data bus.

program execution. The on-board 4K EPROM available for the user is for permanent storage of software programs. The system also has a serial audio cassette interface for bulk storage and RS-232C I/F to connect any CRT console. There is an on-board EPROM programmer to burn the developed software programs into EPROM directly from RAM. Facility also exists for expanding the memory upto 32K of RAM or EPROM (or any mix of these two memories). The microprocessor has a powerful on-board system monitor program in its 4K EPROM which enables the user to load any software program into the on-board RAM through the key-board or through the audio cassette interface or from additional on-board EPROM. The system monitor program also helps the user to edit and debug any software programs being developed. The system monitor can also support TTY interface which uses 20 mA current loop. Intel 8279IC is used for TTY, Key board and display control.

Programmable peripheral interface (PPI) 8255A-5 is used for outputting the pulse sequences, various trigger pulses and also the ADC clock pulses for the signal analyzer when desired. The PPI has three eight-bit I/O (Input/Output) ports, namely port A, B and C. Five bits of the port A, bits 4, 5, 6, 7 & 8 are connected to the BNC connectors (mounted on the side panel of the optional card cage) to output pulse sequences and trigger pulses. Apart from these 24 I/O lines available for the user from PPI 8255A-5 there are 22 parallel I/O lines provided by 8155. All the I/O lines are brought out on a 50 pin connector and are easily available for the user.



All the address, data and control buses, fully buffered, are available as a standard STD bus for easy expansion of the system (STD bus is 56 pin double-sided edge connector standard). With this bus expansion facility we could hook up (i) Real Time controller card which has 8253 counter timer for real time applications, (ii) ADC/DAC card and (iii) Memory expansion card. In fact, any STD compatible card can be hooked up for increasing the processing capabilities of the microprocessor.

The hardware interrupt facility available for the user makes it possible to have programmed jumps and dynamic reconfiguration of the software programs (e.g. changing from "set mode" to "measure mode" etc., see section II.E for details).

The programmable timer/counter 8253 provided on STD compatible RTC card is useful for timing generation with good time resolution. This timer has 3 independent 16 bit counters with a count rate upto 2 MHz. The counting operation of each counter is completely independent and they can be programmed to count either in binary or in BCD. Each counter can be programmed independently to operate in one of the six modes to achieve a variety of timing tasks. A control word (which will be stored in the control word register of the timer) must be sent out by the CPU to initialize any desired counter to operate in one of the six modes (the control word also programs the counter to count either in binary or BCD). Use of this timer (8253) for the purpose of pulse sequence generation has considerably improved

pulse width resolution ( $\sim 0.5 \mu\text{sec}$ ) compared to the use of software counters. This is because the timer counts directly the clock cycles (2 MHz). Out of the six modes of operation (namely, Mode 0, Mode 1, Mode 2, Mode 3, Mode 4 and Mode 5) we have used Mode 1 (programmable one shot) for the purpose of pulse sequence generation. The details of Mode 1 are as follows:

The timing diagram of this mode (programmable one short) is given in Fig. II.5. In this mode the output goes low on the count following the rising edge of the gate input and the output goes high on the terminal count (see Fig. II.5a). If a new count value is loaded after the gate has triggered the one-shot, then on a retrigger, the new count value will be used (this property is useful for two pulse sequence generation). The one-shot is retriggered if another rising edge of the gate input appears when the output is low and the count starts freshly from the beginning (see Fig. II.5b) to retain the output low for the entire duration. It is therefore possible to generate the desired pulse sequence at the output by appropriately triggering the one shot (gate input). The output can be passed through an inverter to get proper levels.

## II.D PULSE SEQUENCE GENERATION

The microprocessor in the present spectrometer system is capable of generating under software control; several pulse sequences utilized in modern pulsed NQR/NMR spectroscopy, for

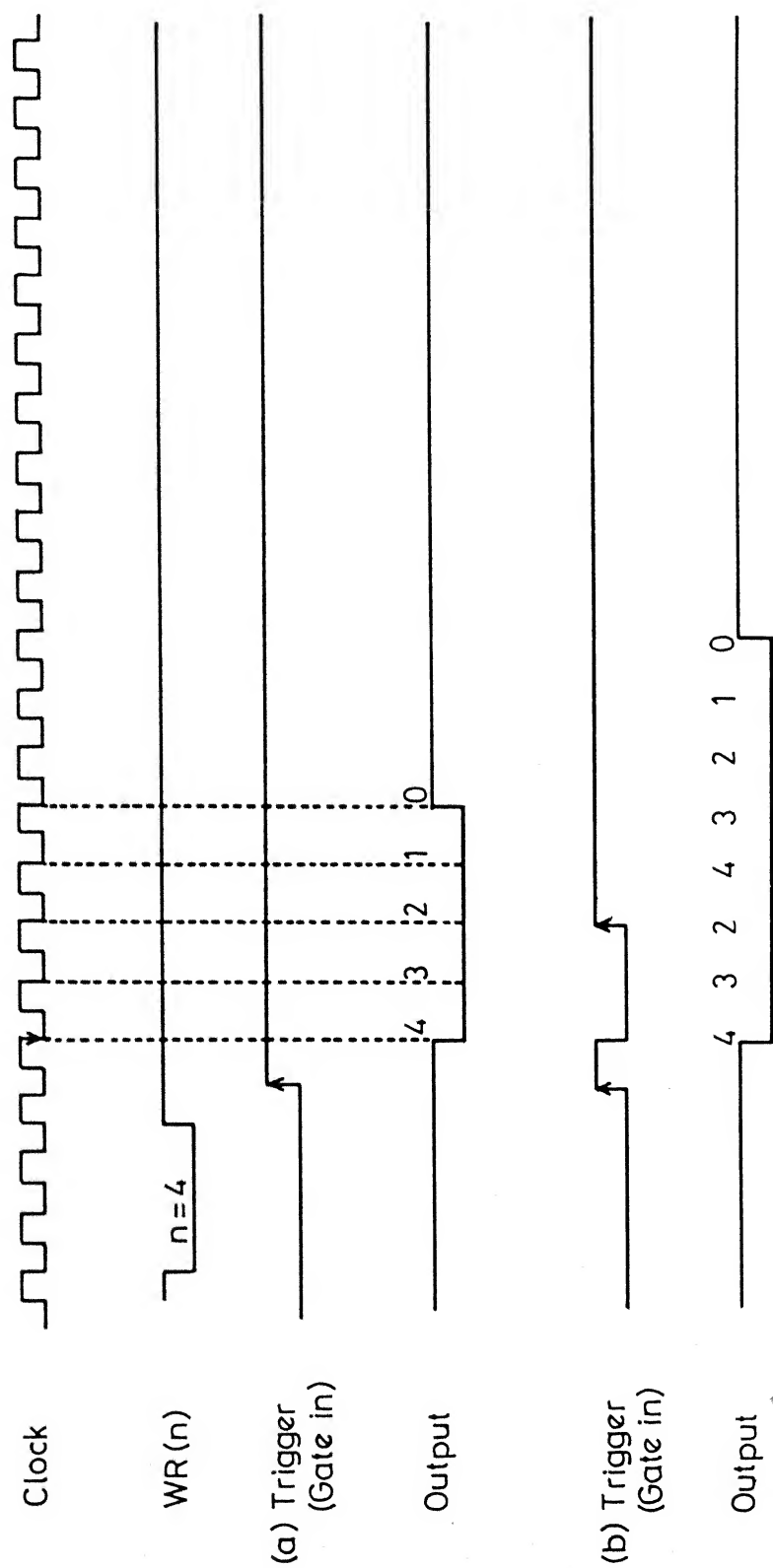


Fig. II.5 Timing diagram for the operation in "Mode-1" (Programmable one-shot) of Intel 8253 timer, (a) indicates a single gate trigger edge, and (b) indicates retriggerable nature of "one-shot" when two trigger edges appear at the gate input.

example, automatic ZSEEM and STEEM (Stimulated echo envelope modulations) sequences and also more sophisticated multiple pulse sequences required for line narrowing and double resonance experiments in NQR. We have generated the following pulse sequences using our microprocessor for which software has been developed:

- i) Single-pulse sequence.
- ii) Two-pulse and three pulse sequences
- iii) Carr-Purcell (CP) and Carr-Purcell-Gill-Meiboom (CPMG) sequences.
- iv) Ostroff-Waugh sequence.
- v) Phase alternated pulse sequence.
- vi) Lee-Goldberg pulse sequence.
- vii) Waugh-Huber-Haeberlen (WAHUHA) 4-pulse, and Mansfield-Rim-Elleman-Vaughan (MREV) 8-pulse sequences.

As has been pointed out in section II.A, the designer may choose different approaches to a timing problem when a computer/micro-processor is readily available. First, one can use some of the output lines of the computer/microprocessor and change their logic levels by a software program, thus realizing a software pulse generator. This method has relatively poor time accuracy. Another elegant way became available to the designer with the development of large scale integration (LSI) programmable timers are now commercially available with counting frequencies of upto 10 MHz [54-58]. These chips offer a powerful structure, with several independent programmable counters triggerable on

edges or levels. They provide greater flexibility at moderate cost, since control functions are programmable from the host computer/microprocessor. We have explored the possibility of realizing pulse sequence generation by the above two methods, namely, (i) software pulse generation and (ii) pulse sequence generation by the use of LSI timer chips using our 8085A based 8-bit microprocessor system. We have used 8253 programmable interval timer for the implementation of the second method. It should be mentioned at this point that the pulse sequence generators built around LSI timer chips (Am 9513) interfaced to mini-computers have been described earlier in the literature by H.S. Jalmes et al. [23] and G.A. Mohr et al. [24].

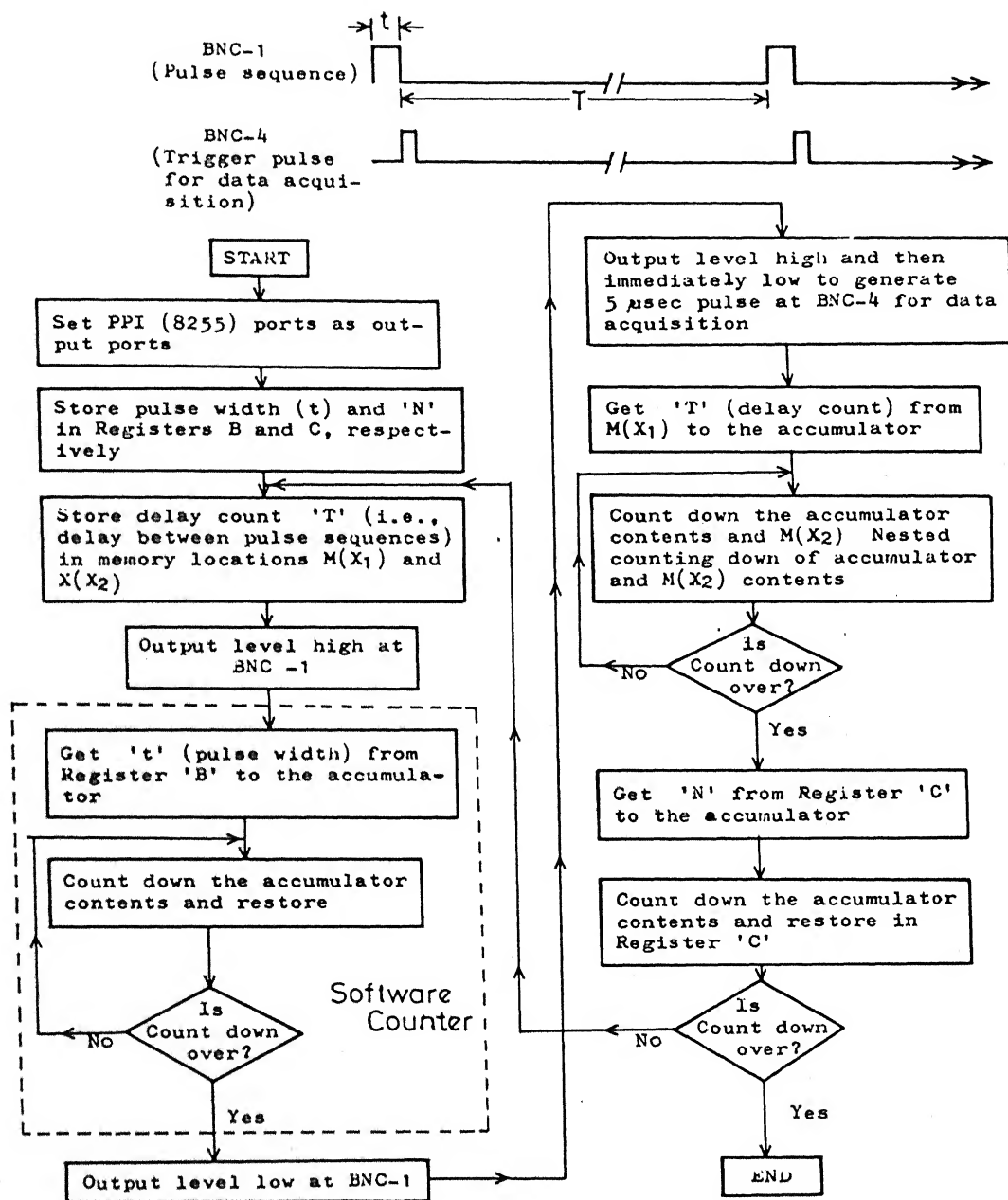
We will first describe the general philosophy followed in the implementation of software pulse sequence generation and then we take up individually the software written for generating various pulse sequences.

For any pulse sequence generation the initial part of the program stores the desired numbers for various parameters of the pulse sequence, namely, the pulse widths of  $\pi/2$  and  $\pi$  pulses (as is required by the sequence of interest), pulse separation(s) (in the case of multiple pulse sequences more than one separation may be required), delay time (repetition rate) and number of repetitions (N) of the sequence ('N' is decided by the required number of coherent averages of the transient signal) either in various registers of 8085A microprocessor chip or in any chosen memory

location and these numbers are translated into time intervals through appropriate delay routines known as software counters. To achieve lowest possible values for pulse widths (and also to achieve better pulse width resolution) we have always stored the corresponding numbers in 8085A registers rather than storing in the memory because the data transfer is faster between various registers and the accumulator than the transfer between memory and accumulator. By the utilization of these registers for storing the numbers corresponding to pulse widths it was possible to obtain a minimum of  $10\mu\text{sec}$  for pulse widths which could be incremented in steps of  $4\mu\text{sec}$ . It should be noted at this point that all the arithmetic and logic operations are performed by the accumulator. Hence, the numbers have to be transferred to the accumulator before translating them into appropriate pulse sequence parameters by the appropriate software counters. The generated pulses are output through one or several of output lines (output channels) of the PPI 8255A-5. These output lines are routed to BNC connectors through current drivers. The pulses which trigger various peripheral devices and signal acquisition unit are output through the channels which are directly connected to BNC connectors without any current drive.

#### II.D(1) Single-Pulse Sequence

In the beginning of the program all the ports of PPI 8255 are set as output ports through appropriate software instructions (see Fig. II.6 for pulse sequence and flow chart of the software



PS = pulse sequence  
 $M(X)$  = memory location ' $X$ '  
 $N$  = number of times PS to be repeated

Fig. II.6 Flow chart of the program for the generation of single pulse sequence.

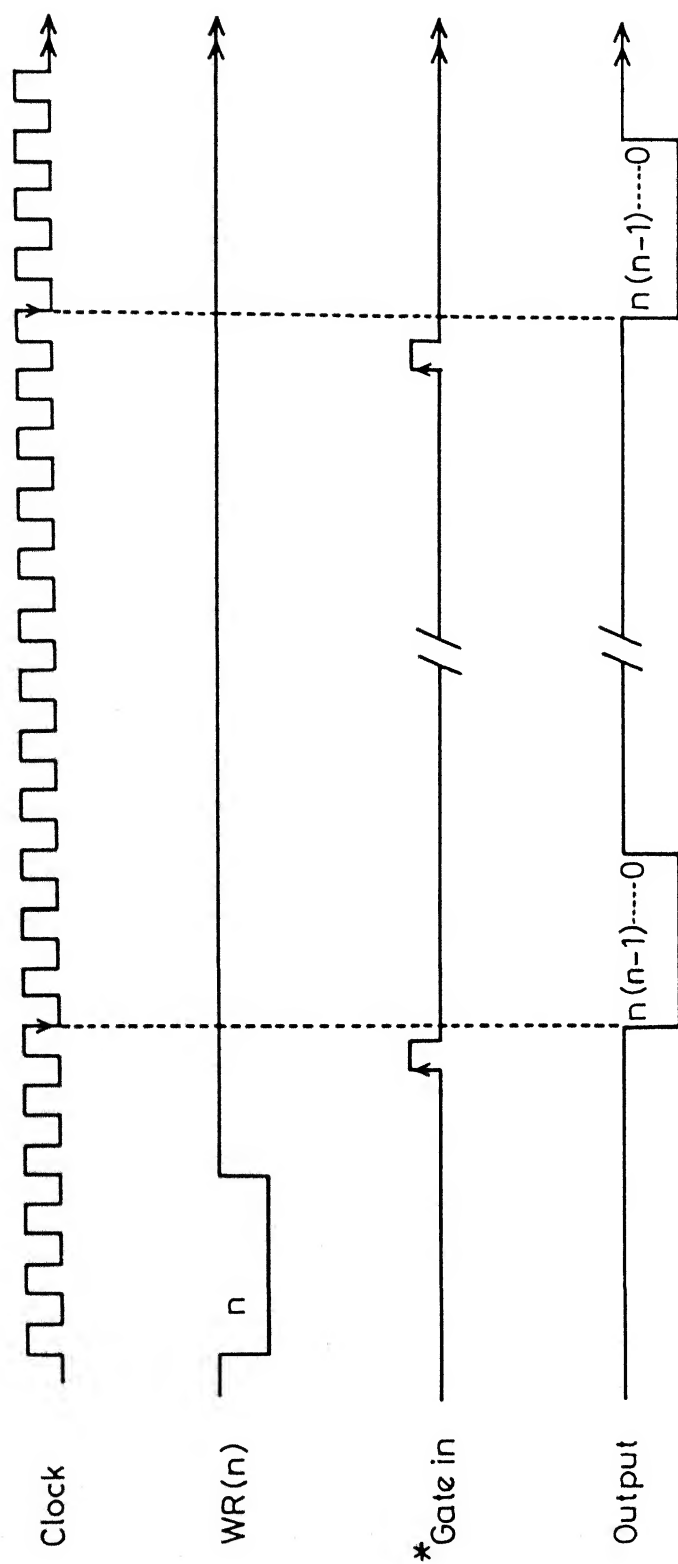
program). Once the PPI ports are set as output ports all the I/O lines of PPI are now ready to output any logic level (high or low) as instructed by the microprocessor. The parameters are then stored for the single pulse sequence, namely, pulse width ( $t$ ) and the number of times pulse sequence to be repeated ( $N$ ) in the registers 'B' and 'C', respectively. The delay count ( $T$ ) is stored in memory locations  $M(x_1)$  and  $M(x_2)$ . After the parameters are stored, the microprocessor outputs logic level 'high' at BNC-1. Immediately after this is done the software program brings register 'B' contents into the accumulator and the "software counter" starts counting down the accumulator contents and checks if the count down process is over (i.e., if the accumulator contents have become zero, see Fig. II.6 for details). During this whole count down process, the logic level at BNC-1 remains high and as soon as the count down process is over the program jumps to the next instruction by which microprocessor outputs the logic level 'low' at BNC-1. It is obvious that the time during which the logic level remains high at BNC-1 is equal to the pulse width ( $t$ ) which can be controlled by the contents of register 'B'. Immediately following the pulse the software program outputs a  $5\mu$  sec trigger pulse at BNC-4 for the initiation of data acquisition by the signal analyzer. It can be mentioned at this point that the data acquisition by the signal analyzer can be initiated immediately after the trigger pulse or if necessary a desired amount of delay following the trigger pulse can be programmed within the signal analyzer. After the  $5\mu$  sec pulse is output the



contents of  $M(x_1)$  are brought to the accumulator which are counted down together with the contents of  $M(x_2)$  in a nested software counter. During this whole nested count down process the logic level at BNC-1 remains low, the time duration of which is equal to the delay count ( $\tau$ ). Now, the program checks if the desired number of pulse sequence repetitions are over. If not, the program jumps for restarting the pulse sequence and if yes, the program ends. It should be noted that when a large number of accumulations of a weak signal are needed an unconditional jump instruction is written after the delay count so that the pulse sequence is generated continuously and the number of averages can be directly programmed in the signal analyzer.

So far we have discussed single pulse sequence generation using the microprocessor working as pure software pulse generator. As has already been pointed out the time resolution of this method is poor because various time intervals are generated through software instructions and the instruction cycle time is generally large ( $1.3 \mu\text{sec}$  in our microprocessor).

We, therefore, have used Intel 8253 programmable timer to improve time resolution. To generate pulse sequences using 8253 timer, one or more of its counters are used and are operated in the Mode 1 (see Fig. II.5 for the timing diagrams of Mode 1). In this method the pulse widths are generated by the hardware counters which directly count the programmed number of clock pluses and the intervals between pulses are generated by software



\* Five  $\mu\text{sec}$  pulses from the microprocessor are used as gate input.

Fig. II.7 Timing diagram for single pulse sequence generation using 8253 timer.

counters as in the case of software pulse sequence generation.

We now illustrate how a single pulse sequence is generated using 8253 timer. First of all a number corresponding to the pulse width (this number is decided by the frequency of the clock signal input to the timer) is stored in one of the counters (in our case counter '0') and 2 MHz clock signal is connected to clock '0'. A single pulse sequence with  $5\mu$  sec pulse width and required amount of repetition time (T) is output through one of the output channels of the microprocessor and this is used as the gate input to the counter '0'. Now, the counter '0' output will be the required single pulse sequence with inverted logic levels (see Fig. II.7). The output has been passed through an inverter to get appropriate logic levels required for the transmitter gating scheme.

#### II.D(2) Two-Pulse Sequence

As in the case of single pulse sequence, the program for two pulse sequence also starts by setting all the ports of PPI-8255 as output ports. Now, pulse widths of  $P_1$  and  $P_2$  pulses ( $t_1$  and  $t_2$ ), and pulse separation  $\tau$  are stored in the Registers 'B', 'D' and 'C', respectively. The number of repetitions of the pulse sequence are stored in register E and the delay count (T) is stored in memory locations  $M(x_1)$  and  $M(x_2)$ . As described in the case of single pulse sequence the microprocessor outputs the logic level 'high' at BNC-1 and retains it 'high' till the

software counter-1 gets the value corresponding to pulse width ( $t_1$ ) from the register 'B' to the accumulator and counts down to zero (see Fig. II.8 for details). Then the microprocessor outputs the logic level 'low' at BNC-1 and retains it 'low' till the software counter-2 gets the value corresponding to pulse separation ( $\tau$ ) from the register 'C' to the accumulator and counts down to zero. Then the microprocessor produces logic level 'high' at BNC-1 for the time duration  $t_2$  ( $P_2$  pulse width) via the software counter-3. After this the output of the BNC-1 is made 'low' for the duration (T) through the nested software counter and this duration is determined by the contents of both the memory locations  $M(x_1)$  and  $M(x_2)$ . Immediately following the second pulse ( $P_2$ ) a short  $5\mu$  sec trigger pulse is output at BNC-4 for data acquisition by the signal analyzer. The pulse sequence program ends after the sequence is repeated a set number (N) of times. The pulse sequence can also be repeated continuously by writing an unconditional jumps instruction after the delay count making it convenient for accumulating large number of transients when weak signals are being observed.

It can be mentioned here that in the case of two pulse experiment of Lee-Goldberg [59] the software for generating the pulse sequence is similar to that of usual two pulse sequence except that the first long pulse is generated using a nested software counter and both the pulses are output in two different BNC-connectors.

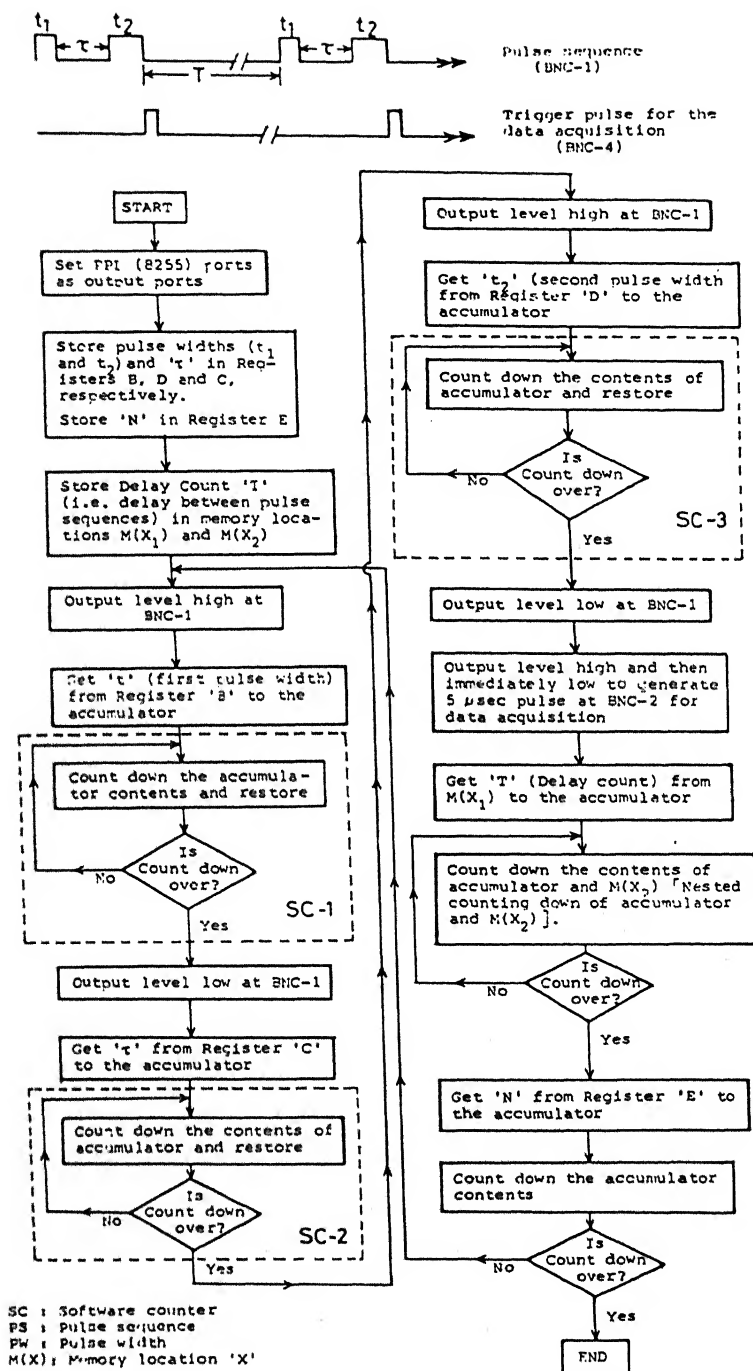


Fig.II.8 Flow chart of the program for generation of two pulse sequence.

We now describe the generation of a two pulse sequence using 8253 programmable timer. In the beginning the microprocessor program stores a number corresponding to  $\pi/2$  pulse width into the counter '0' (counter '0' is used for generating pulses) of 8253. Then the microprocessor outputs a  $5\mu$  sec pulse following which a delay  $\tau$  is generated (by the utilization of a software counter), which is connected to the gate input of the counter '0'. During the delay ( $\tau$ ) the counter is reloaded with a higher number corresponding to  $\pi$  pulse width. At the end of  $\tau$  delay another  $5\mu$  sec pulse is output by the microprocessor which triggers the gate '0'. This process is repeated with a large time delay of  $T$  (generated by nested software counter described earlier). The net result of this process is the generation of the required two pulse sequence at the output of the counter '0' with appropriate pulse widths (see Fig. II.9). Upon passing this sequence through an inverter we can get proper levels for r.f. gating.

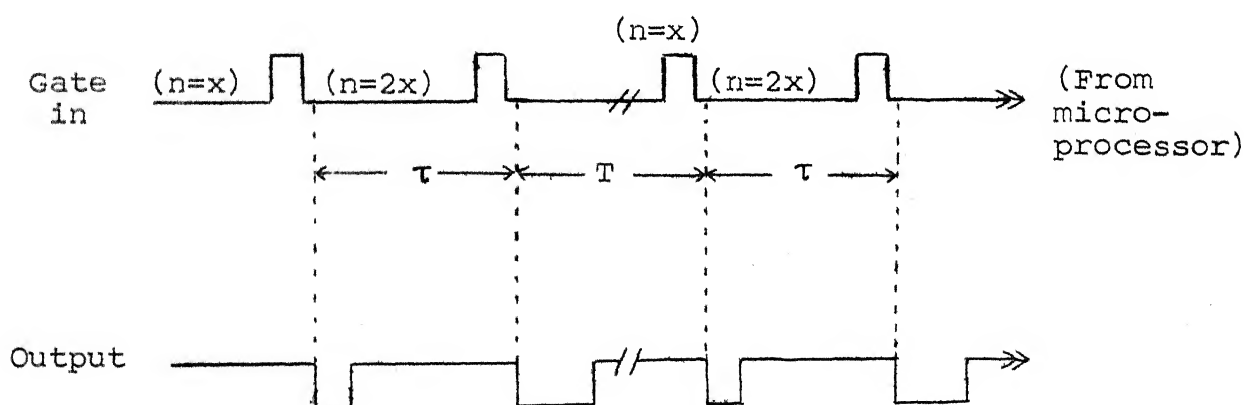


Fig. II.9 Timing diagram for generating two pulse sequence using 8253 timer.

### II.D(3) Multiple-Pulse Sequences

With a view to carry out multiple pulse spin-locking and line narrowing experiments in NQR we have developed software for generating CP [60], CPMG [61], Ostroff-Waugh [62] and phase alternating multiple pulse [63] sequences. Details of the software and gating schemes used for each of these sequences are described.

CP-Sequence: The CP-sequence is represented in Fig. II.10. One of the purpose of the CP-sequence in NMR in solids [63] has been

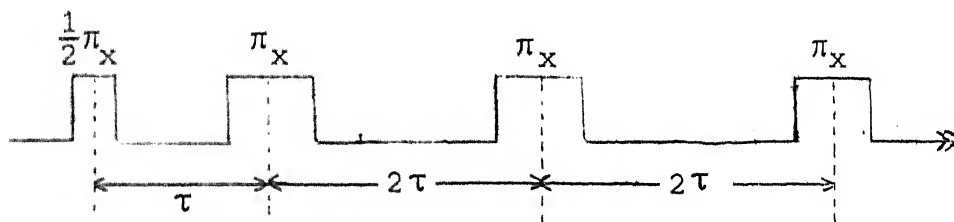


Fig. II.10 Car-Purcell Sequence

to suppress the applied field inhomogeneity term in the effective Hamiltonian. Software for generating this sequence is as follows. After setting all the ports of PPI-8255 as output ports, pulse widths of  $\frac{1}{2}\pi_x$ ,  $\pi_x$  pulses ( $t_1$ ,  $t_2$ ), and separations  $\tau$  &  $2\tau$  are stored in registers 'B', 'C', 'D' and 'E', respectively. The number of  $\pi_x$  pulses ( $n$ ) and the number of repetitions  $N$ , of the sequence are stored in memory locations  $M(x_1)$  &  $M(x_2)$ , respectively, and the delay count,  $T$ , is stored in the locations  $M(x_3)$  &  $M(x_4)$ . The microprocessor now outputs the logic level 'high' at BNC-1 and retains it 'high' till the software counter-1 generates a

delay  $t_1$ , corresponding to  $\frac{1}{2} \pi_x$  pulse (contents of register 'B'). Then the microprocessor outputs logic level 'low' at BNC-1 and retains it 'low' till the software counter-2 generates a delay corresponding to  $\tau$  (contents of register 'D'). After generating the  $\tau$  delay, a logical level 'high' is output by the microprocessor once again at BNC-1 and is retained high till the software counter-3 generates a delay corresponding to  $\pi_x$  pulse and makes the BNC-1 output 'low'. This is followed by the generation of a delay  $2\tau$  by software counter-4 during which period output at BNC-1 remains 'low'. Now the program checks if the desired number of  $\pi_x$  pulses  $n$  have been generated. If not, the program jumps to generate  $\pi_x$  pulse again followed by a  $2\tau$  delay and this continues till the desired number of  $\pi_x$  pulses,  $n$ , are generated. Once this is over a nested software counter generates the delay time,  $T$ , and repeats the entire sequence again at BNC-1 till the sequence is repeated desired number of times ( $N$ ). It should be noted that immediately after the  $\frac{1}{2} \pi_x$  pulse a  $5 \mu \text{sec}$  trigger pulse has been generated at BNC-4 in our experimental setup to acquire the Carr-Purcell echoes into the Signal Analyzer.

The gating scheme for this sequence is quite straightforward (since all the pulses have the same phase) and is similar to the one used in reference [38].

For generating CP pulse sequence using LSI timer we have written a software program which makes the microprocessor output a train of  $5 \mu \text{sec}$  pulses with the intervals shown in Fig. II.10,



as gate input to counter '0'. Before generating this train, the counter is loaded with a number corresponding to  $\pi/2$  pulse width and the number is increased during the period  $\tau$  after  $\pi/2$  pulse. The output of the counter zero will then be the required CP sequence.

### CPMG and Ostroff-Waugh Sequences:

The Gill-Meiboom modification of the CP sequence (CPMG sequence) [61] overcomes the problems such as flip angle errors, r.f. inhomogeneity effects etc. which are associated with original version of the CP pulse train [60]. We utilized CPMG and other versions of CP pulse train such as Ostroff-Waugh [62] and phase alternant [63] sequences to investigate pulsed spin-locking for  $I = 3/2$  spins in NQR spectroscopy.

The CPMG pulse sequence is shown in Fig. II.11(a):

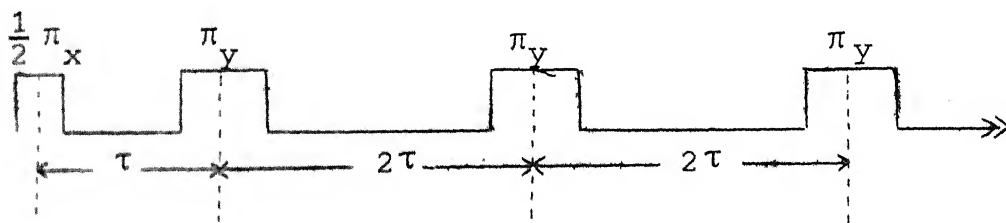


Fig. II.11(a) Gill-Meiboom modification of the Carr-Purcell (CPMG) sequence

For the sake of convenience of r.f. gating the  $\frac{1}{2} \pi_x$  pulse is generated at a different BNC connector (BNC-1) than that of  $\pi_y$  pulses (BNC-2). The combination of these two DC pulses is

achieved using NAND gates to produce OR logic (see Fig. II.11(b) for timing scheme):

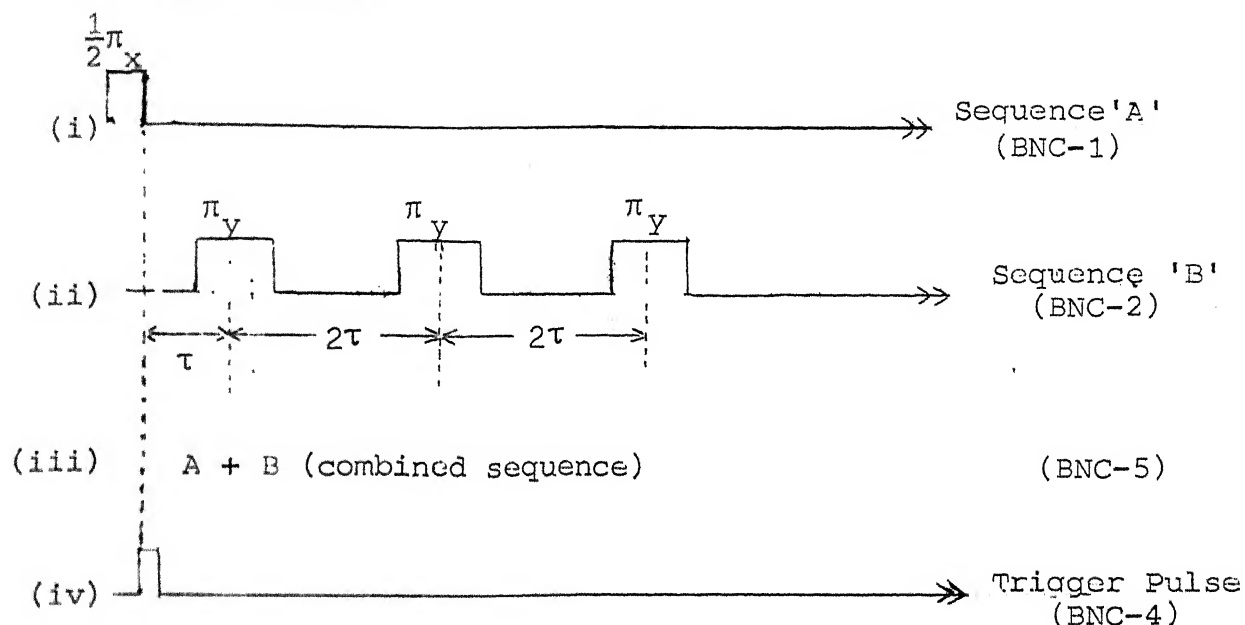


Fig. II.11(b) Timing generation for CPMG sequence

All the parameter storage for CPMG sequence is done similar to that of CP sequence. Once the PPI (8255) ports are set as output ports and parameter storage is done, the microprocessor outputs the sequence 'A' at BNC-1 and the sequence 'B' at BNC-2 using appropriate software counters as discussed earlier.

After this the program generates a long delay ( $T$ ) via a nested software counter as described in earlier programs. Then the program checks if the pulse sequence has been repeated the desired number of times ( $N$ ). If not, the program jumps to repeat the sequence (i.e. sequence 'A' at BNC-1 and sequence 'B' at BNC-2 with appropriate delays) till it is repeated the desired number of times. Immediately after the  $\frac{1}{2}\pi_x$  pulse a  $5\mu\text{sec}$  pulse is



generated at BNC-4 for triggering data acquisition. The r.f. gating scheme used for CPMG sequence is shown in the Fig. II.12. The generation and gating scheme for the Ostroff-Waugh sequence is same as that of CPMG sequence except that all the pulses in the Ostroff-Waugh pulse train are  $\pi/2$  pulses.

The procedure for generation of CPMG sequence using the LSI timer 8253 is same as that of CP sequence except that, here two counters have to be programmed (counter '0' and counter '1'), one for generating  $\frac{1}{2} \pi_x$  pulse and the other for generating rest of the  $\pi_y$  pulses of the train. For Ostroff-Waugh sequence generation, the y-axis pulse train generated by counter '1' are also  $\pi/2$  pulses. The software is same for CPMG and Ostroff-Waugh sequences.

### Phase Alternant Multiple Pulse Sequence

This version of the CP sequence overcomes many of the problems of the original CP sequence and is found to be suitable for multiple-pulse line-narrowing in NQR. The sequence is represented as [63]

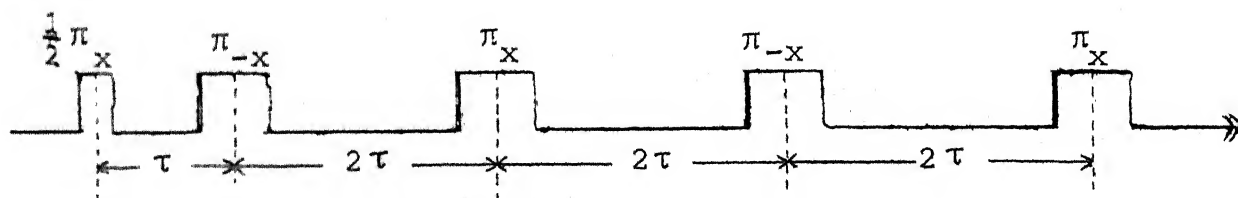


Fig. II.13. Phase alternant multiple pulse sequence

For the sake of convenience of r.f. gating the initial  $\frac{1}{2} \pi_x$  preparation pulse and all the  $\pi_x$  pulses are generated at BNC-1 and all  $\pi_{-x}$  pulses are generated at BNC-2 as shown in the Fig. II.14.

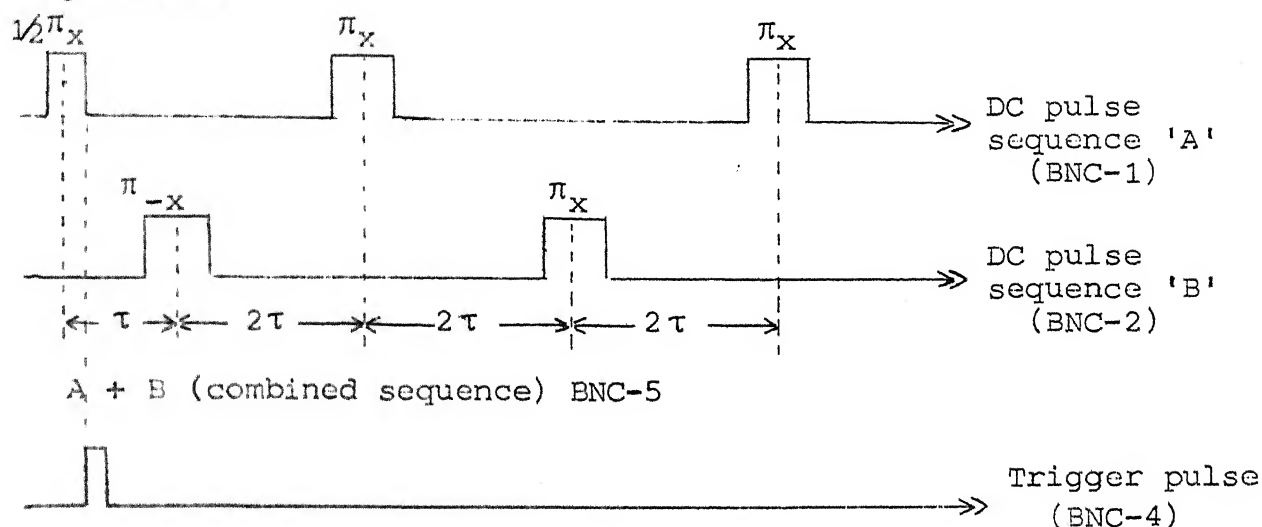


Fig. II.14 Timing generation for phase alternant multiple pulse sequence.

In the beginning of the program all the PPI ports are set as output ports and the parameter storage is done in the same manner as that for CP and CPMG sequences. The program first generates the sequence 'A' at BNC-1 and sequence 'B' at BNC-2 (see Fig. II.14). The program then jumps to generate a large delay ( $T$ ) through a nested software counter similar to the one described earlier. After this delay is produced the program repeats the sequence for the desired number of times. A  $5 \mu\text{sec}$  pulse is also generated immediately after the initial  $\frac{1}{2} \pi_x$  preparation pulse at BNC-4. The phase alternated pulses namely  $\pi_x$  and  $\pi_{-x}$  output at BNC-1 and 2 are combined using the 'OR' logic

and the combined sequence is output through BNC-5. This combination is required by our r.f. gating scheme. The r.f. gating scheme used here is similar to that used for CPMG sequence (Fig. II.12) except that the quadrature hybrid is replaced by a delay line set for a  $180^\circ$  phase shift of an input r.f. signal.

The multiple pulse sequence with the  $180^\circ$  phase shift of alternate pairs of  $\pi$  pulses i.e.,  $[\pi_x, \pi_x]$ ,  $[\pi_{-x}, \pi_{-x}]$  has also been generated in our spectrometer. This sequence has been theoretically shown to be the superior one in NMR [63] among all the modified versions of the CP pulse train though the sequence has not been tried in actual experiments. The pulse sequence is shown in the Fig. II.15.

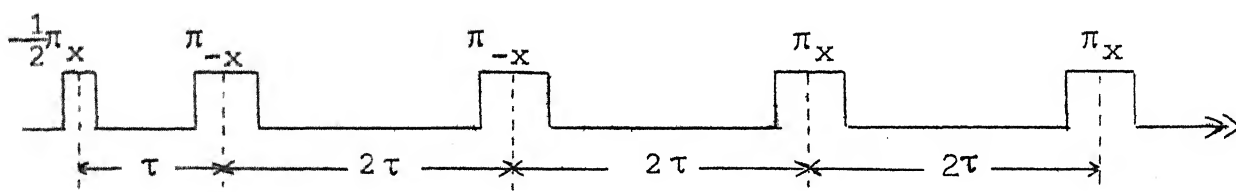


Fig. II.15 Multiple pulse sequence with  $180^\circ$  phase shift of alternate pairs of  $\pi$ -pulses

For the sake of convenience of r.f. gating the following sequences are generated at BNC-1 and BNC-2 (see Fig. II.16). Sequence 'A' and 'B' are generated at BNC-1 and BNC-2 ports with appropriate software counters and the combined sequence (A+B) is output through BNC-5 as mentioned earlier. The r.f. gating scheme is same as that used for phase alternant pulse sequence.

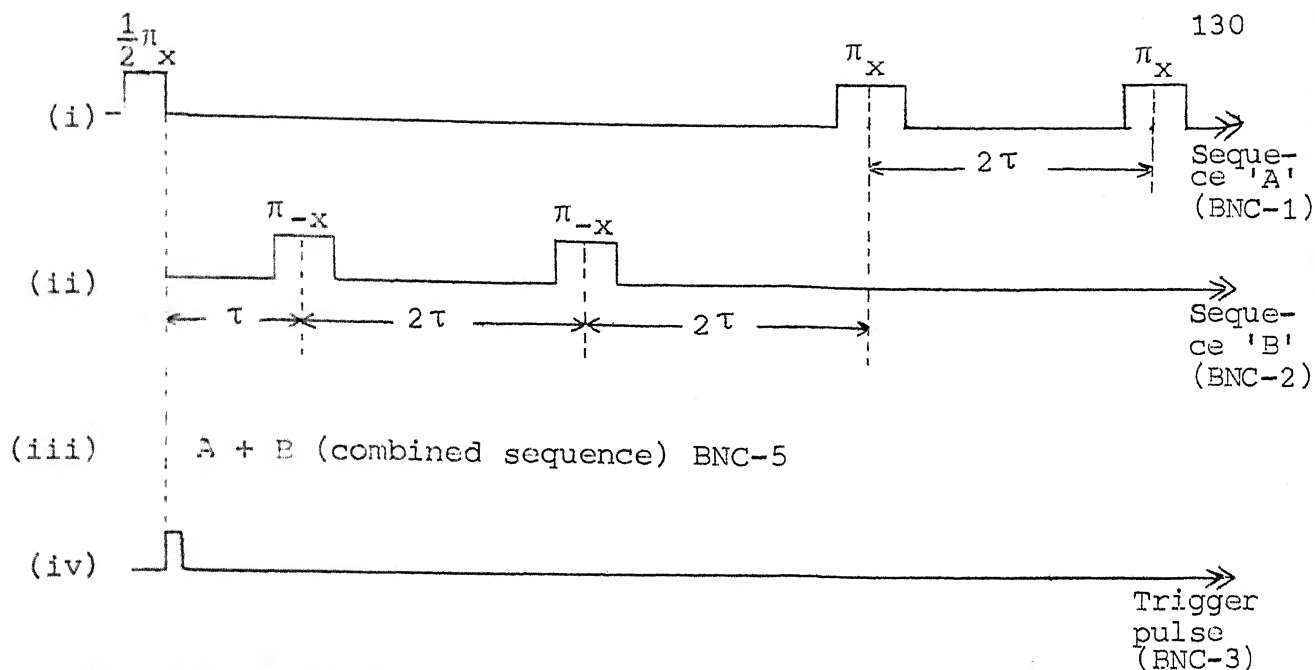


Fig. II.16 Timing generation for the pulse sequence shown in Fig. II.15

The generation of these pulse sequences (PAPS) with the 8253 timer can also be done by generating appropriate timing signals to trigger the gates of counter '0' and counter '1'.

#### II.D(4) WAHUHA four Pulse & MREV-8 Pulse Cycles

This sequence has been designed for the purpose of coherent averaging of dipolar interaction in NMR of solids. It can discriminate between chemical shielding and like-spin dipolar interactions [64]. The sequence has recently been used by V. L. Ermakov and D. Ya Osokin [65] in  $^{14}\text{N}$  NQR spectroscopy. WAHUHA four pulse sequence can be represented as follows:

$$(\pi/2)_x - [\tau - (\pi/2)_{-x} - \tau - (\pi/2)_Y - 2\tau - (\pi/2)_{-Y} - \tau - (\pi/2)_x - \tau]_N$$

The gating scheme used in our spectrometer system for this sequence requires the following timing signals (Fig. II.17) at

various BNC channels of the microprocessor system.

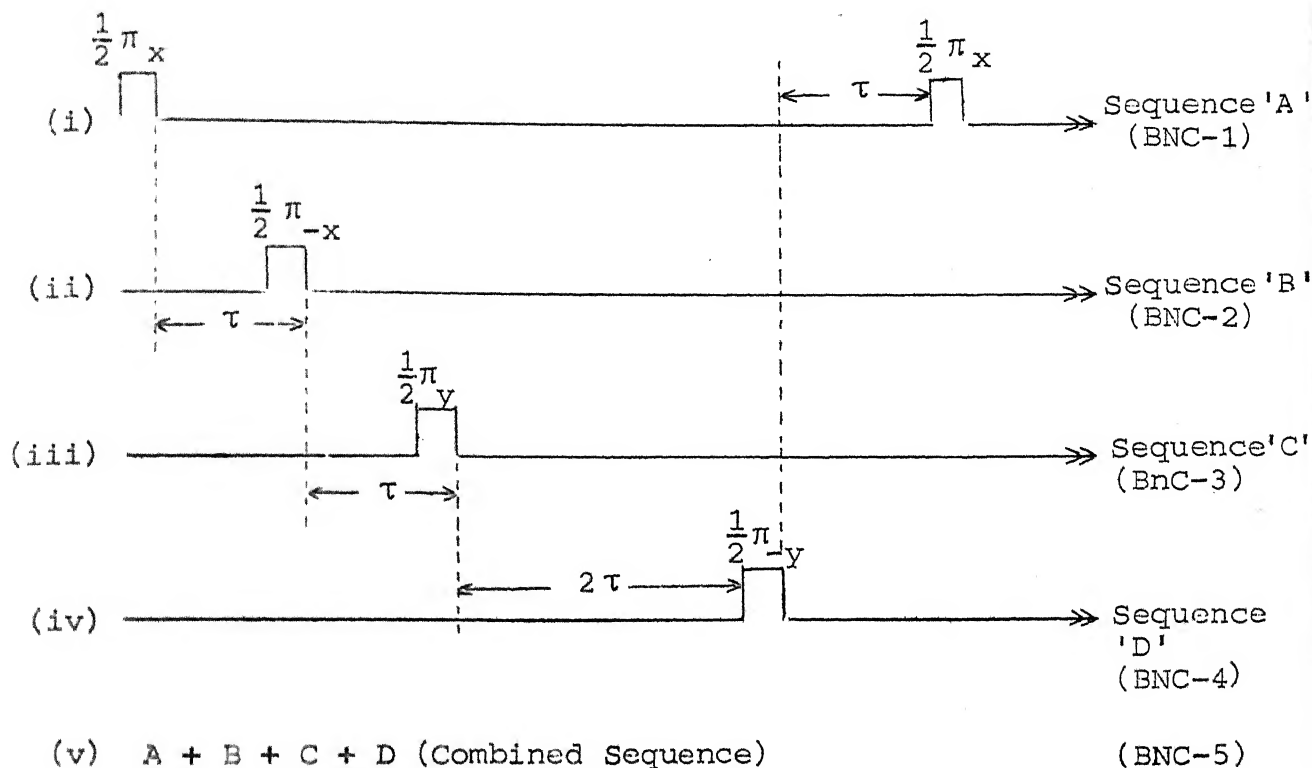


Fig. II.17 Timing generation for the WAHUHA-4 pulse sequence

At the start of the software program for the generation of WAHUHA sequence all the ports of PPI 8255 are set as output ports. The parameter storage is done as follows: (i) pulse width parameter for all the  $\frac{\pi}{2}$  pulses is stored in register 'B', the separation  $\tau$  is stored in register 'C', (iii) the separation  $2\tau$  is stored in the register 'D', (iv) number of pulse sequence cycles (N) is stored in the register 'E', (v) number of repetitions (n) of the sequence is stored in the register 'H' and (vi) the delay count (T) is stored in the memory locations  $M(x_1)$  and  $M(x_2)$ . Once the parameter storage is done the microprocessor program generates a  $\pi/2$



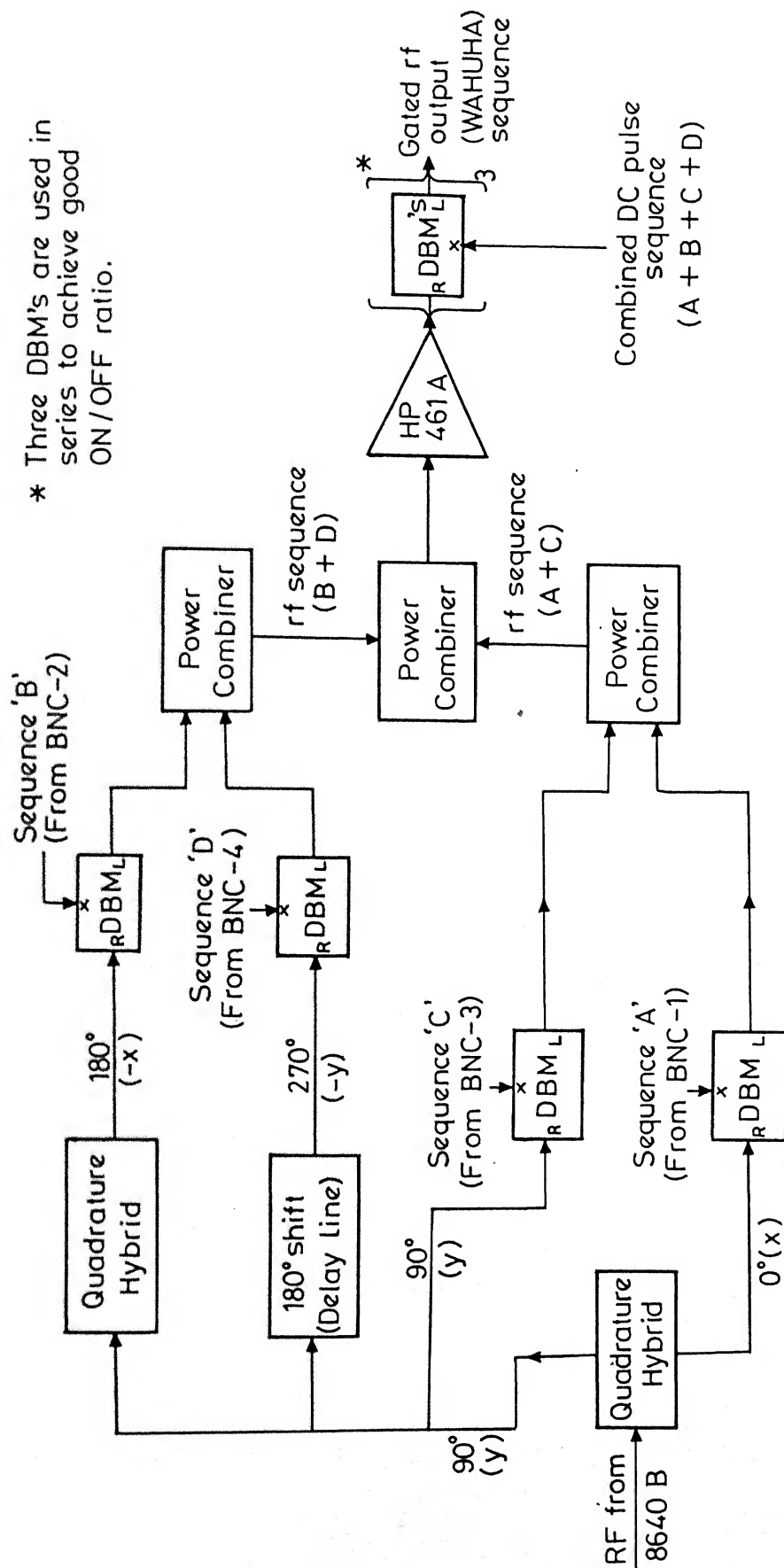


Fig. II.18 RF Gating scheme for WAHUHA four-pulse cycle.

is due to Mansfield and others [66, 67], and is represented as:

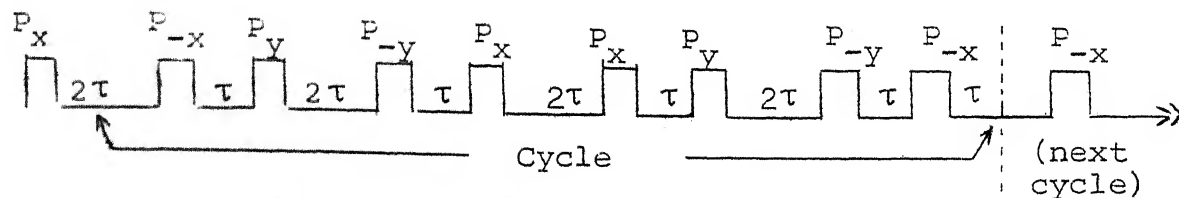


Fig. II.19 MREV 8-pulse cycle

Following timing signals (Fig. II.20) at various BNC-channels of the microprocessor system are generated. Note from Fig. II.20 that the same BNC-channels (as that for WAHUHA cycle) have been used for outputting sequences 'A', 'B', 'C' and 'D' of MREV cycle. The logic of timing generation for MREV 8-pulse cycle is similar to that of WAHUHA 4-pulse cycle except that different timing sequences will have different pulse combinations:

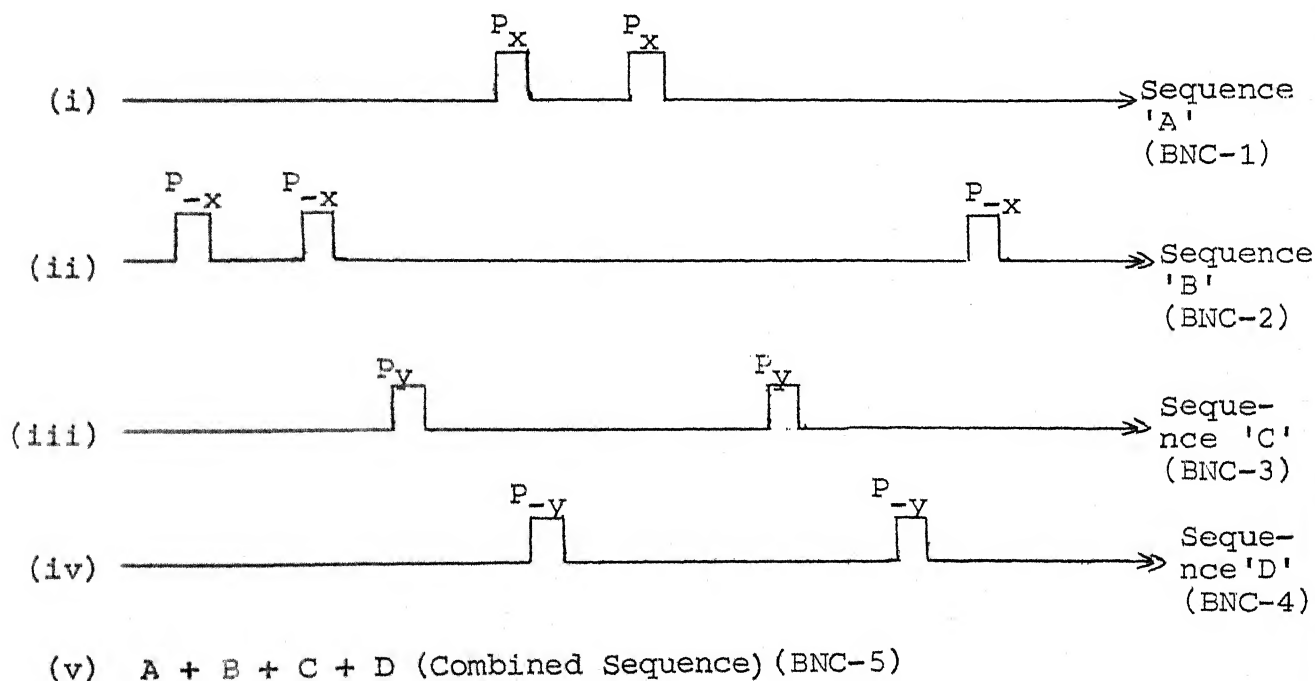


Fig. II.20 Timing generation for the MREV eight-pulse sequence

Out of the nine  $\pi/2$  pulses shown, the first one is the preparation pulse and the rest eight belong to the MREV cycle. This 8-pulse cycle is repeated desired number of times.

The gating scheme used for MREV 8-pulse cycle is same as that for WAHUA 4-pulse cycle.

## II.E AUTOMATION OF VARIOUS PULSED NQR EXPERIMENTS

So far we have discussed the microprocessor software for the generation of various pulse sequences. We shall now consider the automation of various pulsed NQR experiments.

Along with the generation of transmitter and receiver gating pulses the microprocessor also generates appropriate trigger pulses for the data acquisition unit (signal analyzer) and also the clock pulses to the ADC depending on the experiment to be automated. We have automated several NQR experiments with the help of the microprocessor and the signal analyzer. We shall now describe here the automation of a few of these experiments, namely, (i) FT-NQR experiment, (ii) modified Lee-Goldberg experiment, (iii) ZSEEM, (iv) STEEM, and (v) multiple-pulse experiments. It should be mentioned here that in all these experiments the transmitter gating pulses are passed through monostable multivibrators (74121) to increase the width and these pulses are inverted (see Fig. II.21). The inverted pulses are used to block the input to the receiver (receiver gating) during the transmitter pulse. This avoids the undue saturation of the receiver by the high

power r.f. pulses from transmitter.

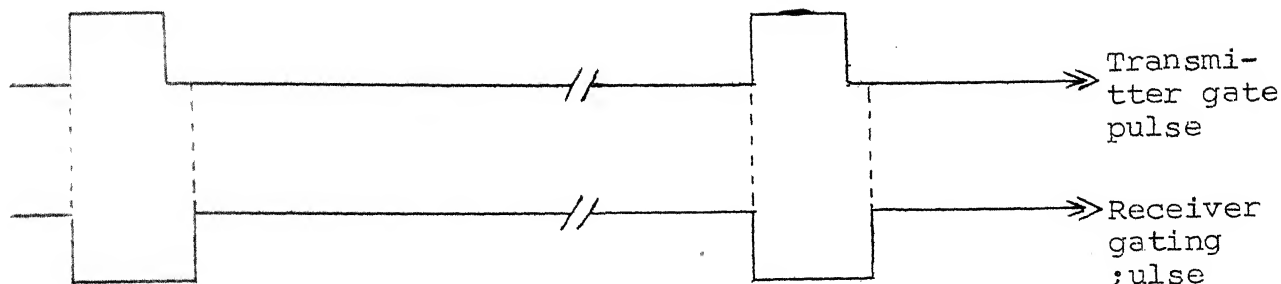


Fig. II.21 Receiver gating pulses

### II.E(1) Automation of FT-NQR Experiment

For the automation of FT experiment the single pulse program (with a trigger pulse following the  $\pi/2$  pulse) is used (section II.D(1)). The signal analyzer, during this experiment, is operated in the BASIC programming mode. The flow chart and the BASIC program for this purpose is given in Fig. II.22. After this program is entered into the BASIC program area, the signal analyzer is switched into the "RUN" mode. Signal analyzer is now ready to accept the input signals as soon as the external trigger pulses for data acquisition appear. The receiver output is connected to one of the two channels of the signal analyzer and then the single-pulse (FID) program is executed by the micro-processor. Now, the signal analyzer acquires and averages the FID signal (the desired number of averages is set by the front pannel keys of the signal analyzer before execution of the BASIC program). The BASIC program stores the averaged signal in

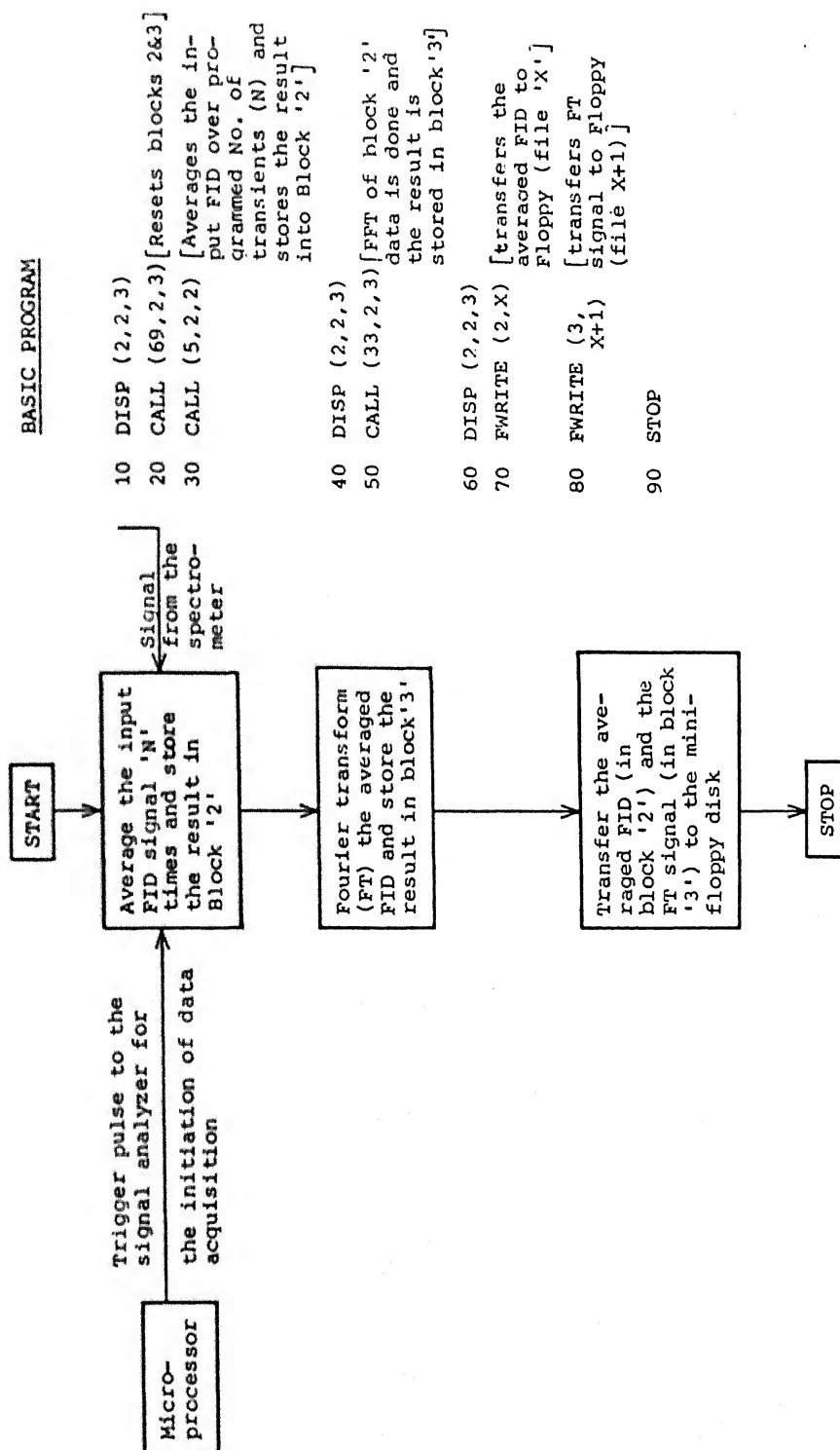


Fig. II.22 Flow chart and the corresponding program in "BASIC" language for the automation of FTNQR experiment.

block '2' of the signal analyzer. The BASIC program then calls the inbuilt FFT routine of the signal analyzer and Fourier transforms the block '2' data. Then the FT-NQR signal is stored into block '3'. The program then transforms the FID (block '2') and FT (block '3') signals to the mini-floppy disk for permanent storage. After this the signal analyzer comes to the monitor mode indicating that the program execution is complete.

The FT-NQR signal stored in the floppy can be brought back to the block memory of the signal analyzer, when desired, and can be recorded by an x-y recorder through the "pen out" of the signal analyzer.

## II.E(2) Automation of Modified Lee-Goldburg Experiment

The modified Lee-Goldburg pulse sequence [59] along with the ADC clock pulse is given in Fig. II.23.

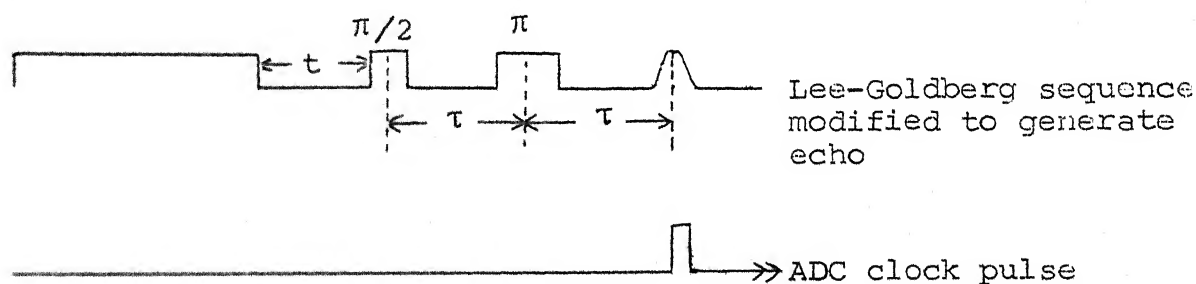


Fig. II.23 Modified Lee-Goldburg pulse sequence

The three-pulse sequence program with the facility to increment width of the first large pulse is executed by the microprocessor. The microprocessor will be operated in the

automode with external clock to the ADC. It can be seen from Fig. II.23 that the echo appears at  $(t + 2\tau)$  after the long off resonant pulse irrespective of its width. The ADC clock pulse is always generated at  $(t + 2\tau)$  after the falling edge of the off resonance pulse. The microprocessor program is now executed with a given initial value of off-resonant pulse width  $t_{p(i)}$ . The ADC clock pulse samples the echo maximum and stores it into the first memory location of the block '2'. Then the microprocessor program increments  $t_p$  (accordingly the ADC clock pulse is shifted) and the signal analyzer samples the corresponding echo maximum to store it into the second location of block '2'. The process continues till the response is recorded for maximum desired value of off-resonant pulse width. The block '2' data at the end of the experiment will be the required Lee-Goldburg sequence response.

### II.E(3) Automation of ZSEEM Experiment

For the automation of ZSEEM experiment various methods have been developed to reduce the experiment time and to improve signal-to-noise ratio (S/N) as much as possible. Three of these methods namely, Method I, Method II and Method III, are described here. In all the three methods basic role of the microprocessor is to generate the echo pulse sequence increment pulse separation and generate trigger pulses with appropriate delay. But the signal acquisition and processing procedure is different

for different methods.

### Method I

In this method the boxcar Integrator (Model CW-1, Princeton Applied Research, USA) is used for single point averaging. The averaged signal is acquired by the signal analyzer in the form of ZSEEM [20].

A suitable software program has been written which enables the microprocessor to generate a two pulse sequence with the separation  $\tau$  automatically incremented and a boxcar sampling pulse at  $2\tau$ . In the initial part of the program the numbers corresponding to, the pulse widths ( $t_1$  and  $t_2$ ) of first and second pulses and pulse separation (see Fig. II.24) are stored in the registers B, D and C, respectively.

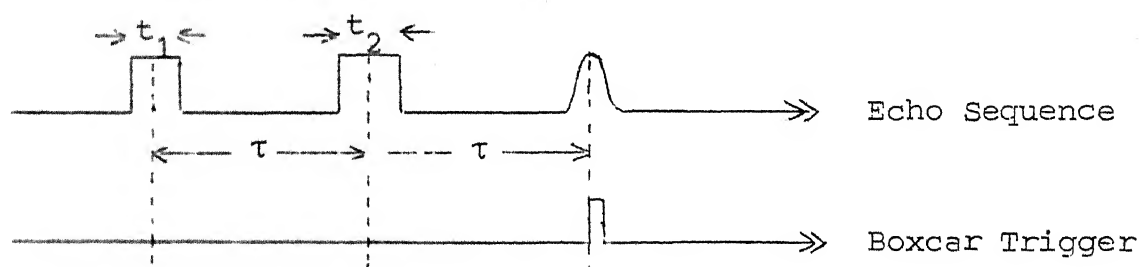


Fig. II.24 Echo pulse sequence with boxcar trigger pulse.

These numbers are translated into time intervals using appropriate software counters as described earlier in this chapter. The software is written in such a way that the pulse sequence is repeated a preset number of times for each value of  $\tau$  in order to enable the boxcar averager to give a stable



voltage output corresponding to the echo maximum at  $2\tau$ . The number of times the pulse sequence has to be repeated is determined by the setting of the time constant of the boxcar integrator, which in turn is optimized for the best S/N ratio. After repeating the sequence, a desired number of times the program increments the contents of C register and generates the sequence with an increased value of  $\tau$ , and the process continues till the maximum desired value of  $\tau$  is reached. The program also generates and outputs through BNC-2 a trigger pulse at  $2\tau$  (from the first pulse of the echo sequence) to open the boxcar gate and to sample the echo maximum. The delay for this trigger pulse at  $2\tau$  will be incremented in synchronization with the increment of separation  $\tau$  between the pulses. Apart from generating the echo sequence and boxcar trigger pulse, the program also generates another pulse at the beginning of the experiment at BNC-3 which initiates the signal analyzer to acquire boxcar output. The program can be run in two modes, namely: (i) "set mode" and (ii) "measure mode" (see Fig. II.25 for details). In the set mode the separation between the pulses ( $\tau$ ) is not incremented and also the trigger pulse to the signal analyzer is not generated. This mode is useful for visual observation of the echo signal on an oscilloscope for adjusting the experimental parameters to optimize the signal. In the "measure mode" the data acquisition by the signal analyzer is initiated for a given value of  $\tau$  (initial value of separation) and the data are acquired

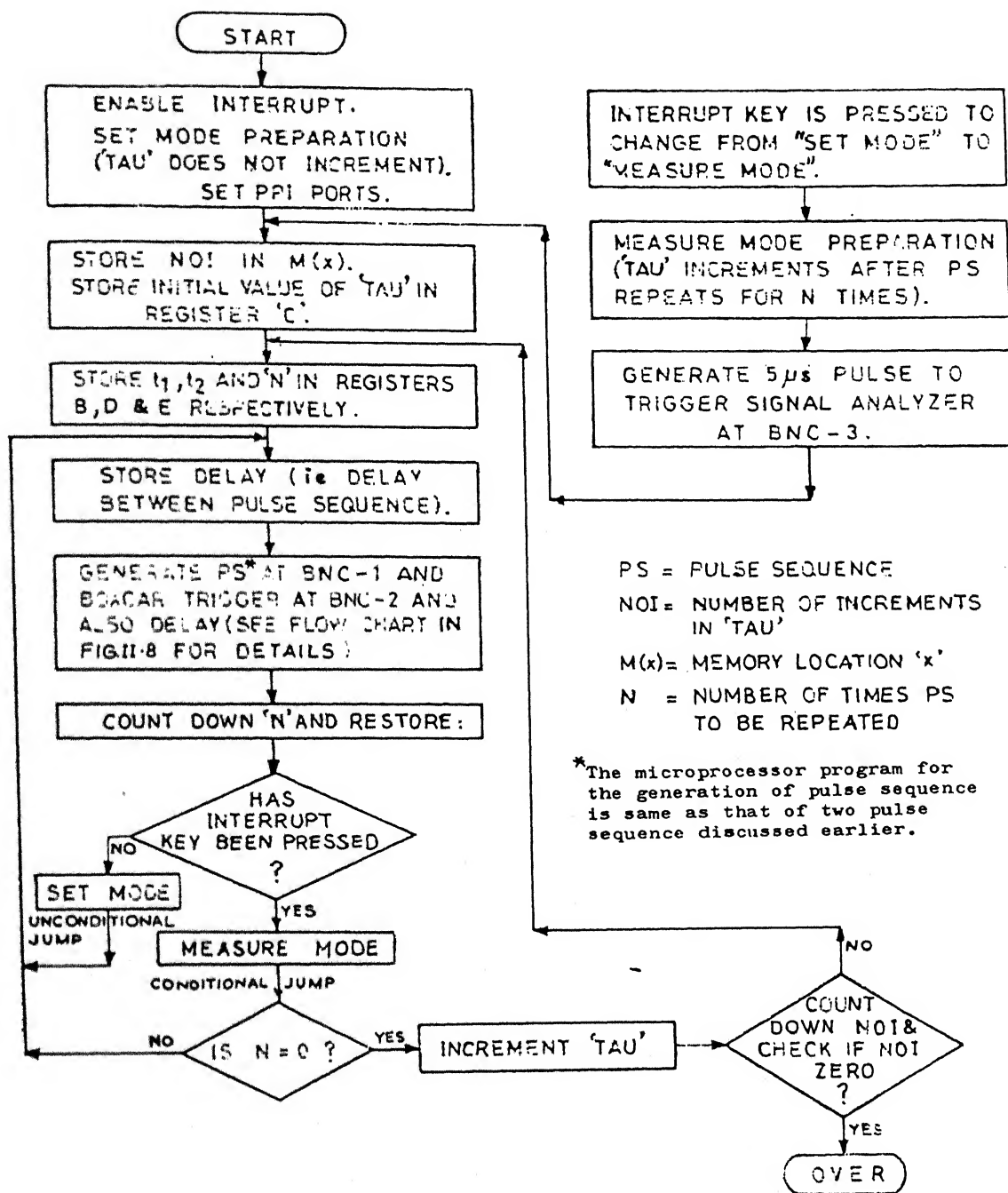


Fig. II. 25 Flow chart of the microprocessor program for automatic acquisition of ZSEEM into the signal analyzer through Boxcar Integrator.

with pulse separation  $\tau$  incremented. The spectrometer is operated in the "measure mode" only when the data are to be acquired after adjusting all the experimental parameters in the "set mode". Transfer from "set mode" to "measure mode" is achieved by the interrupt facility available on board in the microprocessor system [68]. The total experiment time for the acquisition of ZSEEM by this method for a  $\tau$  range of  $22 \mu\text{sec}$  to  $1240 \mu\text{sec}$  is about 40 minutes. This large time is required because sufficient time has to be given at each  $\tau$  value to effect the single point boxcar averaging.

The ZSEEM spectrum acquired into the memory of the signal analyzer is transferred to an inbuilt mini-floppy disk of the signal analyzer for permanent storage. The ZSEEM spectrum stored in the floppy can be taken, when desired, on to an x-y recorder through "pen-out" of the signal analyzer.

To reduce the experiment time and also to improve S/N ratio, we have developed schemes by which the signal is acquired directly by the signal analyzer and these are discussed in the following sub-sections.

## Method II

As has been pointed out the acquisition of ZSEEM by Method I takes considerably long time ( 40 minutes). In order to avoid this we thought it worthwhile to develop a method to directly acquire ZSEEM into the signal analyzer without the

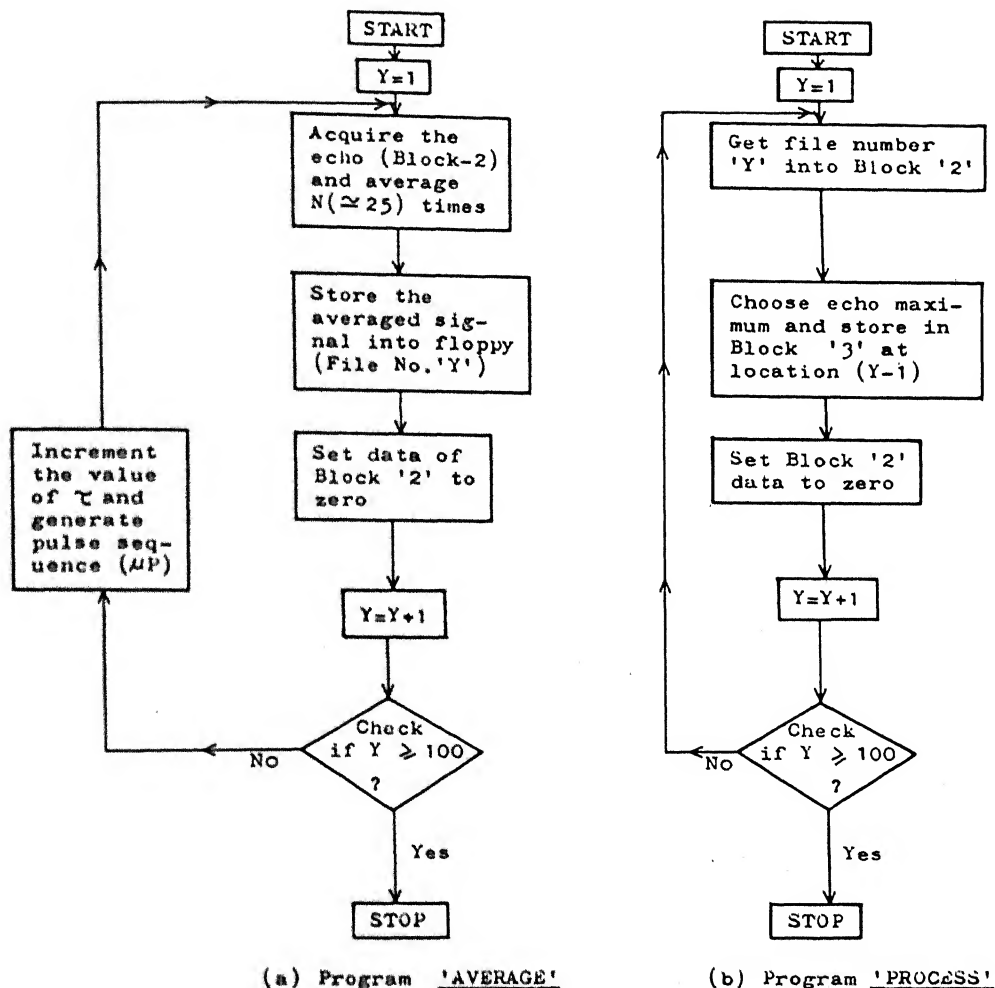
intervention of boxcar averaging. Software program for the microprocessor for this purpose is same as that for the Method I. For the purpose of acquiring ZSEEM directly into the signal analyzer we have used the pulse generated at  $2\tau$  by the microprocessor (see Fig. II.24) as the clock pulse to the ADC of the signal analyzer which is operated in the external clock mode. This clock pulse samples the echo maximum amplitude at  $2\tau$  and stores it into the block memory of the signal analyzer starting from the first memory location of the block '2' for the initial value of  $\tau$ . In this method no waiting time is required after the acquisition of echo maximum for a given value of  $\tau$  and hence  $\tau$  can be incremented immediately after the acquisition of the previous sample. It has been realized in this process that there was a slight mismatch of the ADC clock pulse and the echo maximum amplitude for smaller values of  $\tau$ . The software program has, therefore, been modified to generate five ADC clock pulses around the echo maximum so that five samples around the echo maximum will be acquired into the signal analyzer for each value of  $\tau$ . This data is further processed off-line using BASIC programming facility of the signal analyzer. A program has been written in BASIC language to choose maximum of the five points stored in a given block (source) for each  $\tau$  and to store the maximum value chosen into another block (destination). The total time including off-line processing time required for this experiment scanning a  $\tau$  range of  $26 \mu\text{sec}$  to  $1200 \mu\text{sec}$  is about 4 minutes.

### Method III

In this method the echoes are completely acquired into the signal analyzer operated in the BASIC mode as a function of  $\tau$  and these echoes are processed off-line in the signal analyzer (a "BASIC" language program is written for off-line processing) for obtaining ZSEEM. The flow chart of the program (BASIC program which is synchronized with the microprocessor pulse sequence program) for the acquisition of echoes and processing for ZSEEM by this method is given in Fig. II.26. These programs are named "AVERAGE" and "PROCESS" respectively.

The microprocessor generates the pulse sequence and the trigger pulse for the acquisition of echoes into the signal analyzer. The trigger pulse is generated at  $(\tau_{\text{minus}} 10) \mu \text{ sec}$  after the second pulse so that the echoes are acquired starting from a point much before the echo maximum. The signal analyzer is programmed to average the echoes  $\approx 25$  times for each value of  $\tau$  and store the result in block '2'. The program "AVERAGE" then transfers the averaged echo into the floppy disk following which the data of block '2' is erased. Once this process is over the microprocessor program increments  $\tau$  and generates the next pulse sequence and the trigger pulse with the increased value of  $\tau$  and the corresponding echo is acquired by the signal analyzer.

It should be mentioned here that, after the echo signal is averaged ( $\approx 25$  times in our experiments) for a given value of  $\tau$  it has to be transferred to the floppy disk before the



Y = File number of the echoes stored in the floppy

Note: Y = 100 (i.e. totally 99 echoes are recorded for different values of  $\tau$ )

Fig. II.26 Flow chart of the program in BASIC language for the ZSEEM experiment by method III (a) The program "AVERAGE" and (b) The program "PROCESS".

microprocessor program generates the next sequence with increased  $\tau$ . Hence, the microprocessor has to wait until this transfer is done by the signal analyzer. As there is no provision in the signal analyzer to indicate to the microprocessor about the completion of the transfer we have adopted the following procedure for synchronizing the microprocessor program and the program "AVERAGE" executed by the signal analyzer. The pulse sequence is repeated nearly 30 times for a given value of  $\tau$ , whereas the trigger pulse for the data acquisition is generated only for the first 25 repetitions. The subsequent five repetitions will be dummy, during which period the averaged echo signal is transferred to the floppy. With this, the acquisition and transfer of echoes into the floppy disk by the signal analyzer under the BASIC program control is synchronized with the microprocessor program. In this way the signal analyzer acquires the desired number of echoes ( $\approx 100$ ) into the floppy (with file number 'one' for the first echo and 'two' for the second echo and so on) for various  $\tau$  values starting from about  $40 \mu\text{sec}$  to  $1150 \mu\text{sec}$ . The subsequent processing of the echo data stored in the floppy to obtain ZSEEN can be done off-line by the program "PROCESS" written in the BASIC language.

Upon the execution of the program "PROCESS" the off-line processing of the data starts and the first echo (from file number "one") is brought to block '2' from the floppy disk. The program then chooses the echo maximum and stores this maximum

value into the first memory location of Block '3'. After this is done the program erases the Block '2' data and brings the second file (second echo with the increased  $\tau$  value) from the floppy disk to the Block '2' and then chooses the echo maximum to store it in the second memory location of Block '3'. The process continues till all the 100 echoes are processed and at the end the ZSEEM spectrum stored in the block '3' is displayed.

From the point of view of data acquisition time and S/N ratio Method III is the optimum. In this method the averaging and acquisition of echoes (100 echoes) takes about 5 minutes and the off-line processing of these to obtain ZSEEM takes about 15 minutes for a typical  $\tau$  range of  $\approx 90 \mu\text{sec}$  to  $1200 \mu\text{sec}$ . Method III takes much less time and effort than Method I and at the same time gives improved signal-to-noise ratio. Method II takes an overall time of 6 minutes to obtain single ZSEEM pattern. Out of this about two minutes are spent for the acquisition and rest of the time for processing. Though, this method takes less time among all the three methods the S/N ratio is less than that obtained by Method III and is comparable with that obtained by Method I. ZSEEM spectra of  $^{35}\text{Cl}$  in powdered  $\text{KClO}_3$  recorded by the three methods are compared in Fig. II.27.

#### II.E(4) Automation of STEEM Experiment

For the automatic acquisition of STEEM signal, schemes similar to Method II and Method III of ZSEEM acquisition have



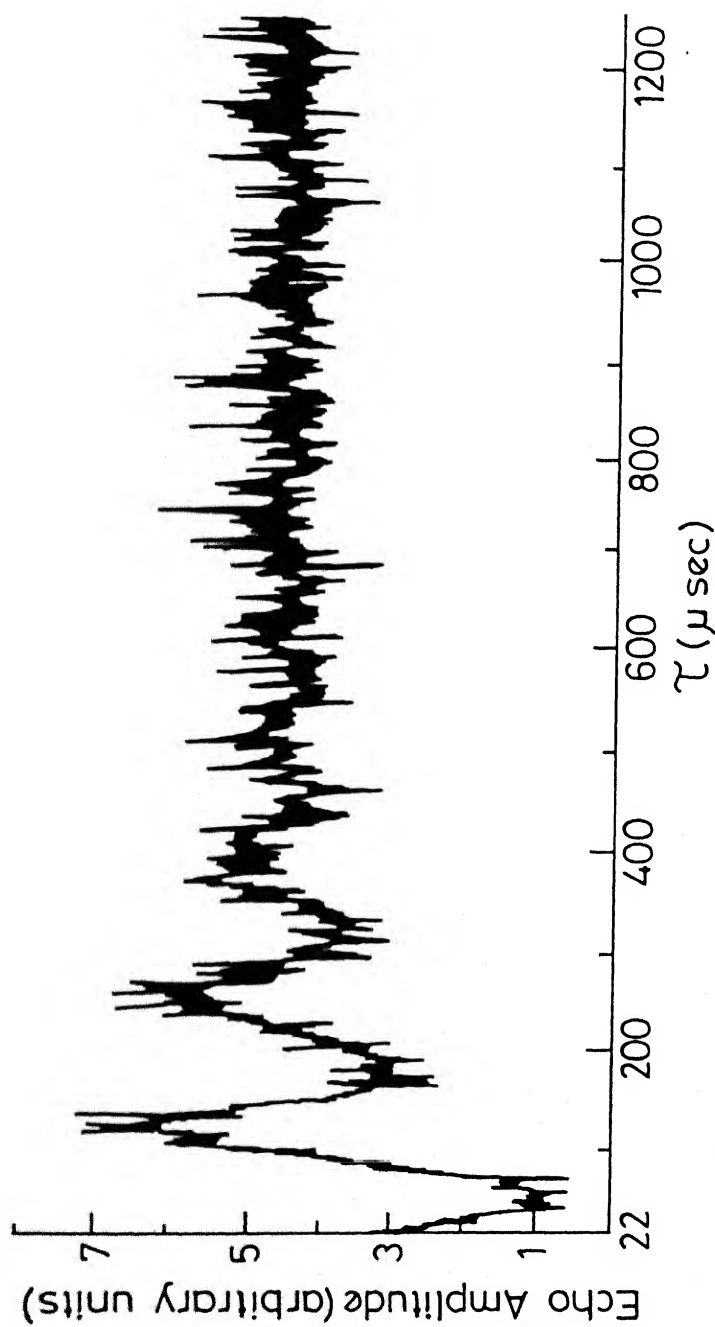


Fig.II.27 (a) Experimental  $^{35}\text{Cl}$  ZSEEM pattern in  $\text{KClO}_3$  obtained by Method I ( $\omega_0 = 28.0896 \text{ MHz}$ ) at  $\approx 298 \text{ K}$  with a magnetic field  $\approx 13.5 \text{ Gauss}$ .

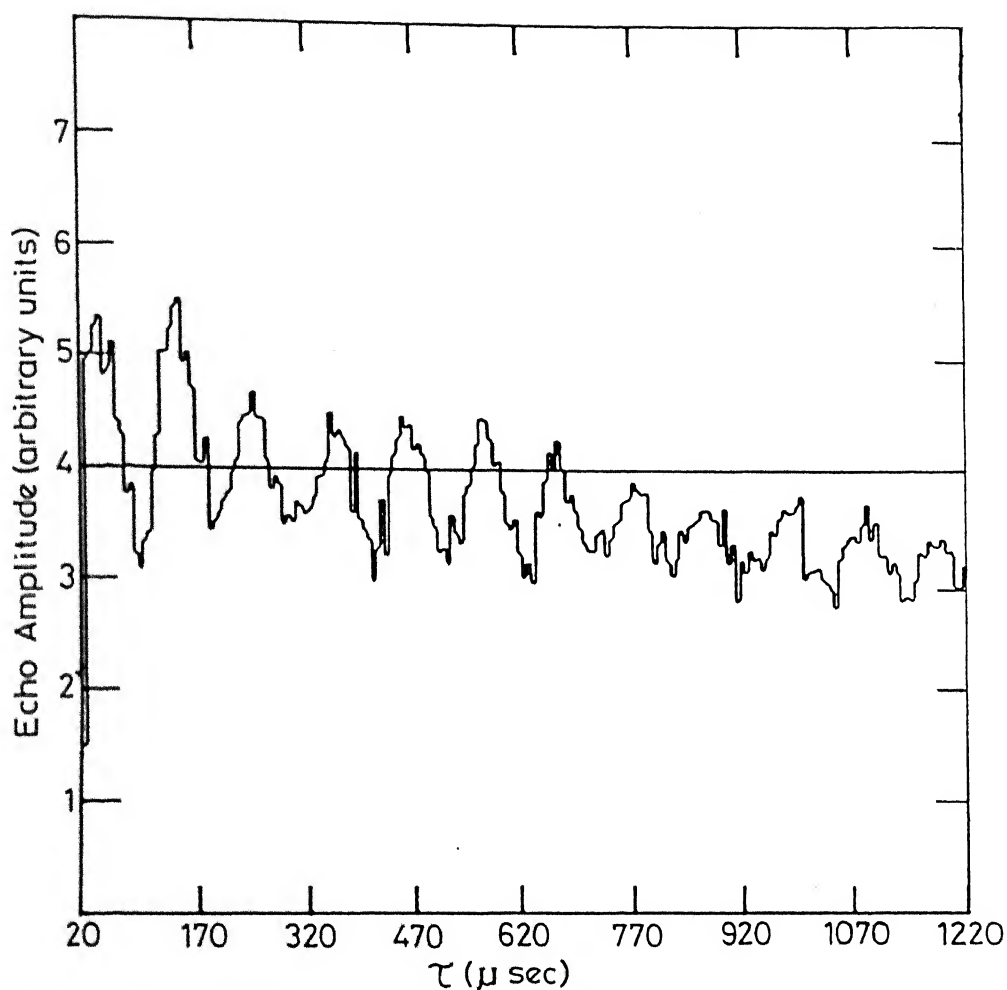


Fig.II.27(b) Experimental  $^{35}\text{Cl}$  ZSEEM pattern in  $\text{KClO}_3$  obtained by-  
Method II at  $\approx 298\text{K}$  ( $\omega_0 = 28.0896\text{MHz}$ ) with a magnetic  
field of  $\approx 13.5$  Gauss.

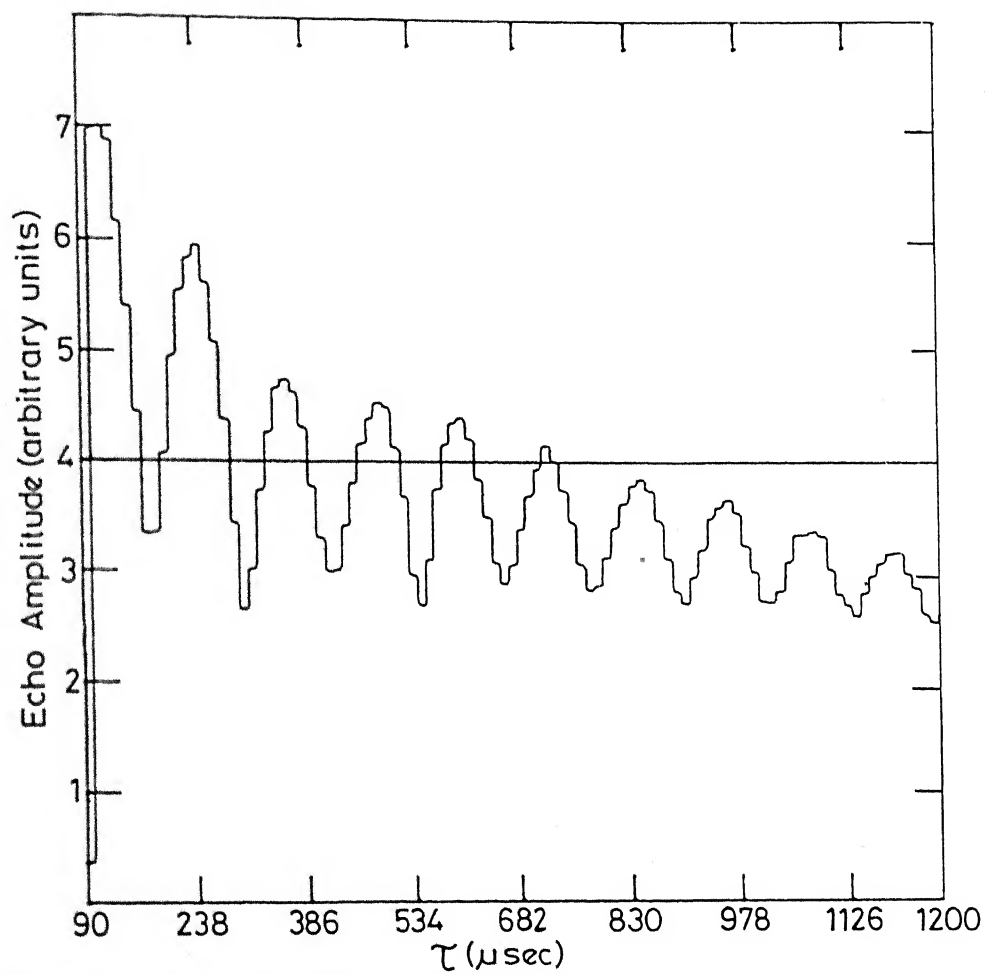


Fig.II-27(c) Experimental  $^{35}\text{Cl}$  ZSEEM pattern in  $\text{KClO}_3$  obtained by Method III at  $\approx 298\text{K}$  ( $\omega_0 = 28.0896\text{ MHz}$ ) with a magnetic field of  $\approx 13.5\text{ Gauss}$ .

been developed. A suitable software program has been written which enables the microprocessor to generate a three-pulse sequence as shown in Fig. II.28.

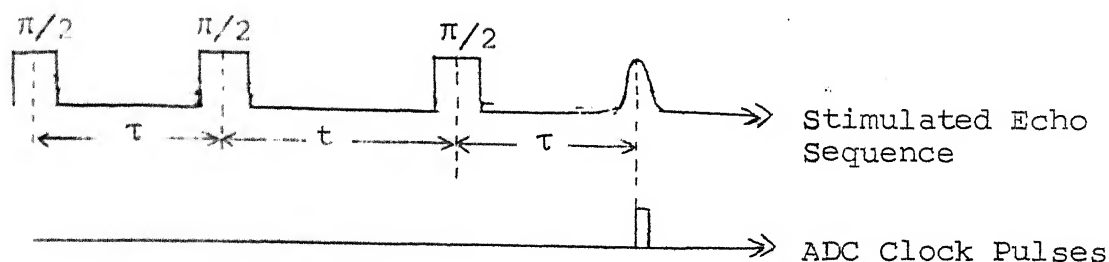


Fig. II.28 Stimulated echo sequence together with the ADC clock pulse for sampling the echo maximum

In the STEEM experiment one studies the stimulated echo amplitude as a function of the separation ' $t$ ' between the second and third pulses with a constant ' $\tau$ ' value. The stimulated echo forms after a time ' $\tau$ ' from the third pulse. Hence the ADC clock pulses (five) to the signal analyzer are generated by the microprocessor around  $\tau$  (in the Fig. II.28 only one ADC clock pulse is shown, but in the actual experiment five clock pulses are generated around the echo maximum). The microprocessor also generates a trigger pulse at the beginning of the experiment which enables the signal analyzer to start data acquisition. The data is acquired into 1 K of memory corresponding to two hundred ' $t$ ' values ranging from  $300 \mu\text{sec}$  to  $1300 \mu\text{sec}$ . This data is processed to choose the maximum of the five points using the BASIC language facility of the signal analyzer with the same program described earlier (in the Method II of ZSEEM) to obtain STEEM

pattern. The STEEM spectrum obtained by this scheme has poor S/N ratio. For this reason a method similar to that of Method III for ZSEEM is developed by the use of same BASIC programs written for ZSEEM (namely AVERAGE and PROCESS). For this purpose the ADC clock pulse shown in the Fig. II.28 is used for triggering the signal analyzer to capture the echo (in this case the trigger pulse is generated at  $(\tau_{\text{minus}} 10) \mu\text{sec}$  after the third pulse in order that the signal analyzer captures the echo starting from a point much before the echo maximum). In this way nearly hundred stimulated echoes are acquired (each averaged 25 times) for different values of 't' (ranging from  $\approx 300$  to  $1300 \mu\text{sec}$ ). As in the case of ZSEEM the acquisition is done under the control of BASIC program AVERAGE. The subsequent off line processing of these stimulated echoes to obtain STEEM patterns is done by the signal analyzer using the BASIC program "PROCESS" described earlier.

## II.F CAPABILITIES AND PERFORMANCE EVALUATION OF THE SPECTROMETER

In order to assess the performance of any scientific instrument and attach significance to the results produced by the instrument, it is necessary to first check if it is capable of reproducing known results. In this section we describe the capabilities of our microprocessor-controlled pulsed NQR spectrometer and present typical results obtained from various pulsed and multiple-pulse experiments. These results on known samples are

presented here to demonstrate the capabilities and quality of performance of the instrument.

## II.F(1) Typical FT-NQR Recordings

In this experiment signal averaging is required for improving signal-to-noise ratio. For this purpose a highly stable frequency source is required. In our spectrometer system the frequency of the r.f. source (HP-8640B) has been locked to an internal 1 MHz crystal source during the averaging process. The FID signals are first acquired and averaged by the signal analyzer under the supervision of the microprocessor (see section II.E), then the FFT of the FID is performed automatically under the BASIC program control. The FID of  $^{35}\text{Cl}$  in powder sample of  $\text{NaClO}_3$  obtained by an averaging over 500 transients is shown in Fig. II.29(a) and the corresponding FT-NQR signal is presented in Fig. II.29(b). The complete processing time for averaging and Fourier Transformation to obtain these signals was about a minute with the signal analyzer operated in the "BASIC" mode. The S/N ratio of the FT-NQR spectrum is comparable with CW NQR spectrum obtained from an injection- and phase-locked SRO spectrometer [69] averaged over a period of five minutes. Fig.II.29(c) presents the FT-NQR spectrum of  $^{35}\text{Cl}$  in powdered sample of  $\text{NaClO}_3$  with a Zeeman field ( $H_0$ ) of  $\approx 12$  Gauss. Here  $H_0$  has been applied in perpendicular direction to the coil axis and the spectrum has been obtained by averaging over 20,000 transients in  $\approx 30$  minutes.

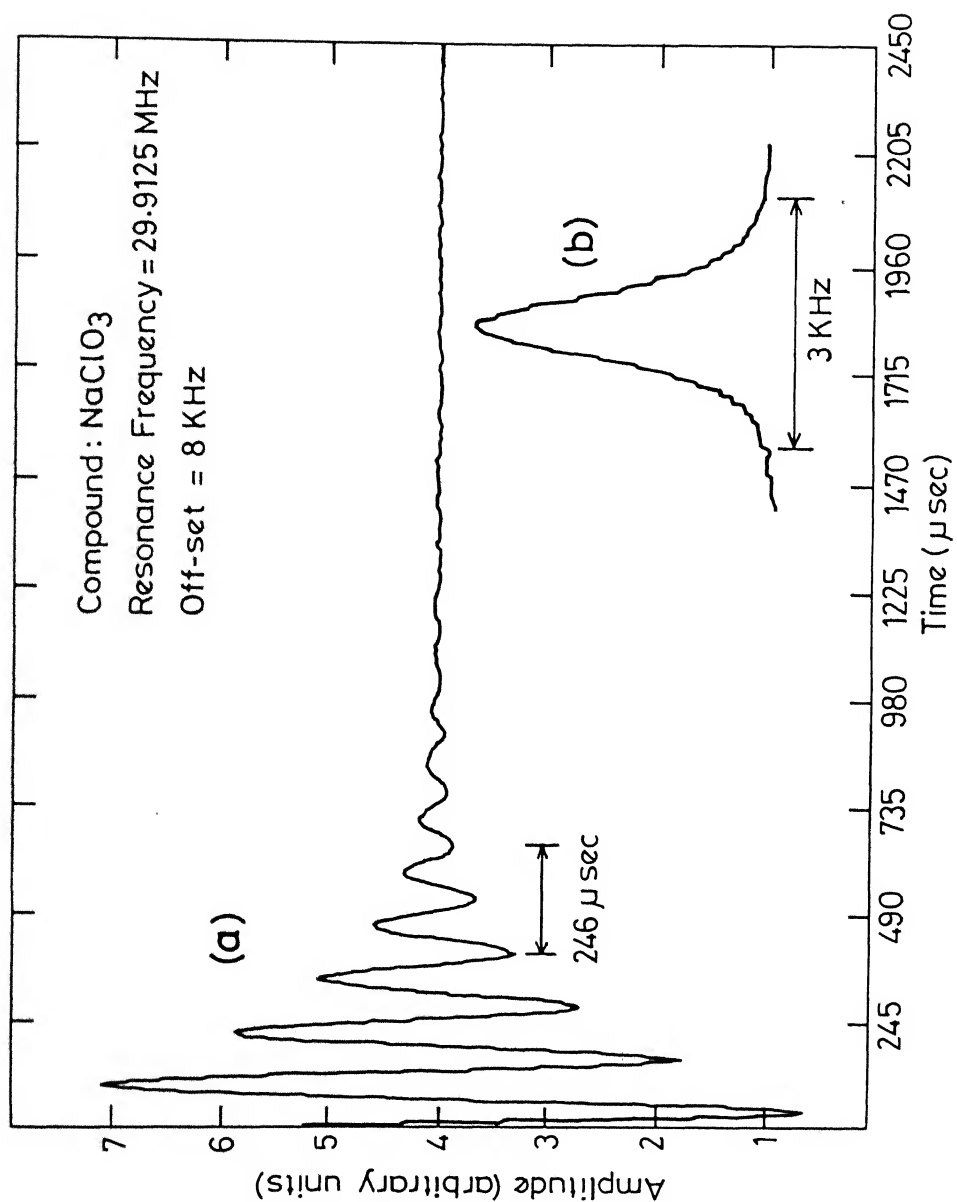


Fig. II.29 (a)  $^{35}\text{Cl}$  off-resonant FID from  $\text{NaClO}_3$  at room temperature.  
(b) FT-NQR spectrum of the above FID.

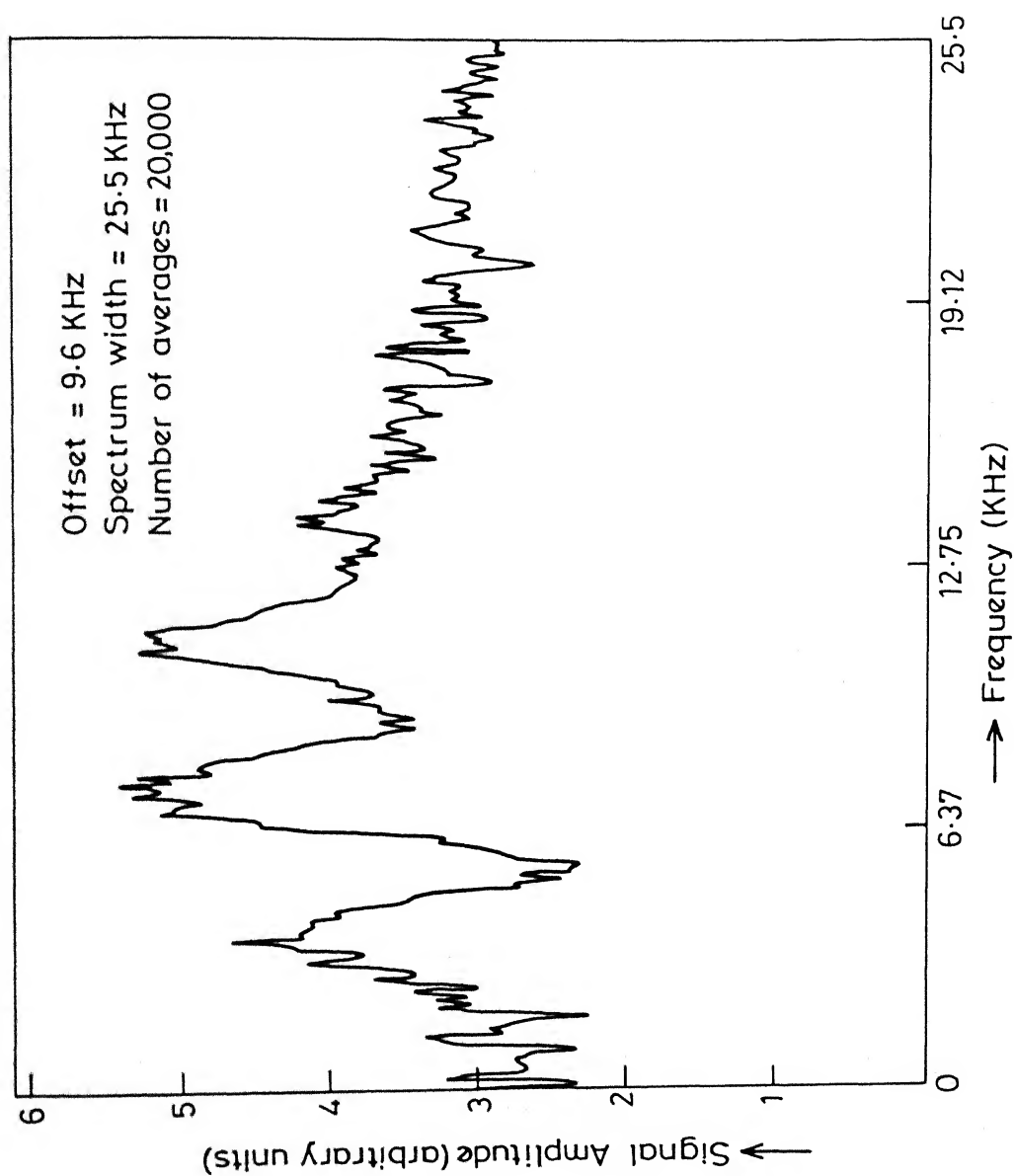


Fig. II.29 (c) Zeeman FT-NQR spectrum from  $^{35}\text{Cl}$  in  $\text{NaClO}_3$  ( $\omega_0 = 29.9524 \text{ MHz}$ ) with a magnetic field  $\approx 12 \text{ Gauss}$  ( $H_0 \perp H_1$ )



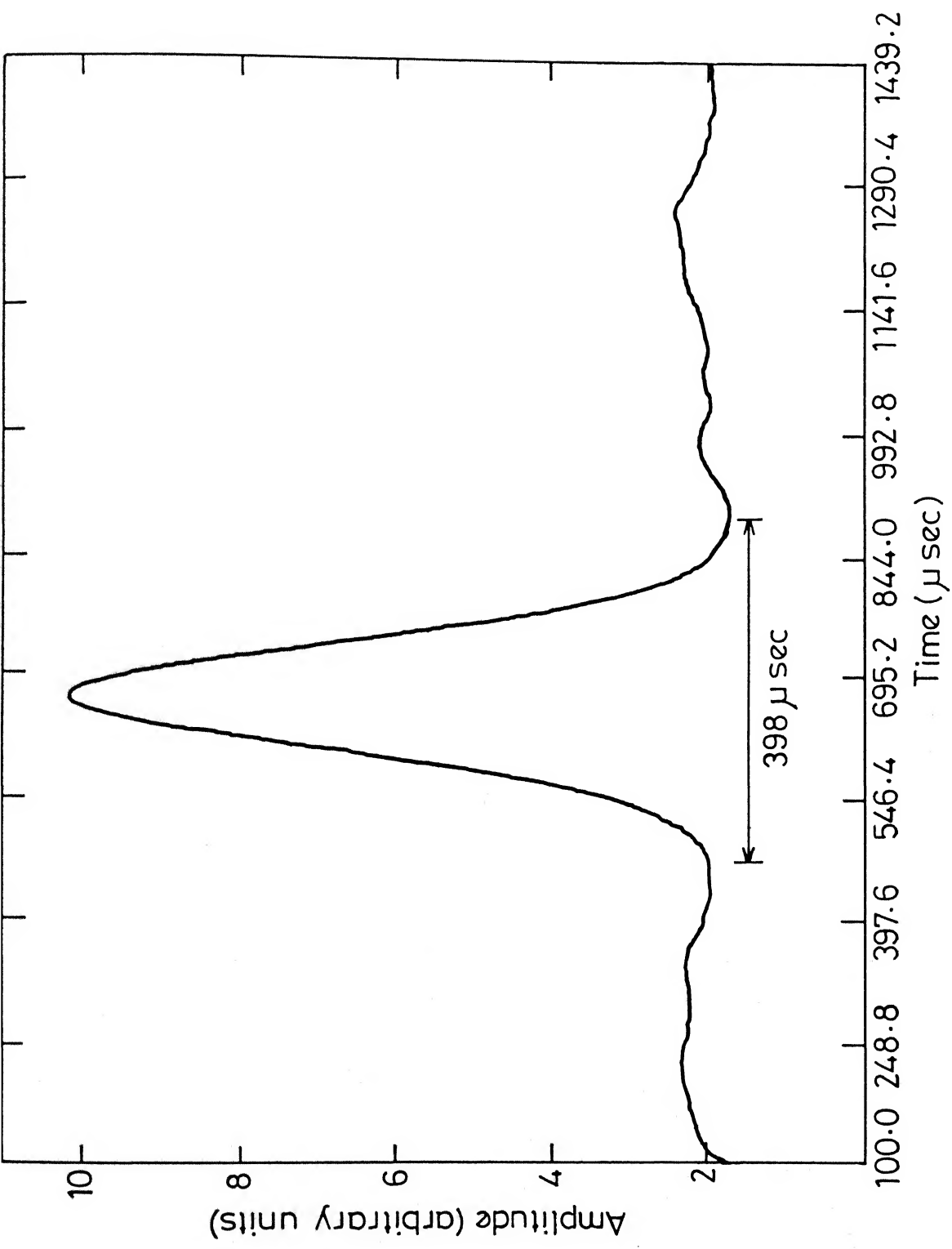


Fig.II.30 Spin echo signal of  $^{35}\text{Cl}$  in  $\text{NaClO}_3$  ( $\omega_0 = 29.9117 \text{ MHz}$ ) at room temperature ( $H_0 \approx 6 \text{ Gauss}$ ).

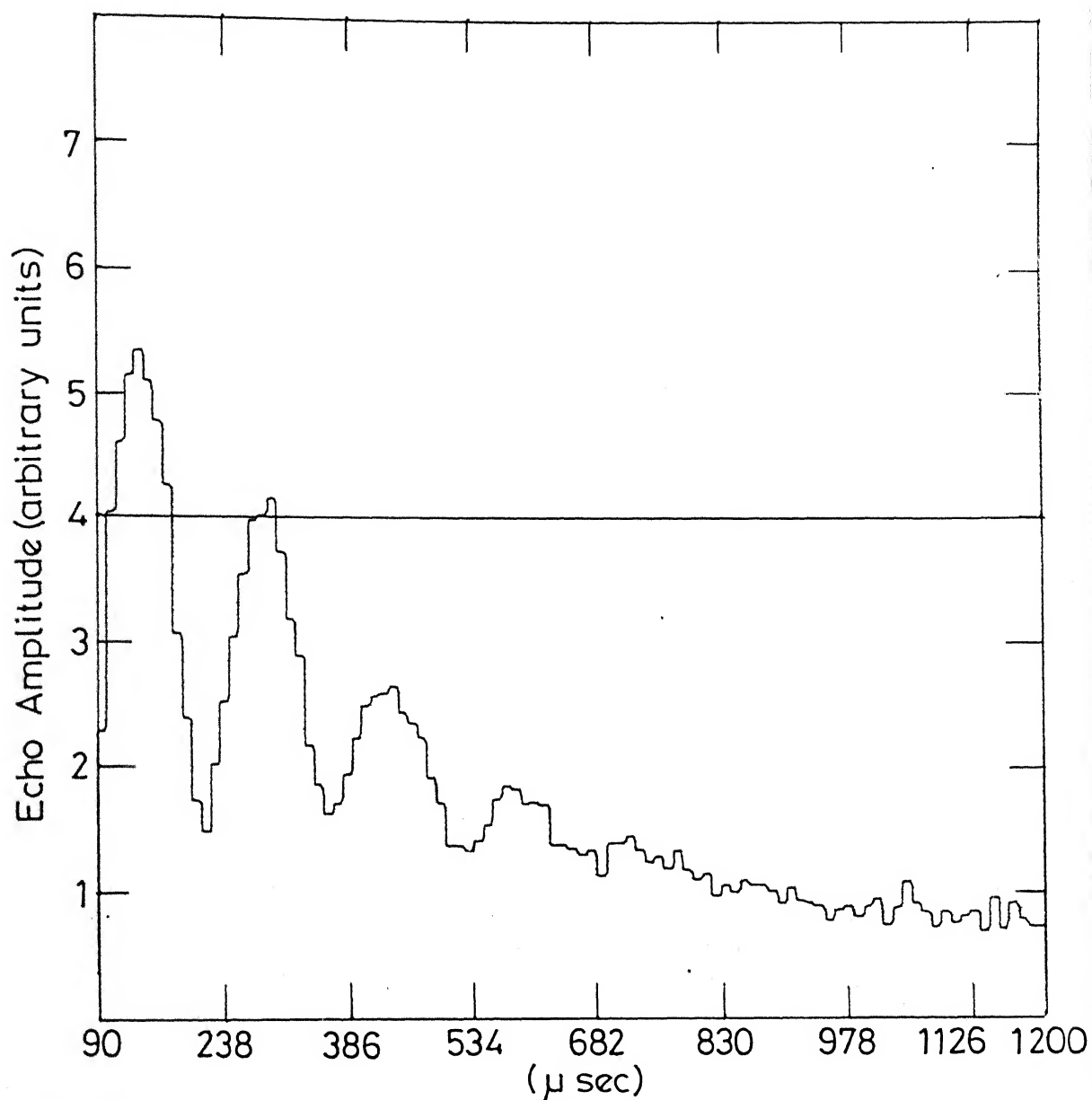


Fig.II.31 Experimental ZSEEM pattern from  $^{35}\text{Cl}$  in powdered sample of  $\text{SbCl}_3$  (site II;  $\omega_0 = 19.1713 \text{ MHz}$ ) with a magnetic field of  $\approx 9.75 \text{ Gauss}$  obtained from a series of two pulse experiments.

Clearly the FT method has resolved all the four lines which is not usually possible with C.W. methods where modulation broadening effects are severe.

## II.F(2) Spin Echo and ZSEEM Experiments

The  $^{35}\text{Cl}$  spin-echo signal obtained from a sample of powder  $\text{NaClO}_3$  in the presence of a weak Zeeman field of  $\approx 6$  Gauss and averaged over 100 repetitions is shown in Fig. II.30.

The ZSEEM pattern acquired by the signal analyzer under the supervision of the microprocessor and in the BASIC program control (see Method III in section II.E) from  $^{35}\text{Cl}$  nucleus in powder  $\text{SbCl}_3$  (Site 2,  $\omega_0 = 19.1713$  MHz) with a Zeeman field strength of 9.75 Gauss is presented in Fig. II.31. The above site in this compound has a non-zero asymmetry parameter (0.16) and has a short  $T_2$  value. These two factors are clearly seen from the ZSEEM spectrum. The pattern also agrees well with the one reported earlier [53] for this compound using an unautomated spectrometer.

## II.F(3) Response of Lee-Goldberg Experiment

Our present spectrometer is also capable of automatically acquiring the response of modified Lee-Goldberg experiment (see section II.E). This off-resonant experiment has been widely used in high resolution NMR of solids and also to some extent in NQR [70]. To evaluate the performance of the spectrometer we obtained the responses of  $^{35}\text{Cl}$  nucleus in a powder sample of  $\text{AgClO}_3$  to the

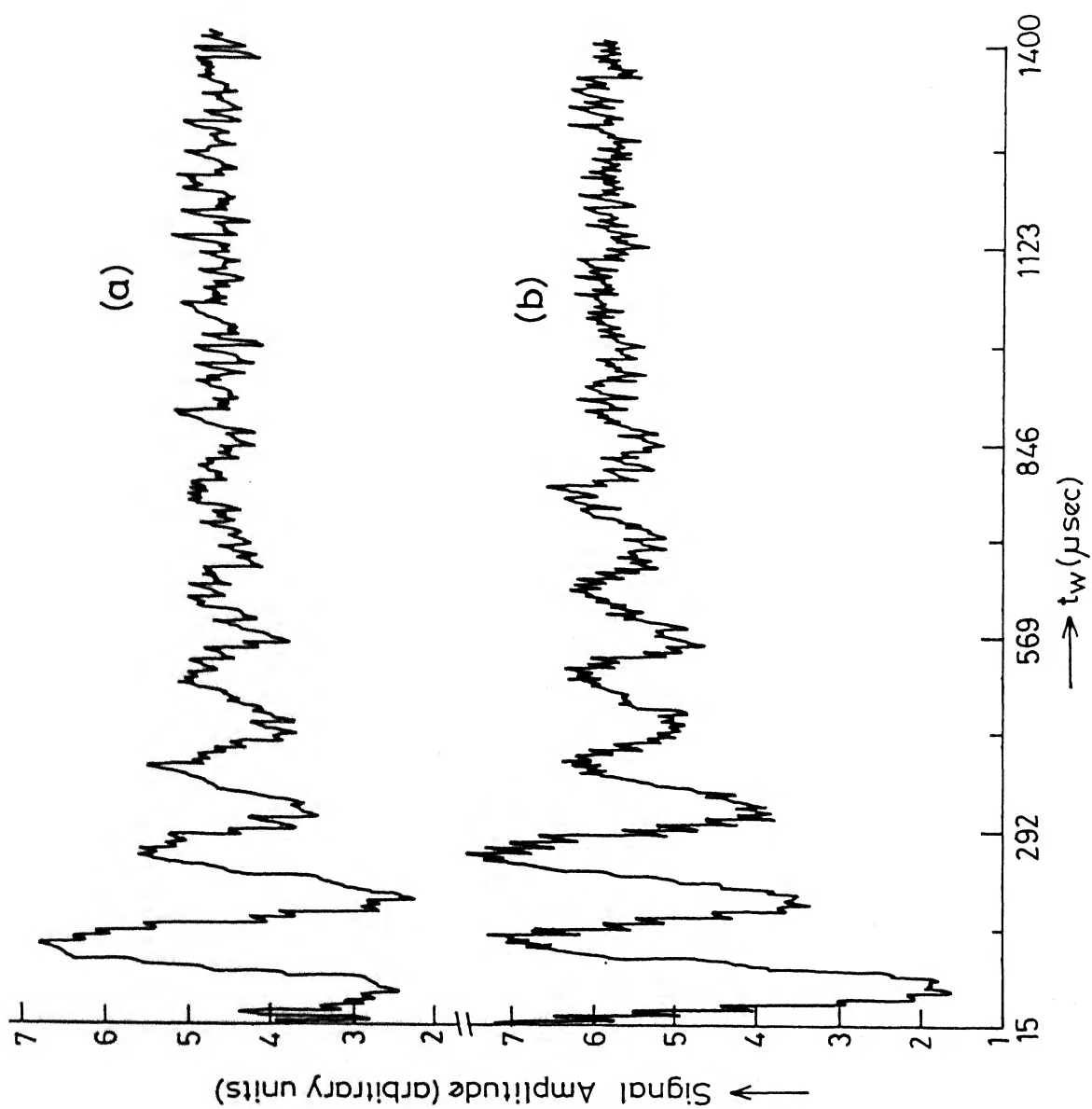


Fig. II-32 Response of  $^{35}\text{Cl}$  in powdered  $\text{AgClO}_3$  to modified Lee-Goldberg sequence: (a)  $H_0 = 0$  and (b)  $H_0 \approx 6.75$  Gauss.

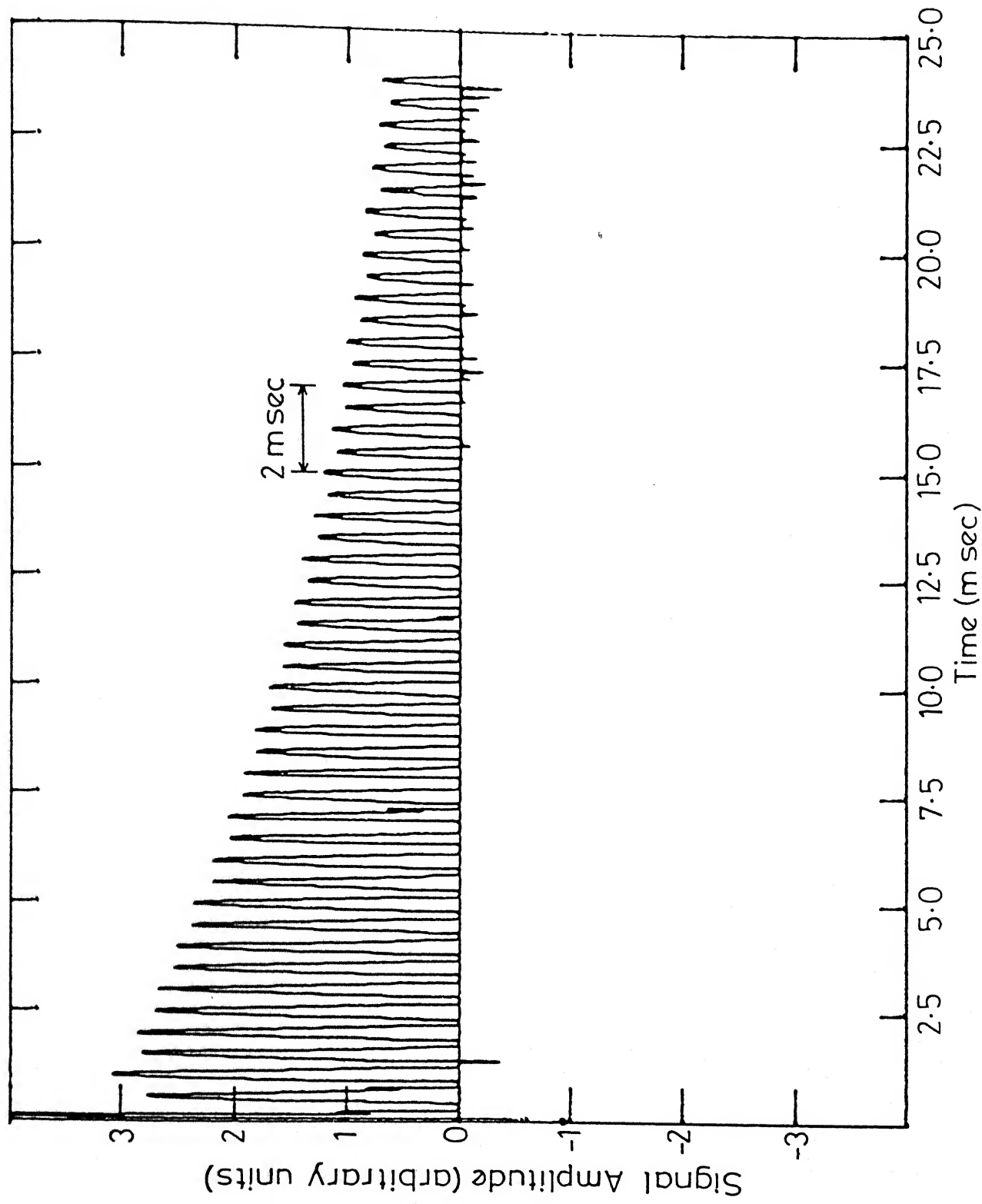


Fig.II.33 Response of  $^{35}\text{Cl}$  in powdered sample of  $\text{KClO}_3$  to CPMG pulse sequence in zero applied field

modified Lee-Goldberg sequence in the presence of a weak Zeeman field and without Zeeman field. These responses recorded with an off-set ( $\Delta\omega$ ) of 2 KHz are shown in the Fig. II.32(a) and Fig. II.32(b). The response shown in Fig. II.32(b) is comparable with that obtained earlier by plotting the Lee-Goldberg sequence response point-by-point as a function of the off-resonant pulse width [71].

#### II.F(4) Multiple-Pulse Response

The results of various multiple-pulse experiments on spin  $I = 3/2$  powder samples using the present microprocessor-controlled pulsed NQR spectrometer are presented in Chapter IV of the present thesis. As an example, we present here the response of  $^{35}\text{Cl}$  in the powdered sample of  $\text{KClO}_3$  to CPMG pulse sequence ( $\Delta\omega = 2.5$  KHz) in zero applied field (Fig. II.33). The response to 48  $\pi$ -pulses (applied along Y-axis) of the CPMG sequence with a value for  $\tau$  of 250  $\mu$  sec has been shown in the figure. This compound has a spin-spin relaxation time ( $T_2$ ) of the order of a msec. However, it can be seen from the Fig. II.33 that multiple-pulse response in this compound persists for a time much longer than  $T_2$  which is an indication of the elongation of transverse relaxation time under the influence of the CPMG sequence.

The results presented in this section clearly indicate the reliable performance and versatility of the spectrometer. Minor modifications of the spectrometer can enhance its capabilities

to study  $^{14}\text{N}$  nuclei at low frequency end, and also nuclei at the higher frequency end such as  $^{79,81}\text{Br}$ ,  $^{127}\text{I}$  etc.

### Summary

In this chapter, the details of automation and control of our pulsed NQR spectrometer using a microprocessor have been presented. Hardware details of the microprocessor and the software developed to generate various pulse sequences have been discussed. It has been demonstrated that the use of a microprocessor in pulsed NQR instrumentation gives considerable flexibility to perform virtually any kind of experiment that is known in modern pulse/multiple pulse NQR spectroscopy. Automation of various pulse experiments including ZSEEM and STEEM experiments have been described. BASIC programming facility of the signal analyzer together with the microprocessor has been used for the automation of these experiments. The performance capabilities of the spectrometer have been demonstrated by illustrating various experimental results obtained with different types of pulsed experiments.

In the next chapter the results of our experimental ZSEEM investigations using the microprocessor controlled pulsed NQR spectrometer will be presented. The results on the implementation of extended-time excitation technique to obtain ZSEEM in NQR will also be described in the next chapter.

REFERENCES

- [1] E.L. Hahn, Phys. Rev., 80, 580 (1950).
- [2] M. Bloom and R.E. Norberg, Phys. Rev., 93, 638 (1954).
- [3] E.L. Hahn and B. Herzog, Phys. Rev., 93, 639 (1954).
- [4] A. Geiger and M. Holz, J. Phys. E: Sci. Instrum., 13, 697 (1980).
- [5] P. Lalanne and S. Eletr, Rev. Sci. Instrum., 41, 71 (1970).
- [6] A.C. Lind, Rev. Sci. Instrum., 43, 1800 (1972).
- [7] D.J. Adduci, P.A. Hornung and D.R. Torgeson, Rev. Sci. Instrum., 48, 661 (1977).
- [8] J.D. Ellett Jr., M.G. Gibby, U.Haeberlen, L.M. Huber, M. Mehring, A. Pines and J.S. Waugh, Adv. Magn. Reson., 5, 117 (1971).
- [9] R.K. Shenoy, J. Ramakrishna and R. Srinivasan, J. Phys. E: Sci. Instrum., 9, 779 (1976).
- [10] G.B. Matson, Chem. Instrum., 6, 187 (1975).
- [11] Interface Technology, Inc., California, U.S.A.
- [12] R.F. Karlicek and I.J. Lowe, J. Magn. Reson., 32, 199 (1978).
- [13] Bruker, Spectrospin AG, Zurich, Switzerland.
- [14] C. Lapray, A. Briguet, J.C. Duplan and J. Delman, J. Magn. Reson., 23, 129 (1976).
- [15] D.J. Toms, Rev. Sci. Instrum., 45, 534 (1974).
- [16] F. Cavon and R.F. Herzog, J. Magn. Reson., 31, 357 (1978).
- [17] D.A. Wright and M.T. Rogers, Rev. Sci. Instrum., 44, 1189 (1973).
- [18] S.G. Huang and M.T. Rogers, Chem. Instrum., 8, 17 (1977).
- [19] A. Geiger and H.G. Hertz, J. Solution Chem., 5, 365 (1976).



- [20] Narsimha Reddy, Arun Bhavsar and P.T. Narasimhan, *Z. Naturforsch.*, 41a, 449 (1986).
- [21] R.E. Ader, A.R. Lepley and D.C. Songco, *J. Magn. Reson.*, 29, 105 (1978).
- [22] D.J. Adduci and B.C. Gerstein, *Rev. Sci. Instrum.*, 50, 1403 (1979).
- [23] H.S. Jalmes and Y. Barjhoux, *Rev. Sci. Instrum.*, 53, 1 (1982).
- [24] G.A. Mohr and Carl M. Edwards, *Rev. Sci. Instrum.*, 54, 1238 (1983).
- [25] M.E. Hale, H. Peemoeller, A.R. Sharp, *Rev. Sci. Instrum.*, 57, 689 (1986).
- [26] For example, as in the Bruker B-KR 300S spectrometer series.
- [27] M. Mehring and J.S. Waugh, *Rev. Sci. Instrum.*, 43, 649 (1972).
- [28] R.E.J. Sears, *Rev. Sci. Instrum.*, 55, 1716 (1984).
- [29] G. Bodenhausen, *J. Magn. Reson.*, 34, 357 (1979).
- [30] M. Hintermann, L. Braunschweiler, G. Bodenhausen, and R.R. Ernst, *J. Magn. Reson.*, 50, 316 (1982).
- [31] T. Frenkiel and J. Keeler, *J. Magn. Reson.*, 50, 479 (1982).
- [32] V. Radeka, R.L. Chase, M. Petrinovic and J.A. Glasel, *Rev. Sci. Instrum.*, 41, 1766 (1970).
- [33] K.E. Kisman and R.L. Armstrong, *Rev. Sci. Instrum.*, 45, 1159 (1974).
- [34] M.S. Conradi, *Rev. Sci. Instrum.*, 48, 359 (1977).
- [35] I.J. Lowe and C.E. Tarr, *J. Phys. E: Sci. Instrum.*, 1, 320 (1968).
- [36] P.K. Grannell, M.J. Orchard, P. Mansfield, A.N. Garroway and D.C. Stalker, *J. Phys. E: Sci. Instrum.*, 6, 1202 (1973).

- [37] D.I. Hoult and R.E. Richards, J. Magn. Reson., 22, 561 (1976).
- [38] R. Ramachandran and P.T. Narasimhan, J. Phys. E: Sci. Instrum., 16, 643 (1983).
- [39] Hewlett-Packard, California, U.S.A.
- [40] D.J. Adduci, P.A. Harnung and D.R. Torgeson, Rev. Sci. Instrum., 47, 1503 (1976).
- [41] M.R. Stoll, Rev. Sci. Instrum., 52, 391 (1980).
- [42] T.C. Farrar and E.D. Becker, "Pulse and Fourier Transform NMR", Academic Press, London (1971).
- [43] J.W. Cooper, "Topics in Carbon-13 NMR Spectroscopy," ed. G.C. Levy, Wiley Press, New York (1976).
- [44] "Progress in Nuclear Magnetic Resonance Spectroscopy," Vol. 14, p. 27-66 (1982), Ed. J.W. Emsley, J. Feeney and L.H. Sutcliffe.
- [45] T. Merrick, S. Smiriga and A. Pines, J. Magn. Reson., 14, 270 (1974).
- [46] S.D. Kunz and A.G. Redfield, Rev. Sci. Instrum., 54, 503 (1983).
- [47] N.L. Rhodes, B.P. Cross, S.L. Tignov and S.B.W. Roedev, Rev. Sci. Instrum., 44, 659 (1973).
- [48] D. Giesendanner, S. Sengupta and G. Litzistorf, J. Molec. Struct., 58, 519 (1980).
- [49] M. Gourdji and A. Pèneau, J. Molec. Struct., 83, 361 (1982).
- [50] D. Giesendanner, R. Lenk and G. Litzistorf, J. Phys. E: Sci. Instrum., 8, 8 (1975).
- [51] M.R. Smith and S. Cohn-Sfetcu, J. Phys. E: Sci. Instrum., 8, 515 (1975).

- [52] G.B. Matson, J. Magn. Reson., 25, 477 (1977).
- [53] R. Ramachandran and P.T. Narasimhan, Molec. Phys., 48 267 (1983).
- [54] 8253 Programmable Interval Timer, Intel Corporation, Santa-Clara, California, U.S.A.
- [55] MC-6840 Programmable Timer Module, Motorola Inc., Phoenix, Arizona, U.S.A.
- [56] MK-3886 Combo, Mostek Corporation, Carrollton, Texas, U.S.A.
- [57] Z8036 Counter/Timer and Parallel I/O Unit, Zilog Inc., Campbell, California, U.S.A.
- [58] Am-9513 System Timing Controller, Advanced Micro Devices, Sunnyvale, California, U.S.A.
- [59] M. Lee and W.I. Goldberg, Phys. Rev., A140, 1261 (1965).
- [60] H.Y. Carr and E.M. Purcell, Phys. Rev., 94, 630 (1954).
- [61] D. Gill and S. Meiboom, Rev. Sci. Instrum., 29, 688 (1958).
- [62] E.D. Ostroff and J.S. Waugh, Phys. Rev. Lett., 16, 1097 (1966).
- [63] U. Haeberlen, "High Resolution NMR in Solids: Selective Averaging," Supplement 1 to Advances in Magnetic Resonance, Ed. J.S. Waugh, page 74-77, Academic Press (1976).
- [64] J.S. Waugh, L.M. Huber and U. Haeberlen, Phys. Rev. Lett., 20, 180 (1968).
- [65] V.L. Ermakov and D. Ya. Osokin, Molec. Phys., 53, 1335 (1984).
- [66] P. Mansfield, J. Phys., C4, 1444 (1971).
- [67] W.K. Rhim, D.D. Elleman and R.W. Vaughan, J. Chem. Phys., 58, 1772 (1973).
- [68] The RST 7.5 Interrupt is enabled in the beginning of the program. If the vector interrupt key (VI) which is

provided on-board is pressed during program execution, the program jumps to location "20CE". Hence we write appropriate instructions required for the "measure mode" starting from location "20CE".

- [69] V. Harihara Subramanian, P.T. Narasimhan and K.R. Srivatsan, J. Phys. E: Sci. Instrum., 14, 870 (1981).
- [70] A.E. Mefed and B.N. pavlov, J. Molec. Struct., 83, 131 (1982).
- [71] R. Ramachandran, Ph.D. Thesis, Department of Chemistry, I.I.T., Kanpur (1982), Kanpur, India.

### CHAPTER III

ZEEMAN PERTURBED NUCLEAR QUADRUPOLE  
SPIN-ECHO ENVELOPE MODULATION (ZSEEM)  
STUDIES ON SPIN  $I = 3/2$  NUCLEI IN  
POWDER SPECIMENS

Equation (III.1) it is clear that the experimental measurement of the pure quadrupole resonance frequency  $\nu_Q$  alone is inadequate to determine the two unknown parameters  $e^2qQ$  and  $\eta$ . The application of an external Zeeman field is necessary to lift the degeneracy of the energy levels, so as to result in four transition frequencies centered around the pure quadrupole frequency. These frequencies can then be used to obtain the two NQR parameters  $\eta$  and  $e^2qQ$  [1]. Zeeman NQR spectroscopy has been utilized in the literature to obtain these parameters in both single crystal [2] and polycrystalline specimens [3-5]. Treating the Zeeman interaction as a perturbation on the quadrupolar interactions, Morino and Toyama [3] have shown that  $\eta$  can be determined accurately from the Zeeman NQR line shapes obtained for parallel orientation of r.f. and Zeeman fields in polycrystalline samples. The salient features in the powder pattern, for non-zero  $\eta$ , are the singularities at

$$\nu = \nu_Q \rho + (1 \pm \eta) \nu_0 \quad \dots \text{(III.2)}$$

$$\text{and } \nu = \nu_Q \rho - (1 \pm \eta) \nu_0 \quad \dots \text{(III.3)}$$

$$\text{where } \nu_Q = \frac{e^2qQ}{2h}$$

$$\text{and } \nu_0 = \frac{\gamma}{2\pi} H_0$$

here  $\nu_0$  is the Larmor frequency, and  $\rho = (1 + \frac{\eta^2}{3})^{1/2}$  can be determined from the splitting of the adjacent singularities.

To first order in  $\eta$  and  $H_0$ , the separation between the adjacent

singularities is given by

$$\Delta\nu = 2 \eta\nu_0 \quad \dots \text{ (III.4)}$$

Morino and Toyama [3] have described an extrapolation method for obtaining  $\eta$  from powder Zeeman NQR spectra recorded at several Zeeman fields. Due to the fact that the experimental Zeeman NQR spectra, in general, have very poor signal-to-noise ratios, the unambiguous measurements of splittings are difficult. Hence, several workers [4, 5, 6-8] have used the method of direct comparison of computer simulated Zeeman NQR powder patterns and the experimental Zeeman NQR spectra usually at lower fields to obtain  $\eta$  values. The method of Morino and Toyama is devoid of a principal error that plagues the single crystal experiments (i.e. the error due to misalignment of the crystal with respect to the external field direction). However, the powder method suffers from the drawback that the intensity of the signal deteriorates even at relatively low Zeeman field strengths before the paired singularities become well resolved. In order to increase the signal-to-noise ratio in the Zeeman NQR spectrum, one increases the modulation depth in CW spectrometers. It is well known that the increase in the modulation depth increases the width of NQR lines and the spurious kinks in the modulation broadened spectra may be erroneously identified as " $\eta$ -kinks" [5]. This was infact the reason for the discrepancy in the  $\eta$  values obtained for  $\text{HgCl}_2$ , at the site of  $^{35}\text{Cl}$ ,

from single crystal and powder studies. Harihara Subramanian and Narasimhan [5] have discussed the origin of the discrepancy in the  $\eta$  values obtained from the two methods and attributed to the erroneous identification of the  $\eta$ -kinks to modulation-broadened background of the steady-state powder Zeeman NQR spectra. They used an injection- and phase-locked SRO type NQR spectrometer and employed coherent signal averaging technique which improved the signal-to-noise ratio and reduced the possibility of modulation broadening and compared their experimental powder Zeeman spectra with those of computer simulated ones. By this method they could get  $\eta$  value for  $\text{HgCl}_2$  which is in good agreement with single crystal results.

The higher sensitivity and convenience of employing long-term signal averaging in pulsed NQR spectrometers (see section III.D) is expected to further facilitate the evaluation of  $\eta$  from Zeeman NQR studies of polycrystalline samples. The Zeeman-perturbed spin echo envelope modulation (ZSEEM) function,  $\mathcal{E}(2\tau)$ , is expected to contain information on  $\eta$ , since the energy levels of a Zeeman perturbed quadrupolar nucleus are  $\eta$ -dependent. A systematic analysis of ZSEEM pattern is therefore expected to give valuable information on the asymmetry parameter  $\eta$ . To understand and appreciate the information content of echo envelope modulation it is necessary to study the origin of modulation and conditions required for observing these modulations. These



aspects are discussed in the following section (section III.B).

### III.B GENERAL BACKGROUND ON SPIN ECHO ENVELOPE MODULATION

In spin-echo experiments a periodic variation of amplitude associated with small splittings of the resonance line is observed in the envelope of echoes which is obtained by plotting the echo amplitude against the pulse separation  $\tau$ . This effect can be used to measure finer splittings even when they are too small to be resolved by CW methods in the presence of inhomogeneous line broadening. The origin of resonance line splitting, which is responsible for echo envelope modulation, is different in different branches of magnetic resonance. Whereas in the case of NMR the indirect J-coupling [9] is responsible for the modulation, in electron paramagnetic resonance [10-12] it is the hyperfine coupling and in NQR spectroscopy, the Zeeman splitting and also J-coupling [13] are responsible for these modulation effects. Two-pulse and stimulated echo sequences can both be used for this study. The two-pulse echo envelope contains sum and difference of split frequencies apart from actual splitting frequencies ( $\omega_a$  and  $\omega_b$ ). A display of the splitting frequencies without such combinations can, however, be obtained by performing a stimulated echo experiment and plotting the echo amplitude as a function of the time ( $t$ ) between second and third pulses. Fig. III.1 shows a general case of splitting associated with two sets of spin states  $|\alpha\rangle$  and  $|\beta\rangle$ . It shall be noted that

transitions are possible from each  $|\alpha_i\rangle$  state to more than one  $|\beta_j\rangle$  states (branching transitions):

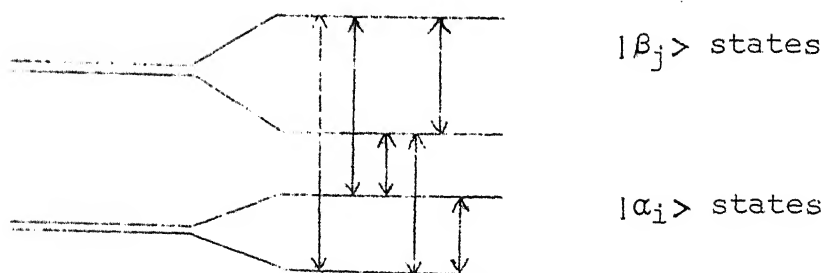


Fig. III.1 Splitting of degenerate spin states due to fine interaction.

The branching of transitions is responsible for the observation of echo envelope modulation effect. When branching transitions occur, the resonant pulses induce coherent relationships between the states within the  $\alpha$  and  $\beta$  manifolds as well as between states in opposite manifolds. This leads to interference effects in the spin echo and hence to the modulation of the echo envelope. Experimentally, only those modulation frequencies which lie within  $2\gamma H_1$  ( $H_1$  is the strength of resonant field) are effectively in resonance with the alternating field and are therefore able to contribute to the modulation effects [14]. It is, therefore, not possible to observe the modulation effect in the echo envelope with low  $H_1$  field when the energy level splittings are large.

If we now consider the special case of a Zeeman perturbed quadrupolar spin system with  $I = 3/2$ , it is evident that a

coherent pulse excitation of all the branching transitions would lead to spin echo envelope modulations, with frequencies corresponding to the Zeeman splittings  $\omega_a$  and  $\omega_b$ , and also their sum and differences frequencies in the case of a two-pulse experiment. Due to the insensitivity of the spin echo signal to

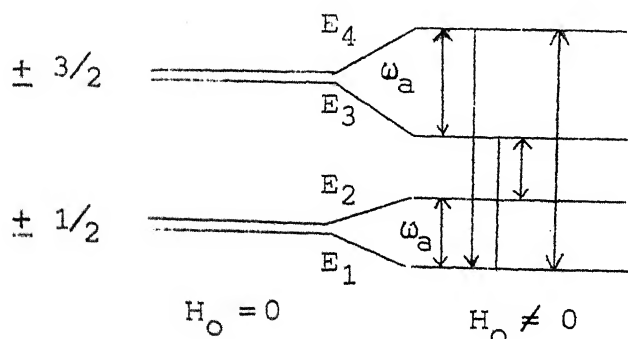


Fig. III.2 Zeeman splittings of the nuclear quadrupole energy levels of spin  $I = 3/2$  systems

static inhomogeneities, small Zeeman splittings will also be observed as echo envelope modulations even when they are obscured in the steady-state experiments. Apart from its dependence on  $\eta$ , the spin echo envelope modulation function,  $\mathcal{E}(2\tau)$ , is also dependent on the angles  $\theta$  and  $\phi$ , depending the mutual orientation of the external fields and the principal axes of the efg tensor, owing to the dependence of the various energy levels and the transition probabilities on these angles. There are two conditions required to be fulfilled to observe Zeeman-perturbed spin echo envelope modulation, namely, i) the Zeeman splittings  $\omega_a$  and  $\omega_b$  of the upper and lower levels, respectively

but  
7 ph

(see Fig. III.2) should be larger than the frequency width of the spin packets that make up the inhomogeneously broadened NQR line, and (ii) the r.f. field is such that  $\gamma H_1 \gg \omega_a$  and  $\omega_b$ . The first condition ensures the occurrence of several modulation periods within the echo decay time, the latter ensures the excitation of all the branching transitions.

Sapozhnikov and Yasman [13] have attempted an analysis of the polycrystalline specimen ZSEEM patterns for spin  $I = 3/2$  nuclei, for a parallel orientation of the external magnetic field and the exciting r.f. field. Their method of simulation of ZSEEM is of questionable validity due to the assumption that  $\mathcal{E}(2\tau)$  contains frequency components at only  $\omega_b$ , that corresponds to the Zeeman splitting of the lower energy level. In reality  $\mathcal{E}(2\tau)$  contains  $\omega_a$ ,  $\omega_b$  and  $(\omega_a + \omega_b)$  and  $(\omega_a - \omega_b)$  components in a two-pulse experiment [14, 15]. Ainbinder et al. [16] obtained an expression for  $\langle I_x \rangle$  by examining the problem for an arbitrary spin and an arbitrary orientation of the external magnetic field relative to the principal axes of the efg tensor when  $H_1 = H_{1x}$  for the case of single crystals. Hence, this study is of little use for a detailed analysis of the Zeeman-perturbed SEEM patterns obtained from polycrystalline specimens. Zakirov and Safin [17] have calculated the echo envelope shape in powders for spin  $3/2$  nuclei. They have obtained relation between  $\eta$  and experimentally measured parameters. They have not given details of their calculation explicitly. Ramachandran and Narasimhan [15]

have used the density matrix formalism to compute the response of a Zeeman-perturbed nuclear quadrupole spin  $I = 3/2$  ensemble to a resonant two-pulse excitation. They have considered the parallel orientation of the external fields,  $H_1$  and  $H_0$ , and calculated  $\epsilon(2\tau)$  for arbitrary orientation of these fields with respect to cpg principal axes. They have powder averaged the theoretical response on a computer and compared theoretically simulated ZSEEM spectra with experimental ones to determine  $\eta$  values. They have used for recording the experimental ZSEEM a pulsed spectrometer [18], where the settings of pulse separation ( $\tau$ ) and of the delay for opening the boxcar sampling gate are manually adjusted and they found it extremely cumbersome to perform these experiments [15]. To overcome these difficulties we have used the microprocessor-controlled pulsed NQR spectrometer system [19] described in Chapter II of the present thesis, for these studies.

We now briefly outline the theoretical analysis of ZSEEM from spin  $3/2$  powder samples in the following section (section III.C).

### III.C THEORETICAL ANALYSIS OF ZSEEM FOR SPIN $3/2$ NQR SYSTEMS

In Chapter I (see section I.B(2)) we discussed the utility of density matrix formalism to obtain theoretical expression for the transient response from a spin  $I = 3/2$  NQR system as a result of the application of a resonant r.f. pulse of duration

$t_w$ . Echo envelope modulation can be studied using a series of two-pulse experiments. We shall extend here the analysis of section I.B(2) to the response of spin  $3/2$  systems to a two-pulse sequence with a pulse separation of  $\tau$ . We then go on to calculate the response of the system to a two-pulse sequence in the presence of small Zeeman field which yields ZSEEM and which is the subject matter of this chapter.

### III.C(1) Response of Spin $I = 3/2$ Systems to a Two-Pulse Sequence in the Absence of Zeeman Field

Let us consider a two pulse sequence with equal pulse width and a separation of  $\tau$  as depicted in Fig. III.3.

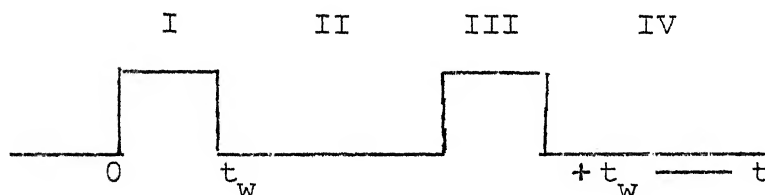


Fig. III.3 Two-pulse spin echo sequence

We are concerned here with the calculation of the signal induced in the r.f. coil after the second pulse. By following the theoretical analysis discussed in Chapter I (see section I.B(2)) we can calculate the evolution of the spin system during two sets of periods of nutation (periods I and III) and free precession (periods II and IV) and occur in a spin echo sequence (Fig. III.3). The evolution operators being  $\exp(-i\mathcal{H}^*t)$  for

the regions I and III and  $\exp[-\frac{i(\Delta\omega)}{2}\mathcal{H}_Q t]$  for regions II and IV. Here  $\mathcal{H}^*$  is the effective Hamiltonian in the interaction representation defined in Chapter I (section I.B.(2)) and  $\Delta\omega$  is the offset. The definition of 't' for various regions is as follows:

$$0 \leq t_1 \leq t_w \quad (\text{for region I})$$

$$t_w \leq t_2 \leq \tau \quad (\text{for region II})$$

$$\tau \leq t_3 \leq (\tau + t_w) \quad (\text{for region III})$$

$$t_4 > (\tau + t_w) \quad (\text{for region IV})$$

We then obtain the density matrix  $\rho(t_4)$  describing the evolution of the system after the second pulse (region IV in Fig. III.3).

$$\rho(t_4) = U_4 U_3 U_2 U_1 \rho(0) U_1^{-1} U_2^{-1} U_3^{-1} U_4^{-1} \quad \dots(\text{III.5})$$

where  $U_1$ ,  $U_2$ ,  $U_3$  and  $U_4$  are the evolution operators in the four regions depicted in Fig. III.3 and are given by

$$U_1 = \exp(-i\mathcal{H}^* t_1) \quad \dots(\text{III.5(a)})$$

$$U_2 = \exp[-\frac{i}{2}(\Delta\omega) \mathcal{H}_Q t_2] \quad \dots(\text{III.5(b)})$$

$$U_3 = \exp(-i\mathcal{H}^* t_3) \quad \dots(\text{III.5(c)})$$

$$U_4 = \exp[-\frac{i}{2}(\Delta\omega) \mathcal{H}_Q t_4] \quad \dots(\text{III.5(d)})$$

The details of the calculation for the evolution of the density matrix can be found in references [15, 22].

Once we have the density matrix in hand we can calculate the expectation value of  $I_x$  and hence the signal ( $\Delta V_x$ ) induced in the coil. Thus, we find

$$\Delta V_x = K\sqrt{3} \left(\frac{\omega_0^2}{4KT}\right) \left\{ \sin \alpha \cos^2 \frac{\alpha}{2} \cos \omega_0 t + \sin \alpha \cos \alpha \cos [\omega_0(t-\tau)] - \sin \alpha \sin^2 \frac{\alpha}{2} \cos [\omega_0(t-2\tau)] \right\} \quad \dots \text{(III.6)}$$

Introducing the spread in resonance frequencies one obtains,

$$\begin{aligned} \Delta V_x = K\sqrt{3} \left(\frac{\omega_0^2}{2KT}\right) \left\{ \sin \alpha \cos^2 \frac{\alpha}{2} \cos \omega_0 t \exp\left(-\frac{t^2}{2T_2^{*2}}\right) \right. \\ \left. + \sin \alpha \cos \alpha \cos [\omega_0(t-\tau)] \cdot \exp\left[-\frac{(t-\tau)^2}{2T_2^{*2}}\right] \right. \\ \left. - \sin \alpha \sin^2 \frac{\alpha}{2} \cos [\omega_0(t-2\tau)] \cdot \exp\left[-\frac{(t-2\tau)^2}{2T_2^{*2}}\right] \right\} \\ \dots \text{(III.6(a))} \end{aligned}$$

where  $\alpha = \frac{\sqrt{3}}{2} \gamma H_1 t_w$

and  $t \geq \tau + t_w$  and  $\tau \gg t_w$ .

The first term in the equation (III.6(a)) represents the remnants of the FID following the first pulse. If  $\tau \gg T_2^*$ , this signal will decay before the application of the second pulse, the second term gives the FID following the second pulse which has a maximum at  $t = \tau$ . The third term represents the echo signal which has a maximum at  $t = 2\tau$ . The envelope of the echo maximum



plotted as a function of  $\tau$ , decays with an exponential time dependence, characterized by the time constant  $T_2$ , where  $T_2$  is the spin phase memory time or the spin-spin relaxation time.  $T_2$  usually has a higher value than  $T_2^*$  [20]. While  $T_2^*$  has contributions from both inhomogeneous and homogeneous line broadening mechanisms,  $T_2$  has contributions only from the latter.

Although the case of two pulses of equal widths has been considered, the results are similar for any combination of two pulse sequence. Only the overall signal amplitude will differ, depending on the magnitudes of constant factors involving trigonometric functions of  $(\omega_1 t_w)$ .

### III.C(2) Response of Spin I = 3/2 Systems to a Two-Pulse Sequence in the Presence of Perturbing Zeeman Field

In the presence of a finite magnetic field ( $H_0$ ), the doubly degenerate nuclear quadrupole energy levels split (see, Fig. III.2) depending upon the strength and the direction of  $H_0$  relative to the principal axes of the efg tensor we wish to calculate the echo intensity  $\mathcal{E}(2\tau)$  as a function of  $\tau$ , due to the excitation of branching transitions between various quadrupolar levels split by the Zeeman field. Relaxation processes, in general, cause the echo to decay. These effects are not considered in the calculation of  $\mathcal{E}(2\tau)$ . The damping of echo envelope modulation due to relaxation process can be incorporated into  $\mathcal{E}(2\tau)$  later on.

The total Hamiltonian for a spin  $I = 3/2$  nucleus in an asymmetric efg ( $\eta \neq 0$ ) and a Zeeman field is,

$$\mathcal{H}_0 = \mathcal{H}_Q + \mathcal{H}_Z \quad \dots (III.7)$$

$$\text{where } \mathcal{H}_Q = \frac{e^2 q Q}{4I(2I-1)} \left[ 3 \hat{I}_Z^2 - \hat{I}^2 + \eta (\hat{I}_x^2 - \hat{I}_y^2) \right] \quad \dots (III.8)$$

$$\text{and } \mathcal{H}_Z = - \gamma \hbar \hat{H} \cdot \hat{I} \quad \dots (III.9)$$

For arbitrary  $\eta$  values, considering the approximation  $|\mathcal{H}_Q| \gg |\mathcal{H}_Z|$ , the wavefunctions and the energy levels can be obtained by treating the Zeeman term as a perturbation on the quadrupole levels [21]. This solution gives the required transformation matrix  $[T]$ , between the pure quadrupole basis  $(\phi_i)$  and Zeeman basis  $(\xi_i)$  [15, 22] i.e.,

$$[\xi_i] = [T][\phi_i] \quad \dots (III.10)$$

In this section we are concerned with two-pulse response in the presence of a Zeeman field. The main difference between the present case and that discussed in section III.C(2) is that, here we have the thermal equilibrium reduced density matrix over Zeeman basis to start with. Further, the nutation and free precession occur in the presence of Zeeman interaction apart from the main quadrupolar interaction. However, it should be noted that during the nutation periods the evolution is considered by

neglecting Zeeman interaction for simplicity. Then the evolution operators are transformed into the Zeeman basis.

Adapting the density matrix formalism (see section I.B(2) of Chapter I) for this case we can arrive [15] at the density matrix  $\rho(t_4)$  describing the evolution of the spin system after the second pulse of echo sequence. For this purpose it is advantageous to go to an interaction representation defined earlier in Chapter I (section I.B(2)).

$$\rho(t_4) = S_4 S_3 S_2 S_1 \rho(0) S_1^{-1} S_2^{-1} S_3^{-1} S_4^{-1} \quad \dots \text{(III.11a)}$$

$$\text{(or)} \quad \rho(t_4) = S \rho(0) S^{-1} \quad \dots \text{(III.11b)}$$

where  $S = S_4 S_3 S_2 S_1$  and the evolution operators  $S_1$ ,  $S_2$ ,  $S_3$  and  $S_4$  correspond to the regions I, II, III and IV, respectively, of Fig. III.3. From the density matrix (equation III.11b) we can obtain the expectation values of  $\langle I_i \rangle$   $i = x, y, z$  i.e.,

$$\langle I_i \rangle_{i=x, y, z} = \text{Tr} [\rho(t_4) I_i] \quad \dots \text{(III.11c)}$$

The induced signal can be obtained from the expectation values of  $I_i$  ( $i = x, y, z$ ) resolved along the axis of the coil, i.e.,

$$I(t) = I_x \sin\theta \cdot \cos\phi + I_y \sin\theta \cdot \sin\phi + I_z \cos\theta \quad \dots \text{(III.11d)}$$

where  $\theta$  and  $\phi$  are polar angles defining the mutual orientation

of the external fields ( $H_1$  and  $H_0$ ) and the principal axes of the efg tensor. The induced signal is proportional to the time derivative of  $I(t)$ , i.e.,

$$\varepsilon(t) \propto \dot{I}(t) \quad \dots (III.12)$$

Now, the expression for the Zeeman perturbed spin echo envelope modulation function  $\varepsilon(2\tau)$  is given by [15].

$$\begin{aligned} \varepsilon(2\tau) = & K \frac{(\omega_Q)^2}{(2I+1)KT} \sin(2\lambda\gamma H_1 t_w) \sin^2(\lambda\gamma H_1 t_w) \\ & \{ A_1 P_1 [\exp(-i\omega_a \tau) + \exp(i\omega_b \tau) - \exp(-i(\omega_a - \omega_b)\tau)] \\ & + B_1 Q_1 [\exp(-i\omega_a \tau) + \exp(-i\omega_b \tau) - \exp(-i(\omega_a + \omega_b)\tau)] \\ & + C_1 R_1 [\exp(i\omega_a \tau) + \exp(i\omega_b \tau) - \exp(i(\omega_a + \omega_b)\tau)] \\ & + D_1 S_1 [\exp(i\omega_a \tau) + \exp(-i\omega_b \tau) - \exp(i(\omega_a - \omega_b)\tau)] \\ & + [E_1 P_1 + F_1 Q_1 + G_1 R_1 + H_1 S_1] \} \quad \dots (III.12a) \end{aligned}$$

Here  $t$  is replaced by  $2\tau$  and the expression for  $A_1, B_1, C_1, D_1, E_1, F_1, G_1, H_1, P_1, Q_1, R_1$  and  $S_1$  are given in the reference [15]. The function  $\varepsilon(2\tau)$  (equation III.12(a)) is obtained for an arbitrary orientation  $(\theta, \phi)$  of the external fields ( $H_1$  and  $H_0$ ) with respect to the efg principal axes system. The response of quadrupolar spin ensemble in a polycrystalline samples, where all values of  $\theta$  and  $\phi$  occur with equal probability is obtained

by considering a weighted averaging overall orientations.

$$\overline{\langle \epsilon(2\tau) \rangle} = \frac{1}{4\pi} \int_0^{2\pi} \int_0^\pi \epsilon(2\tau) \sin\theta \, d\theta \, d\phi \quad \dots \text{(III.13)}$$

The integral in the above equation (III.13) can be evaluated numerically on a digital computer to simulate ZSEEM patterns from polycrystalline specimens.

#### III.D EXPERIMENTAL STUDY OF ZSEEM FROM SPIN 3/2 POWDER SAMPLES USING TWO PULSE ECHO METHOD

The microprocessor-controlled pulsed NQR spectrometer [19] described in Chapter II has been employed to investigate  $^{35}\text{Cl}$  ZSEEM patterns in polycrystalline specimens of  $\text{KClO}_3$ ,  $\text{HgCl}_2$  (two sites),  $\text{SbCl}_3$  (two sites) in order to explore the possibility of determining  $\eta$ . All the experimental investigations were carried out at room temperature. The external fields ( $H_1$  and  $H_0$ ) were oriented in a parallel configuration in all the experiments and the pulse sequence used was a  $(\pi/2 - \tau - \pi)$  sequence. The static Zeeman field was produced by a Helmholtz coil arrangement, which was energized using a regulated power supply (Model 726AR, Hewlett-Packard, USA). The magnetic field ( $H_0$ ) produced by the Helmholtz coil for a given current was measured and calibrated by a low field EPR set-up Alfa Model AL-55 (Alfa Laboratories, USA) using DPPH signal. For the purpose of r.f. power amplification we have used an ENI (Electronic Navigation Industries, Inc.) power amplifier to drive the final stage of the home-made tuned

power amplifier [18]. This combination gives an overall power output of  $\sim 800$  watts. For automatic processing of ZSEEM patterns we have developed several methods (see section II.E(3) of Chapter II), out of which we have used method III (see section II.E(3) for details) for recording all the ZSEEM patterns presented in this section. In this method the complete echo is acquired and averaged over a desired number of transients (25 transients in all the recordings presented here) by the signal analyzer for a given initial value of  $\tau$  and then transferred to the mini floppy disc. Next, the  $\tau$  is incremented by the microprocessor and the corresponding echo is captured. In this way nearly hundred echoes are stored in the floppy for different  $\tau$  values. These echoes are then processed Off-line by the utilization of BASIC language programming facility of the signal analyzer to obtain ZSEEM patterns. We have recorded ZSEEM spectra for the compounds mentioned above at various Zeeman field values ranging from 6 to 20 Gauss. The ZSEEM spectra obtained from  $^{35}\text{Cl}$  in  $\text{KClO}_3$  at three different Zeeman field values are presented in Figs. III.4(a) to III.4(c). The number of modulation peaks in the pattern clearly increases as the Zeeman field increases. Even at very small fields (6 Gauss the modulation peaks could be easily resolved in the ZSEEM spectra. These patterns agree well with the corresponding theoretically simulated ZSEEM patterns for the case of  $\eta = 0$  and also with the experimental ZSEEM obtained earlier for this compound [15]. Figs. III.5(a) to III.5(c) show our experimental ZSEEM patterns

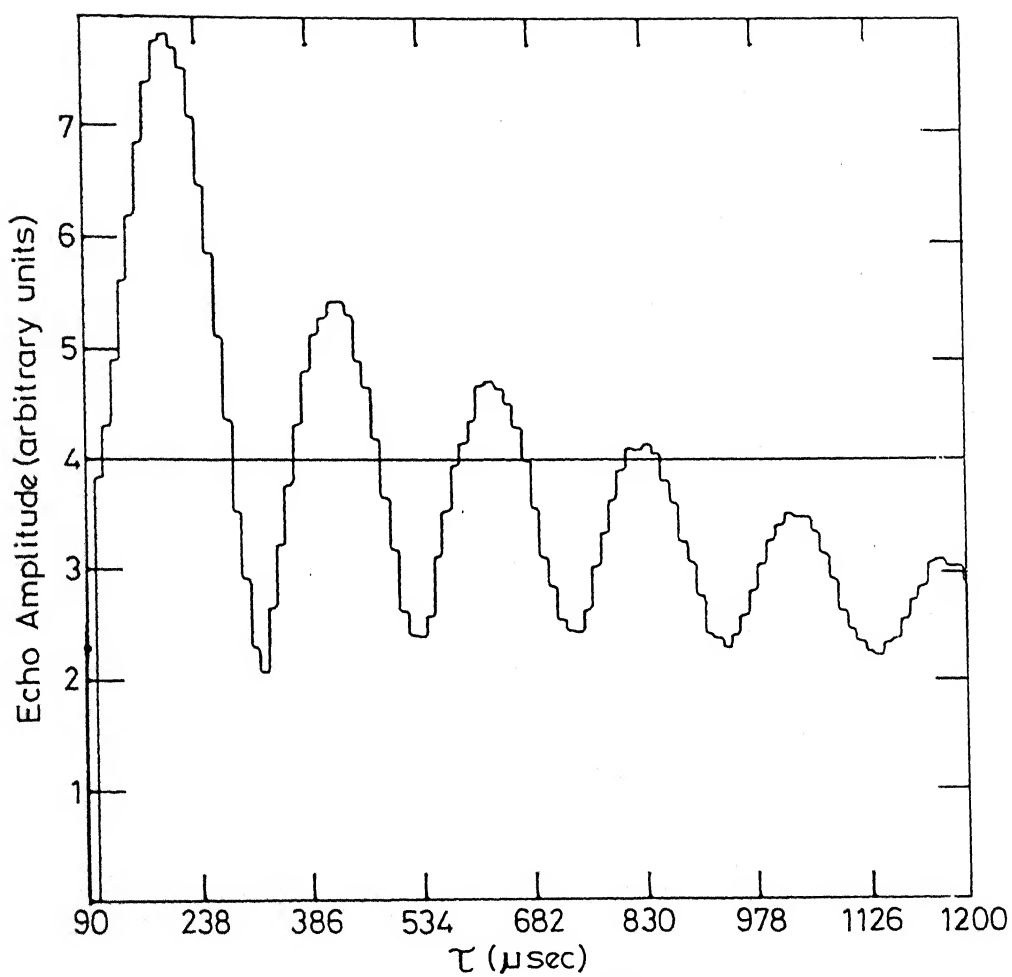


Fig. III-4(a) Experimental ZSEEM pattern from  $^{35}\text{Cl}$  in powdered sample of  $\text{KClO}_3$  ( $\omega_0 = 28.0948 \text{ MHz}$ ) with a magnetic field of 6.5 Gauss obtained from a series of two pulse experiments.

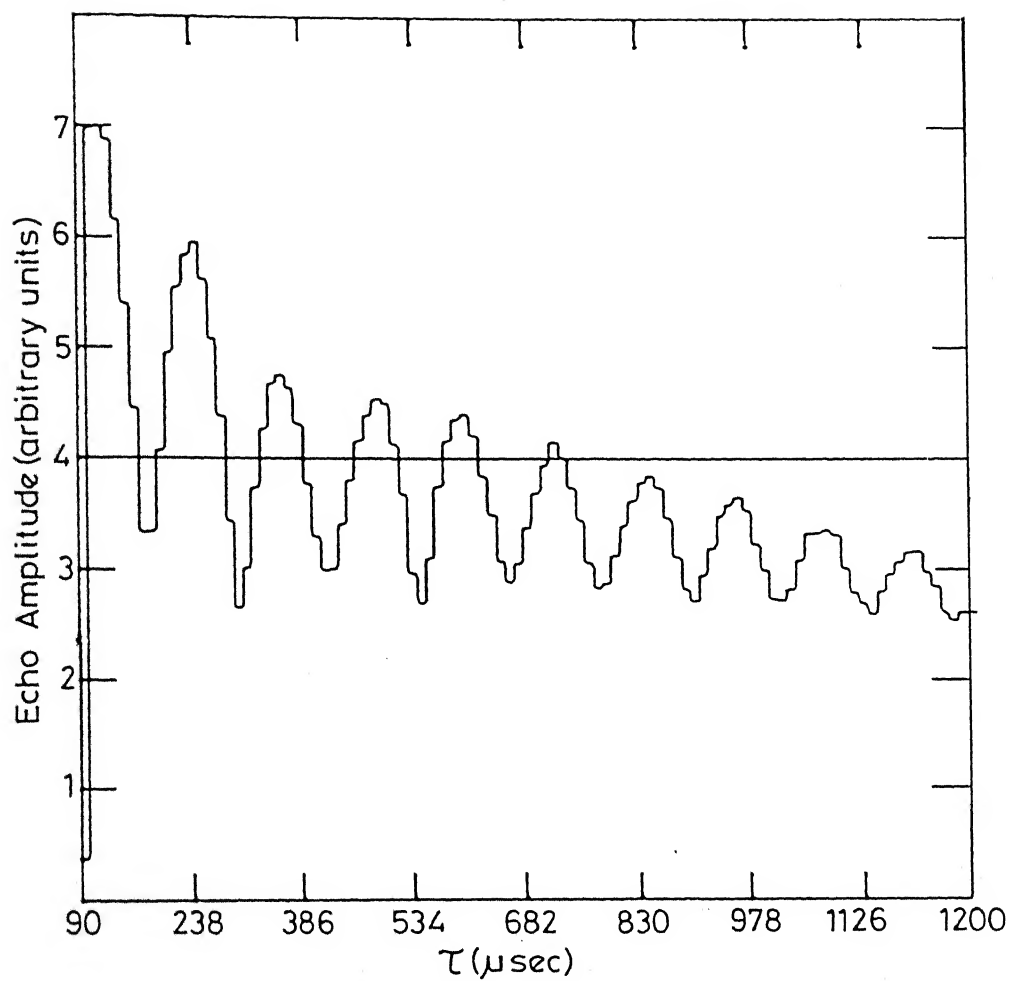


Fig.III-4(b) Same as in Fig.III-4(a) with a magnetic field of  $\approx 13$  Gauss.



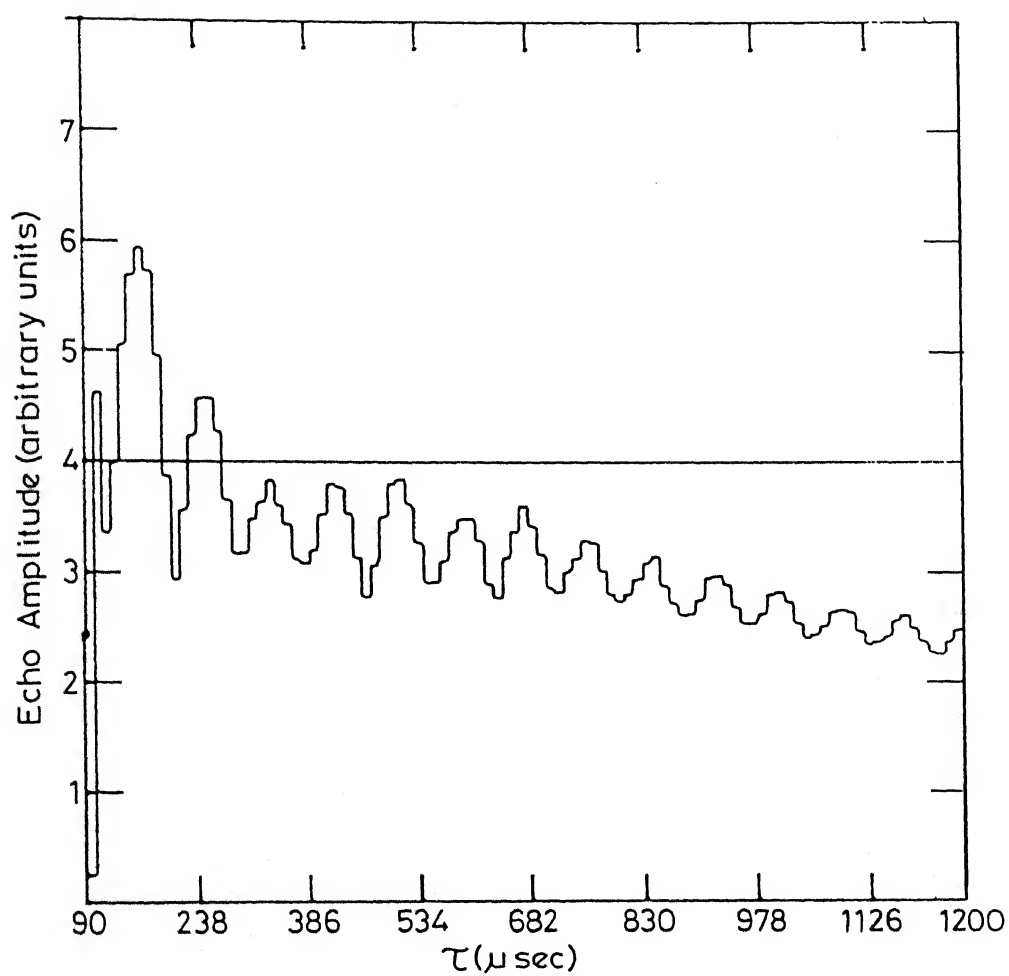


Fig.III-4(c) Same as in Fig.III-4(a) with magnetic field of  $\approx 19.5$  Gauss.

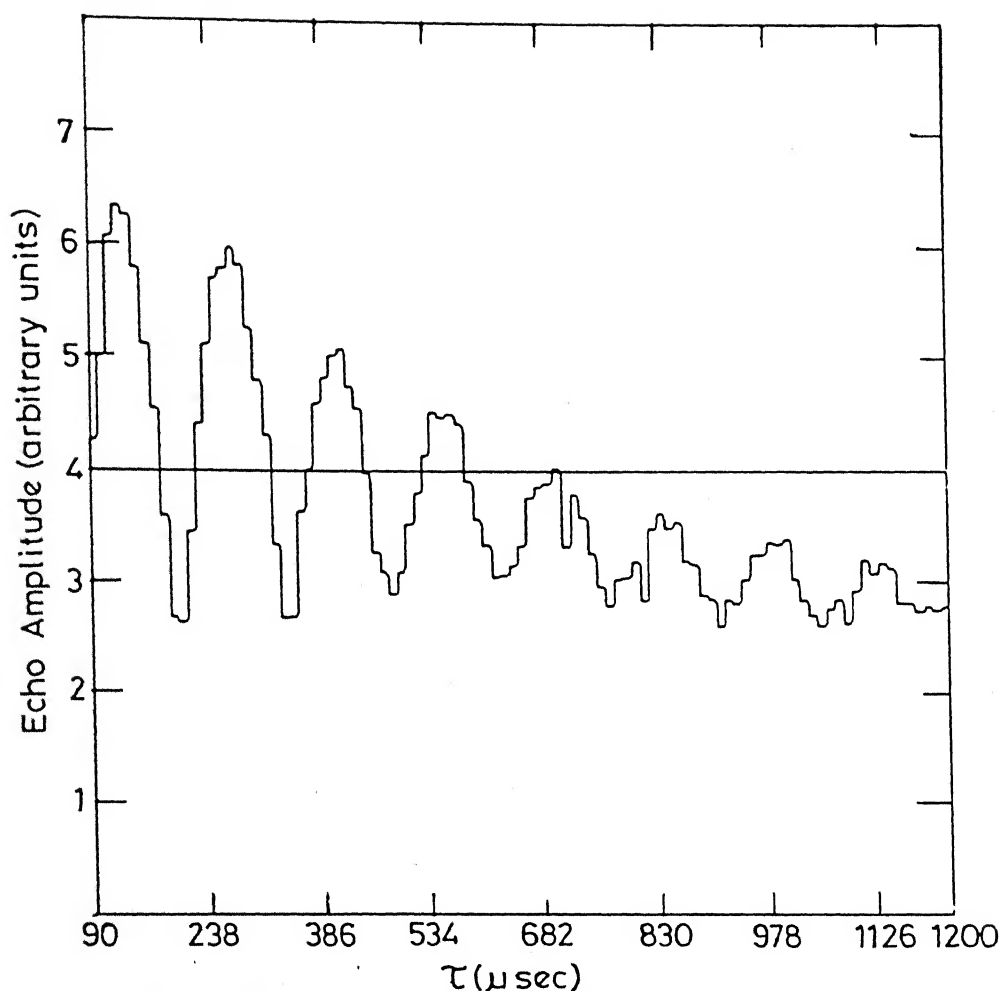


Fig.III.5(a) Experimental ZSEEM pattern from  $^{35}\text{Cl}$  in powdered sample of  $\text{HgCl}_2$  (site I,  $\omega_0 = 22.0599\text{ MHz}$ ) with a magnetic field of  $\approx 9.75\text{ Gauss}$  obtained from a series of two pulse experiments.

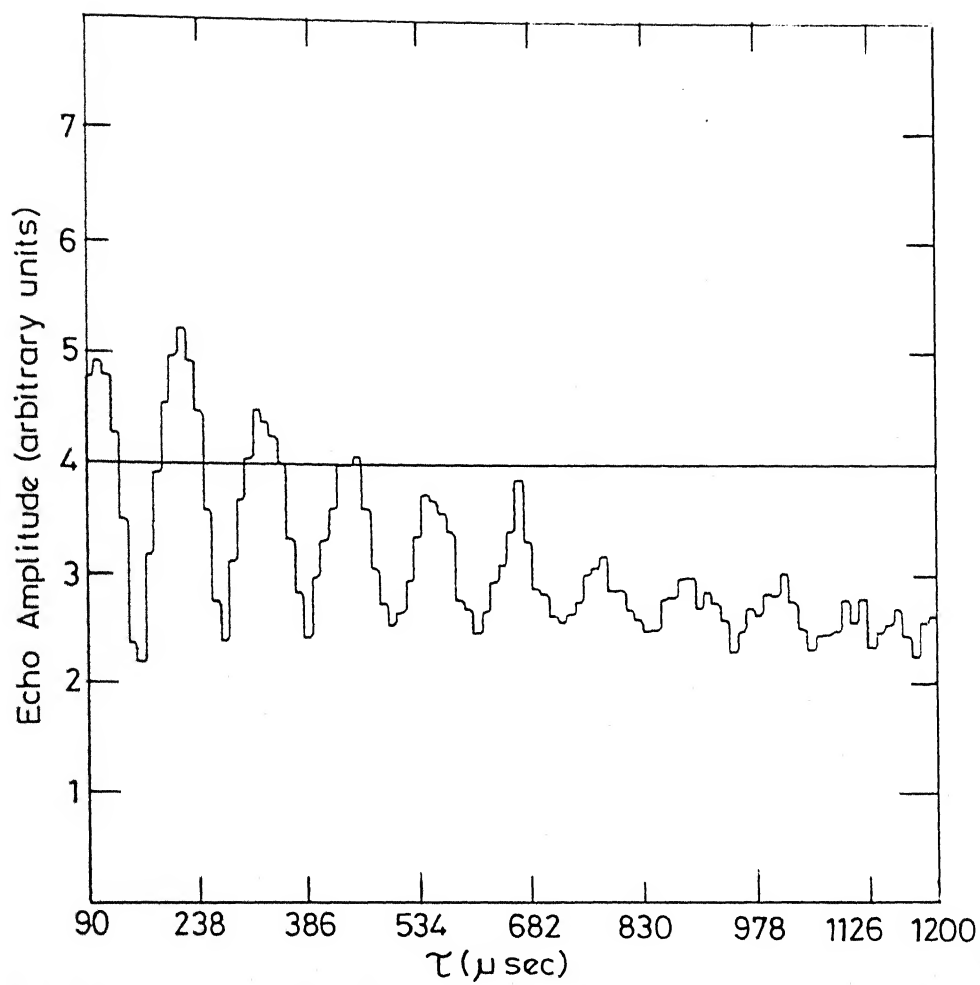


Fig.III.5(b) Same as in Fig.III.5(a) with a magnetic field of  $\approx 13$  Gauss.

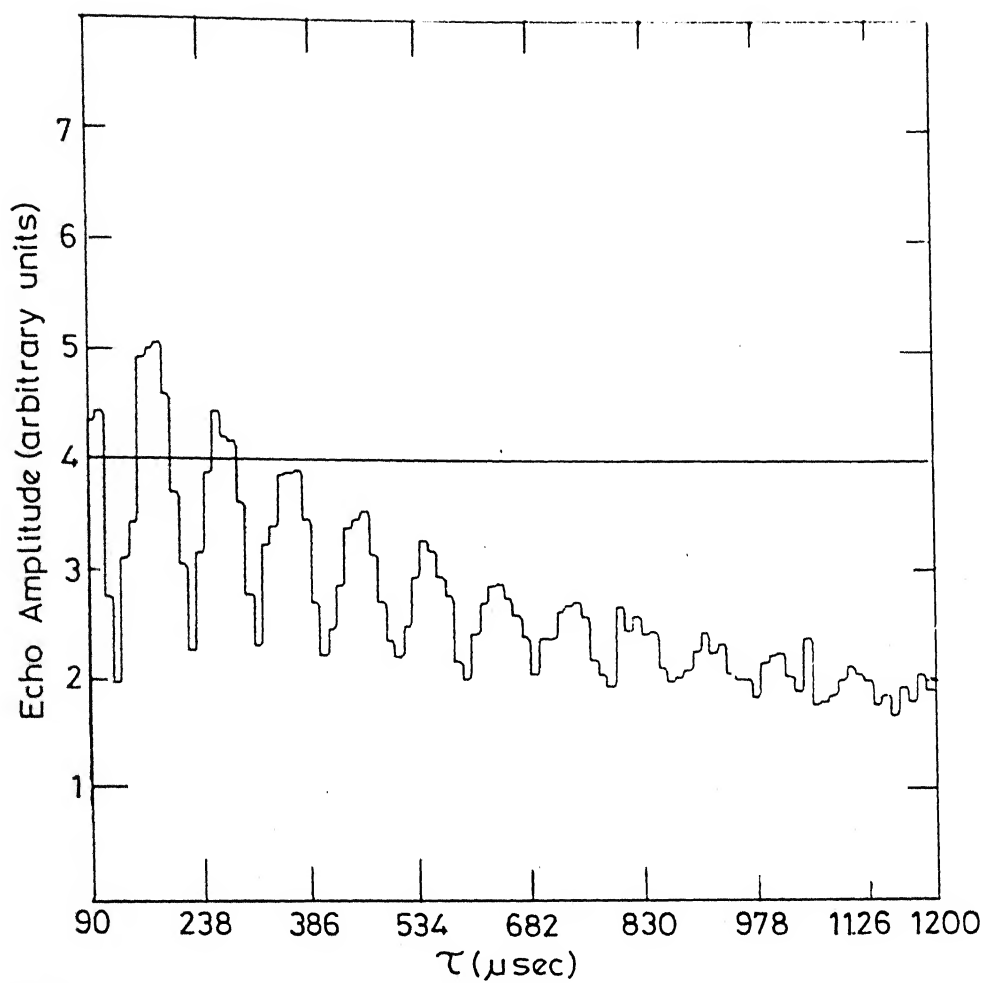


Fig.III.5(c) Same as in Fig.III.5(a) with a magnetic field of  $\approx 16.25$  Gauss.

obtained for the  $^{35}\text{Cl}$  nuclei in  $\text{HgCl}_2$  at three different magnetic fields (in the range 10-20 Gauss) for the site I, while Figs. III.6(a) to III.6(c) show ZSEEM spectra for  $^{35}\text{Cl}$  (site II) in this compound with the same magnetic field values. It is pertinent to mention here that  $\eta$  values ranging from 0.08 to 0.7 for the two  $^{35}\text{Cl}$  sites have been reported from powder studies in the literature for this compound. From comparison of the ZSEEM patterns recorded using our microprocessor-controlled pulsed NQR spectrometer (Figs. III.5(c) and III.6(c)) with the theoretically simulated ones at the corresponding static magnetic field values [15] it is apparent that the  $\eta$  values for the two  $^{35}\text{Cl}$  sites in  $\text{HgCl}_2$  lie very close to zero. This is in agreement with the conclusions drawn by earlier investigators of our laboratory [5, 15] and also with the work of Lucken and coworkers [23].

We have also investigated the ZSEEM patterns for the two  $^{35}\text{Cl}$  sites in  $\text{SbCl}_3$ . Figs. III.7(a) to III.7(c) present the experimental ZSEEM spectra for site I and Figs. III.8(a) to III.8(c) present the ZSEEM spectra for site II at three Zeeman field values ranging from 10-20 Gauss. It is clearly reflected in these patterns that the two  $^{35}\text{Cl}$  sites in this compound have different asymmetry parameter values. The ZSEEM patterns of site I show the typical oscillatory decay for a  $\eta \approx 0$  case whereas the ZSEEM spectra for site II show clearly the decay pattern behaviour corresponding to non-zero  $\eta$  value (Figs. III.8(a) to III.8(c)). Our experimental ZSEEM pattern for this

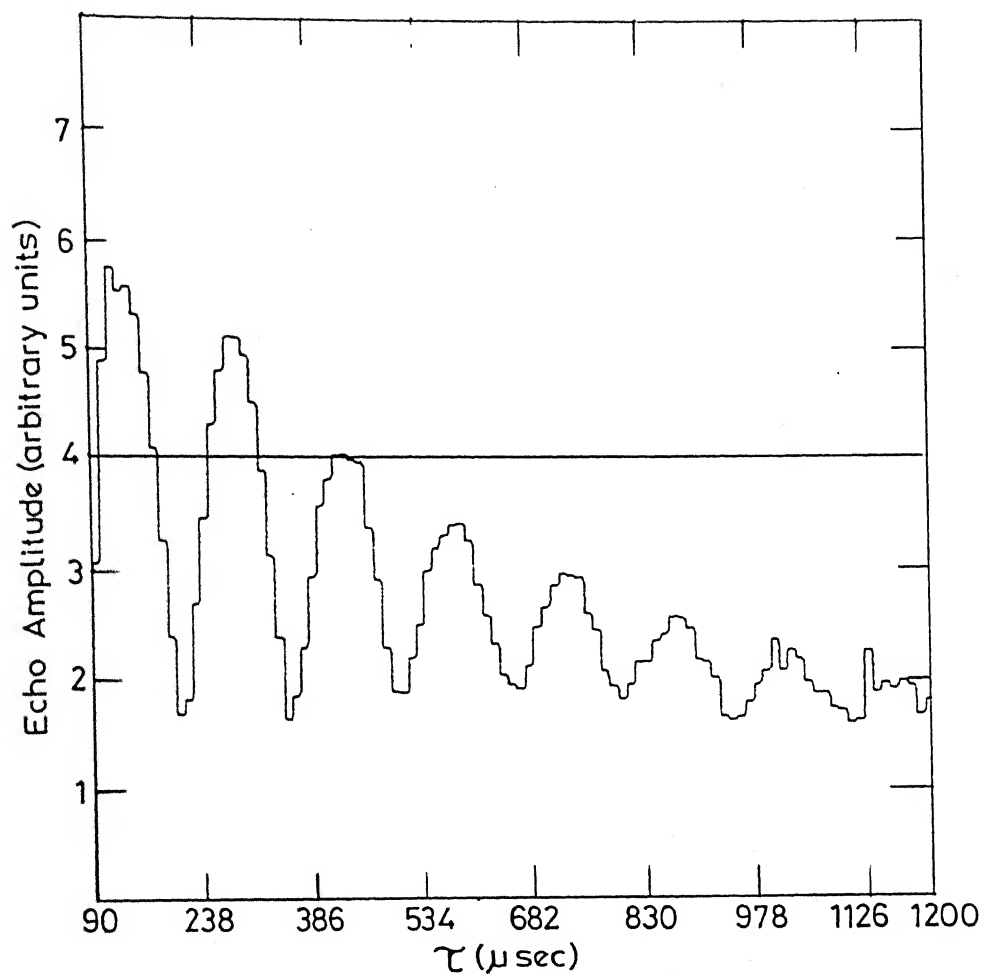


Fig.III.6(a) Experimental ZSEEM pattern from  $^{35}\text{Cl}$  in powdered sample of  $\text{HgCl}_2$  (site II;  $\omega_0 = 22.2389 \text{ MHz}$ ) with a magnetic field of  $\approx 9.75 \text{ Gauss}$  obtained from a series of two pulse experiments.

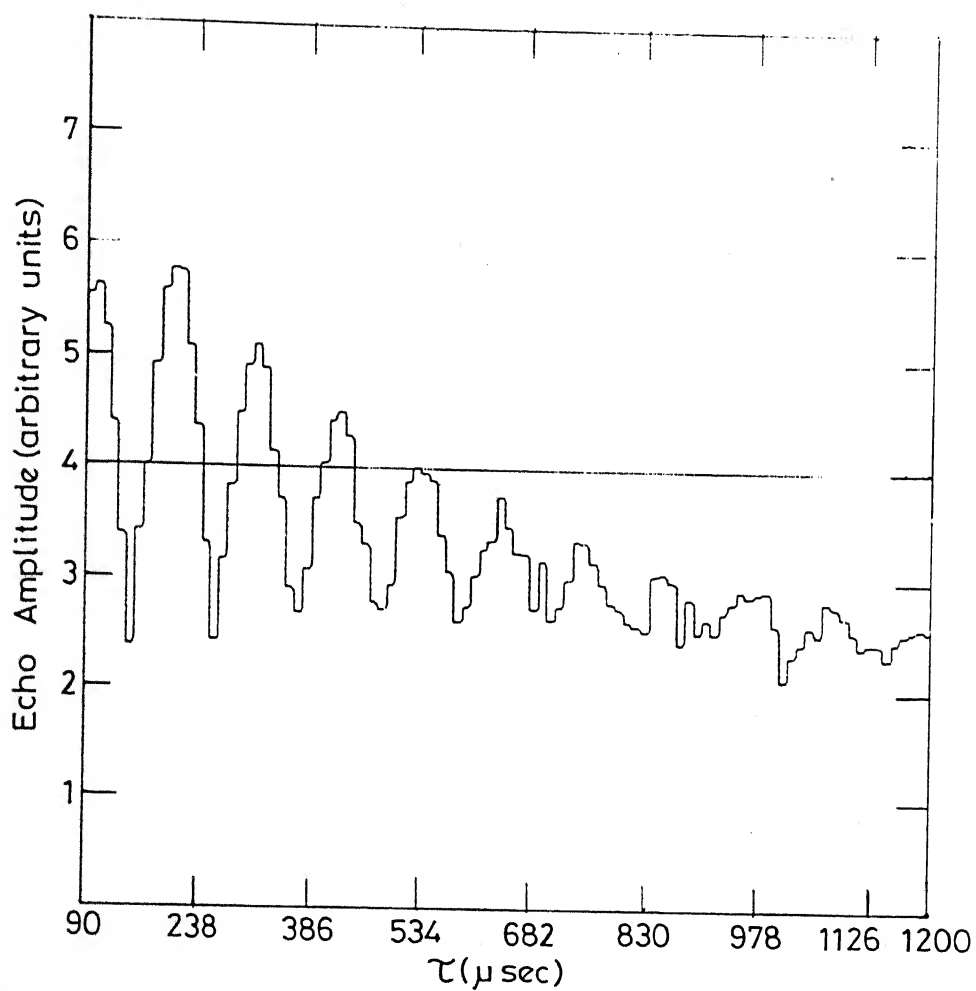


Fig.III.6(b) Same as in Fig.III.6(a) with a magnetic field of  $\approx 13$  Gauss.

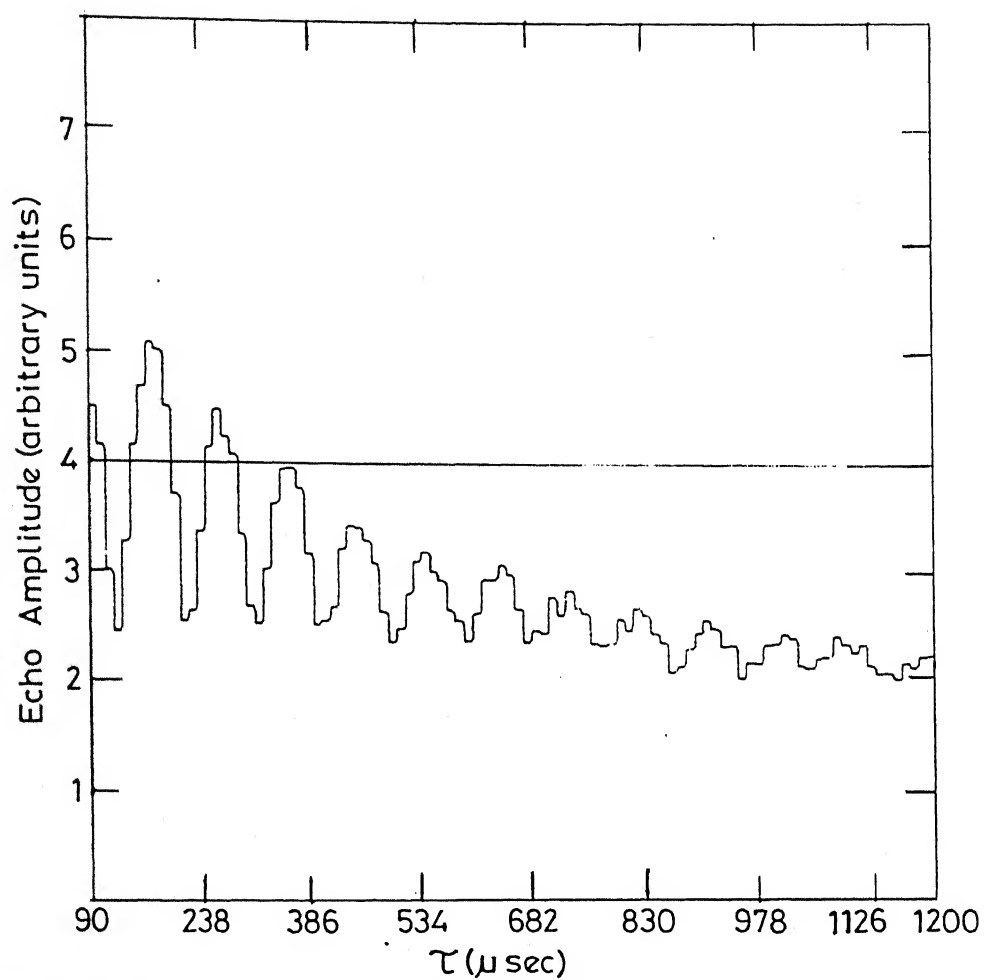


Fig.III.6(c) Same as in Fig.III.6(a) with a magnetic field of  $\simeq 16.25$  Gauss.



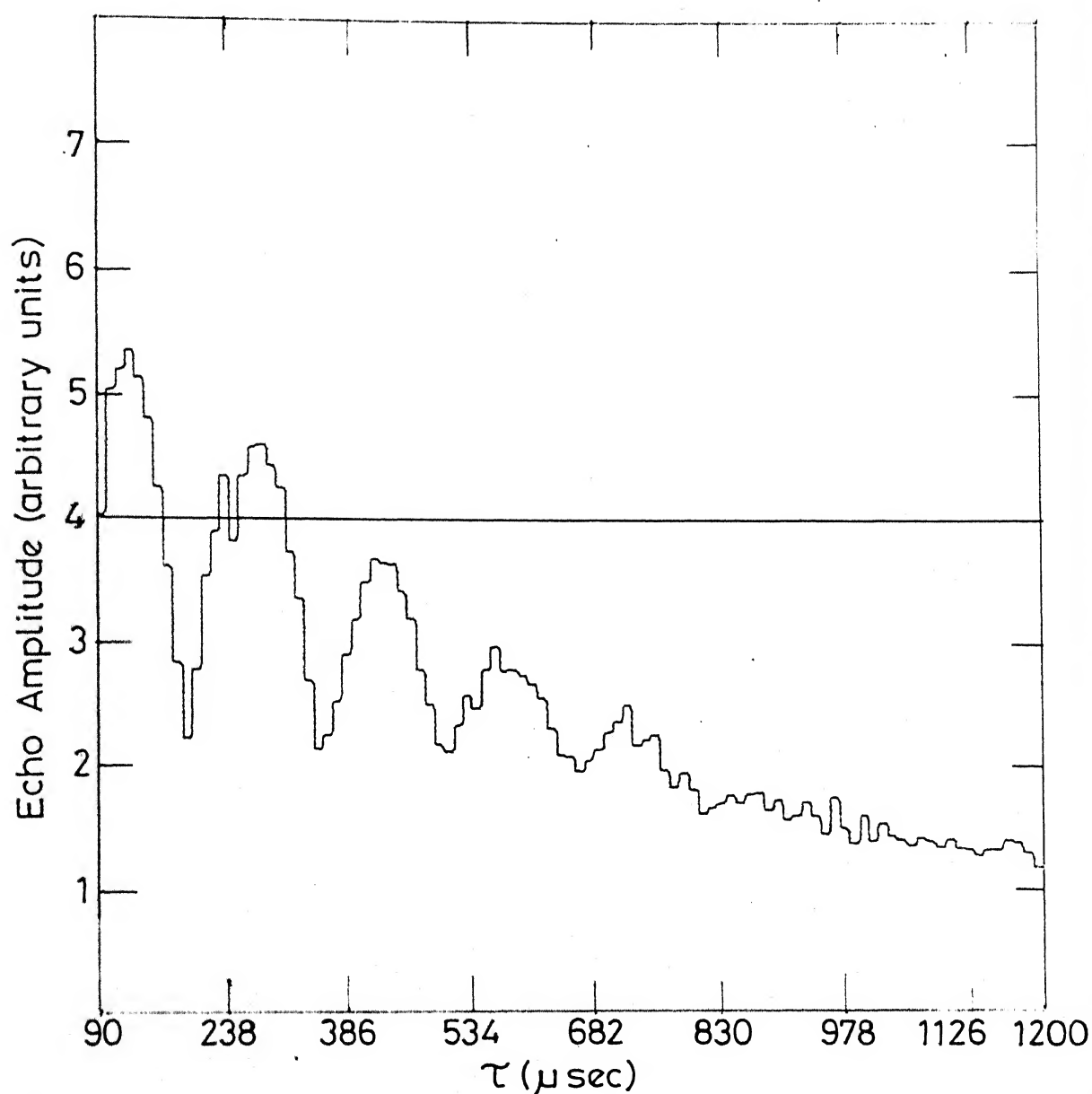


Fig.III.7(a) Experimental ZSEEM pattern from  $^{35}\text{Cl}$  in powdered sample of  $\text{SbCl}_3$  (site I;  $\omega_0 = 20.4015 \text{ MHz}$ ) with a magnetic field of  $\approx 9.75 \text{ Gauss}$  obtained from a series of two pulse experiments.

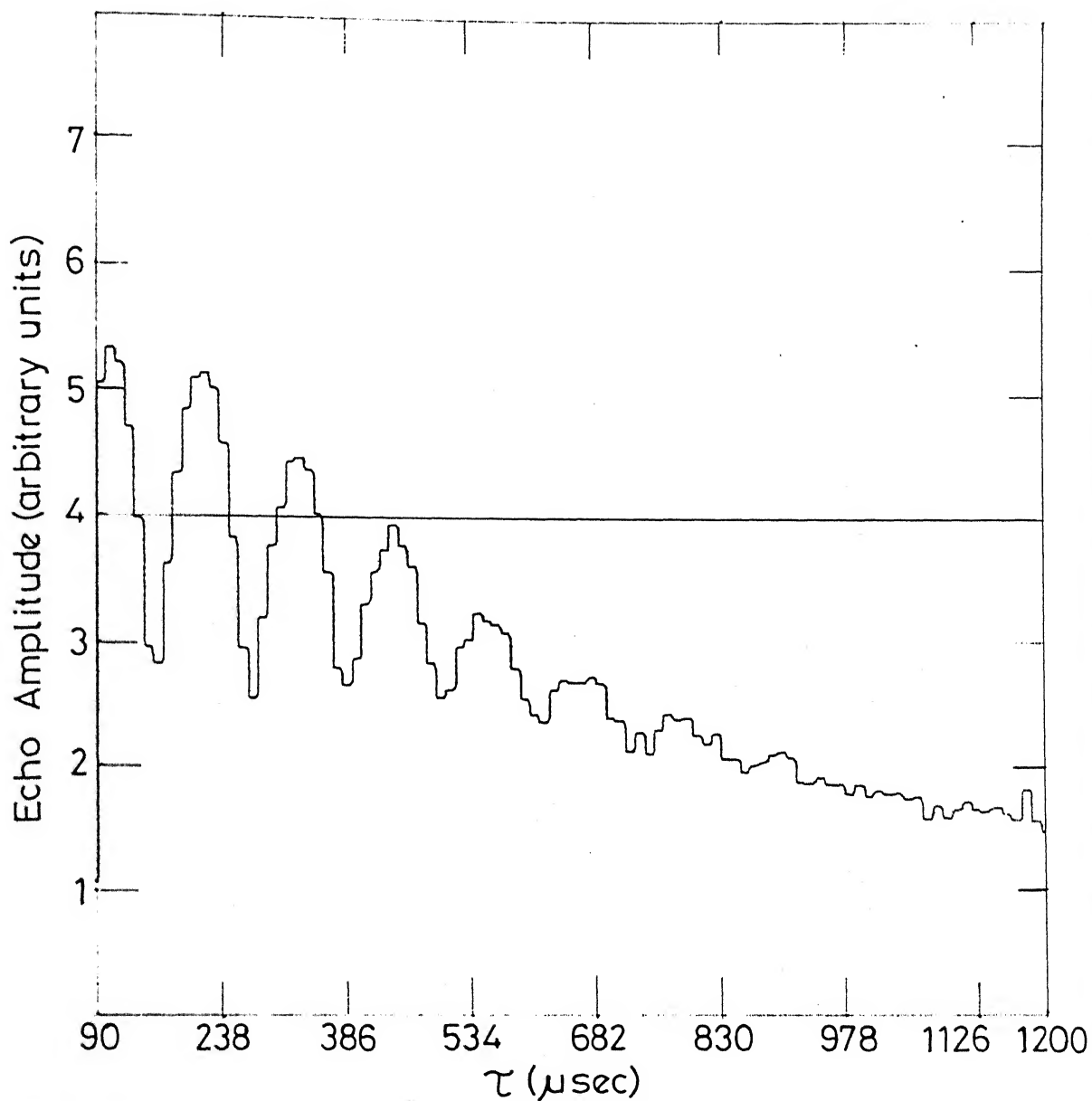


Fig.III.7(b) Same as in Fig.III.7(a) with a magnetic field of  $\approx 13$  Gauss.

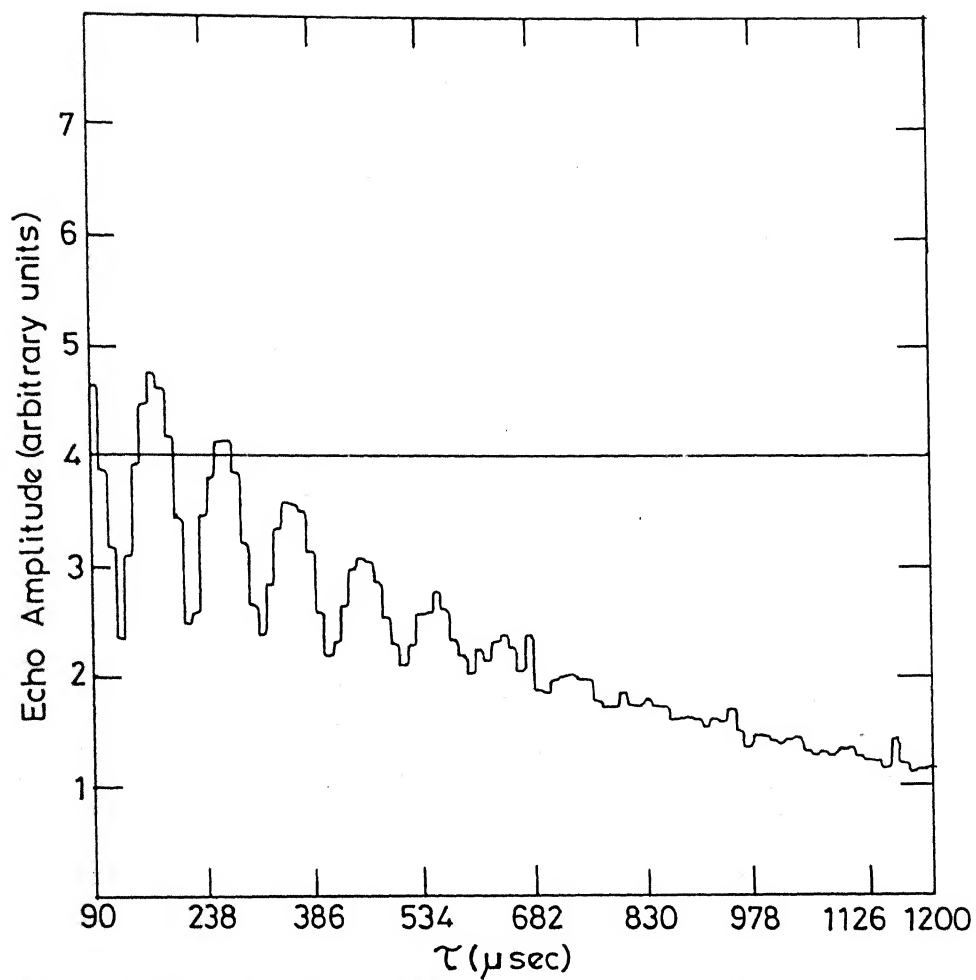


Fig.III.7(c) Same as in Fig.III.7(a) with a magnetic field of  $\approx 16.25$  Gauss.

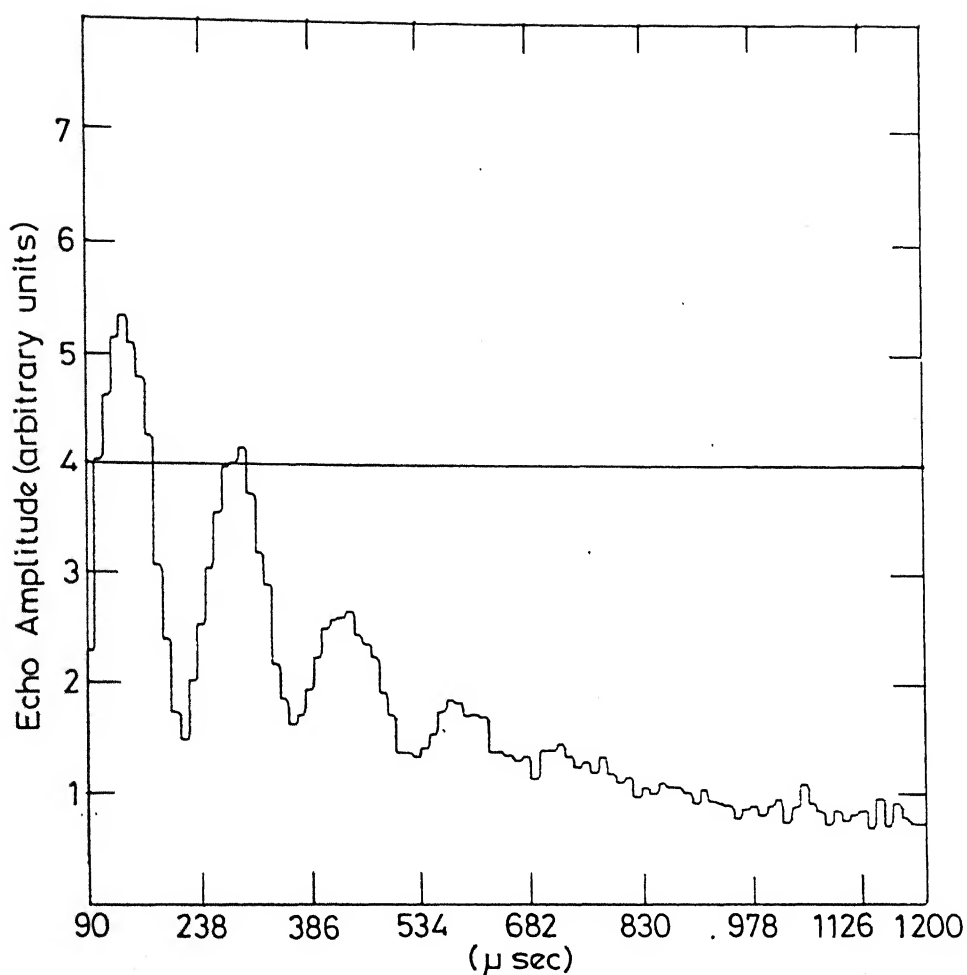


Fig. III.8(a) Experimental ZSEEM pattern from  $^{35}\text{Cl}$  in powdered sample of  $\text{SbCl}_3$  (site II;  $\omega_0 = 19.1713$  MHz) with a magnetic field of  $\approx 9.75$  Gauss obtained from a series of two pulse experiments.

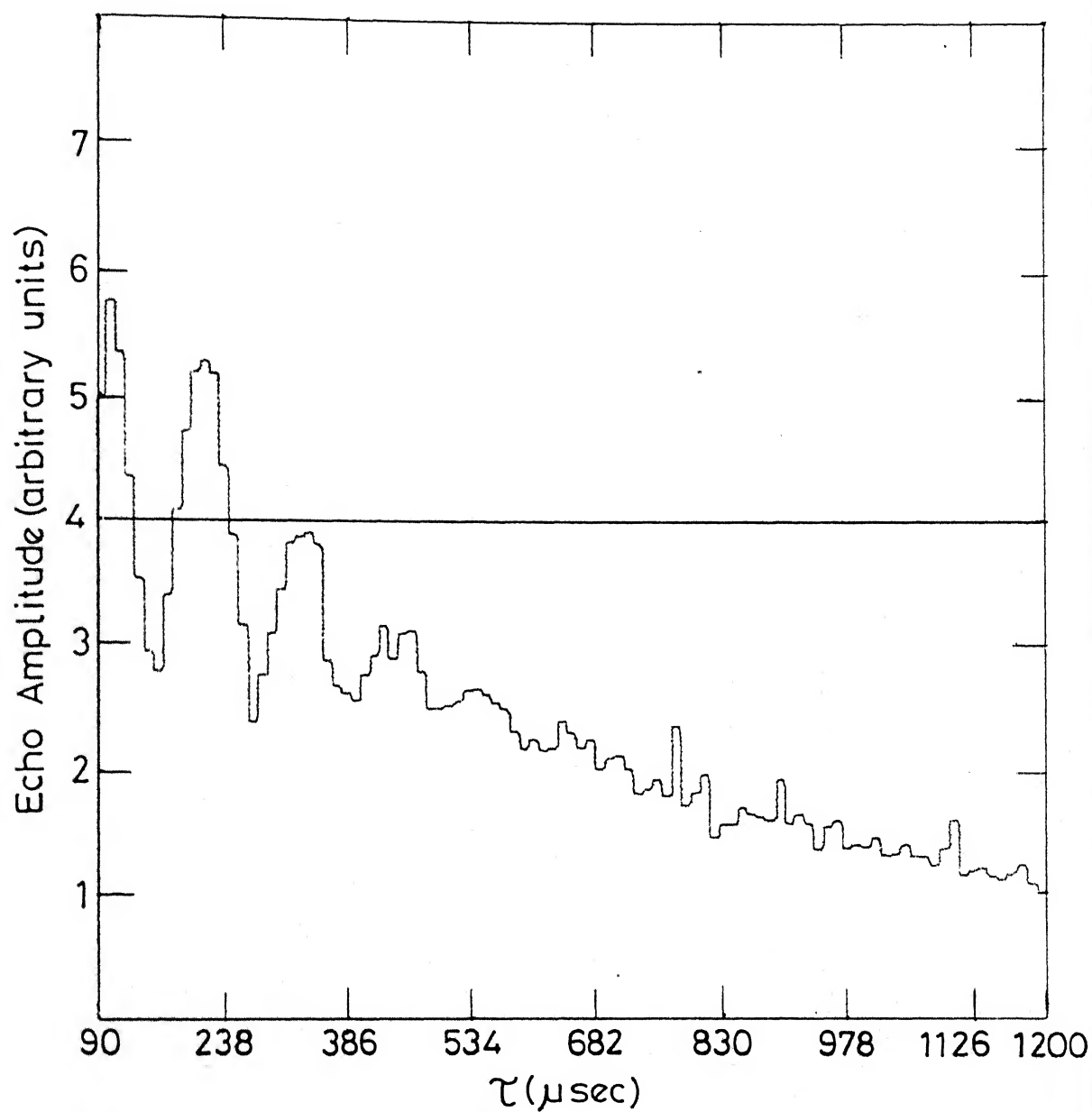


Fig. III.8(b) Same as in Fig. III.8(a) with a magnetic field of  $\simeq 13$  Gauss.

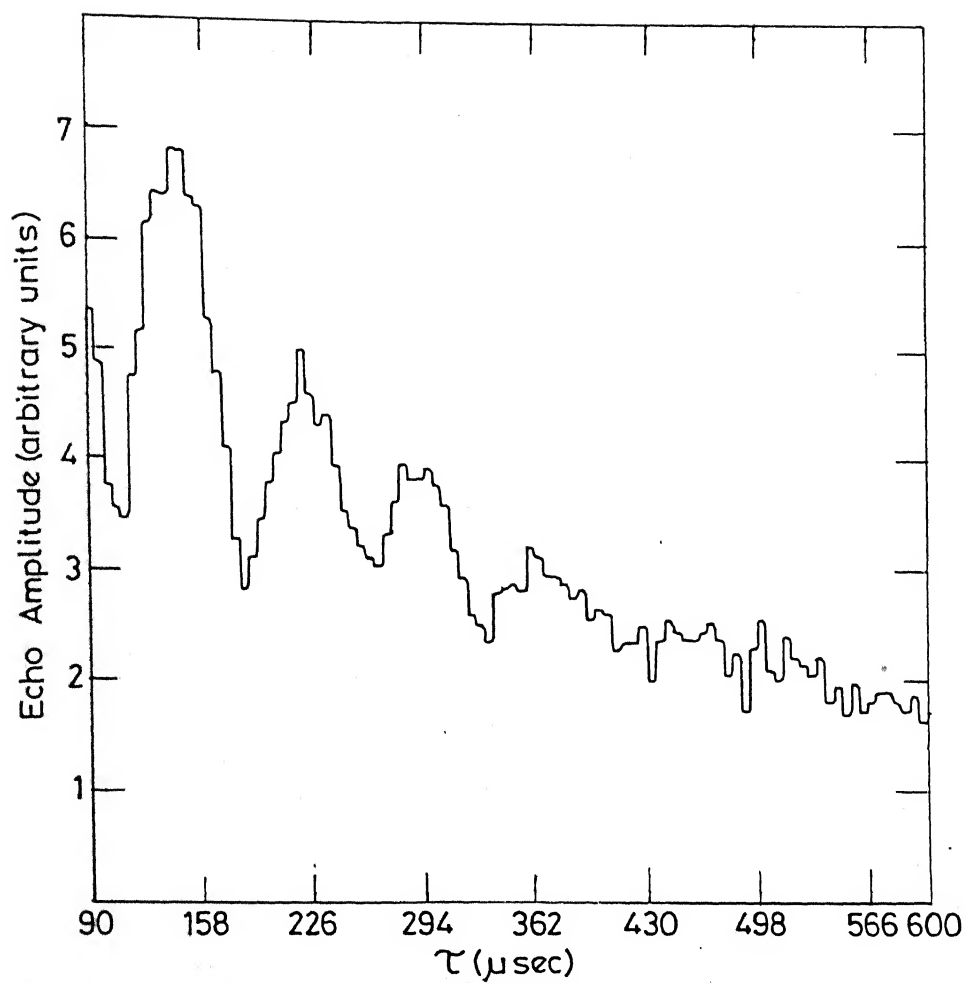


Fig.III.8(c) Same as in Fig.III 8(a) with a magnetic field of  $\approx 19.50$  Gauss.

site recorded at -19.5 Gauss shows a good agreement with the theoretically simulated pattern [15] for  $\eta = 0.15$  with the inclusion of exponential damping pre-factors in the expression for  $\epsilon(2\tau)$  (see Fig. 9(b) of reference [15]). Ramachandran and Narasimhan [15] incorporated two exponential damping factors  $T_2$  and  $T_2'$  to account for the overall  $^{35}\text{Cl}$  ZSEEM signal decay from site II in  $\text{SbCl}_3$ . The time constant  $T_2$  was incorporated to take into account the general exponential decay of the echo signal while  $T_2'$  was incorporated by them to account for the additional much faster decay of the modulations on the echo envelope, as a function of  $\tau$ , relative to the echo itself. They optimized the values of  $T_2$  and  $T_2'$  to obtain visual agreement between their theoretical and experimental patterns [15]. A comparison of our present experimental ZSEEM pattern with their theoretical pattern confirms the value of  $\eta = 0.15$  for the second site of  $^{35}\text{Cl}$  in  $\text{SbCl}_3$ .

Our experimental study on polycrystalline samples using the microprocessor-controlled pulsed NQR spectrometer suggests that the two-pulse ZSEEM method is suitable for obtaining values from polycrystalline samples, since these patterns are highly sensitive to the  $\eta$  value. The automation introduced by the microprocessor control has considerably increased the ease of performing the ZSEEM experiment in a much shorter time compared to unautomated systems [19] thus removing one of the important bottlenecks in the use of the ZSEEM technique in NQR spectroscopy.

As we have seen so far, obtaining ZSEEM using conventional two-pulse method involves the measurement of echo amplitude as a function of  $\tau$  in a series of experiments. In the next section (section III.E) we present a new method of obtaining ZSEEM in a single experiment. The method is based on extended time preparation of the spin system using weak r.f. perturbation.

### III.E EXTENDED TIME EXCITATION TECHNIQUE FOR OBTAINING ECHO ENVELOPE MODULATION

#### III.E(1) Introduction

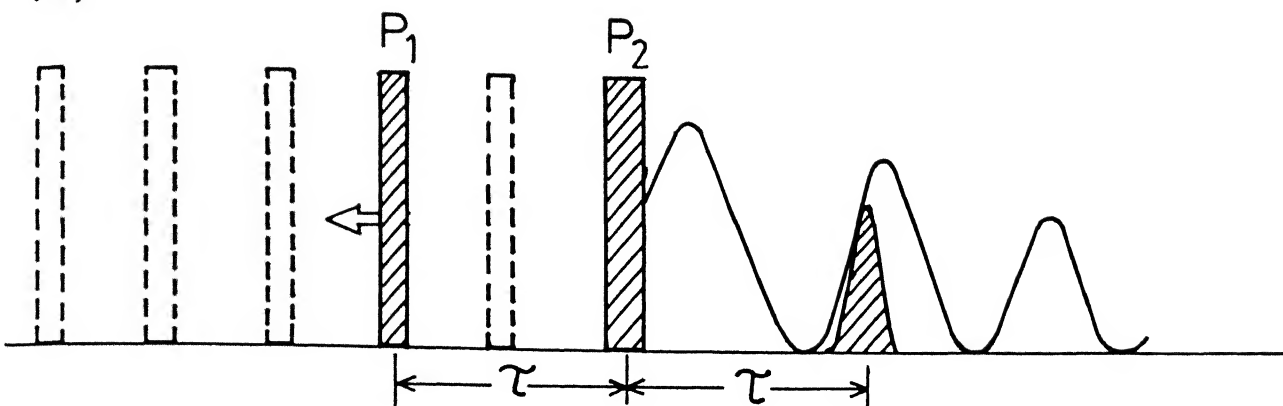
Usually the entire spin echo envelope modulation is obtained by a point-by-point measurement of the echo maximum amplitude as a function of the pulse separation ( $\tau$ ) in a sequence of two-pulse experiments. The measurement of echo-envelope modulation by this method is, therefore, tedious and time consuming [15], unless one has automated the complete experiment [19].

Recently, Schweiger et al. [24] have reported an alternative approach which permitted them to obtain the entire electron spin echo-envelope modulation in a single experiment using extended time excitation. This experiment provides a continuous refocusing of interactions of the spin system. Extended time excitation experiments used for the purpose of information storage have been discussed previously in the literature [25-31]. Fernbach and Proctor [25] first showed in their paper on "Spin-echo memory device" that an applied sequence of events can be



recalled by means of a short powerful 'reading pulse'. They have subjected a proton rich sample placed in a strong inhomogeneous magnetic field to a pattern of relatively weak r.f. pulses (sequences of pulses with varying amplitudes) at the Larmor frequency. The pattern was then recalled by applying a strong r.f. pulse at a latter time as in the spin-echo technique. They have also showed mathematically that such a series of pulses, varying in amplitude can be "memorized" by the spin-system of protons for times much larger than  $T_2^*$ . The corresponding information storage effects have also been described recently in coherent optics [28-31]. In these experiments it was shown that a complex laser pulse-shape information can be stored in and recalled from the 'spectral distribution of the population in one terminal level' of an inhomogeneously broadened optical transition [31]. In contrast to these investigations Schweiger et al. [24] have employed the technique to map interactions inherent within the spin system itself. Instead of applying an initial  $\pi/2$  pulse ( $\rho_1$ ) followed by a  $\pi$ -refocusing pulse ( $\rho_2$ ) (see Fig. III.9(a)), Schweiger et al. [24] have excited the system by a low-level irradiation  $V(t)$  for an extended time  $\tau_0$  prior to the refocusing pulse (Fig. III.9(b)). In the linear response approximation, each time interval within the excitation period  $\tau_0$  causes an echo in the corresponding time interval in symmetric position after the  $\pi$ -pulse [24] (time reversal occurs). The superposition of all these echoes leads then to a continuous echo

(a)



(b)

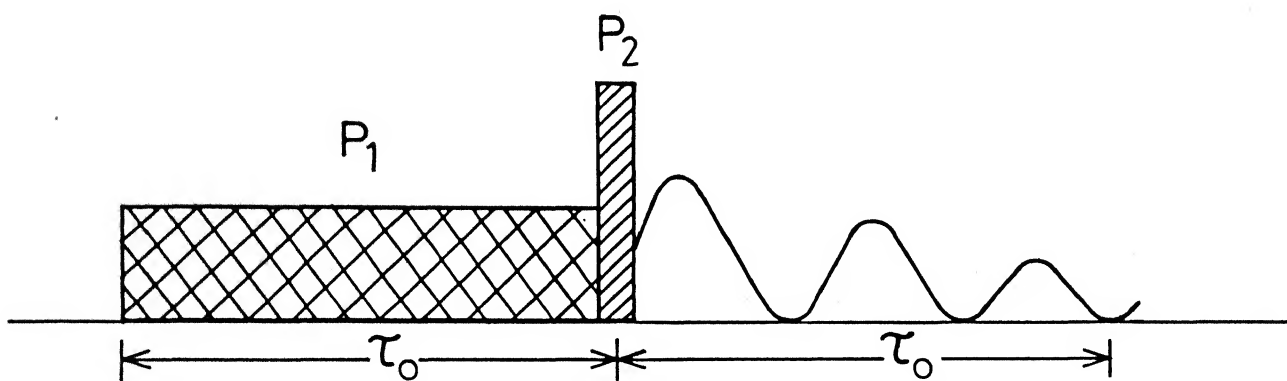


Fig. III.9 (a) Conventional two-pulse SEEM experiment where the echo amplitude is measured pointwise by stepping up  $\tau$  from experiment to experiment. (b) Extended time excitation experiment with soft-pulse excitation followed by a strong refocussing  $\pi$ -pulse producing the entire echo envelope modulation in a single experiment.

flip angle pulses. Schweiger et al. have shown from their experimental studies on electron spin-echo spectroscopy that all the three methods yield spin-echo envelope modulation.

We have investigated the possibility of obtaining ZSEEM patterns in NQR spectroscopy using the extended time excitation method. We have chosen to investigate the Zeeman perturbed nuclear quadrupole spin system ( $I = 3/2$ ) using a soft-pulse excitation followed by a strong  $\pi$ -pulse for refocusing. Our results are presented in the following section (section III.E(2)).

### III.E(2) Experimental Study on Extended Time Excitation in NQR of Spin $I = 3/2$ Powder Samples to Obtain ZSEEM

The microprocessor-controlled pulsed NQR spectrometer has been utilized for this experiment. The r.f. gating scheme used is shown in Fig. III.10. The timing signals generated by the microprocessor system, for the purpose of r.f. gating are shown in Fig. III.11. For r.f. power amplification, we have used an ENI (Electronic Navigation Industries, Inc.) model A300 power amplifier to drive the final stage of the home-made tuned power amplifier [18]. This combination gives a stable r.f. pulse power of  $\approx 800$  watts for the hard  $\pi$ -pulse ( $\approx 50 \mu$  sec) and the soft pulse power is controlled by reducing the input to the power amplifier using an attenuator in the r.f. gating scheme (see Fig. III.10). The output of the power amplifier is coupled to the sample probe and the response of the sample is amplified

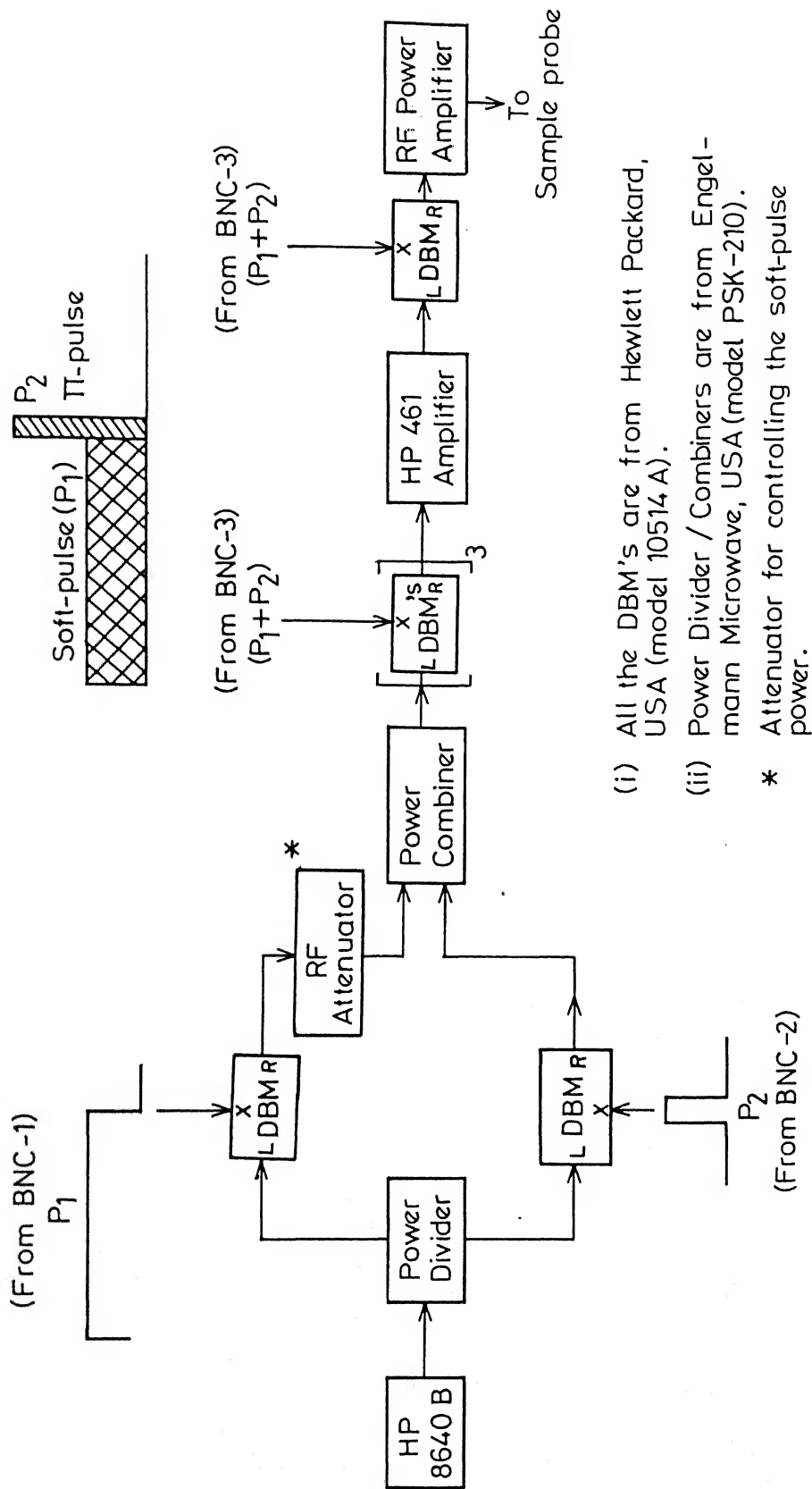
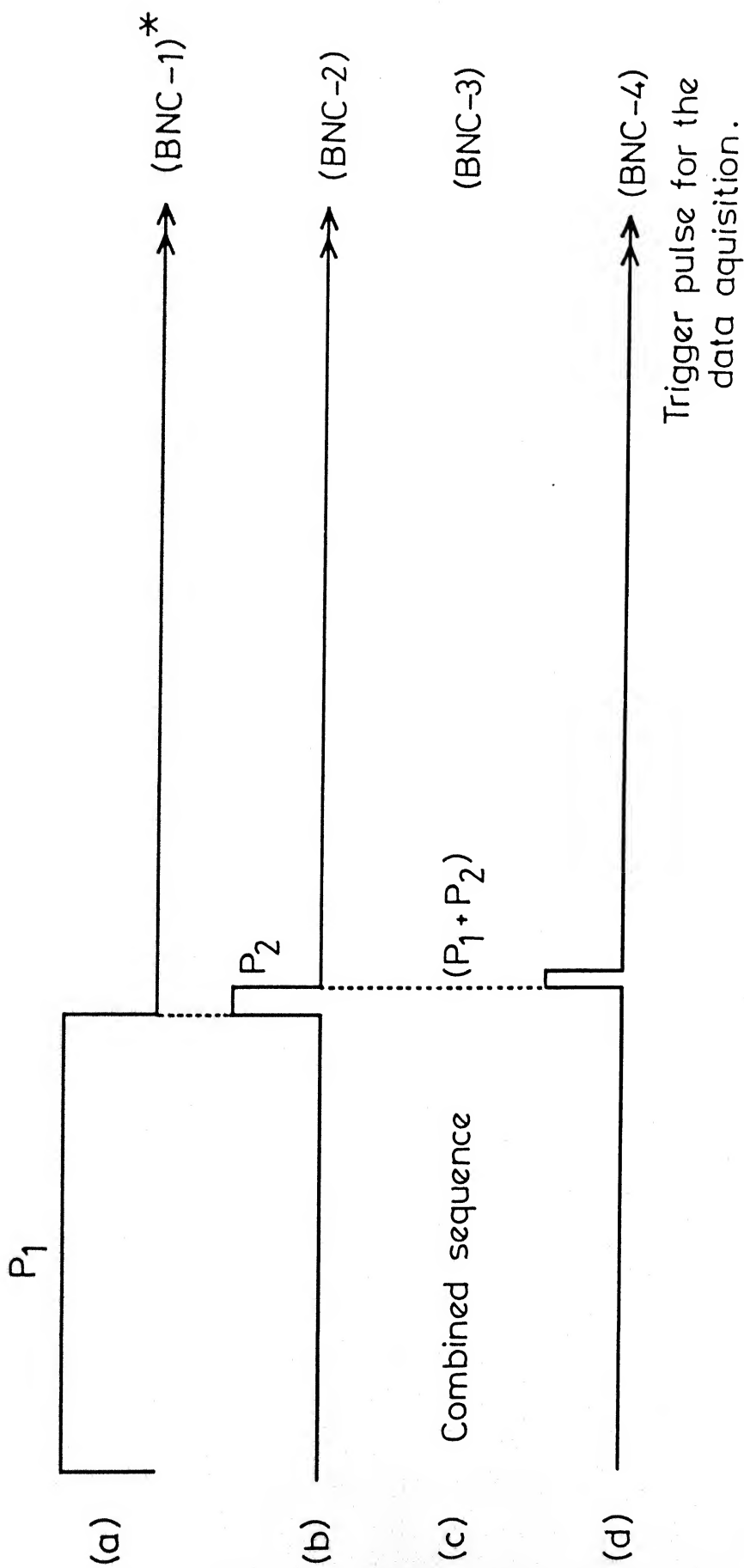


Fig. III.10 RF Gating scheme for soft-pulse based extended time excitation experiment.



\* Various "BNC" connectors are mounted on the card cage of the microprocessor.

Fig. III. 11 Timing singnals required for the RF gating scheme for soft-pulse excitation experiment.

and detected. Sufficient care has been taken to blank the receiver during the long soft-pulse excitation period and the subsequent  $\pi$ -pulse. We have infact used a cascade of two gates for this purpose. Even after the use of such a scheme, a delay of  $100\mu\text{ sec}$  following the  $\pi$ -pulse had to be given before acquiring the response. This was mainly because of overloading of the receiver for long periods by the extended time preparation pulse. Receiver ouput which is the response of the soft-pulse has been acquired into the signal analyzer (SM-2100B, from Iwatsu Electric Co. Ltd., Tokyo, Japan). It should be mentioned here that the amplitude of the soft pulse response in the case of electron spin echo modulation [24] is about ten percent of the Hahn two-pulse echo. Using this as a guide we have coherently averaged the soft pulse responses over hundred repetitions to improve S/N ratio. The complete soft pulse excitation experiment takes less than half a minute as compared to  $\approx 20$  mts. for the two-pulse experiment with the present spectrometer system.

The response to soft-pulse excitation followed by a  $\pi$ -pulse from  $^{35}\text{Cl}$  in a powdered sample of  $\text{KClO}_3$  with a magnetic field of 9.75 Gauss, applied parallel to  $H_1$  is shown in Fig. III.12. As has been mentioned earlier, if one prepares the system for a duration  $\tau_0$  by using extended time excitation then one obtains ZSEEM only for a period  $\tau_0$  after the refocusing  $\pi$ -pulse. Unless otherwise mentioned in all our experiments we have prepared the system for a period  $\tau_0 = 1200\mu\text{ sec}$  using soft-pulse excitation. The response has therefore been recorded for

1200  $\mu$ sec after the  $\pi$ -pulse with an initial delay of 100  $\mu$ sec. The  $\pi$ -pulse length used has been chosen to be same as that which gives maximum echo signal (maximum refocusing) in powdered sample (see section I.B(2)). The  $^{35}\text{Cl}$  site in  $\text{KClO}_3$  has an asymmetry parameter value of zero. A closer look at the ZSEEM obtained from soft-pulse excitation experiment (Fig. III.12) shows that the latter portion of the response starting from 350  $\mu$ sec from the  $\pi$ -pulse agrees well with the ZSEEM obtained from the conventional two-pulse method (Fig. III.13) at the same magnetic field value. The modulation period (140  $\mu$ sec) calculated from the latter portion of the soft-pulse excitation response is in agreement with that obtained from the conventional two-pulse method. This observation confirms the possibility of obtaining Zeeman perturbed SEEM patterns in NQR from powder samples using the extended time excitation method. Further confirmation is obtained from a comparison of ZSSEEM patterns shown in Figs. III.14 and III.15 recorded with a magnetic field of  $\approx 13$  Gauss by the two methods. The nature of the signal obtained immediately following the  $\pi$ -pulse in the case of the soft excitation method is different from that obtained for short  $\tau$  values in the case of the two-pulse method and the reason for this lies in the magnitude of  $T_2^*$  for the NQR powder sample used in the study. This aspect of the problem will be discussed later (see III.E(3)). For the present we may note that the response after a period of 350  $\mu$ sec following the  $\pi$ -pulse is in agreement with the result of the two-pulse

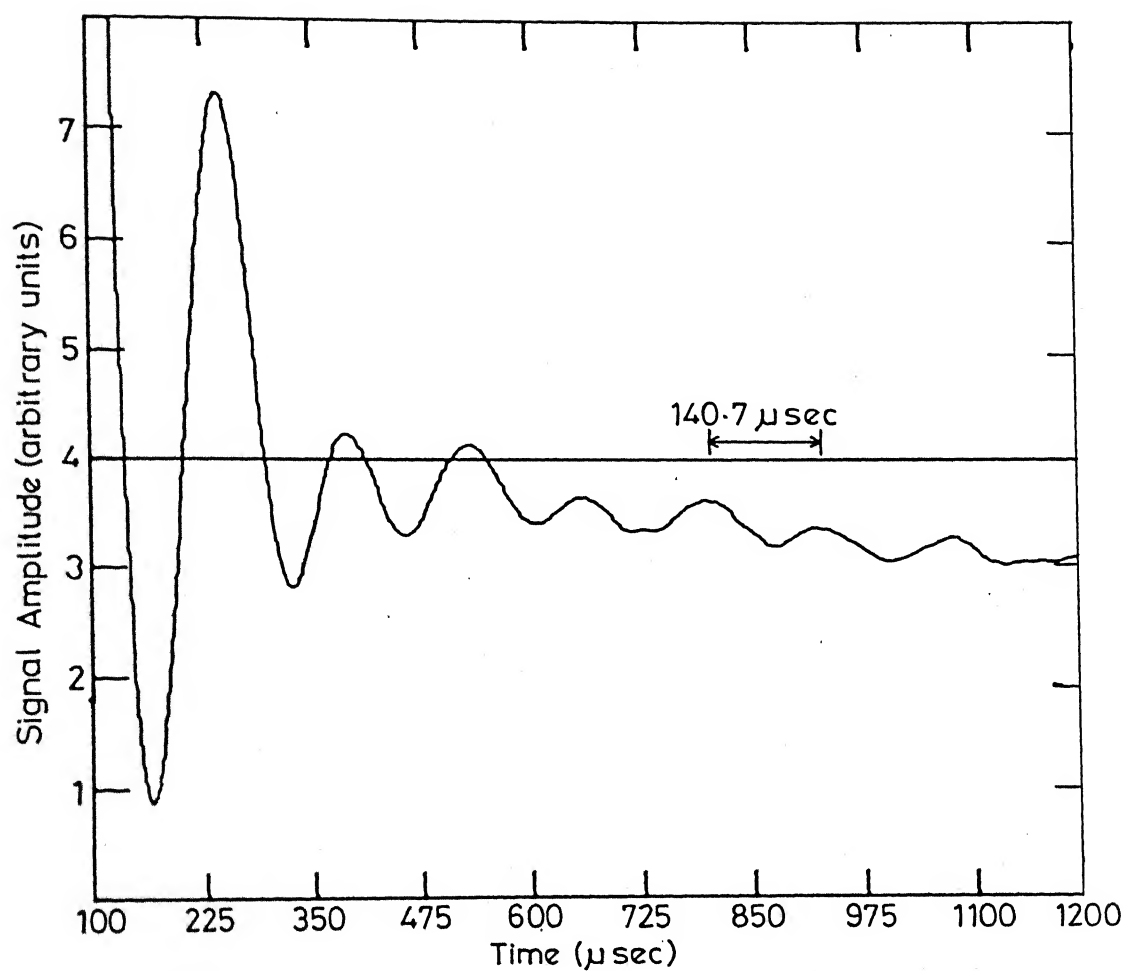


Fig.III.12 Response of soft-pulse excitation from  $^{35}\text{Cl}$  in powdered sample of  $\text{KClO}_3$  ( $\omega_0=28.0948\text{MHz}$ ) with a magnetic field of  $\approx 9.75\text{ Gauss}$ .



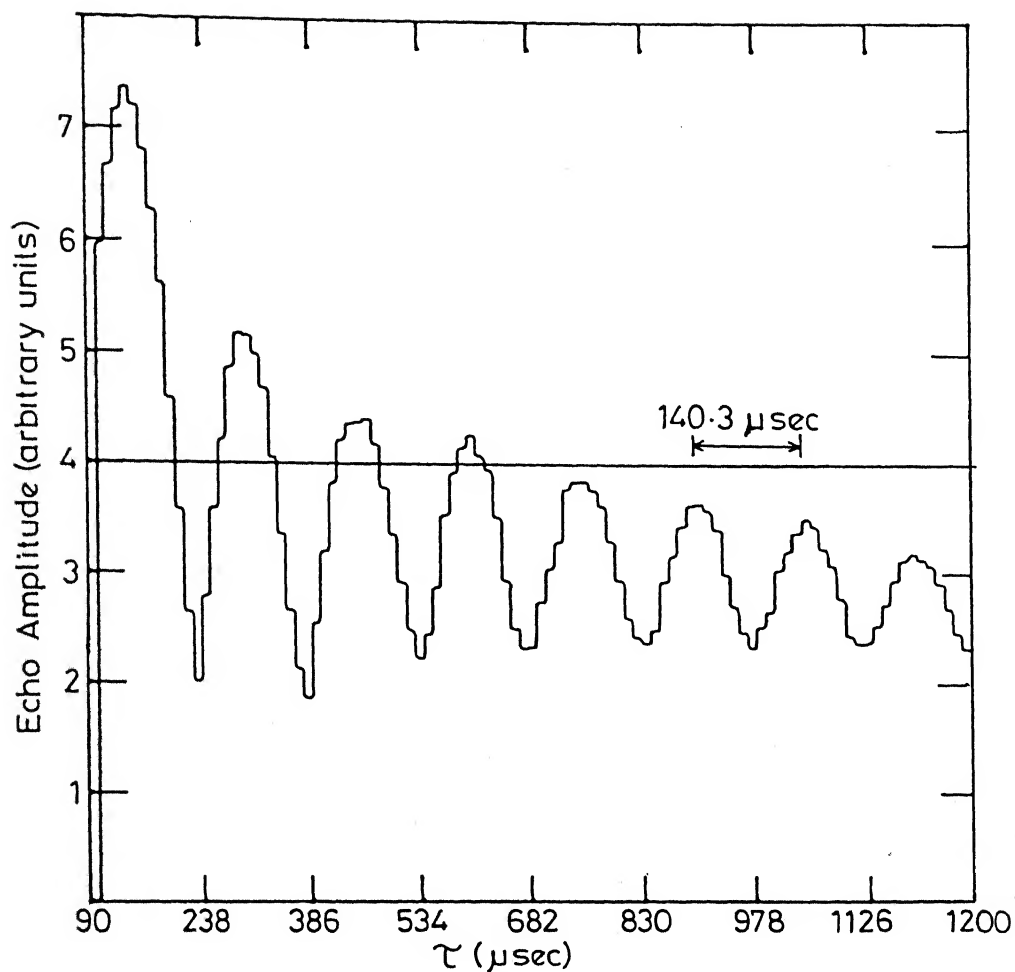


Fig.III.13 ZSEEM pattern obtained from  $^{35}\text{Cl}$  in powdered sample of  $\text{KClO}_3$  ( $\omega_0 = 28.0948\text{MHz}$ ) with a magnetic field of  $\approx 9.75$  Gauss obtained from a sequence of basic two pulse experiments.

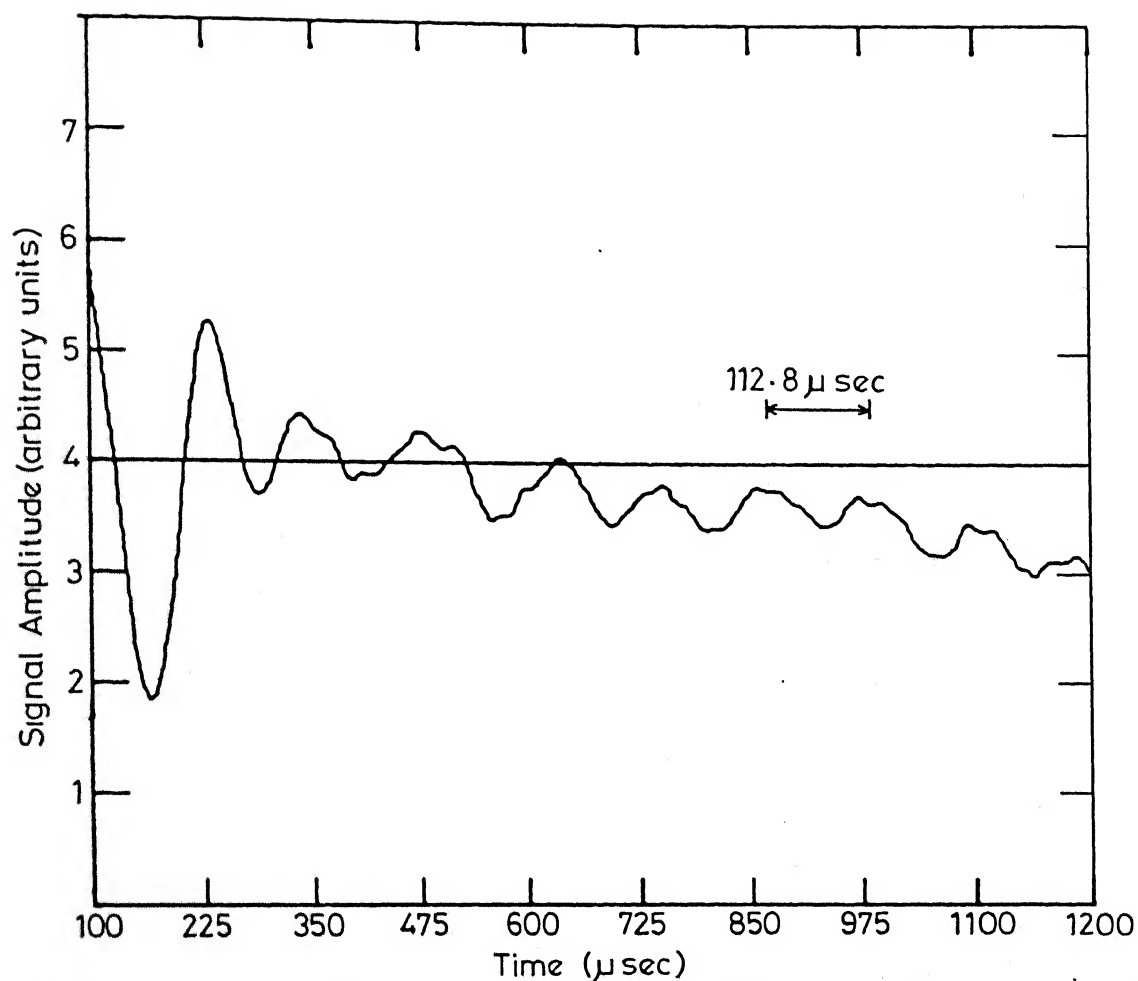


Fig.III.14 Response of soft pulse excitation from  $^{35}\text{Cl}$  in powdered sample of  $\text{KClO}_3$  ( $\omega_0=28.0948\text{MHz}$ ) with a magnetic field of  $\approx 13\text{ Gauss}$ .

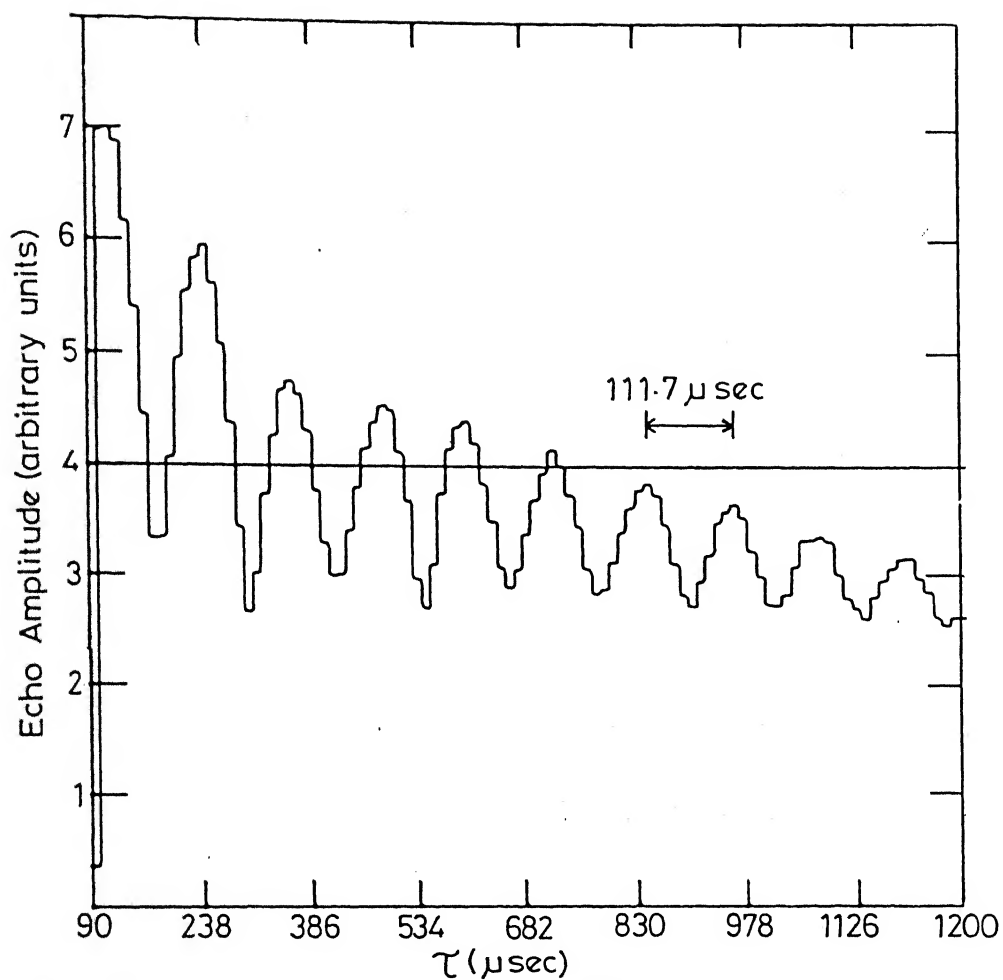


Fig.III.15 ZSEEM pattern obtained from  $^{35}\text{Cl}$  in powdered sample of  $\text{KClO}_3$  ( $\omega_0 = 28.0948 \text{ MHz}$ ) with a magnetic field  $\simeq 13$  Gauss obtained from a sequence of basic two pulse experiments.

method for this compound.

A factor which is crucial for getting reliable ZSEEM patterns by soft-pulse excitation is the soft-pulse power. In order to optimize the response we have performed the experiments as a function of soft-pulse power ranging from 5 to 25 watts. The results of this study on  $^{35}\text{Cl}$  in powdered  $\text{KClO}_3$  for a magnetic field value of 9.15 Gauss are shown in Figs. III.16 to III.21. The total transmitter power for the  $\pi$ -refocusing pulse in all these recordings has been kept constant at 800 watts. It is seen from these results that as the soft-pulse power is increased the response improves but at higher power values the modulations tend to be smoothened out. For a soft-pulse power of about 13 watts a clear and undistorted ZSEEM pattern (Fig. III.18) is obtained.

From the present study it is evident that one can obtain ZSEEM by means of the extended excitation method provided the linear regime is maintained for the soft-pulse. This was indeed the observation of Schweiger et al. [24] in electron spin-echo spectroscopy.

With a view to extend the soft-pulse based ZSEEM experiment to other compounds with non-zero asymmetry parameter, we have studied the 19.1713 MHz transition (site II) of  $^{35}\text{Cl}$  in  $\text{SbCl}_3$ . The responses (ZSEEM) to soft-pulse followed by a  $\pi$ -pulse from  $^{35}\text{Cl}$  in powdered sample of  $\text{SbCl}_3$  for the above-mentioned site were studied at various magnetic field values in the range of

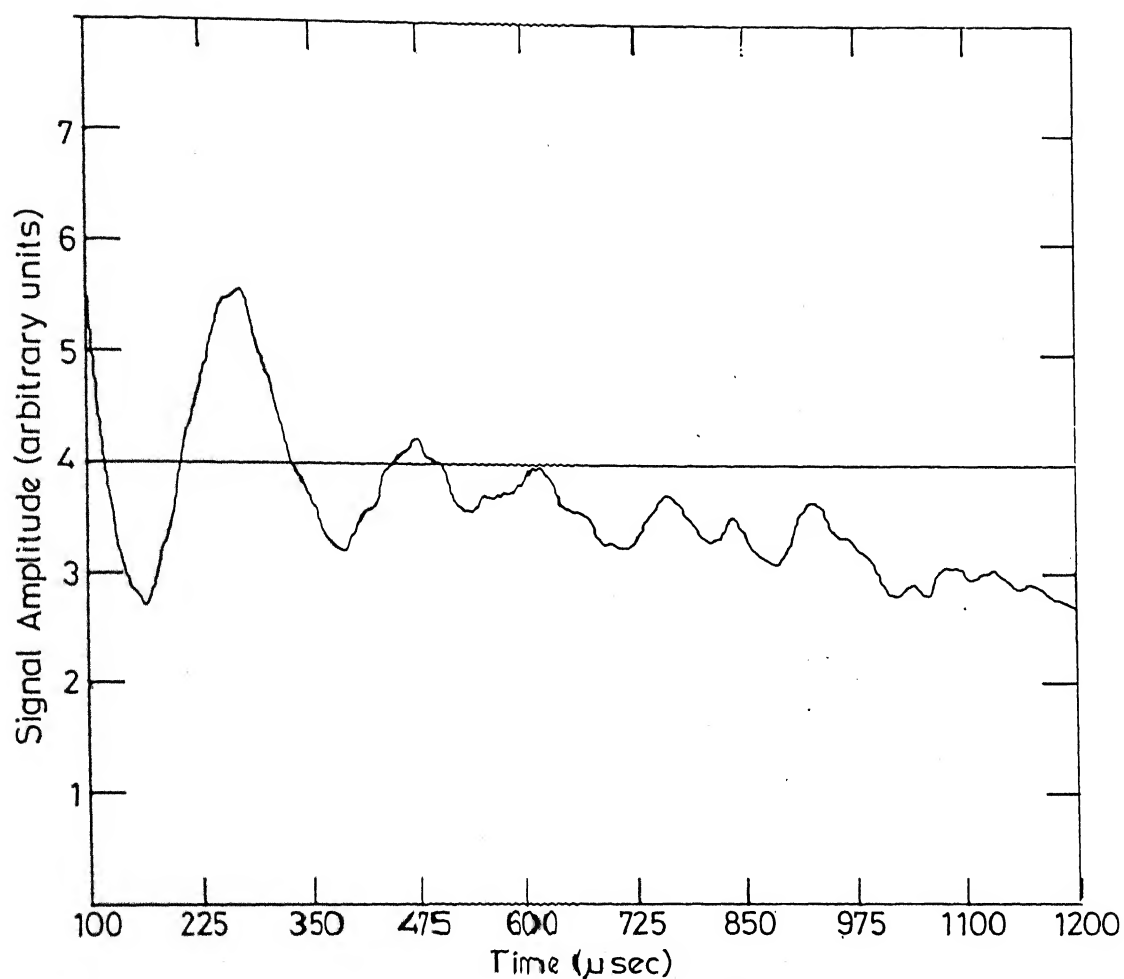


Fig.III.16 Response of soft-pulse excitation from  $^{35}\text{Cl}$  in powdered sample of  $\text{KClO}_3$  ( $\omega_0=28.094\text{MHz}$ ) with a magnetic field  $\approx 9.75$  Gauss and a soft-pulse power of  $\approx 5$  Watts.

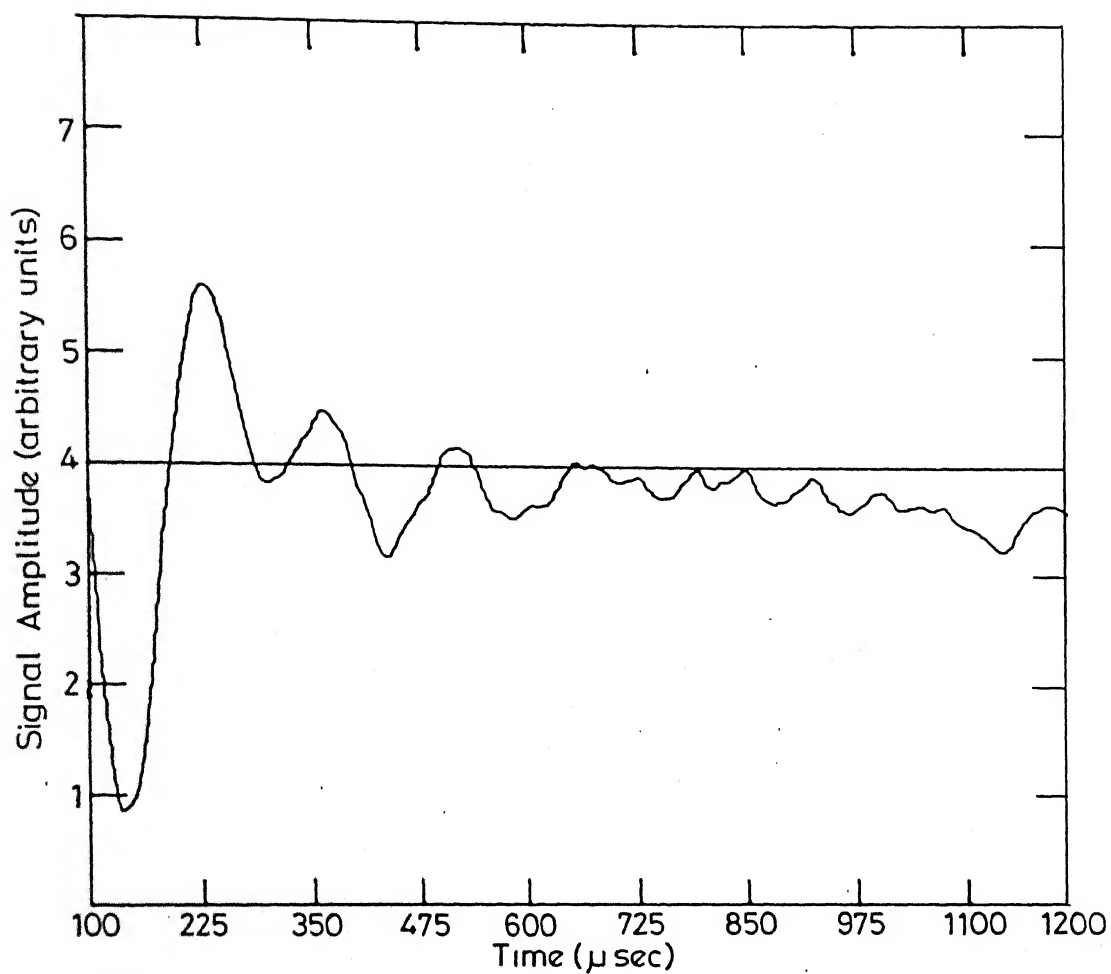


Fig.III.17 Same as in Fig.III.16, but with a soft-pulse power of  $\approx 7.5$  Watts.

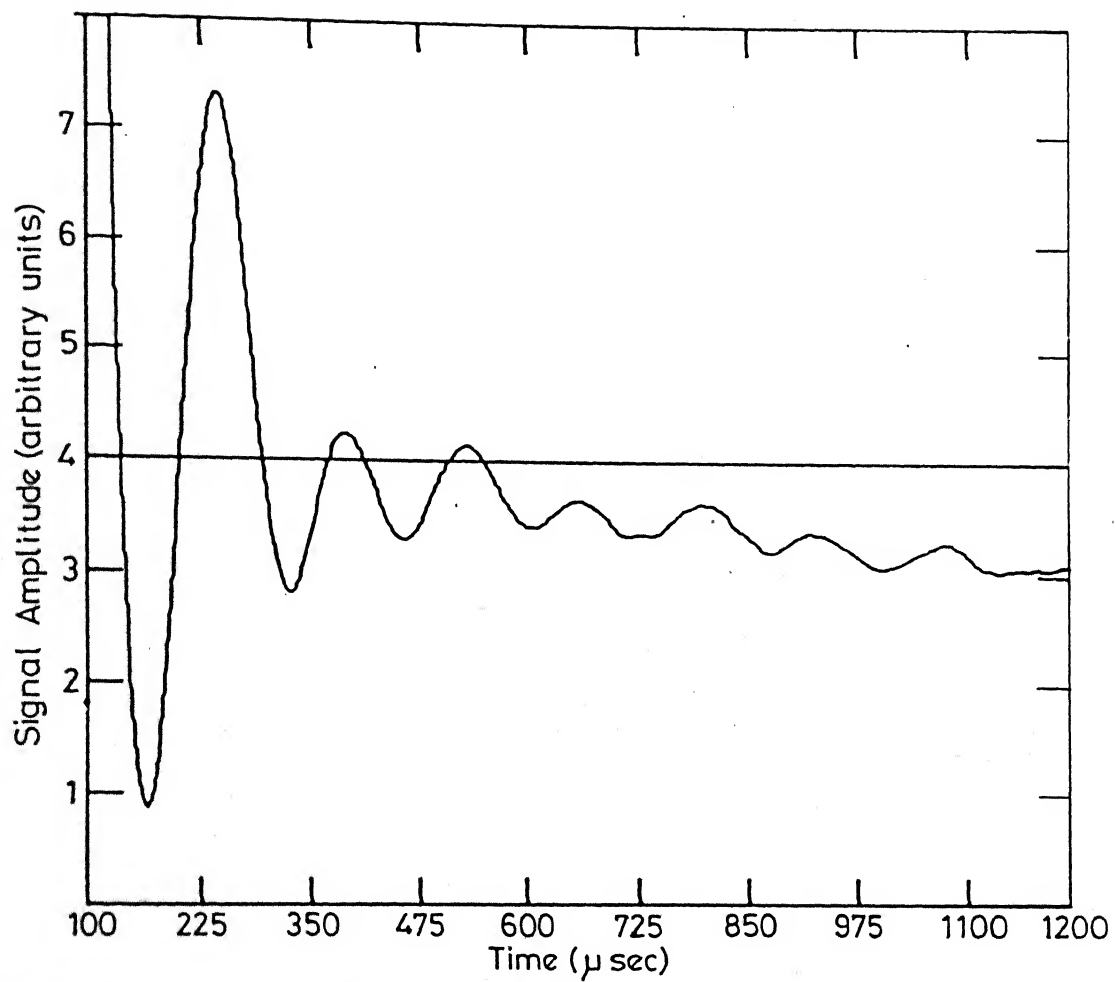


Fig.III.18: Same as in Fig.III.16, but with a soft-pulse power of  $\approx 13$  Watts.

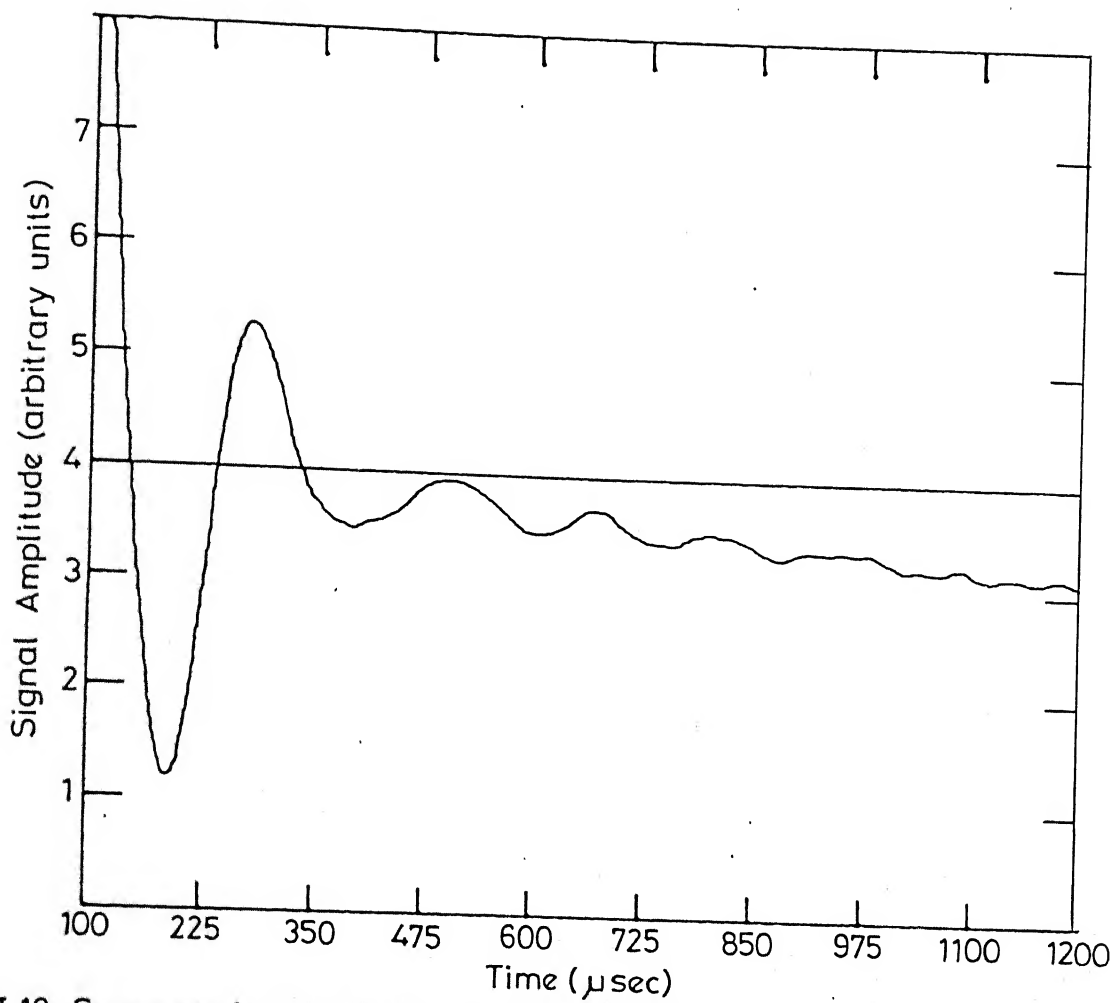


Fig.III.19 Same as in Fig.III.16, but with a soft-pulse power of  $\approx 19$  Watts.



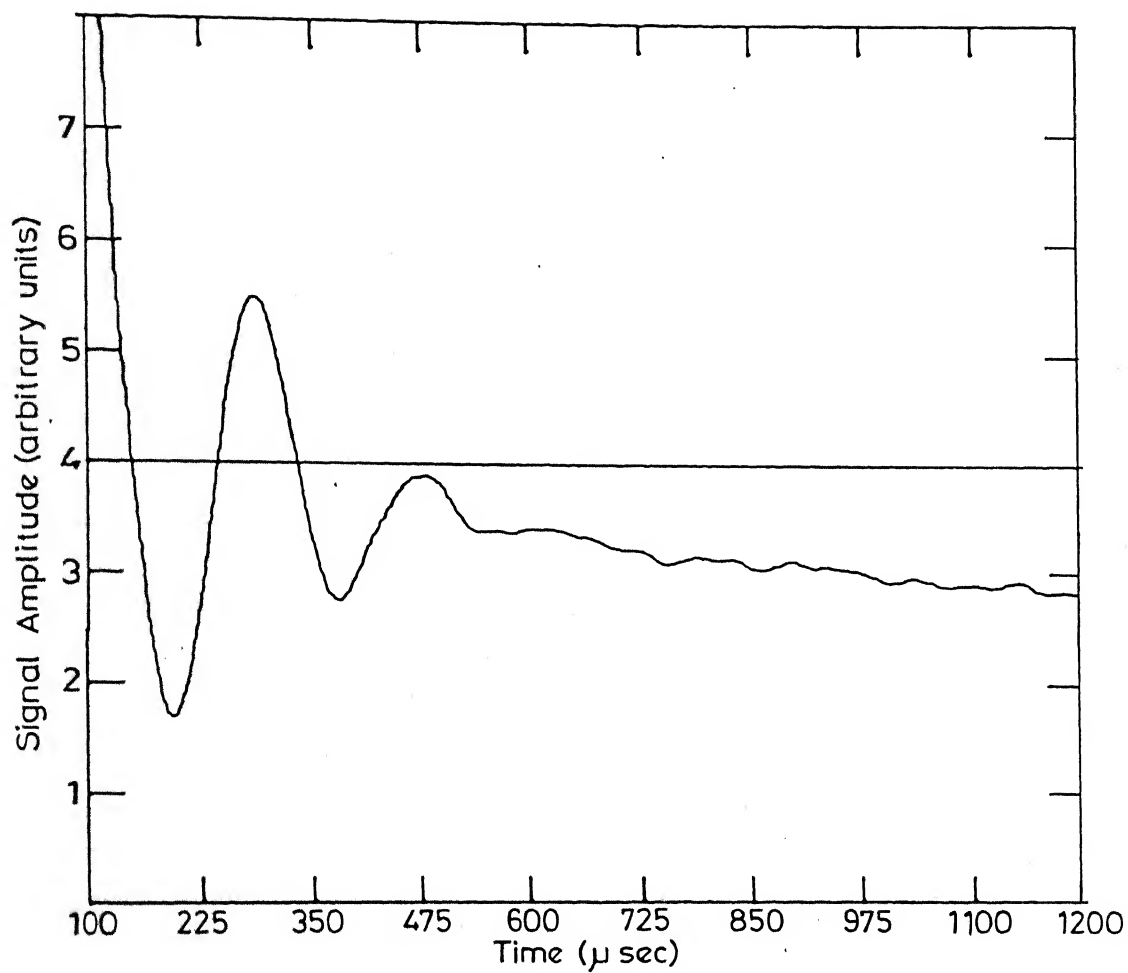


Fig.III.20 Same as in Fig.III.16, but with a soft-pulse power of  $\approx 22$  Watts

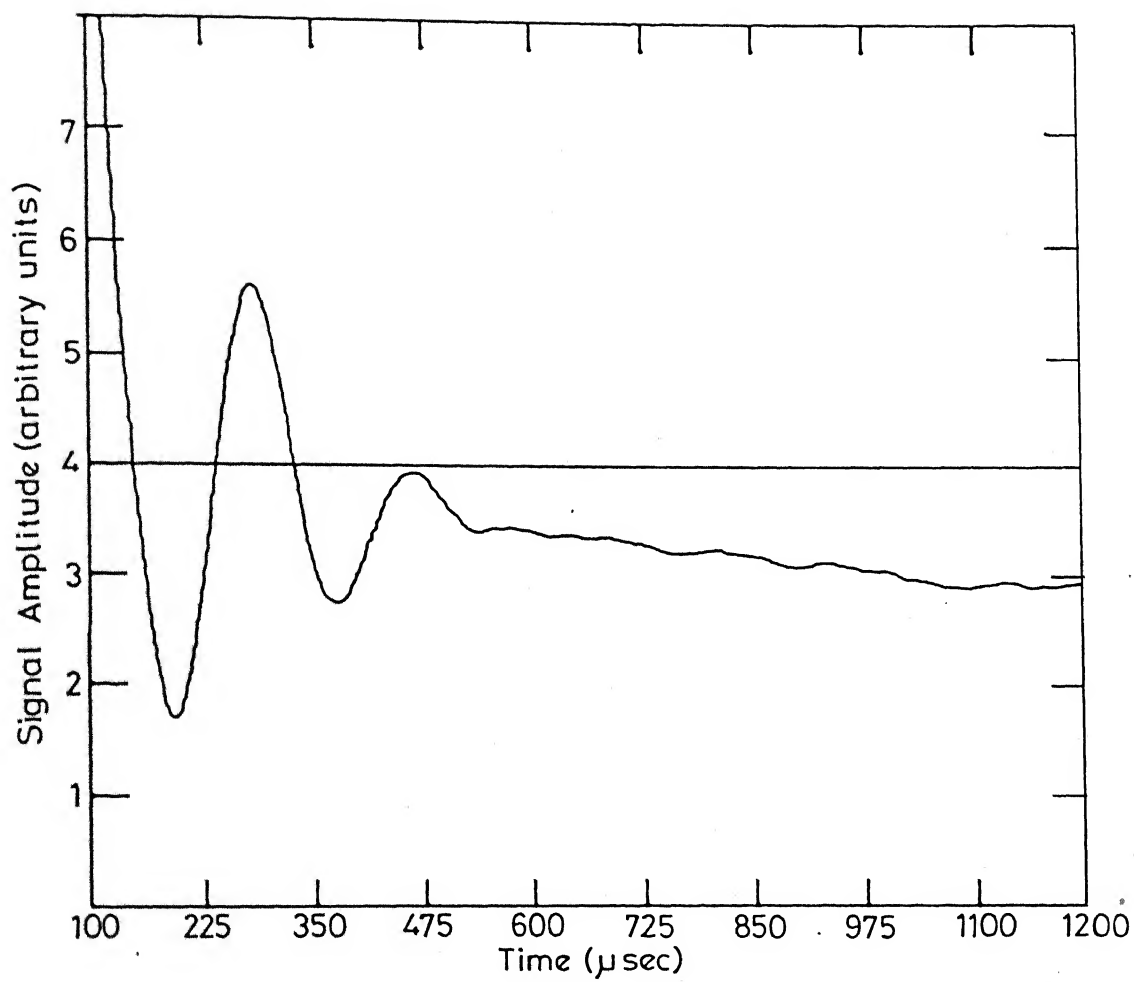


Fig.III.21 Same as in Fig.III.16, but with a soft-pulse power of  $\approx 25$  Watts.

9 to 20 Gauss. The ZSEEM spectra so obtained are presented in Figs. III.22(a) to III.22(c). It should be mentioned that the value of  $T_2$  for this compound is short and hence the modulations on the echo envelope die off faster. We have, therefore, studied the soft-pulse response in this compound for a duration of  $675 \mu\text{sec}$  only. Since we have reduced the length of the soft-pulse, the receiver dead time has also been decreased and the response could therefore be acquired with a delay of only  $50 \mu\text{sec}$  from the  $\pi$ -pulse. Except for the initial period of  $\approx 150 \mu\text{sec}$ , these responses agree with those recorded for this site at corresponding magnetic field values by the two-pulse method (see Figs. III.8(a) to III.8(c)). The responses clearly show the decay patterns corresponding to a non-zero  $\eta$  value for this site in  $\text{SbCl}_3$ . It is also interesting to note that excluding the initial  $150 \mu\text{sec}$ , the pattern shown in Fig. III.22(c) agrees well with the pattern simulated theoretically by Ramachandran and Narasimhan [15] (see Fig. 9(b) of this reference) at approximately the same magnetic field with a value of  $\eta$  of 0.15. We thus see clearly the feasibility of obtaining  $\eta$  values for spin  $3/2$  case from the ZSEEM patterns obtained by the soft-pulse excitation method for powder specimens.

### III.E(3) A Comparative Study of the Two Methods of Obtaining ZSEEM From Powder Samples

The results of soft-pulse excitation presented in the previous section (section III.E(2)) are quite encouraging and informative. However, it is clear from a comparison of the

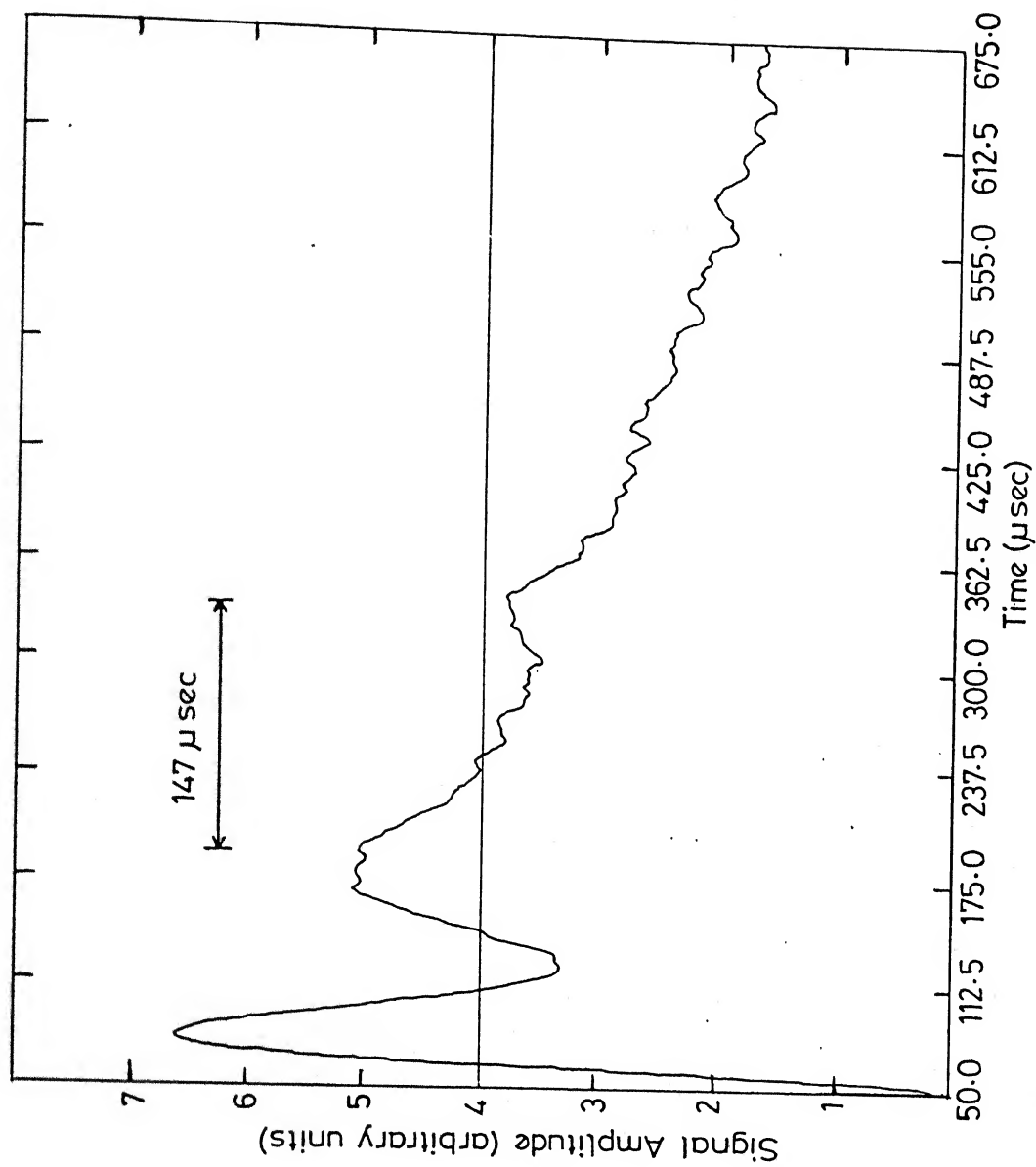


Fig.III.22(a) Response of soft pulse of excitation from  $^{35}\text{Cl}$  in powdered sample of  $\text{SbCl}_3$  ( $\omega_0 = 19.1713 \text{ MHz}$ ) with a magnetic field  $\approx 9.75 \text{ Gauss}$ .

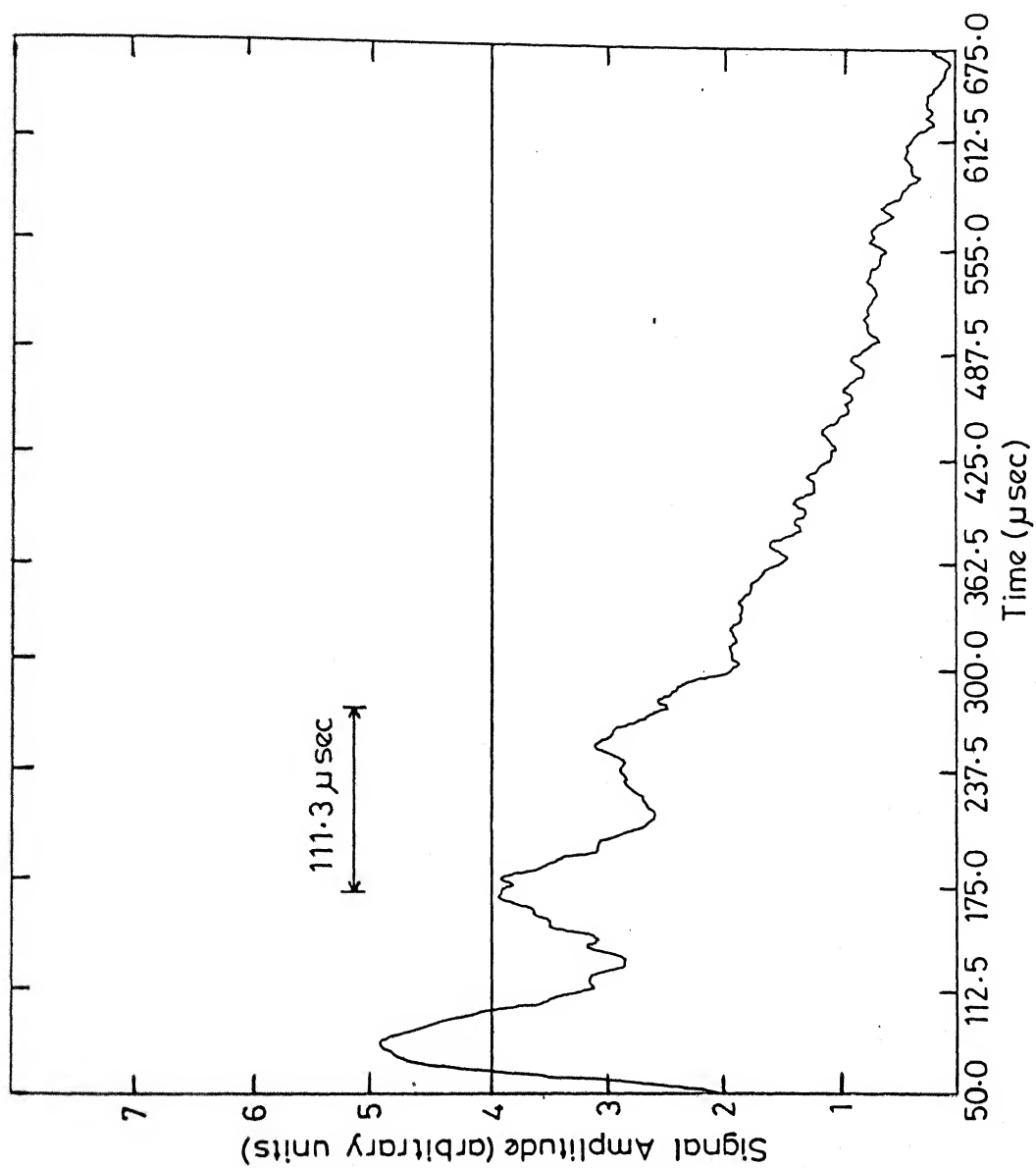


Fig. III 22(b) Same as in Fig. III 22(a), but with a magnetic field  $\approx 13$  Gauss.

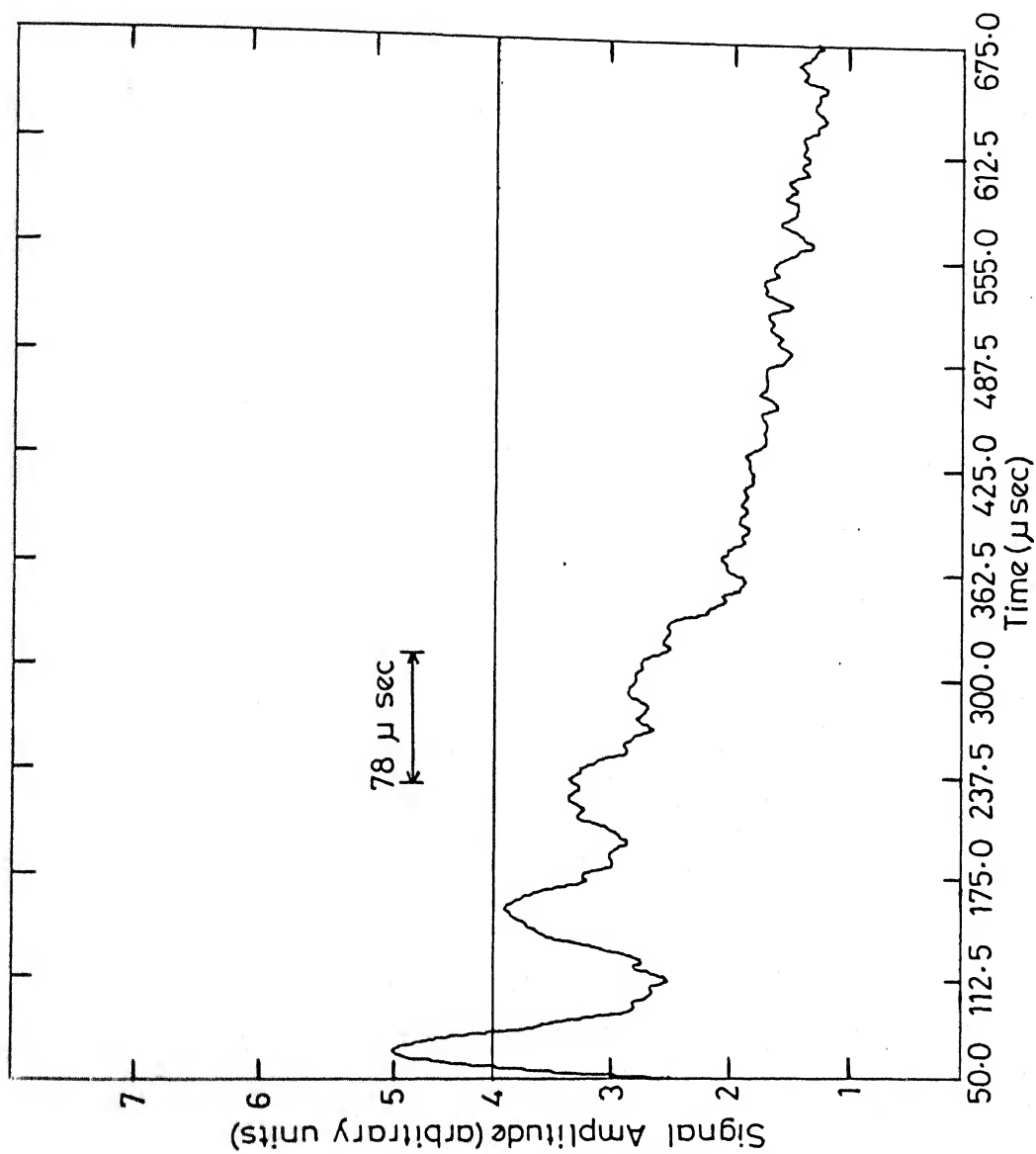


Fig.III.22(c) Same as in Fig.III.22(a), but with a magnetic field  $\approx 19.5$  Gauss.

initial portion of the experimental ZSEEM obtained from the two-pulse method and the extended time excitation method that the response from soft-pulse excitation is quite intense for  $\approx 350 \mu$  sec in the case of  $\text{KClO}_3$  and  $\approx 150 \mu$  sec in the case of  $\text{SbCl}_3$ . In these regions there is no one-to-one correspondence between the patterns obtained from the two methods. It should be mentioned here that such a difference has not been observed by Schweiger and coworkers [24] in the case of electron spin-echo envelope modulation (ESEEM) spectroscopy.

In our view the following may be responsible for this difference; (1) the  $\pi$ -pulse applied in our studies may not be a "hard"  $\pi$ -pulse with the result the origin of the time reversal is not well-defined. This would result in a smearing and low-pass filtering of the modulation patterns [34]. This factor, however, does not seem to be affecting the soft-pulse response in our experiments because the modulation patterns in the long time (large  $\tau$ ) region are in agreement with those from the two-pulse method. Further investigation of this point needs increased r.f. power capabilities in our spectrometer system.

The second and main factor which we feel is responsible for the observed difference between the soft-pulse excitation response and the one from the two-pulse method is that the  $\pi$ -pulse may not be properly refocusing the interactions after the sample has been prepared by the soft-pulse excitation on account of the random orientation of efg axes in powder samples. That part of the

magnetization which is not refocused remanant magnetization, may be responsible for the large initial signal which decays with a shorter time constant ( $T_1^*$ ) compared to the echo decay time constant ( $T_2$ ).

Although the use of single crystals would improve matters concerning the proper definition of the  $\pi$ -pulse with respect to the principal efg axes,  $H_1$  inhomogeneities (if present) could still contribute to the deviation in the pulse angle over different regions in the sample. Since we are interested in the determination of asymmetry parameter of the efg tensor in powder specimens containing spin  $3/2$  nuclei we shall concern ourselves here with the evaluation of the applicability of the extended excitation technique for powder samples. In this context we investigated the use of a composite  $\pi$ -refocusing pulse in conjunction with the soft excitation pulse hoping that this would reduce the deviation from the  $180^\circ$  rotation angle experienced by various crystallites. In particular, we employed a composite  $\pi_x$ -pulse [35] consisting of three pulses viz.,  $(\frac{1}{2}\pi_x - \pi_y - \frac{1}{2}\pi_x)$  as the refocusing pulse. This pulse did not improve matters in our experiments possibly because of the large time duration ( $\approx 120\mu$  sec) required for the composite  $\pi$ -pulse itself with our present transmitter (R.F. power  $\approx 800$  watts). As has been pointed out earlier in this section, long refocusing pulses are not conducive for obtaining clear modulation patterns since the origin of the time reversal will not then be well-defined and a



low pass filtering action would take place [34]. In order to prove the fact that the large initial signal with faster decay rate is due to  $\pi$ -pulse which is enable to refocus completely the magnetization in powder samples used in our studies, we performed a soft-pulse excitation experiment on  $^{35}\text{Cl}$  in powdered  $\text{KClO}_3$  with  $H_0 = 9.75$  Gauss and used a delay of  $450\mu$  sec between the soft-pulse and the  $\pi$ -pulse. The response was acquired with a delay of  $100\mu$  sec following the  $\pi$ -pulse (Fig. III.23). The signal so obtained indeed contains the initial large signal which decays faster (with a time constant  $T_2^*$ ). It is also apparent from the figure (III.23) that the signal after  $450\mu$  sec following the  $\pi$ -pulse is due to the soft-pulse excitation response and this portion of the response is identical to that shown in Fig. III.12 obtained at the same magnetic field (9.75 Gauss). This clearly confirms the fact that the initial fast-decaying large amplitude signal is due to "non-echo" response. This signal decays with a time constant  $T_2^*$  ( $200\mu$  sec in  $\text{KClO}_3$ ) and after a period of 300-400 $\mu$  sec its effect on the response is not significant. Mention may be made here of the fact that the echo envelope modulations decay with a time constant  $T_2$  which is of the order of a msec in this compound. It is, therefore, seen in our soft-pulse excitation experiments that, once the initial high intensity signal decays, the ZSEEM pattern is clear and this latter portion of the response is in complete agreement with that from the two-pulse method (see section III.E(2)). Figure III.23 also shows the soft-pulse excitation response (dotted lines) without any

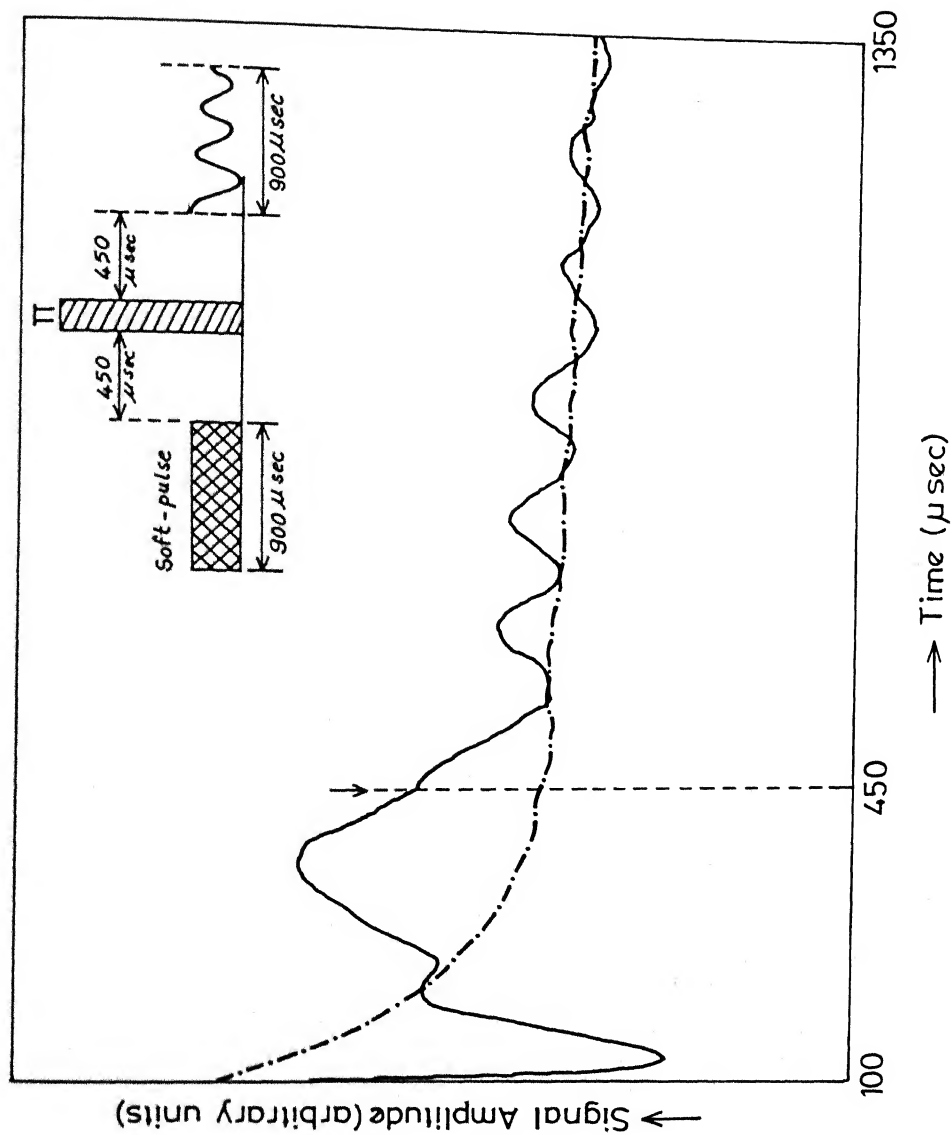


Fig. III.23 Soft-pulse excitation response obtained from  $^{35}\text{Cl}$  in powdered  $\text{KClO}_3$  ( $H_0 = 9.75$  Gauss) with a delay time of  $450 \mu\text{sec}$  between the excitation pulse and the refocusing pulse. Dot-Dash lines show the echo decay obtained from the soft-pulse excitation without any magnetic field.

magnetic field which clearly shows an unmodulated echo decay pattern and also contains an initial fast-decaying large amplitude signal with characteristic time constant  $T_2^*$ . We may, therefore conclude that the soft-pulse excitation method, as applied to powder samples in NQR spectroscopy, is suitable for compounds having short  $T_2^*$  and long  $T_2$  values. The ESEEM spectra obtained by Schweiger et al. did not show any interference from signals due to unrefocused components immediately following the  $\pi$ -pulse. This point could be easily understood in terms of the high Zeeman field used in their experiments which provides a common axis of quantization for all the spins in the sample and the fact that the  $180^\circ$  refocussing pulse is a "hard" and "clean"  $\pi$ -pulse. Consequently, the "non-echo" response is practically absent in their experiment, unlike the NQR case. Further work in the direction of finding out suitable schemes for suppressing the uninteresting  $T_2^*$  decay signal in powder samples and enhancing the ZSEEM intensity in the short  $\tau$  region is in progress in our laboratory.

### III.E(4) Conclusion

The extended-time excitation method is a fast and convenient method of obtaining ZSEEM spectra in NQR Spectroscopy compared to the conventional two pulse method. The asymmetry parameter  $\eta$  can be obtained for spin  $I = 3/2$  nuclei by a comparison of soft-pulse response in the longer  $\tau$  region with the

theoretically simulated ZSEEM spectra [15].

Though, we have utilized a microprocessor-controlled pulsed NQR spectrometer equipped with a signal analyzer for this experiment, it should be pointed out that this experiment could also be performed with unautomated spectrometer systems equipped with just (i) a hardware pulse generator capable of generating two-pulse sequence, and (ii) a transient recorder or a time averager. The soft pulse excitation technique is, therefore, an easier alternative way of obtaining ZSEEM and thereby  $\eta$ . However, it should be mentioned that method is limited to compounds having short  $T_2^*$  and long  $T_2$  values.

### Summary

In this chapter an experimental investigation on the possibility of evaluating  $\eta$  for spin 3/2 powder samples through ZSEEM analysis has been undertaken. The experimental investigations were carried out using a microprocessor-controlled pulsed NQR spectrometer (described in Chapter II) operated in the automatic ZSEEM acquisition mode. A brief survey of CW methods of obtaining  $\eta$  from spin 3/2 powder samples and an introduction to spin-echo envelope modulation studies has also been presented. Our experimental ZSEEM investigations have clearly revealed the fact that it is possible to obtain  $\eta$  values by comparing experimental ZSEEM patterns with the patterns obtained from theoretical simulation. It has also been demonstrated that automation of

the spectrometer system for carrying out ZSEEM investigations using the two-pulse method enormously reduces the experiment time. In this chapter we have also described a new methodology of obtaining SEEM patterns using extended-time excitation technique and implemented the technique for the first time to study ZSEEM of powder samples containing spin  $3/2$  nuclei. It has been pointed out that the method is suitable for compounds having short  $T_2^*$  and long  $T_2$  values.

In the next chapter our experimental investigation on responses to various multiple-pulse sequences of spin  $I = 3/2$  in powder samples will be presented.

REFERENCES

- [1] (a) T.P. Das and E.L. Hahn, "Nuclear Quadrupole Resonance Spectroscopy," Solid State Physics, Supplement 1, Academic Press, New York (1958).  
(b) E.A.C. Lucken, Nuclear Quadrupole Coupling Constants," Academic Press, New York (1969).
- [2] C. Dean, Phys. Rev., 96, 1053 (1954).
- [3] Y. Morino and M. Toyama, J. Chem. Phys., 35, 1289 (1961).
- [4] K.V. Raman and P.T. Narasimhan, Pure appl. Chem., 32, 271 (1972).
- [5] V. Harihara Subramanian and P.T. Narasimhan, J. Molec. Struct., 58, 193 (1980) and references cited therein.
- [6] F.J. Adrian, J. Chem. Phys., 38, 1258 (1963).
- [7] H.R. Brooker and R.B. Creel, J. Chem. Phys., 61, 3658 (1974).
- [8] J. Darville, A. Gerard and M.T. Calende, J. Magn. Reson., 16, 205 (1974).
- [9] E.L. Hahn and D.E. Maxwell, Phys. Rev., 88, 1070 (1952).
- [10] L.G. Rowan, E.L. Hahn and W.B. Mims, Phys. Rev., 137, 61 (1965).
- [11] V.F. Yudanov, A.M. Raitsmirov and Yu.D. Tsvetkov, Teor. Experim. Khim. Akad. Nauk Ukr. SSR, 4, 520 (1968).
- [12] D. Grischkowsky and S.R. Hartmann, Phys. Rev., B2, 60 (1970).
- [13] Yu. E. Sapozhnikov and Ya. B. Yasman, Bull. Acad. Sci. USSR, Phys. Ser., 42, 210 (1978).
- [14] W.B. Mims, Phys. Rev., B5, 2409 (1972).
- [15] R. Ramachandran and P.T. Narasimhan, Molec. Phys., 48, 267 (1983).

- [16] M.E. Ainbinder, V.S. Grechishkin, A.D. Gordeev and A.S. Osipenko, *Sov. Phys. Solid State*, 10, 1592 (1969).
- [17] D.O. Zakirov and I.A. Safin, *J. Molec. Struct.*, 83, 253 (1982).
- [18] R. Ramachandran and P.T. Narasimhan, *J. Phys. E: Sci. Instrum.*, 16, 643 (1983).
- [19] Narsimha Reddy, Arun Bhavsar and P.T. Narasimhan, *Z. Naturforsch.*, 41a, 449 (1986).
- [20] D.E. Woessner and H.S. Gutowsky, *J. Chem. Phys.*, 39, 440 (1963).
- [21] M. Toyama, *J. Phys. Soc. Japan*, 14, 1727 (1959).
- [22] J.C. Pratt, *Molec. Phys.*, 34, 539 (1977).
- [23] S. Sengupta, D. Giezendanner and E.A.C. Lucken, *J. Magn. Reson.*, 38, 553 (1980).
- [24] A. Schweiger, L. Braunschweiler, J.M. Fauth and R.R. Ernst, *Phys. Rev. Lett.*, 54, 1241 (1985).
- [25] S. Fernbach and W.G. Proctor, *J. Appl. Phys.*, 26, 170 (1955).
- [26] P. Mansfield, A.A. Maudsley, P.G. Morris and I.L. Pyckett, *J. Magn. Reson.*, 33, 261 (1979).
- [27] D.F. Hoult, *J. Magn. Reson.*, 35, 69 (1979).
- [28] S.O. Elyutin, S.M. Zakharov and E.A. Manykin, *Zh. Eksp. Teor. Fiz.*, 76, 835 (1979) [*Sov. Phys. JETP*, 49, 421 (1979)].
- [29] V.A. Zulkov, V.V. Samartsev and R.G. Usmannov, *Pis'ma Zh. Eksp. Teor. Fiz.*, 32, 293 (1980) [*JETP Lett.*, 32, 270 (1980)].
- [30] N.W. Carlson, L.J. Rothberg, A.G. Yodh, W.R. Babbitt and T.W. Mossberg, *Opt. Lett.*, 8, 483 (1983).

- [31] D.W. Carlson, Y.S. Bei, W.R. Babbitt and T.W. Mossberg, Phys. Rev., A30, 1572 (1984).
- [32] L. Kevan, M.K. Bowman, P.A. Narayana, R.K. Boeckman, V.F. Yuldanov and Y.D. Tavetkov, J. Chem. Phys., 63, 409 (1975).
- [33] R.M. Macfarlane, R.M. Shelby and R.L. Shoemaker, Phys. Rev. Lett., 43, 1726 (1979).
- [34] L. Breunschweiler, J.-M. Fauth, A. Schweiger and R.R. Ernst, J. Magn. Reson., 64, 160 (1985).
- [35] R. Freeman, S.P. Kempell and M.H. Levitt, J. Magn. Reson., 38, 453 (1980).



## CHAPTER IV

MULTIPLE-PULSE RESPONSES IN  
NQR SPECTROSCOPY : AN EXPERIMENTAL  
STUDY ON POWDER SAMPLES CONTAINING  
SPIN  $I = 3/2$  NUCLEI

This chapter deals with experimental investigations of multiple-pulse responses from  $^{35}\text{Cl}$  ( $I = 3/2$ ) in polycrystalline samples. Section IV.A presents a survey of earlier investigations in the area of multiple-pulse NQR spectroscopy. Section IV.B gives a detailed discussion of our experimental results on responses from spin-3/2 systems in powdered samples to various multiple-pulse sequences and conclusions derived therefrom.

#### IV.A MULTIPLE-PULSE STUDIES IN NQR: A SURVEY

In NMR of solids, the response of  $I = 1/2$  spin systems to various multiple-pulse sequences has been well-studied, and sequences for suppressing the dipolar broadening to obtain high resolution NMR spectra in the solid state are now well-established [1]. Similar experiments carried out in pure quadrupole resonance in the time scales of the order of transverse relaxation times would show how the various factors contributing to the NQR line width respond to strong pulsed r.f. field perturbations, and would indicate pulse sequence characteristics that would lead to narrowing of NQR line widths. Such line narrowing experiments are expected to yield valuable information on the interactions leading to fine structure of NQR lines. Unlike NMR there are very few studies in NQR in the direction of theoretical and experimental investigations with multiple-pulse sequences. Further, we have noticed that in NQR spectroscopy the

majority of investigations on multiple-pulse responses have been carried out on spin  $I = 1$  systems and very little work has been carried out on  $I \geq 3/2$  systems. To the best of our knowledge there is only one experimental investigation reported in the literature [2] concerning multiple pulse spin-locking in pure NQR spectroscopy of spin  $I \geq 3/2$  systems. This study examined the spin-locking effect under the influence of Carr-Purcell-Maiboom-Gill (CPMG) sequence [3]. In this chapter we present the results of our experimental investigations on responses to a variety of multiple-pulse sequences of spin  $I = 3/2$  powder samples.

We shall first review the available literature on multiple-pulse NQR spectroscopy. The first experimental observation of multiple-pulse responses in NQR spectroscopy was due to Marino and Klainer [4]. Their study has been on the  $\nu$  transition ( $0 \leftrightarrow -1$ ) of  $^{14}\text{N}$  ( $I = 1$ ) nuclei in a powdered sample of  $\text{NaNO}_2$  using the Ostroff-Waugh (OW) sequence [5]. Surprisingly, their results were analogous to those observed in nuclear magnetic resonance (NMR) by Ostroff and Waugh [5], and by Mansfield and Ware [6] though the systems studied in both the cases were entirely different. Marino and Klainer have reported that the persistence of the echo train for times much larger than  $T_2$  took place (i) when  $\tau \leq T_2$ , where  $\tau$  is the time spacing between the first two pulses of the excitation sequence, and (ii) when the Carr-Purcell (CP) sequence [7] is modified in the following

two ways: all the pulses are  $90^\circ$  pulses and the first pulse is phase shifted by  $90^\circ$  with respect to all the others (i.e. Ostroff-Waugh sequence). Under these conditions the spin-echo train decays much slower than the usual spin-echo decay. The echo decay process under the influence of spin-locking sequence is characterized by a time constant,  $T_{2\epsilon}$ , which is much longer than  $T_2$ . For  $\tau \leq T_2$  the effective relaxation time  $T_{2\epsilon}$  becomes strongly dependent on  $\tau$ . Marino and Klainer have also shown that when  $T_2 < T_{2\epsilon} < T_1$  the data fit very well by the relation  $T_{2\epsilon} \approx \tau^{-5}$ , supporting strongly the observation of pulsed spin-locking effect in pure quadrupole resonance. One would, therefore, expect that for  $\tau \rightarrow 0$  one would obtain  $T_{2\epsilon} \rightarrow T_{1\rho}$ , the spin-lattice relaxation in the rotating frame and infact Marino and Klainer [4] have observed the echo train which persisted for several seconds even though the spin-spin relaxation time  $T_2$  measured by the  $90^\circ - \tau - 180^\circ$  method is only  $3.4 \times 10^{-3}$  sec in  $\text{NaNO}_2$  for the observed transition. These authors pointed out that this observation promises to improve substantially the effective sensitivity of  $^{14}\text{N}$  NQR by coherently adding the individual echoes within a spin-locked spin-echo sequence.

The next experimental investigation in the area of multiple-pulse NQR is that of Osokin [8-10], who utilized phase alternated multiple-pulse sequence [PAPS], and also the spin-locking sequences of CPMG and OW. He showed in the case of spin-1 systems that the echo decay time constant ( $T_{2\epsilon}$ ) under the

action of the above pulse sequences could be enhanced considerably. He found that the decay time constant of multiple echoes is greatly enhanced when the following cycles are used [18],

1) PAPS:

$$\text{i.e., } \theta_1(x) - [\tau - \theta_2(-x) - 2\tau - \theta_2(x) - \tau]_n$$

2) Spin-locking sequence:

$$\text{i.e., } \theta_1(x) - [\tau - \theta_2(y) - \tau]_n .$$

His experimental results showed that the decay time constant equals in the order of magnitude to the spin-lattice relaxation time ( $T_1$ ). For example, in the case of methylamine  $T_1 \approx 1$  sec at 77 K and the decay time constant obtained was  $\approx 0.5$  sec. In polycrystalline sodium nitrite  $T_1 \approx 12$  sec and the measured decay time constant from these experiments was about 10 sec. Thus, from the correlation between the decay time constants and the  $T_1$  values, Osokin concluded that molecular motions are responsible for the decay of the spin-echo envelope and that all other sources of line broadening averaged out and hence have no influence on the evolution of the spin system during the application of multipulse sequences mentioned above. In addition, it was also noticed by him that the decay time constant,  $T_{2\epsilon}$ , depends on the cycle pulse width  $\theta_2$ . In methylamine  $T_{2\epsilon}$  increased by a factor of about 1.5 as the pulse width was decreased from  $\theta_2 = 2\theta_1$  to  $\theta_2 = \theta_1$  (i.e. when all the pulses are made equal to  $\pi/2$ ).

The third experimental group in the area of multiple-pulse NQR is that of Ainbinder et al. [2]. They have performed spin-locking experiments on  $^{35}\text{Cl}$  ( $I = 3/2$ ) and  $^{123}\text{Sb}$  ( $I = 7/2$ ) in polycrystalline samples using CPMG sequence and confirmed the quasi-equilibrium character of the magnetization decay under spin-locked conditions (i.e. signal decay was observed with a time constant  $T_{2\epsilon} \gg T_2$ ). They have also studied the dependence of  $T_{2\epsilon}$  on  $\tau$  and observed that  $T_{2\epsilon}$  increases as  $\tau$  is decreased but always remains smaller than  $T_{1\rho}$ .

Ermakov and Osokin [11] have also used the WAHUHA 4-pulse sequence which causes selective averaging of homonuclear dipolar interactions in NMR of solids. They studied the NQR of  $^{14}\text{N}$  nuclei ( $I = 1$ ) in a single crystal sample of  $\text{NaNO}_2$ . In order to examine the effect of WAHUHA sequence they used different preparatory pulses to obtain the time dependence of the NQR spin echo intensity. The experiment gave the fast decay of the observed signal on the time of the order of  $T_2$  indicating that none of the interactions could be averaged in this experiment.

Let us now consider various theoretical frame works that have been proposed to interpret the experimental results described above, in the area of multiple-pulse NQR.

A theoretical interpretation for the experimental results of Marino and Klainer has been given by Cantor and Waugh [12]. It is appropriate to point-out that in NMR spectroscopy the time dependence of the observed magnetization (in short time periods)

in the Ostroff-Waugh experiment has been explained using the average-Hamiltonian theory [1,13]. Various approximation methods [14] and spin temperature concepts [15] have been used to explain the long-term behavior.

Coming now to NQR of powder samples the effective pulse angle will not be  $90^\circ$  for all spins, but will vary from one crystallite to the other depending on the relative orientation of the quadrupole principal axis system and the r.f. field direction. The Hamiltonian under the action of OW sequence is therefore not cyclic (i.e. in the appropriate interaction representation it is not periodic in time) and the average-Hamiltonian theory cannot be used for the case of NQR of powder samples. A different theoretical approach is thus required to explain the pulsed spin-locking effect in the case of NQR. Using a model for the polycrystalline sample containing spin-1 nuclei Cantor and Waugh [12] have developed a theoretical method to follow the evolution of the density matrix. They modelled the system as an ensemble of isolated two-spin systems, each system randomly oriented with respect to the r.f. field direction, depending on the orientation of the crystallite in which it is present and also assumed that the quadrupole principal axis system for each of the two spins have the same orientation with respect to r.f. field direction. It should be noted that the time development of the system under the spin-locking (Ostroff-Waugh) sequence has been considered using the reduced density

obtaining qualitative information on short-time behaviour (i.e. the effective spin-locking observed in multiple-pulse NQR) of the system. To understand the long-time behaviour, they have applied a molecular-Chaos approximation [14] to this model system, which leads to the conclusion that the characteristic decay time  $T_{2\epsilon}$  increases as the time between the pulses decreases. However, they have not been able to obtain the functional dependence of  $T_{2\epsilon}$  on  $\tau$ . The non-explicability of the long-time behavior (i.e. the dependence of the magnetization decay time on the pulse sequence parameter  $\tau$ ) of this two-spin model is not surprising because the decay depends intrinsically on the many-spin nature characteristic of the real system.

Recently, Hitrin et al. [18] have developed a theoretical frame work for NQR spin  $I = 1$  systems which predicts the observed short-time and also the long time behavior in pulsed spin-locking experiment of Marino and Klainer [4]. Their theory is based on the canonical transformation technique [19] to obtain the solution for the density matrix and these authors used ensemble averaging over all the orientations of crystallites to obtain the magnetization in powder samples. The long-time behavior predicted by their theory depends on the details of the model system considered. A three-spin model, for instance, predicts that the decay time constant ( $T_{2\epsilon}$ ) is proportional to  $\tau^{-2}$  and a four-spin model predicts  $\tau^{-4}$  dependence. This clearly shows that, as the model approaches the real system (many-spin model)



the predicted long time behavior approaches experimental results ( $\tau^{-5}$  dependence). They have also studied the effect of off-set and spin-lattice relaxation on the evolution of the quasi-steady state magnetization.

It should be mentioned here that as far as the spin-locking sequence of Ostroff and Waugh for NQR systems is concerned the canonical transformation approach of Hiltner et al. is suitable only for the case of spin-1 NQR systems, where the use of spin-1/2 operator formalism could reduce the problem to the one with equidistant spectra. It is only recently that Ainsbinder et al. [20,21] have developed a theory for non-equidistant spectra and arbitrary spin by using the method of canonical transformations and the Krylov-Bogolyubov-Mitropol'skii (K-B-M) averaging method [22]. The K-B-M averaging method is applicable to non-equidistant spectra. Ainsbinder et al. [20,21] have obtained conditions for spin-locking in NQR and have shown that in the multiple-pulse sequence represented below:

$$90_x - [\tau - \theta_{(x+\phi)} - \tau]_n$$

Spin-locking occurs for arbitrary  $\theta$  values when  $\phi = (2k+1)\pi/2$ , where  $k$  is an integer (i.e.,  $k = 0, 1, 2$ ). It should be noted that the experiment by Marino and Klainer [4] corresponds to a particular case where  $\theta = \pi/2$  and  $k = 0$ . Ainsbinder and Furman [20] have pointed out that for any spin system with arbitrary spin it is possible to choose a pulse sequence that can lead to

a spin-locking state thereby averaging the interactions that broaden the spectrum. It should be mentioned here that the theory due to Ainsbinder et al. is general and is applicable to any non-equidistant pure quadrupole spin system with arbitrary spin value. Ainsbinder and Furman [20] have proposed from their theory that similar to that in NMR the multiple-pulse action in NQR spectroscopy leads to two types of averaging of internal interactions which broaden the NQR lines, namely, (i) general averaging and (ii) selective averaging. (i) A pulse sequence that influences right away all the types of interactions regardless of their nature is said to be causing general averaging. Examples of sequences causing this averaging are spin-locking sequence and phase alternated multiple pulse sequence. (ii) The pulse sequences which selectively average particular interactions are said to cause "selective averaging". Unlike NMR, pulse sequences causing "selective averaging" have not so far been designed in NQR literature.

Recently Ainsbinder et al. [2] have proposed a theory for spin-lattice and spin-spin relaxation processes for systems with  $I \geq 1/2$  under the action of multiple-pulse spin-locking sequences. The theory is based on the assumption that for times larger than  $T_2$  after the first pulse of the pulse sequence the decay of magnetization is slow enough to consider it as a quasi-equilibrium process ( $T_2 \approx \omega_{loc}^{-1} = (\gamma H_{loc})^{-1}$ ). They have verified this assumption from their experiments on  $^{35}\text{Cl}$  ( $I = 3/2$ ) and

$^{123}\text{Sb}$  ( $I = 7/2$ ) in polycrystalline samples.

More recently, Matti Maricq [23] has employed Floquet theory to analyze the quasi-stationary state and its decay to equilibrium in the pulsed spin-locking NQR experiment. He has shown that the behavior of the magnetization for  $I = 1$  systems with respect to pulse angle, pulse spacing, and resonance offset is analogous to the NMR case, even though the truncated dipolar Hamiltonian  $\mathcal{H}'_Q$  in the quadrupole rotating frame is not the same as the usual truncated dipolar Hamiltonian in the high field rotating frame. He has shown that the quasi-stationary magnetization decays slowly to an intermediate equilibrium state. The reason for this decay stems from the fact that the higher order correction terms to the average Hamiltonian mix the individual dipolar baths that constitute the quasi-stationary state and the system reaches an equilibrium state. On a longer time scale spin-lattice relaxation will of course, equilibrate this intermediate state with the lattice and the thermal equilibrium is then attained. The theory of Matti Maricq [23] including the higher order average-Hamiltonians for dipolar interaction predicts a long-time magnetization decay in agreement with experiment [4]. This theory also provides a comparison to the predictions made by the canonical transformation theory of Provotorov et al. [18,19].

So far we have discussed the theories that have been developed to explain the results of multiple-pulse spin-locking

experiments. The other multiple-pulse experiment, which has been successfully employed by Osokin [8-10] to achieve general averaging of interactions in spin-1 pure NQR case, is the phase alternated multiple pulse sequence. Osokin himself has given a theoretical interpretation for these results. He has taken advantage of the fact that PAPS is cyclic in NQR and hence average Hamiltonian theory can be used to explain the results of PAPS [8-10]. Using fictitious spin-1/2 operator formalism he has calculated the average Hamiltonians for various internal interactions and has shown that under the influence of PAPS, (i) the average Hamiltonian of inhomogeneous broadening, (ii) the secular part of the Hamiltonian of the interaction of the spin system with torsional oscillations, and (iii) the average Hamiltonian of heteronuclear dipole-dipole interactions commute with the initial density matrix  $\rho_i$ , prepared by the first (preparatory) pulse of the sequence. It should be mentioned at this point that, any broadening interactions will be suppressed if the corresponding average Hamiltonian satisfies the conditions [8]  $\mathcal{H}_{av} = 0$  or  $[\rho_i, \mathcal{H}_{av}] = 0$ . Therefore, he concluded that the pulse sequence under consideration (PAPS) removes the contribution of all the above mentioned interactions to the line width. In subsequent publications [9,10] he has also calculated the average Hamiltonian for homonuclear dipole-dipole interaction to see its commutation properties with the initial density matrix ( $\rho_i$ ) prepared by the first pulse of PAPS and also to see

the effect of this interaction on the response of quadrupolar spin-1 systems under the influence of PAPS. It has been shown that the zero-order average Hamiltonian of homonuclear dipole-dipole interaction does not commute with  $\rho_1$ . However, in the interaction representation the Hamiltonian for this interaction contains a constant term. This implies that the homonuclear dipole-dipole interactions transformed by phase alternated multi-pulse sequence give rise to a quasi-steady state characterized by both the transverse and longitudinal magnetizations. It has also been shown that the ratio of transverse and longitudinal magnetizations in the quasi-steady state depends on the pulse width  $\theta_2$ , but not on the preparatory pulse width  $\theta_1$ . Experimental echo envelope decay in the multiple-pulse responses [8-10] shows that the transverse magnetization approaches to a non-zero steady-state which confirms the theory.

Ermakov and Osokin [24] have also calculated the quasi-steady state magnetization observed in  $^{14}\text{N}$  multiple-pulse (PAPS) experiments. They have used the average Hamiltonian theory to study the influence of PAPS by considering a model system containing two dipolar coupled equivalent spin-1 nuclei each subjected to local efg's. Using the fictitious spin-1/2 operator formalism a general method is developed for solving the Liouville equation leading to results which reproduce the experimentally observed quasi-steady state magnetization. The influence of spin-lattice relaxation on the time evolution of the quasi-steady state has

also been considered by Osokin [25]. The rate equation describing the evolution of quasi-steady state to equilibrium with the lattice is obtained using average Hamiltonian theory. The results agree with the experiment.

To interpret their experimental results from WAHUHA-4 pulse sequence Ermakov and Osokin [11] have developed a theory in which the system is modelled as two equivalent spins with  $I = 1$ . They have pointed out that the observation of the quasi-steady state is not a feature specific to NQR. There is a close analogy between the quasi-steady state and the so-called pedestal observed in the off-resonance WAHUHA experiments in NMR [26,27]. In both the cases the pedestal, or quasi-steady state is caused by the terms of the total Hamiltonian which transform as a first rank irreducible tensor. In the NMR case these are the off-set and chemical shift terms. In NQR, apart from the off-set term, the secular part of the Hamiltonian of homonuclear dipolar interaction has parts which transform as first rank tensors.

It should be mentioned here that the theory of multiple-pulse sequences has been considered earlier by Zueva et al. [28-32]. They have considered the effectiveness of various multiple-pulse sequences for removing contributions to line width from inhomogeneous broadening mechanisms [30-32] and also from the homogeneous dipolar interactions [32].

#### IV. RESPONSE OF $^{35}\text{Cl}$ CONTAINING POLYCRYSTALLINE SAMPLES TO MULTIPLE-PULSE SEQUENCES: EXPERIMENTAL RESULTS

It has been pointed out in Section IV.A that the experiments leading to narrowing of nuclear quadrupole resonance lines are expected to reveal fine structure that is masked in generally broad NQR lines. As a first step in this study of line narrowing we have undertaken multiple-pulse experiments on spin  $I = 3/2$  systems. We have employed various multiple-pulse sequences to investigate their effect in causing averaging of internal interactions in polycrystalline samples containing  $^{35}\text{Cl}$  ( $I = 3/2$ ) nuclei. For this purpose we have considered CP, CPMG, Ostroff-Waugh and phase alternant multiple-pulse sequences (PAPS). Several modifications of some of these sequences have also been investigated by us with a view to understand the effect of flip angle ( $\theta$ ) and phase ( $\phi$ ) of the sequence pulses in establishing the spin-locked state in powder samples. In order to understand the long-time behaviour of the spin system ( $I = 3/2$ ) under the spin-locked state we have investigated the multiple-echo decay time constant,  $T_{2\text{e}}$  as a function of pulse separation  $\tau$ . The effect of off-set and also the magnetic field have been studied. These results on  $^{35}\text{Cl}$  nuclei in powdered  $\text{KClO}_3$  and  $\text{NaClO}_3$  are described in the following sub-sections and critically examined in the light of currently available theories on multiple-pulse responses.

##### IV.B(1) Experimental Details:

All our investigations have been carried out at room temperature employing the microprocessor-controlled pulsed NQR spectro-



meter described in Chapter II of the present thesis. The micro-processor software developed for the generation of various multiple-pulse sequences employed here has been discussed in Chapter II (Section II.D). All the multiple-pulse experiments have been automated to acquire the responses into the signal analyzer and to store into the mini-floppy disk for permanent storage. Appropriate trigger pulses to initiate data acquisition by the signal analyzer have been generated by the microprocessor. When necessary, the microprocessor also generates external ADC clock pulses to the signal analyzer enabling the automatic sampling and acquisition of multiple-echo maxima in the form of echo decay curve.

Some of the important considerations in multiple-pulse experiments are the proper adjustment of phases of r.f. pulses (i.e. alignment of r.f. pulses along particular directions of interest) and adjustment of pulse widths to obtain appropriate flip angles (e.g.,  $\pi$ ,  $\pi/2$ ,  $\pi/4$  etc.). In all our experiments the desired phase difference between various pulse channels has been adjusted by means of phase-sensitive detection when delay lines were employed for phase shifting. No such adjustment was however found necessary when commercial fixed phase shifting devices such as quadrature hybrids were used for a particular phase shift. As far as the pulse flip angle is concerned it should be mentioned that for powder samples the so called  $90^\circ$  pulse which gives maximum FID signal is not equal to  $\pi/2$  but it is equal to  $0.66\pi$  (see Chapter I). Similarly the  $180^\circ$  refocusing pulse for powder is equal to  $1.22\pi$ . In all our multiple-pulse experiments the initial preparatory pulse has been adjusted to  $0.66\pi$  (by maximizing



the FID) and the pulse width of the sequence pulses are adjusted according to the refocusing pulse width requirements (which is decided by maximizing the two-pulse echo amplitude).

It should be mentioned at this point that in our spectrometer system the receiver recovery time increases during multiple pulse experiments. With a view to reduce the recovery time of the receiver and also to minimize the r.f. pulse feed - through to the receiver, we have employed a cascade of two receiver gates (based on HP-10514 A double balanced mixers). Even so, the transmitter pulse feed - through to the receiver could not be completely eliminated in our experiments.

#### IV.B(2) Results from Various Multiple-Pulse Sequences

All the multiple-pulse sequences that were employed in our investigations can be represented by the following two general sequences:

(1)  $90_x - (\tau - \theta_{(x, \emptyset)} - \tau)_n$ , hereafter referred to as the spin-locking sequence ,

and (2)  $90_x - (\tau - \theta_{-x} - 2\tau - \theta_x - \tau)_n$ , the phase alternated multiple pulse sequence (PAPS).

One can get any specific sequence of interest by properly choosing  $\theta$  and  $\emptyset$  in sequence-1, and  $\theta$  in sequence-2. For example, from sequence-1 we get,

1) CP sequence when  $\theta = 180^\circ$  and  $\emptyset = 0^\circ$ ,

ii) CPMG sequence when  $\theta = 180^\circ$  and  $\phi = 90^\circ$ ,  
 iii) Ostroff-Waugh sequence when  $\theta = 90^\circ$  and  $\phi = 90^\circ$ ,  
 and from sequence 2 we get the usual form of phase alternated multiple pulse sequence when  $\theta = 180^\circ$ . In our experimental study we have employed all the above mentioned sequences and also the sequences generated by various other choices of  $\theta$  and  $\phi$  in sequence 1 and  $\theta$  in sequence 2, and observed "spin space" averaging [1]. We will now describe the results of our investigations.

#### IV.B(2.1) Investigations with the spin-locking sequence $[90_x - (\tau - \theta_{(x+\phi)} - \tau)_n]$

We first employed the well-known spin-locking sequence due to Ostroff and Waugh [5] which has been originally used in NMR and later adopted to NQR of spin-1 systems [4]. Using this sequence we observed the persistence of spin echo train for times much longer than  $T_2$ . Figs. IV.1(a) to Fig. IV.1(c) present the responses to Ostroff-Waugh sequence in three regions of time from  $^{35}\text{Cl}$  in polycrystalline sample of  $\text{KClO}_3$ . These responses are presented here after processing in the signal analyzer to remove the transmitter pulse feed-through. Clearly, these responses indicate the observation of the phenomenon of spin-locking in the powder NQR sample containing spin  $3/2$   $^{35}\text{Cl}$  nuclei. We have also observed spin-locking using CPMG and other analogous multiple-pulse sequences with varying phase shifts ( $\phi$ )

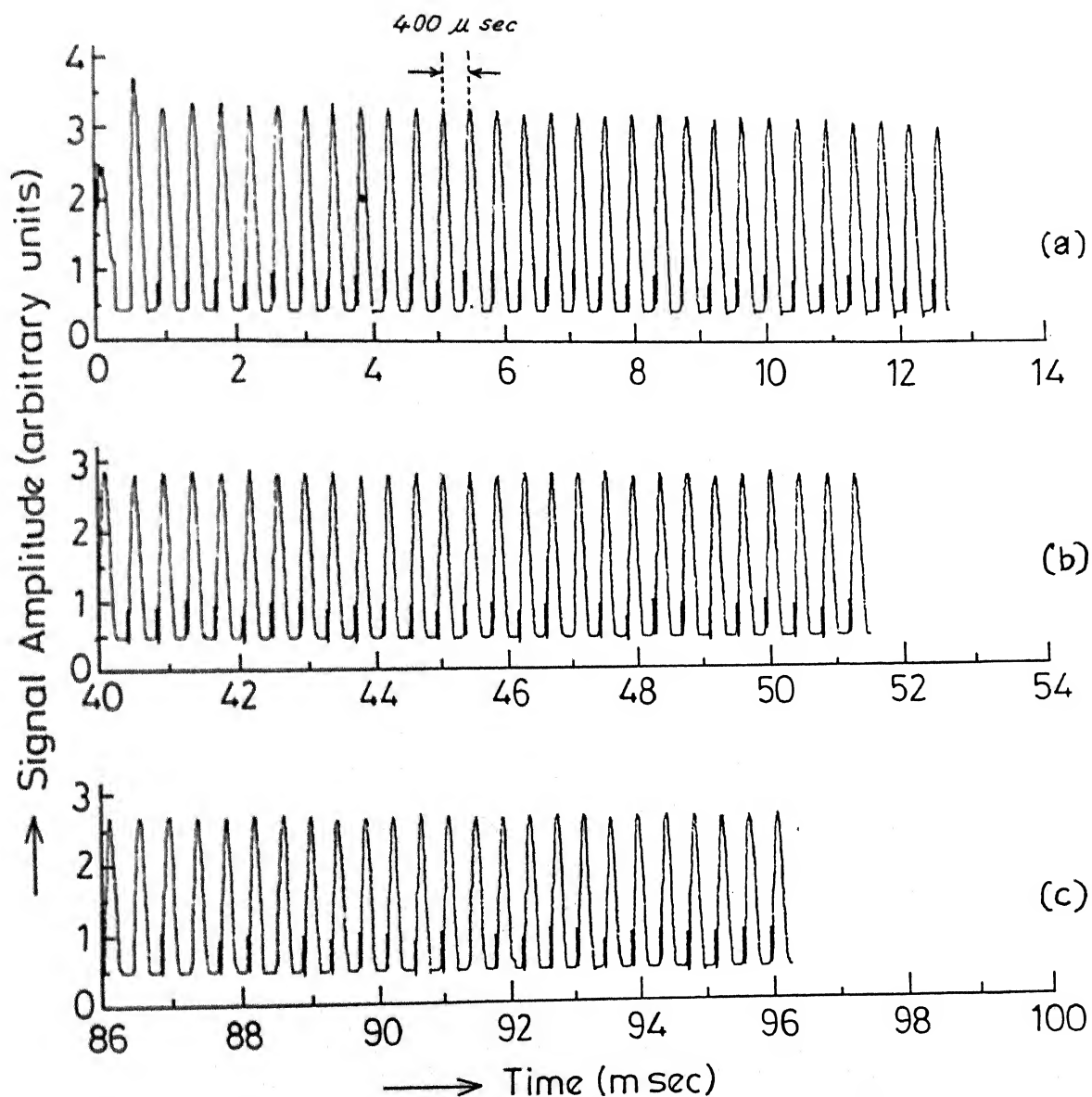


Fig.IV.1 Response from  $^{35}\text{Cl}$  in powdered sample of  $\text{KClO}_3$  to Ostroff-Waugh sequence ( $\tau = 200 \mu\text{sec}$  and  $\Delta\omega = -2 \text{ KHz}$ ); (a) response of initial 32 pulses, (b) response of 100-128 pulses, and (c) response of 215-240 pulses. (Relative amplitudes of multiple-echoes in all the three Figures are in the same units).

between the preparatory pulse and the sequence pulses and also with arbitrary " $\theta$ " values. These results are discussed below.

#### IV.B(2.1.a) Study of $\theta$ -dependence

In this study we have fixed the value of " $\theta$ " (the phase shift between the preparatory pulse and the sequence pulses) to  $90^\circ$ , i.e.,  $90_x - (\tau - \theta_y - \tau)_n$  has been used with a value of  $\tau \approx 200$   $\mu$ sec. The responses to this sequence as a function of " $\theta$ " have been recorded from  $^{35}\text{Cl}$  nuclei in powdered  $\text{NaClO}_3$  and  $\text{KClO}_3$ . We have observed spin-locking with on-resonance as well as off-resonance conditions. However, it has been observed that the multiple-echoes are intense when small amount of off-set is given. It can be seen from our studies on off-set dependence that the echo decay time constant ( $T_{2\epsilon}$ ) does not vary significantly. We have, therefore, presented all our results with small amount of off-set. Typical recordings obtained from  $\text{NaClO}_3$  with an off-set  $\approx -3.5$  KHz and with " $\theta$ " value of  $180^\circ$ ,  $130^\circ$ ,  $90^\circ$  and  $45^\circ$  are shown in Figs. IV.2(a) to IV.2(d), respectively. These responses correspond to initial 30 pulses of the sequence. However, it should be noted that the response to  $\approx 80$  pulses has been recorded for the purpose of calculation of the effective echo decay time constant ( $T_{2\epsilon}$ ) in all these experiments. From the responses shown in Figs. IV.2(a) to IV.2(d) it is clear that the spin-locking state is achieved for any arbitrary value for " $\theta$ ". From these Figures it can also be seen that the magnetization decay

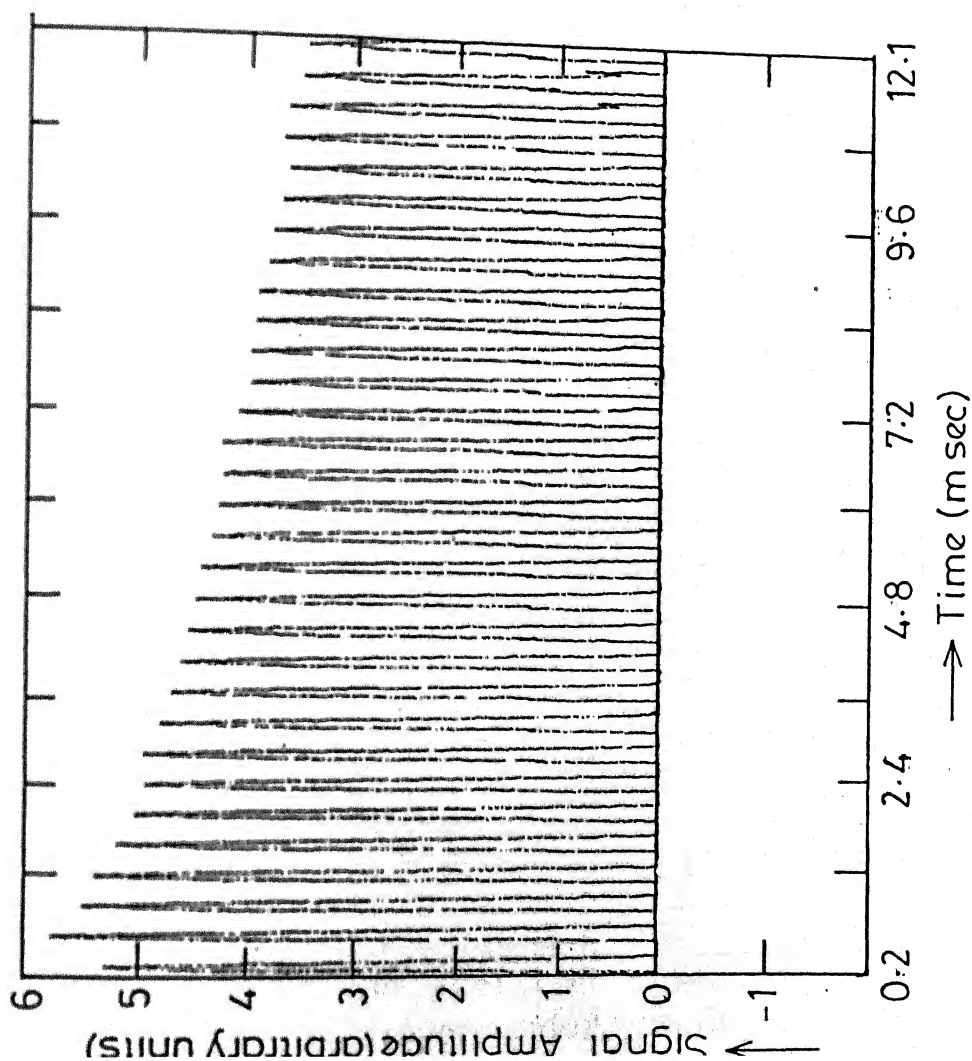


Fig. IV.2(a) Response from  $^{35}\text{Cl}$  in powdered sample of  $\text{NaClO}_3$  to spin-locking sequence with a value for  $\theta = 180^\circ$  ( $\tau = 200 \mu\text{sec}$ ,  $\phi = 90$  and  $\Delta\omega \approx -3.5 \text{ KHz}$ ).

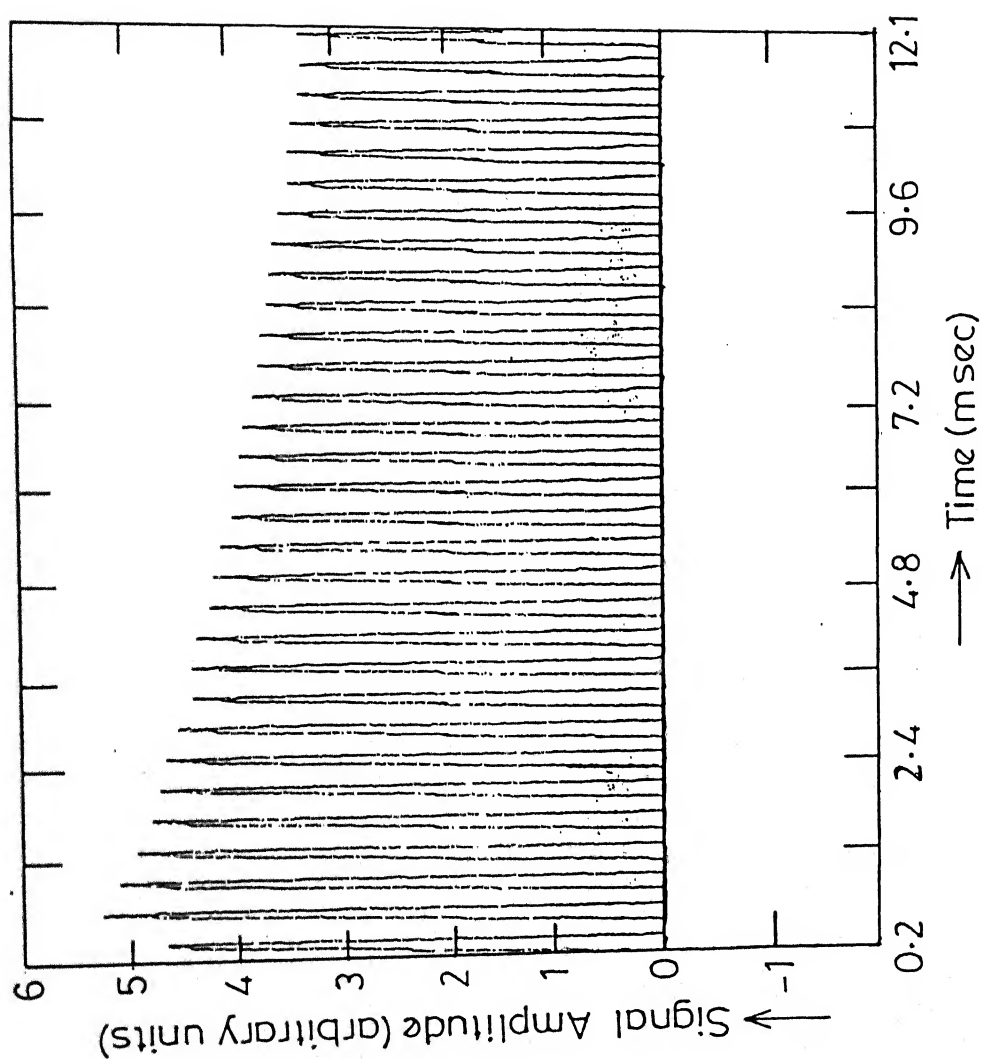


Fig.IV.2(b) Same as that of Fig.IV.2(a) with a value for  $\theta = 130^\circ$ .

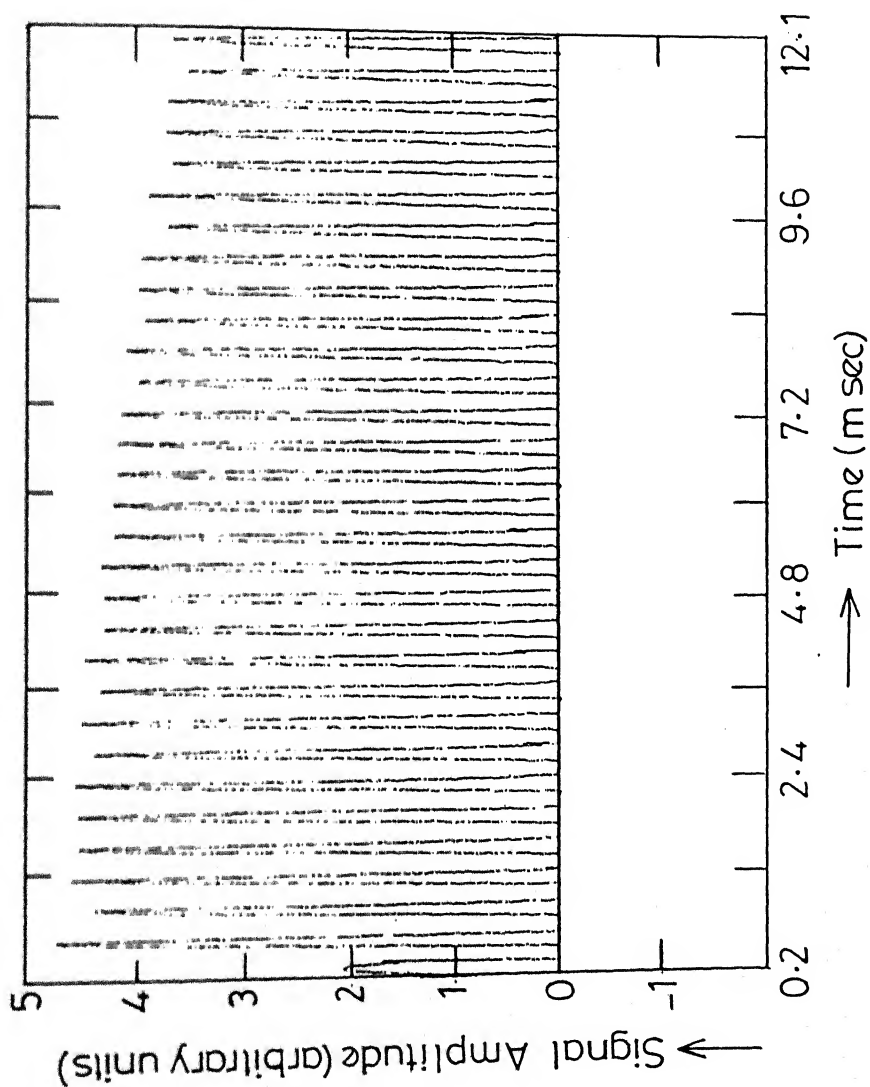


Fig. IV.2(c) Same as that of Fig. IV.2(a) with a value for  $\theta = 90^\circ$ .

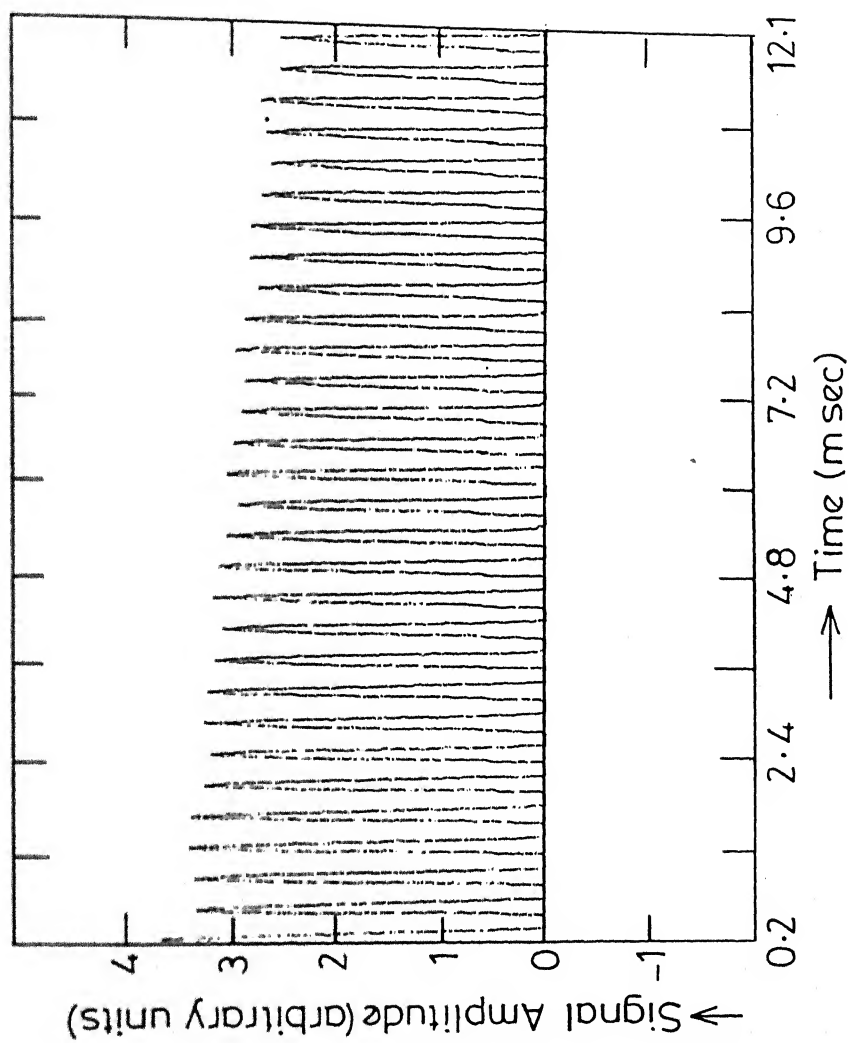


Fig. IV-2(d) Same as that of Fig. IV-2(a) with a value for  $\theta = 45^\circ$ .



(echo decay) is slower at lower values of pulse angle ( $\theta$ ). In otherwords, the effective echo decay time constant ( $T_{2\epsilon}$ ) increases as the pulse angle ( $\theta$ ) is decreased. Typical results confirming this observation are presented in Table IV.1. The  $T_{2\epsilon}$  values given in this table are calculated from the responses recorded (with an off-set  $\approx 3.5$  KHz) as a function of " $\theta$ ". It should be mentioned here that there is an error of  $\approx 5\%$  in calculation of  $T_{2\epsilon}$  in all the results presented in this chapter.

Table IV.1 Effective echo decay time constant ( $T_{2\epsilon}$ ) measured as a function of  $\theta$  with a resonance frequency off-set of  $\approx 3.5$  KHz from  $^{35}\text{Cl}$  in powdered  $\text{NaClO}_3$

| Sl.No. | Flip angle ( $\theta$ ) | $T_{2\epsilon}$ (msec) |
|--------|-------------------------|------------------------|
| 1.     | $180^\circ$             | 13.6                   |
| 2.     | $130^\circ$             | 15.0                   |
| 3.     | $90^\circ$              | 19.5                   |
| 4.     | $45^\circ$              | 22.5                   |

A similar  $\theta$  dependence has been observed by Rhim et al. [33] in NMR spectroscopy. It is clear from the above data that spin locking occurs with the above sequence for different  $\theta$  values and this corresponds to the "general averaging" as mentioned by Ainbinder and Furman [20]. The spin-spin relaxation time  $T_2$

for this compound is of the order of a msec and the spin-lattice relaxation time  $T_1$  at 297 °K is  $\approx 45$  msec [34]. Under the influence of the above spin-locking sequence the effective echo decay time constant  $T_{2\epsilon}$  is much larger than  $T_2$  and approaches  $T_1$  in the order of magnitude.

We have also investigated the variation of  $T_{2\epsilon}$  as a function of " $\theta$ " in the presence of a small Zeeman field. The results obtained from  $^{35}\text{Cl}$  in powdered  $\text{KClO}_3$  with a Zeeman field  $\approx 9.75$  Gauss and an off-set of -3 KHz are presented in Table IV.2.

Table IV.2. Variation of  $T_{2\epsilon}$  as a function of  $\theta$  obtained from  $^{35}\text{Cl}$  in  $\text{NaClO}_3$  with a magnetic field  $\approx 9.75$  Gauss

| Sl. No. | Flip angle ( $\theta$ ) | $T_{2\epsilon}$ (msec) |
|---------|-------------------------|------------------------|
| 1.      | $180^\circ$             | 16.5                   |
| 2.      | $90^\circ$              | 19.7                   |
| 3.      | $45^\circ$              | 21.6                   |

These results also are quite indicative of the fact that  $T_{2\epsilon}$  increases as " $\theta$ " is decreased. The magnitudes of  $T_{2\epsilon}$  values measured by us are not very accurate because of the uncertainty in the measurement of the amplitudes of multiple echoes in the presence of transmitter pulse feed-through in our spectrometer

system. Further work is in progress in order to improve the accuracy of these results.

#### IV.B(2.1.b) Study of $\phi$ -dependence:

This study has been performed for various values of " $\phi$ " ranging from  $0^\circ$  to  $360^\circ$ . Two typical values for pulse angle ( $\theta$ ) have been considered and the pulse separation  $\tau$  has been fixed at  $\sim 200$   $\mu$ sec. We first employed the modified CP sequence (i.e.  $\phi = 0^\circ$  as in the original CP sequence, with  $\theta = 90^\circ$ ). Hereafter, wherever we say modified CP sequence, we mean the above modification in terms of " $\theta$ " alone). The response to modified CP sequence in three regions of time from  $^{35}\text{Cl}$  in powdered  $\text{KClO}_3$  are presented in Figs. III.3(a) to Fig. III.3(c). ? The three time regions chosen here are same as those for the Ostroff-Waugh sequence response shown in Figs. III.1(a) to III.1(c). It is surprising to note that the spin-locked state is established even with the modified CP-sequence which involves no phase shift ( $\phi = 0$ ) between the preparatory pulse and sequence pulses. Also, a closer look at Figs. III.1 and III.3 shows that the responses to Ostroff-Waugh and modified CP-sequence are comparable and spin-locking is achieved in both the cases. This fact is further confirmed from responses to these two sequences recorded from  $^{35}\text{Cl}$  in powdered  $\text{NaClO}_3$  (see Figs. III.4 and III.5). We have also observed spin-locking using the simple CP-sequence ( $\phi = 0^\circ$  and  $\theta = 180^\circ$ ). Table IV.3 presents our results employing

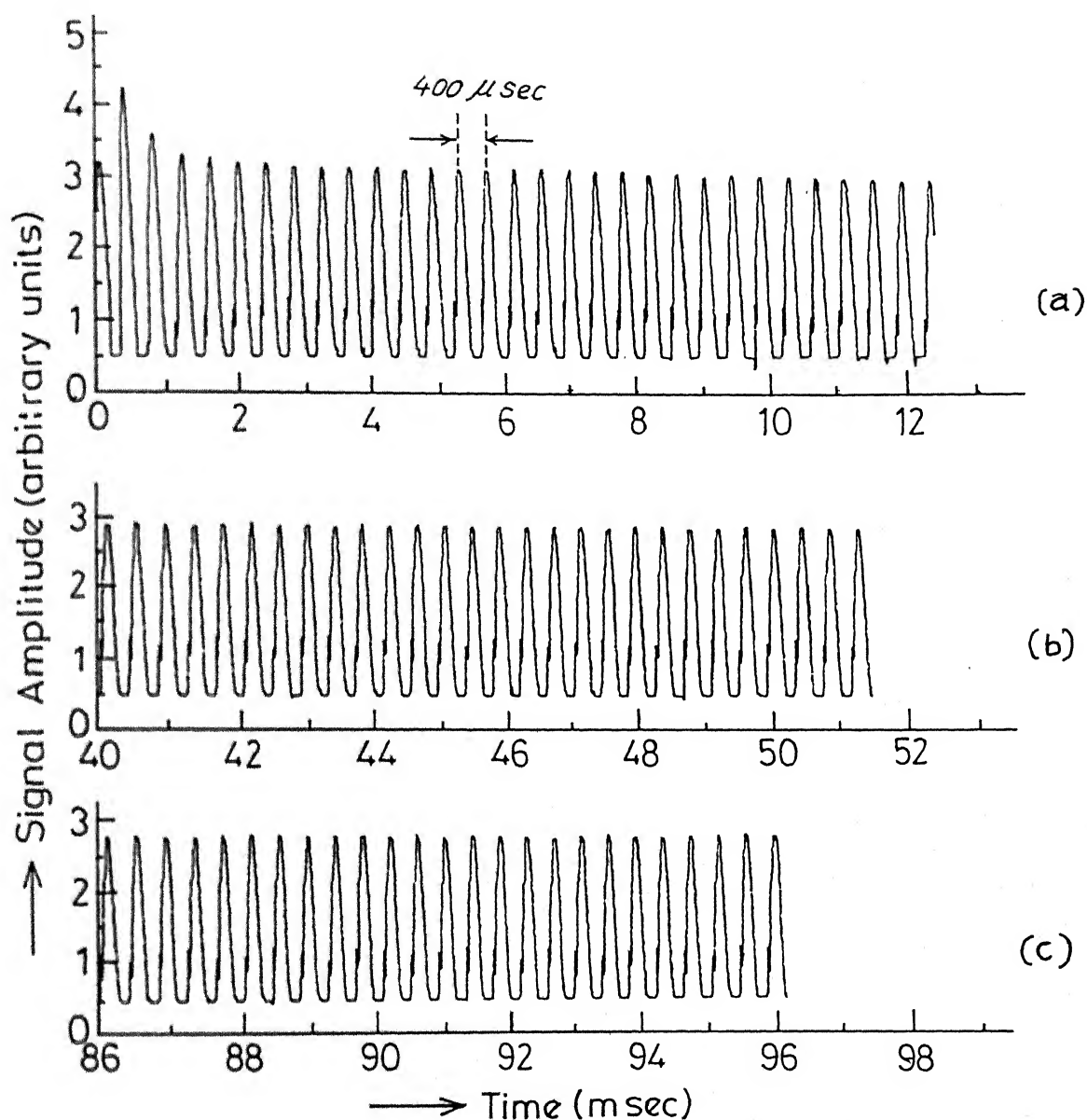


Fig.IV.3 Response from  $^{35}\text{Cl}$  in powdered sample of  $\text{KClO}_3$  to modified CP-sequence ( $\tau=200\ \mu\text{sec}$  and  $\Delta\omega=-2\text{KHz}$ ); (a) response of initial 32 pulses, (b) response of 100-128 pulses, and (c) response of 215-240 pulses (Relative amplitudes of multiple-echoes in all the three Figures are in the same units).

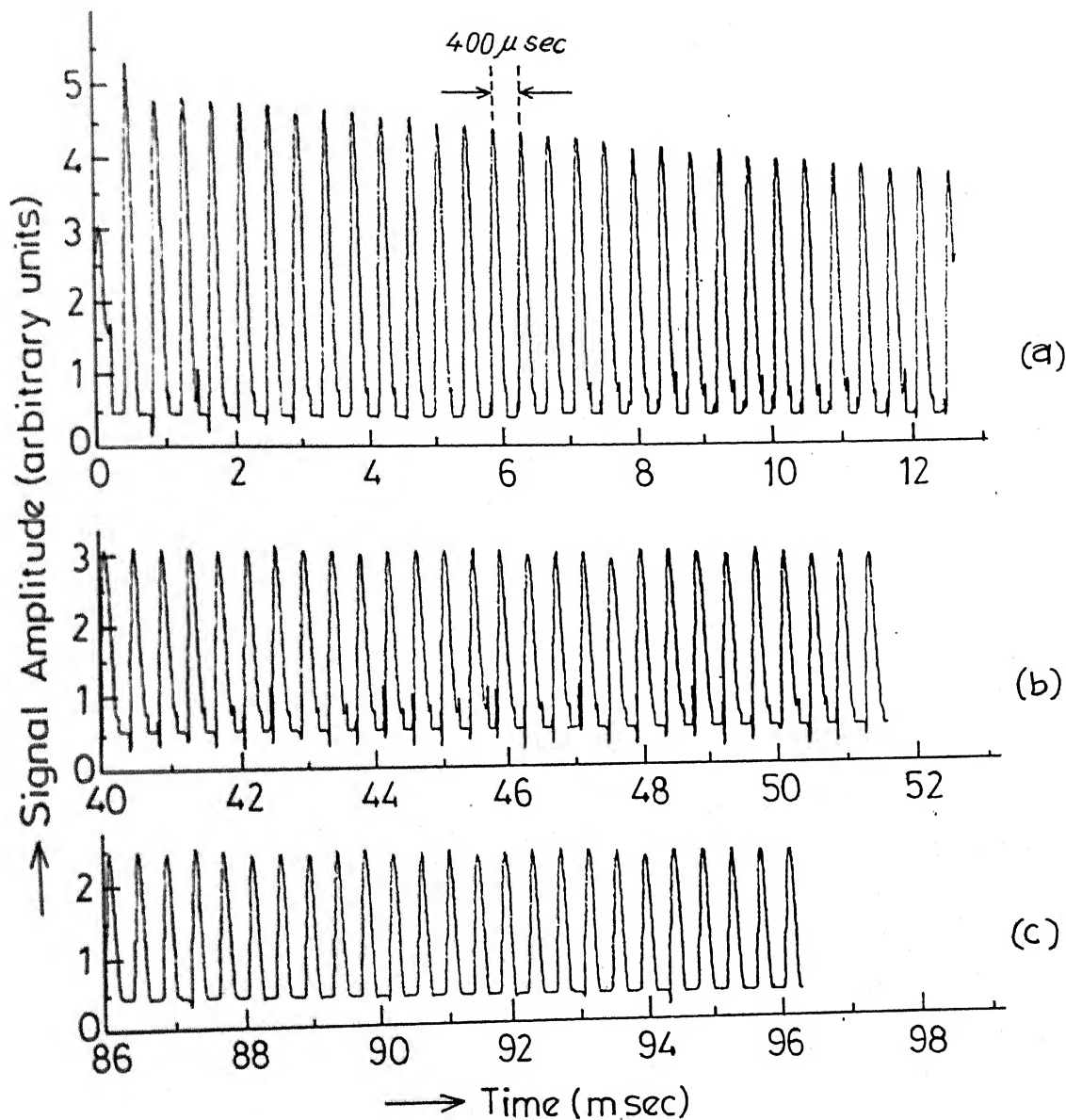


Fig.IV.4 Response from  $^{35}\text{Cl}$  in powdered sample of  $\text{NaClO}_3$  to Ostroff-Waugh sequence ( $\tau = 200 \mu\text{sec}$  and  $\Delta\omega = -2\text{KHz}$ ); (a) response of initial 32 pulses, (b) response of 100-128 pulses and (c) response of 215-240 pulses (Relative amplitudes of multiple-echoes in all the three Figures are in the same units).

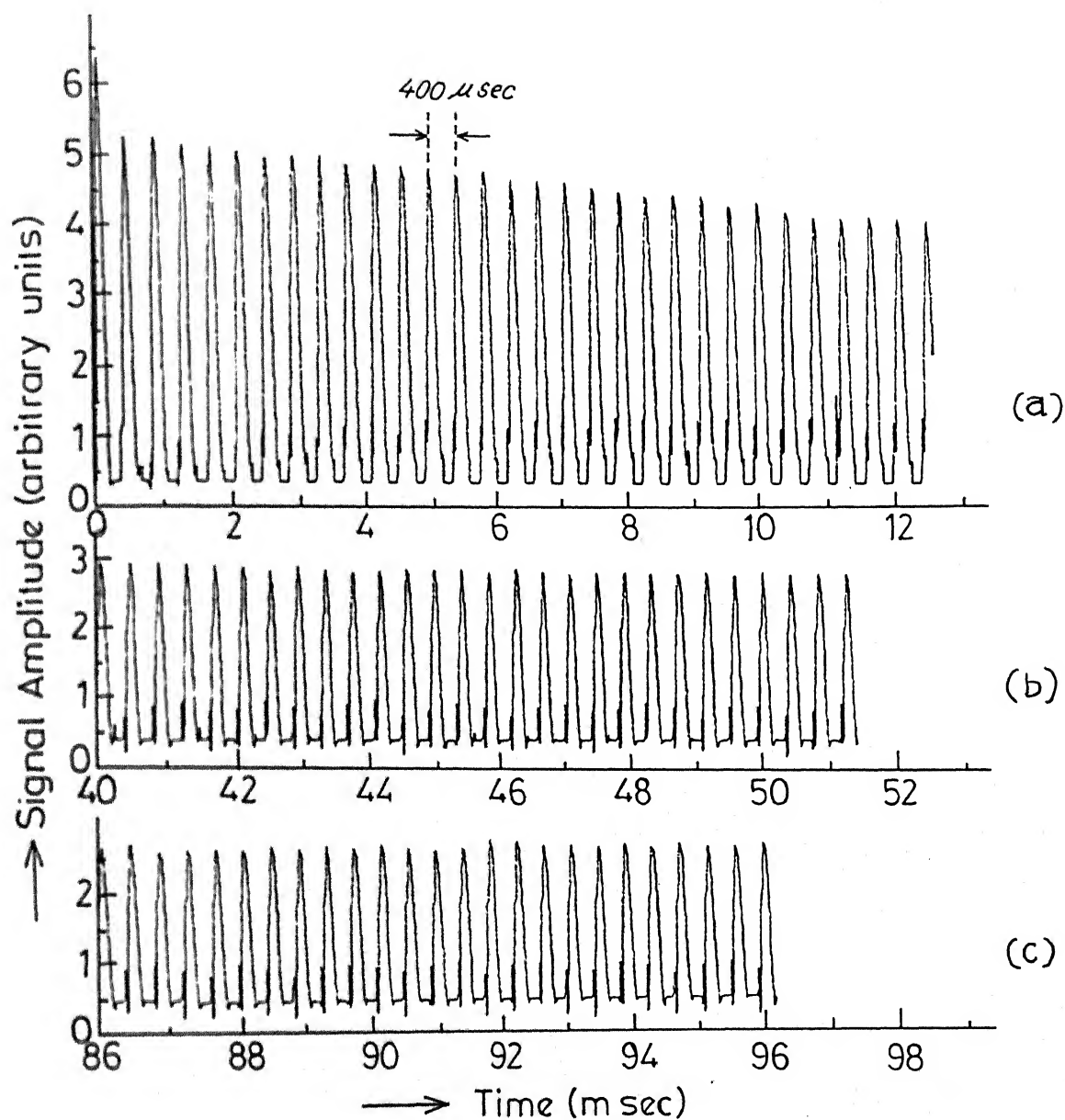


Fig. IV.5 Same as that of Fig. IV.4 with modified CP-sequence.

(i) a  $90^\circ$  phase shift ( $\phi = 90^\circ$ ) and (ii) without any phase shift ( $\phi = 0^\circ$ ) with an off-set of  $\approx 3.5$  KHz. These results clearly confirm the fact that, in the case of spin  $3/2$  nuclei in powdered samples, the spin-locked state is achieved not only by the application of pulse sequences involving  $90^\circ$  phase shift (i.e., CPMG and Ostroff-Waugh sequences) but also by the application of those involving no phase shift (i.e., CP- and modified CP-sequences).

Table IV.3 Comparison of results obtained with and without phase shift using spin-locking sequence

| Sl.<br>No. | $\phi$     | $\theta$                 | $T_{2E}$<br>(msec) |
|------------|------------|--------------------------|--------------------|
| 1.         | $0^\circ$  | $180^\circ$ (CP)         | 14.3               |
|            |            | $90^\circ$ (modified CP) | 17.6               |
| -----      |            |                          |                    |
| 2.         | $90^\circ$ | $180^\circ$ (CPMG)       | 13.6               |
|            |            | $90^\circ$ (OW)          | 19.5               |

It is worth mentioning at this juncture that, this result (i.e. the observation of spin-locking effect with CP- and modified CP-sequences) is not obtained in NMR spectroscopy of solids, because the flip angle errors associated with CP-sequence cause multiple echoes to decay faster. Also, this aspect ( $\phi$ -dependent study) has not been given much importance earlier in the literature of multiple-pulse spin-locking using powder NMR samples.

We have carried out spin-locking experiment employing  $\theta$  values in the general sequence  $90_x - [\tau - \theta_{(x+\theta)} - \tau]_n$ . Surprisingly, we were able to observe spin-locked state with any arbitrary  $\theta$  value ranging from  $0^\circ$  to  $360^\circ$  (for typical results, see Figs. IV.6(a) to IV.6(d)). These results on powder NQR samples containing  $^{35}\text{Cl}$  ( $I = 3/2$ ) nuclei cannot be explained on the basis of any of the presently available theories on multiple-pulse responses of NQR systems. The most general theory for multiple-pulse spin locking presently available is that of Ainbinder and Furman [20]. This theory is applicable to NQR systems with arbitrary spin. This theory, however, predicts that the spin-locking state can be realized by the above sequence (for an arbitrary  $\theta$ ) only if the phase  $\theta = (2k + 1)\pi/2$ , where  $k = 0, 1, 2$ ; i.e., one can observe spin-locking only for the  $\theta$  values of  $\pi/2, 3\pi/2$  and  $5\pi/2$  ( $\equiv \pi/2$ ). On the other hand, we have observed spin-locking in powders even in cases which do not satisfy this phase condition. Therefore, a suitable theoretical framework to explain the present experimental results on spin  $3/2$  nuclei in polycrystalline samples needs to be developed. To our knowledge, no study has been carried out to date on  $\theta$ -dependence in single crystals. Such studies would also be of help in assessing the validity of the Ainbinder and Furman theory for spin  $I = 3/2$  case. The unexpected result that spin-locking state is achieved independent of phase  $\theta$  is most likely due to the powdered nature of the samples used in the present study, where the efg axes of various crystallites are oriented randomly in space.



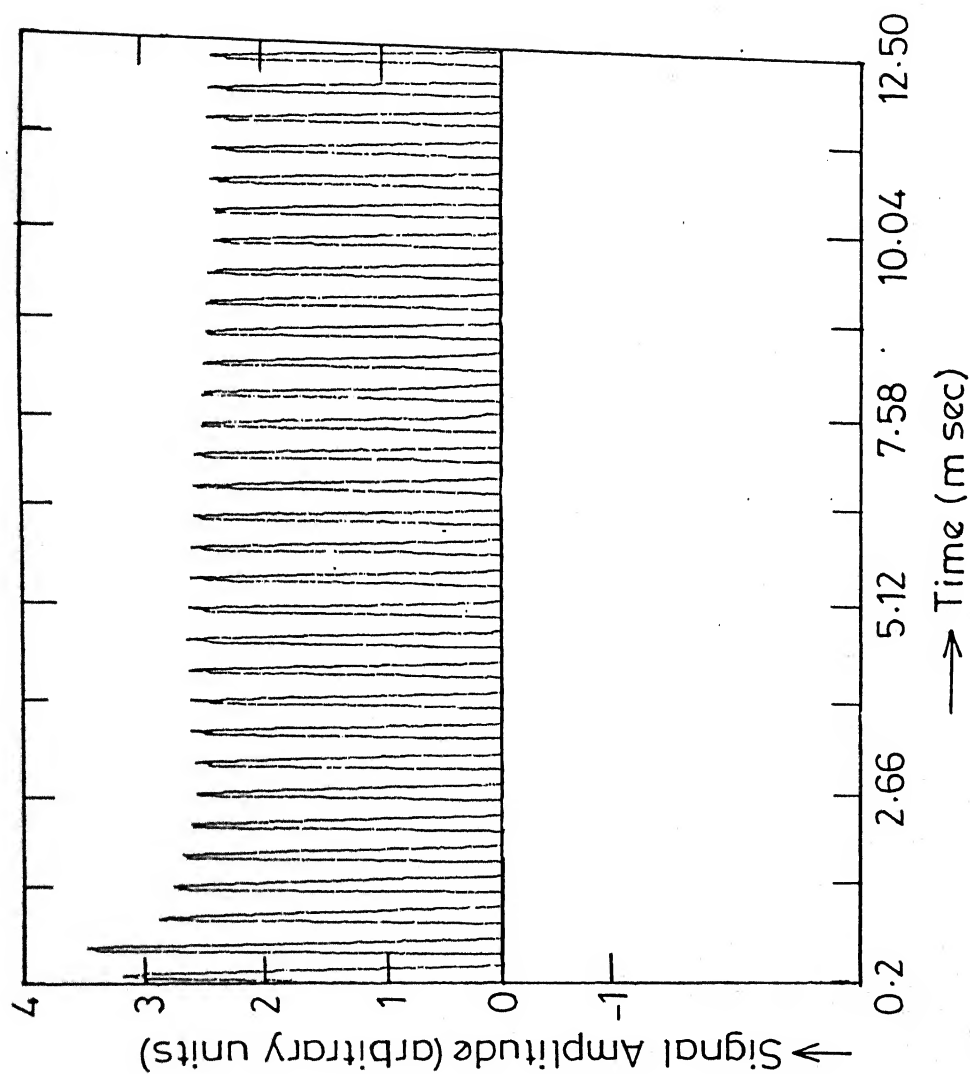


Fig.IV.6(a) Response from  $^{35}\text{Cl}$  in powdered sample of  $\text{KClO}_3$  to spin-locking sequence with a value for  $\phi = 45^\circ$  ( $\theta = 90^\circ$ ,  $\tau = 200 \mu\text{sec}$  and  $\Delta\omega = -3.5 \text{ KHz}$ ).

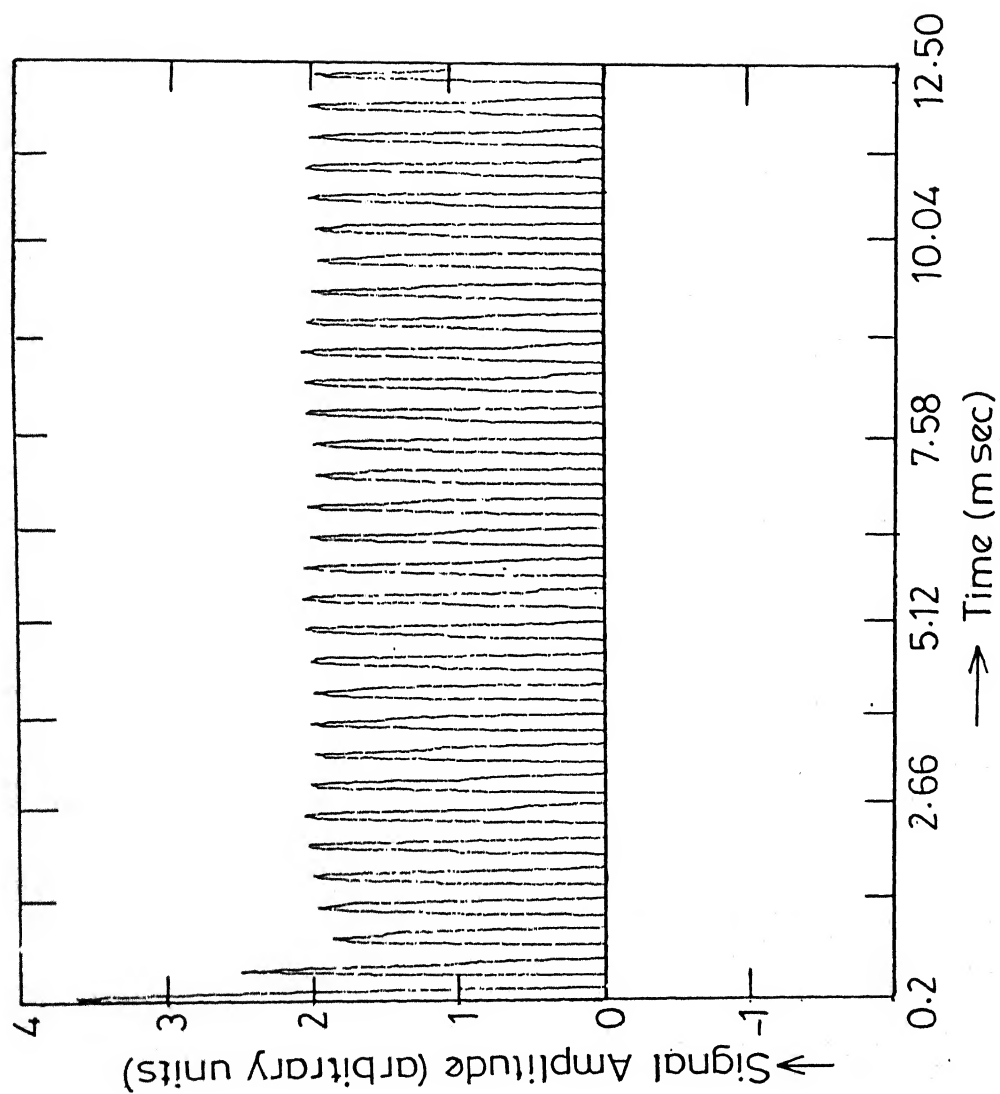


Fig. IV.6 (b) Same as that of Fig. IV.6(a) with a value for  $\phi = 135^\circ$ .

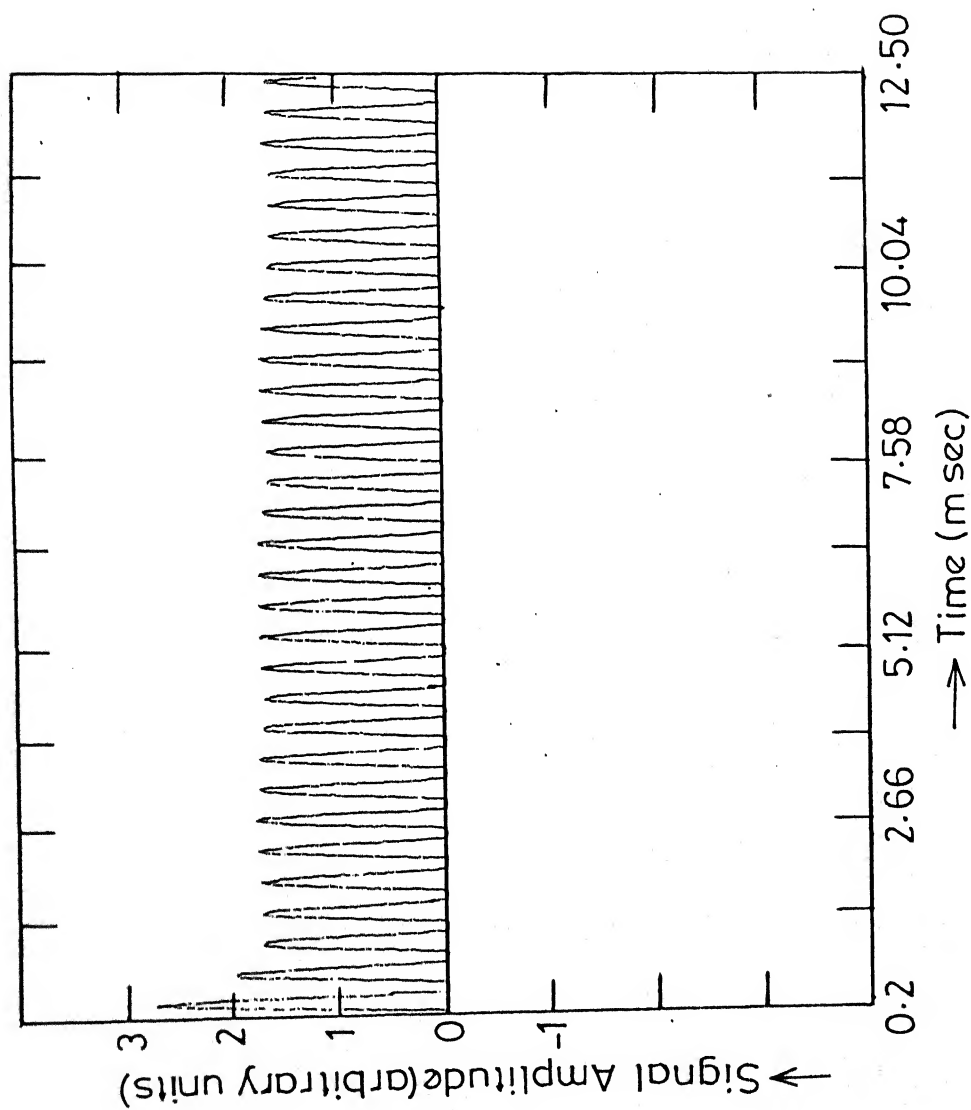


Fig.IV.6(c) Same as that of Fig.IV.6(a) with a value for  $\phi = 225^\circ$ .

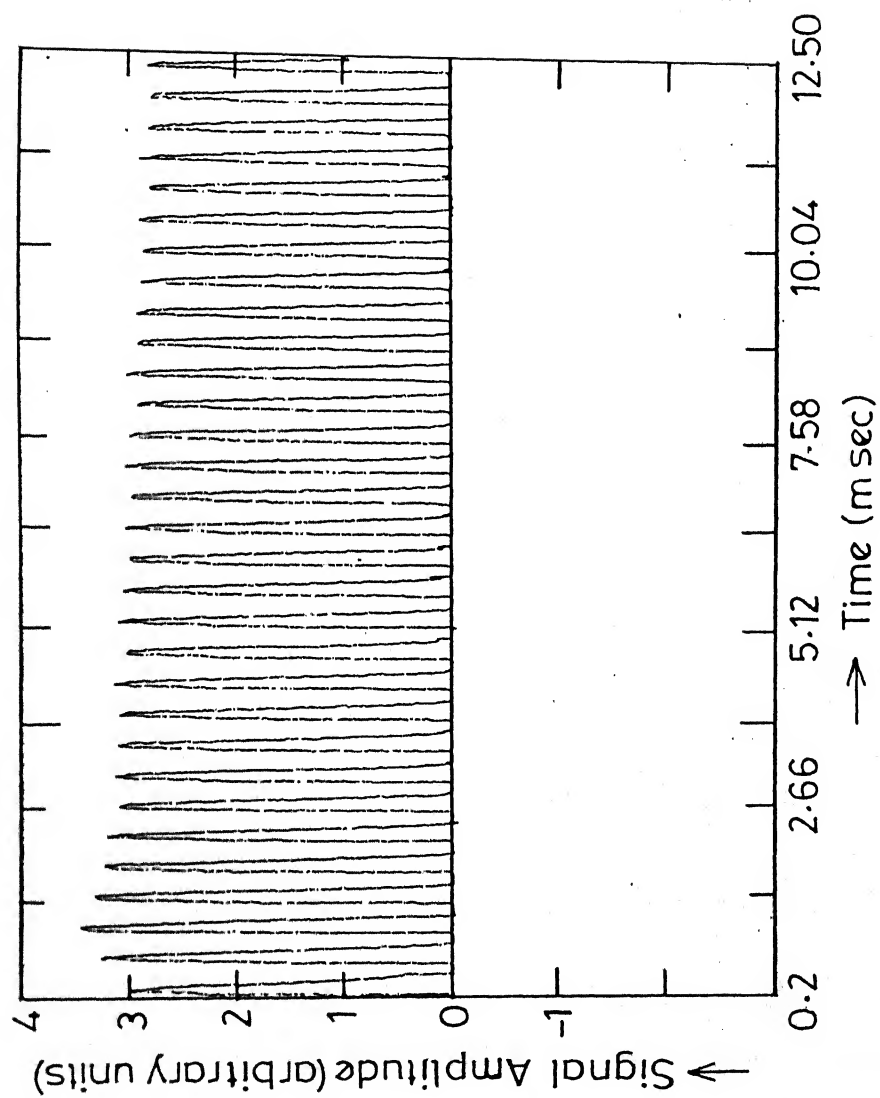


Fig. IV.6(d) Same as that of Fig. IV.6(a) with a value for  $\phi = 315^\circ$ .

#### IV.B(2.i.c) Study of off-set dependence:

We chose the CPMG-sequence ( $\alpha = 90^\circ$  and  $\theta = 180^\circ$ ) for this study. The pulse separation,  $\tau$ , in all these experiments has been kept constant at  $\approx 200 \mu\text{sec}$ . We have performed our experiments in the off-set range of  $-7 \text{ KHz}$  (i.e.,  $7 \text{ KHz}$  below the resonance) through the resonance condition to  $+7 \text{ KHz}$  (i.e.,  $7 \text{ KHz}$  above the resonance). Spin-locking could be achieved in the complete range of offset studied. Typical responses obtained from  $^{35}\text{Cl}$  in powdered  $\text{KClO}_3$  at off-set values of  $-3 \text{ KHz}$  and  $+5 \text{ KHz}$  are presented in Figs. IV.7 and IV.8, respectively. The effective echo decay constant  $T_{2\text{e}}$  did not vary significantly as a function of off-set but remained constant at  $\approx 20 \text{ msec}$  in the whole off-set range covered in our investigations. It should be mentioned here that the  $T_1$  values for this compound at  $300^\circ\text{K}$  is  $21 \text{ msec}$  [34] and the  $T_{2\text{e}}$  obtained in our experiments approached this value. A plot of the quasi-stationary magnetization in the spin-locked state as a function of off-set is shown in Fig. IV.9. This plot is similar to the theoretically predicted one for powdered samples containing spin-1 systems [23].

We have also investigated the effect of off-set in the presence of a finite magnetic field of  $\approx 9.75 \text{ Gauss}$ . Here again  $T_{2\text{e}}$  remained constant at  $\approx 20 \text{ msec}$  over the complete range of off-set indicating that  $T_{2\text{e}}$  is not affected by a small magnetic field.

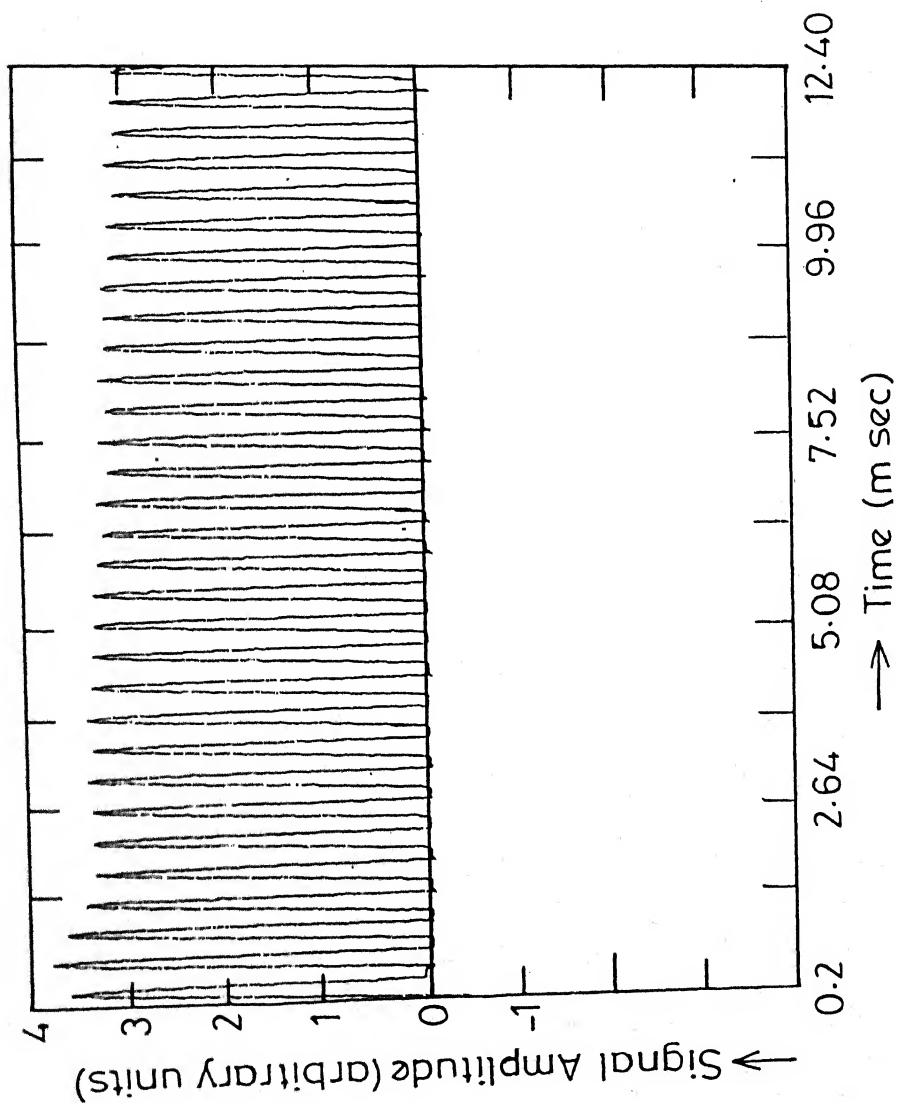


Fig.IV.7 Response from  $^{35}\text{Cl}$  in powdered sample of  $\text{KClO}_3$  to CPMG sequence with an off-set =  $-3\text{ KHz}$  ( $\tau = 200\text{ }\mu\text{sec}$ ).

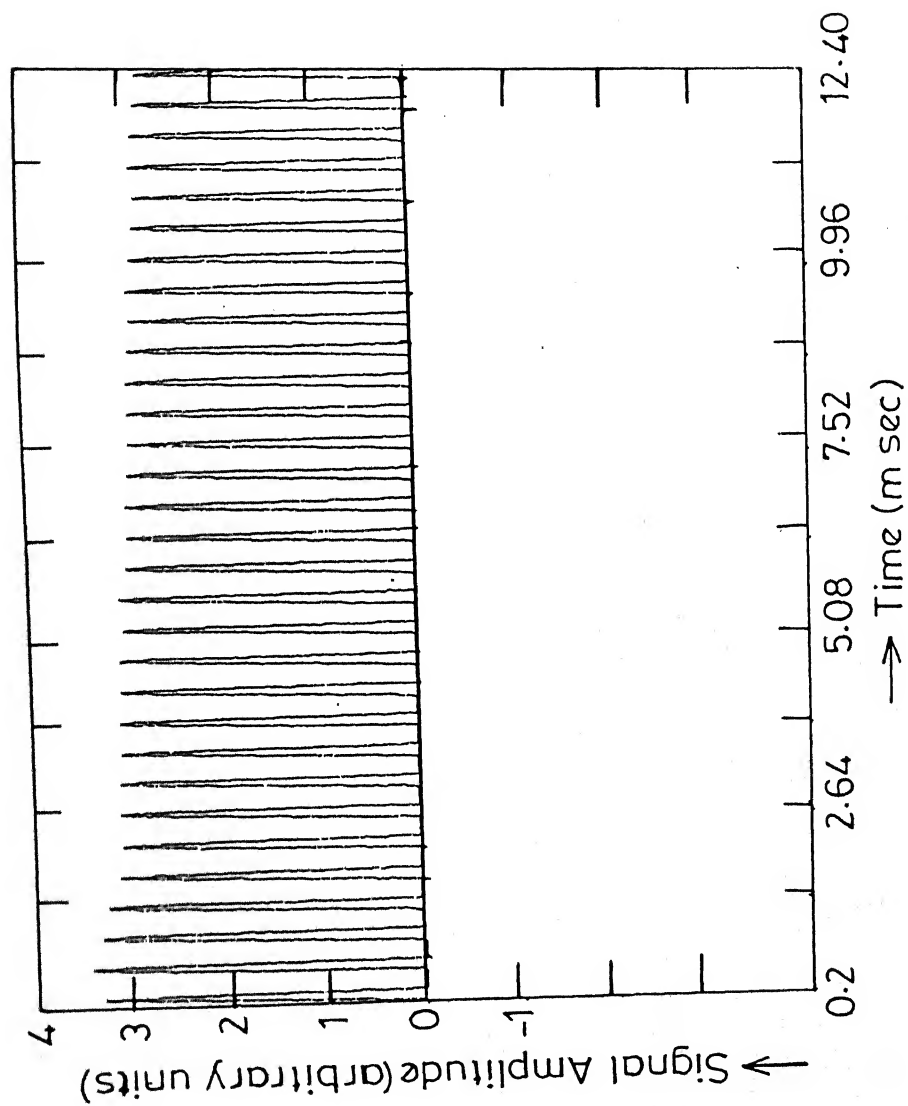


Fig.IV.8 Same as that of Fig.IV.7 with an off-set = +5KHz.

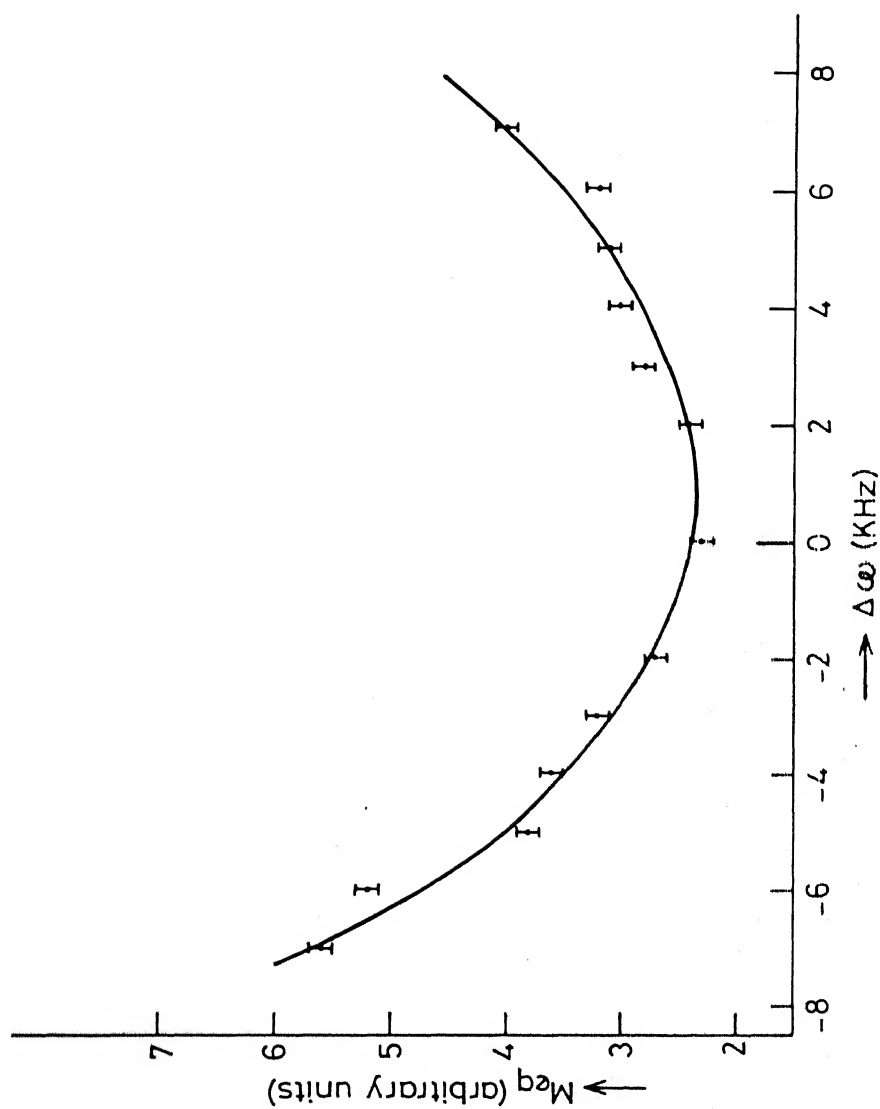


Fig. IV.9 A plot showing the dependence on off-set of the quasi-equilibrium magnetization as measured from  $^{35}\text{Cl}$  in powdered  $\text{KClO}_3$  using CPMG sequence.



#### IV.B(2.i.d) Study of $\tau$ -dependence:

In the literature on multiple pulse NQR of spin-1 systems there are varying propositions about the long-time behavior of the magnetization in a spin-locking experiment (i.e. the dependence of the echo decay time constant on  $\tau$ ). The original experiment of Marino and Klainer [4] showed a  $\tau^{-5}$  dependence. With a view to obtain a functional dependence of  $T_{2\text{eff}}$  on  $\tau$ , we have carried out spin-locking experiments in the  $\tau$  range of 100  $\mu\text{sec}$  to 900  $\mu\text{sec}$ . We used the Ostroff-Waugh sequence ( $\phi = 90^\circ$  and  $\theta = 90^\circ$ ) for this purpose. The investigations were carried out on  $^{35}\text{Cl}$  in  $\text{KClO}_3$  and  $\text{NaClO}_3$  in the above mentioned  $\tau$  range. Spin-locking effect was observed in the complete  $\tau$  range in both the compounds ( $T_2$  for both of the compounds is of the order of a msec). Typical responses obtained from  $^{35}\text{Cl}$  in powdered  $\text{KClO}_3$  at  $\tau$  values of  $\approx 150 \mu\text{sec}$  and  $\approx 300 \mu\text{sec}$  are presented in Figs. IV.10 and IV.11, respectively. It should be mentioned here that, though we have observed spin-locking state in the complete  $\tau$  range it was not possible to obtain a functional dependence of  $T_{2\text{eff}}$  on  $\tau$  because of the following reason. It has been pointed out earlier in this chapter that the transmitter pulse feed-through appears at the receiver output in our spectrometer system. Because of the presence of the feed-through pulses in our responses the echo base-line could not be identified properly. Particularly in the region of lower  $\tau$  values this problem was more severe. Consequently, the magnitude of the calculated

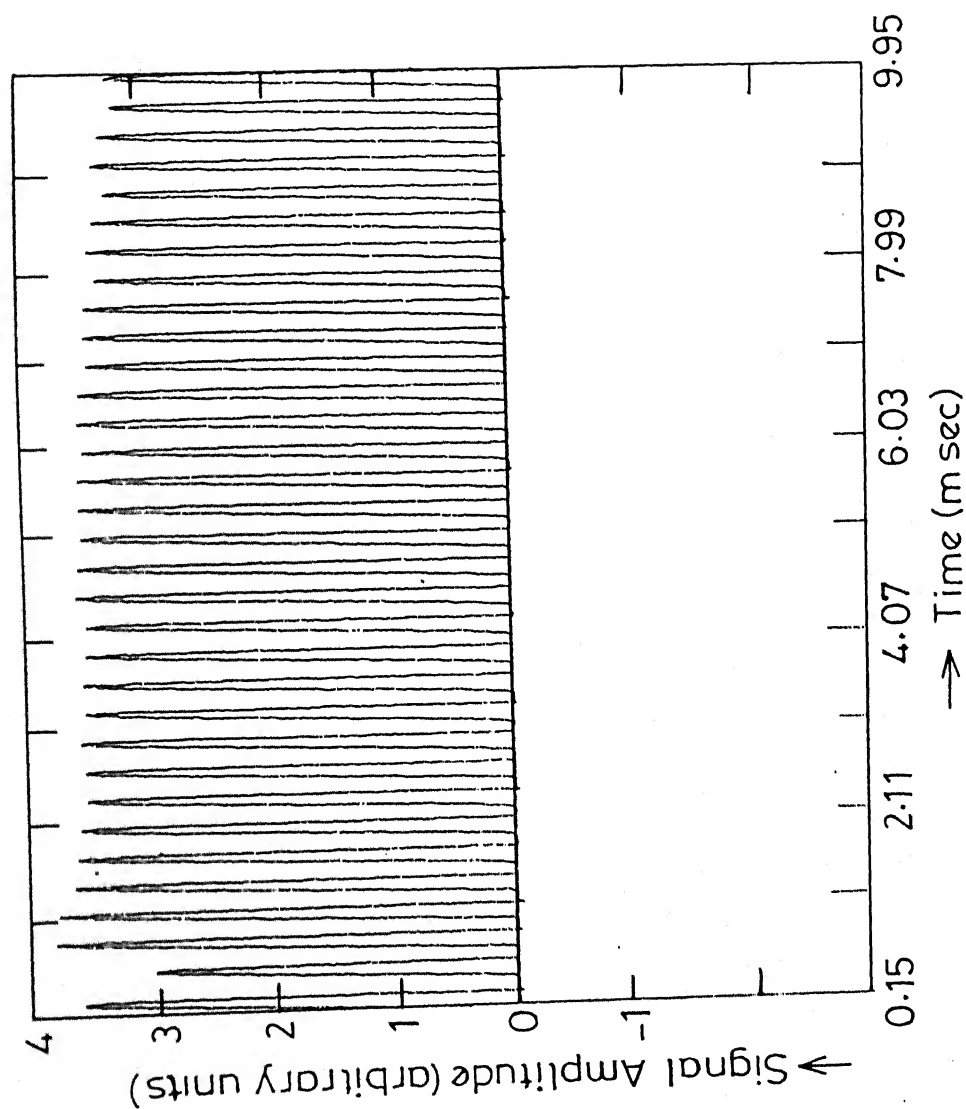


Fig.IV.10 Response of  $^{35}\text{Cl}$  in powdered  $\text{KClO}_3$  to Ostroff-Waugh sequence with a value for  $\tau \approx 150 \mu\text{sec}$ .

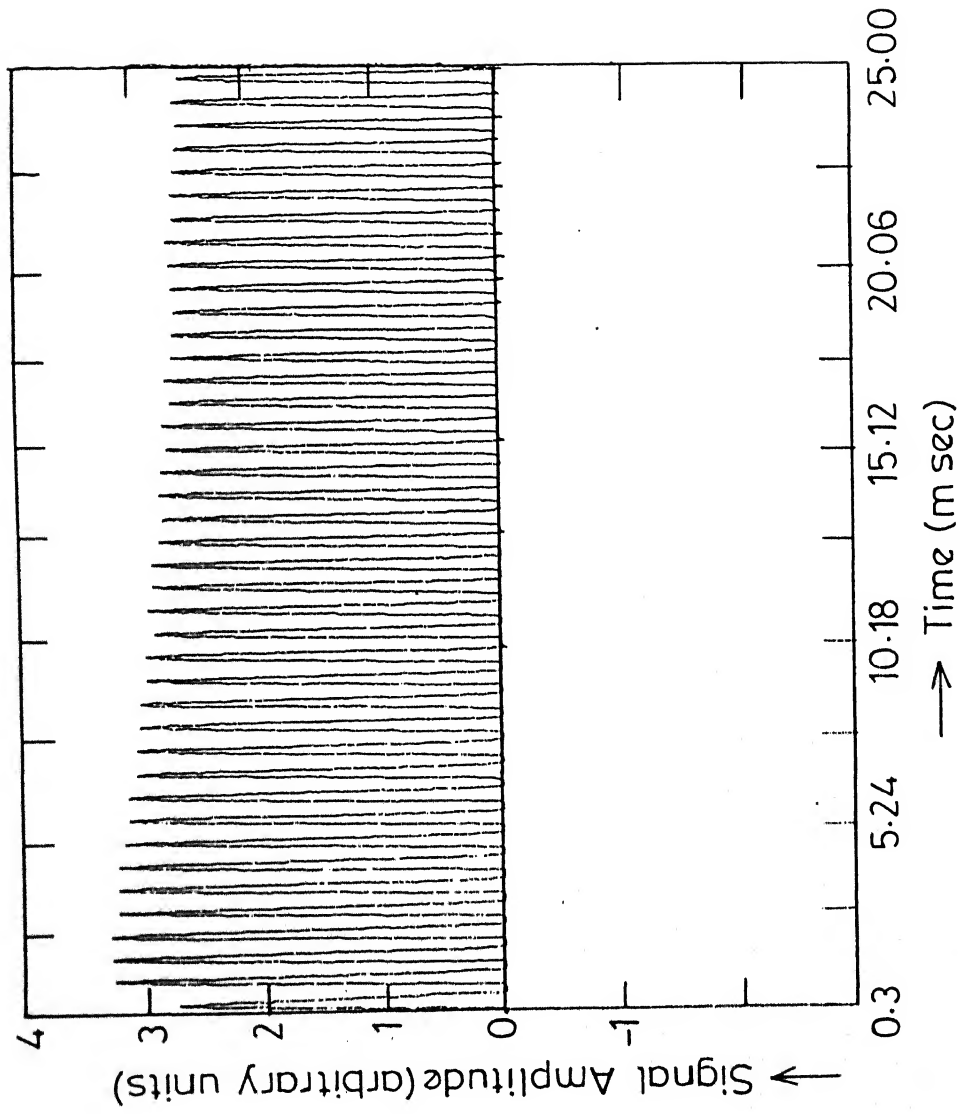


Fig.IV.11 Same as that of Fig.IV.10 with a value for  $\tau \approx 300 \mu\text{sec}$ .

$T_{2e}$  values were not accurate and it was not possible to obtain a precise functional relation between  $T_{2e}$  and  $\tau$ .

#### IV.B(2.ii) Investigations using phase alternated multiple pulse sequence (PAPS)

In multiple-pulse NQR spectroscopy, the theoretical and experimental investigations employing PAPS have been done by Osokin [8-10, 24, 25] on powdered samples containing spin-1 nuclei. To the best of our knowledge, there has been no investigation in the literature concerning the action of PAPS on spin-3/2 systems. Typical recordings obtained for three different " $\theta$ " values, namely,  $180^\circ$ ,  $90^\circ$  and  $45^\circ$  on-resonance from  $^{35}\text{Cl}$  in  $\text{KClO}_3$  using PAPS are presented in Figs. IV.12(a) to IV.12(c). Response to only the first thirty phase alternated pulses have been shown in these figures with a  $\tau$  value of  $\approx 200 \mu\text{sec}$ . However, in actual recordings responses to more than 100 phase alternated pulses have been observed and the magnetization persisted for more than 100 msec in the case of  $\text{KClO}_3$  and  $\approx 200 \text{ msec}$  in the case of  $\text{NaClO}_3$ . This clearly shows that spin space averaging of NQR line broadening interactions can be achieved using PAPS in spin-3/2 nuclei in powdered samples. The  $T_{2e}$  values calculated as a function of  $\theta$  with a resonance off-set of -3 KHz ( $\tau \approx 200 \mu\text{sec}$ ) obtained from  $^{35}\text{Cl}$  in  $\text{NaClO}_3$  are tabulated in Table IV.4.

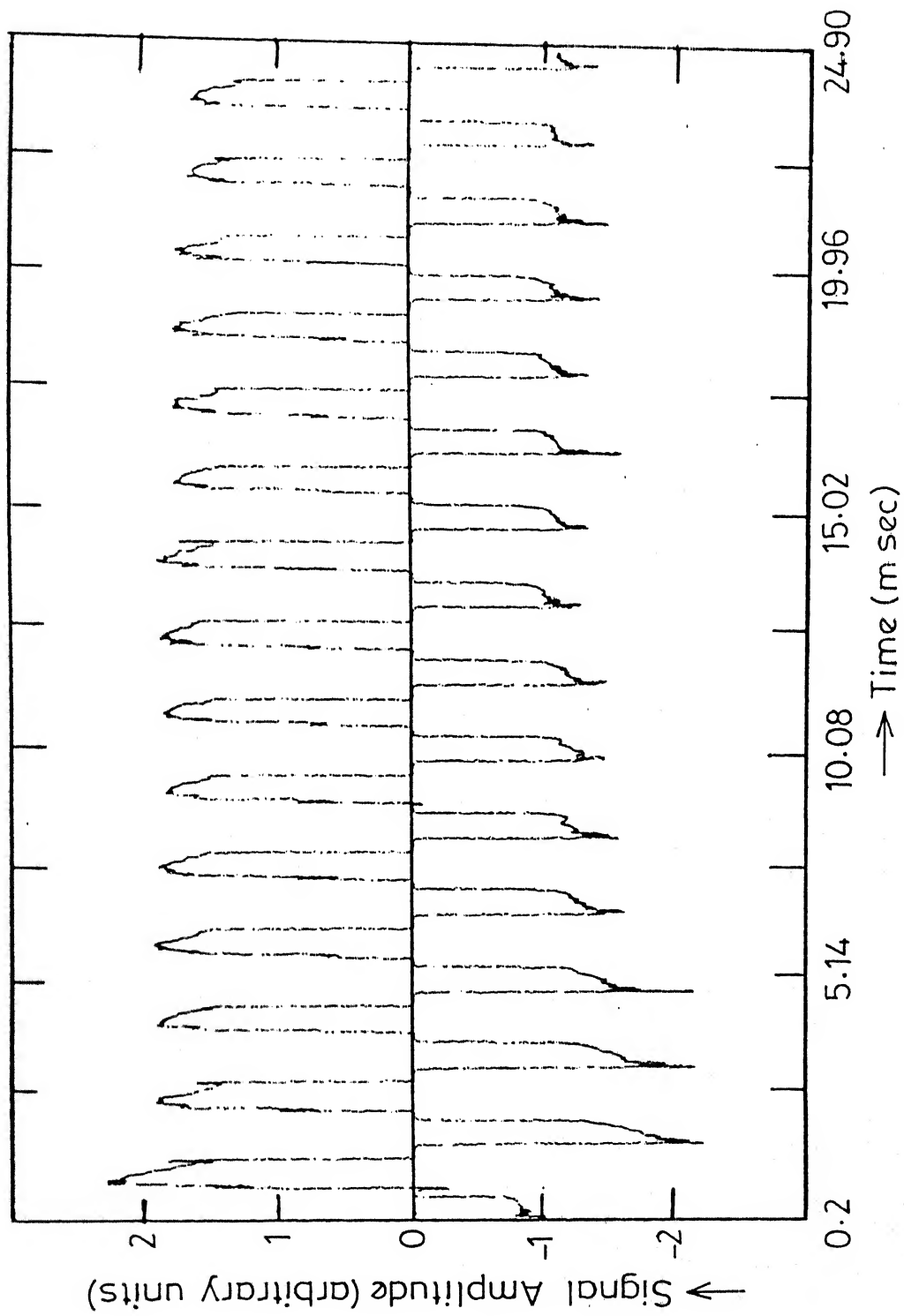


Fig.IV.12(b) Same as that of Fig.IV.12(a) with a value for  $\theta=90^\circ$ .

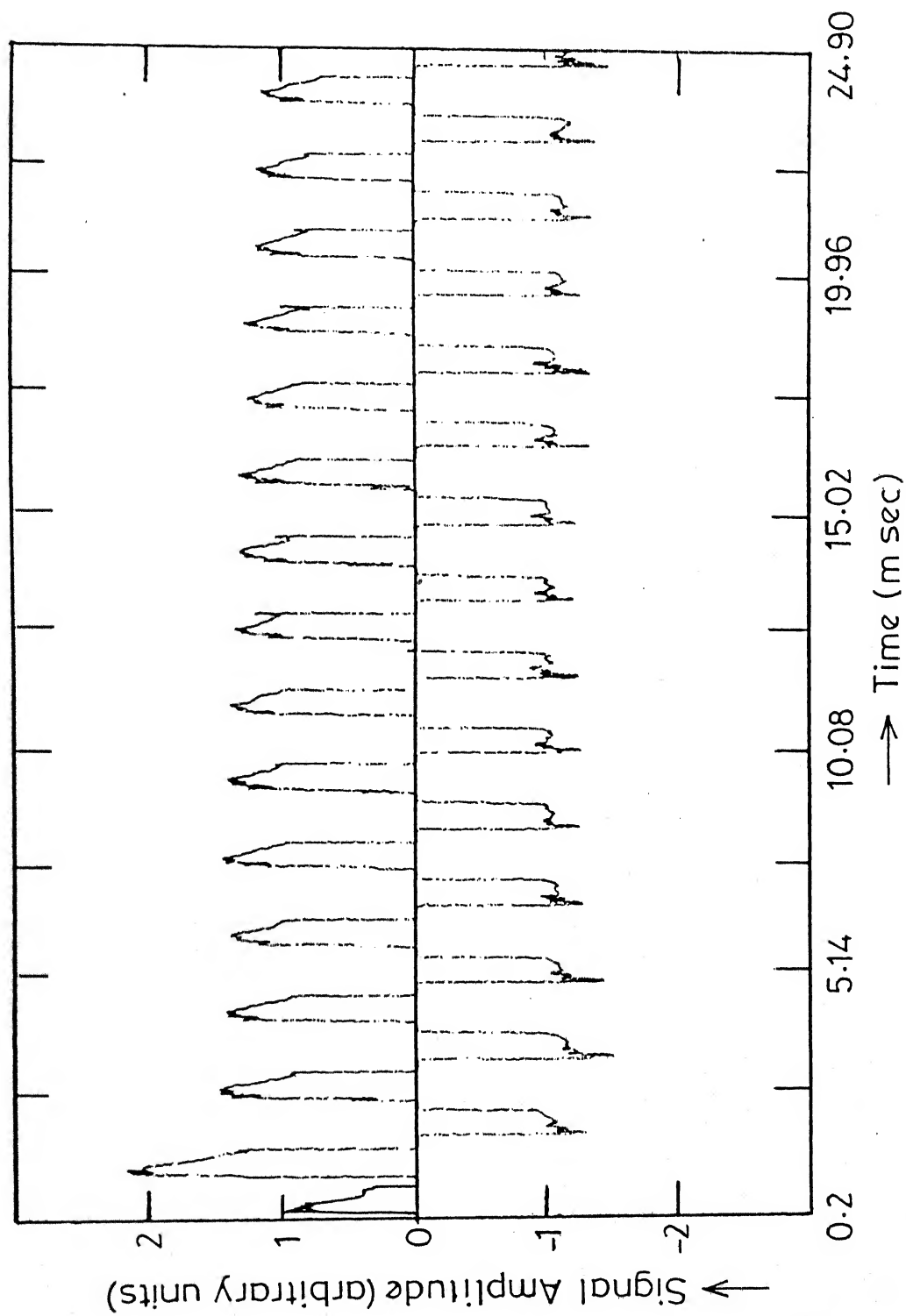


Fig.IV 12(c) Same as that of Fig.IV.12(a) with a value for  $\theta = 45^\circ$ .

Table IV.4 Variation of  $T_{2\epsilon}$  with " $\theta$ " as observed by PAPS from  $^{35}\text{Cl}$  in powdered  $\text{NaClO}_3$

| Sl. No. | $\theta$    | $T_{2\epsilon}$ (msec) |
|---------|-------------|------------------------|
| 1.      | $180^\circ$ | 26.90                  |
| 2.      | $90^\circ$  | 32.12                  |
| 3.      | $45^\circ$  | 37.53                  |

It is clear from the table that  $T_{2\epsilon}$  increases as " $\theta$ " is decreased and approaches very close to the value of 45 msec, the spin-lattice relaxation time ( $T_1$ ) for this compound.

We have also observed the elongation of echo decay time employing PAPS for  $\tau$  values ranging from 100 to 600  $\mu\text{sec}$  and the averaging effect has been observed throughout the  $\tau$  range. However, our calculated  $T_{2\epsilon}$  values, particularly at lower  $\tau$  values, were not accurate enough to enable us to come up with a functional relation between  $T_{2\epsilon}$  and  $\tau$  on account of the transmitter pulse feed through problem. Efforts in the direction of quantifying the long time behavior of the magnetization are in progress.

#### IV.B(2.iii) Conclusions

Multiple-pulse line narrowing by means of averaging in the spin space has been achieved in NMR of solids by the utilization of two different classes of pulse sequences, namely, multiple-

pulse sequences leading to (i) "general averaging," and (ii) "selective averaging" very little work in this area has been done in NQR, particularly in the case of  $I \geq 3/2$  systems. We have carried out our investigations employing spin-locking and phase alternated multiple-pulse sequences on powdered samples containing  $I = 3/2$  nuclei. Following conclusions are drawn from our studies:

(1) We have observed the spin-locked state by employing CPMG and OW pulse sequences. Apart from the usual spin-locking sequence that has so far been used in NMR and NQR literature, namely,  $90_x - [\tau - \theta_{(x+90)} - \tau]_n$  we have employed a more general sequence, namely,  $90_x - [\tau - \theta_{(x+\emptyset)} - \tau]_n$  in our experiments. Our results on powder samples have shown that spin-locking can be achieved for any arbitrary phase difference ( $\emptyset$ ) between preparatory pulse and the sequence pulses. So far in the literature of NQR there is only one theoretical frame work due to Averbinder and Furman [20] which is valid for any general spin. Using the canonical transformation technique and K-B-M averaging method they have obtained the average Hamiltonian  $\bar{\mathcal{H}}$  which describes the spin system under the action of the multiple-pulse sequence. It is known that spin-locking state will be realized upon satisfaction of the condition  $[\tilde{\rho}_+(0), \bar{\mathcal{H}}] = 0$ , here  $\tilde{\rho}_+(0)$  is the density matrix immediately following the first pulse. The above condition means that, for obtaining spin-locked state, the orientation of the magnetization of the spin system after the preparatory pulse should coincide with the orientation of



the effective field produced by the multiple-pulse sequence. Following these ideas and by using the above mentioned technique for obtaining  $\overline{H}$ , Ainbinder and Furman have come up with a condition on phase ( $\phi$ ) requirements for achieving the spin-locked state in NQR (see Section IV.A). However, it should be noted that, we have observed spin-locking in the case of powder samples containing spin-3/2 nuclei without satisfying the conditions that have been imposed on phase requirements by the theory of Ainbinder and Furman. This means that their theory is not of such general validity as one would have thought of at first. Detailed phase ( $\phi$ ) dependent studies on single crystal samples on a large variety of spin systems would help in further evaluating the general validity of the Ainbinder-Furman theory.

(2) Our multiple-pulse investigations have shown that the echo decay time constant,  $T_{2\epsilon}$ , approaches the spin-lattice relaxation time,  $T_1$ . For example, we have obtained a value for  $T_{2\epsilon} \approx 20$  msec in the case of  $KClO_3$  and  $\approx 37$  msec in the case of  $NaClO_3$ , indicating the attainment of high resolution ( $\approx 25$  to 50 Hz). Here the numbers for the resolution have been estimated by taking inverse of the observed  $T_{2\epsilon}$  values. Also, as pointed out by Marino and Klainer [4] one can take advantage of enhancing the S/N ratio by co-adding the multiple echoes within a spin-locked spin-echo sequence. Thus, by employing multiple-pulse technique one can simultaneously enhance the resolution and

S/N ratio in a much shorter time. The technique can therefore be exploited to detect weak NQR signals from powder samples containing spin-3/2 nuclei. It should be mentioned that our results on  $\theta$ -dependence have shown that for powder samples  $\theta$ -requirements are less stringent and hence the S/N ratio can be easily enhanced in powder samples containing  $I = 3/2$  nuclei.

(3) In our experiments, the value of  $T_{2\theta}$  has increased as  $\theta$  is reduced for a given value of  $\tau$  in the spin-locking sequence. The study as a function of  $\tau$  has indicated that the spin-locking can be observed as long as  $\tau \leq T_2$ . These results are consistent with that obtained in NMR [33] and also in the case of spin-1 NQR systems [8].

(4) We have also investigated the influence of PAPS on spin-3/2 powder samples. The results show that the spin space averaging could be obtained using PAPS and the echo decay time constant could be enhanced to approach  $T_1$  with this sequence. Studies as a function of  $\theta$  in PAPS experiment have also shown that  $T_{2\theta}$  increases as  $\theta$  is decreased. This result is consistent with that observed by Osokin [8-10] in the case of powder samples containing spin-1 NQR systems.

### Summary

In this chapter we presented the results of our experimental investigations on multiple-pulse responses from  $^{35}\text{Cl}$  ( $I = 3/2$ ) containing polycrystalline samples. Several multiple-pulse

sequences were considered for this purpose. These investigations were carried out employing the microprocessor-controlled pulsed NQR spectrometer described in Chapter II. After surveying the available literature on multiple-pulse studies in NQR, the experimental results obtained from various multiple-pulse sequences have been presented. Two general sequences were considered for the purpose of spin space averaging, namely, (i) the spin-locking sequence, i.e.,  $90_x - [\tau - \theta_{(x+\phi)} - \tau]_n$ , and the phase alternated multiple-pulse sequence, i.e.,  $90_x - [\tau - \theta_{-x} - 2\tau - \theta_x - \tau]_n$ . An interesting observation was made by us that spin-locking with arbitrary  $\phi$  values using the sequence (i) above could be achieved in  $^{35}\text{Cl}$  containing powdered samples. The only theoretical framework for spin-locking in NQR that is applicable for any general spin is due to Ainsbinder and Furman. However, this theory predicts spin-locking only when  $\phi = (2k+1)\pi/2$ . Clearly, our experimental results show that the phenomenon of spin-locking in powder samples in NQR is not restricted to these  $\phi$  values alone. The results from our experimental investigations as a function of  $\theta$ , off-set and  $\tau$  were also presented in this chapter. It has been pointed out that significant resolution and S/N improvement can be achieved from spin-locking experiments.

We have also observed the lengthening of the transverse magnetization under the action of phase alternated multiple-pulse sequence (PAPS) which is the result of spin space general

averaging. The averaging effect has been observed for arbitrary  $\theta$  (see sequence (ii) above) and for  $\tau < T_2$  using PAPS.

This chapter ends with the conclusions drawn from the present multiple-pulse investigations on powder samples containing spin-3/2 nuclei.

REFERENCES

- [1] U. Haeblerlen, "High Resolution NMR in Solids: Selective Averaging," Supplement-1 to Advances in Magnetic Resonance, Ed. J.S. Waugh, Academic Press (1976).
- [2] N.E. Ainbinder, G.B. Furman, G.E. Kibrik, A. Ya. Poljakov and I.G. Shaposhnikov, Z. Naturforsch., 41a, 366 (1986).
- [3] D. Gill and S. Meiboom, Rev. Sci. Instrum., 29, 688 (1958).
- [4] R.A. Marino and S.M. Klainer, J. Chem. Phys., 67, 3388 (1977).
- [5] E.D. Ostroff and J.S. Waugh, Phys. Rev. Lett., 16, 1097 (1966).
- [6] P. Mansfield and D. Ware, Phys. Lett., 22, 133 (1966).
- [7] H.Y. Carr and E.M. Purcell, Phys. Rev., 94, 630 (1954).
- [8] D. Ya. Osokin, Phys. Stat. Sol. (b) 102, 681 (1980).
- [9] D. Ya. Osokin, Phys. Stat. Sol. (b) 109, K7 (1982).
- [10] D. Ya. Osokin, J. Molec. Struct., 83, 243 (1982).
- [11] V.L. Ermakov and D. Ya. Osokin, Molec. Phys., 53, 1335 (1984).
- [12] R.S. Cantor and J.S. Waugh, J. Chem. Phys., 73, 1054 (1980).
- [13] J.S. Waugh, C.H. Wang, L.M. Huber and R.L. Vold, J. Chem. Phys., 48, 662 (1968).
- [14] J.S. Waugh and C.H. Wang, Phys. Rev., 162, 209 (1967).
- [15] W.K. Rhim, D.P. Burum and D.D. Elleman, Phys. Rev. Lett., 37, 1764 (1976).
- [16] S. Vega, J. Chem. Phys., 63, 3769 (1975); 68, 5518 (1978).
- [17] S. Vega and A. Pines, J. Chem. Phys., 66, 5624 (1977).
- [18] A.K. Hitrin, G.E. Karnaukh and B.N. Provotorov, J. Molec. Struct., 83, 269 (1982).

- [19] B.N. Provotorov, E.B. Feldman, Zh. Exsp. Teor. Fiz., 79, 2206 (1980).
- [20] N.E. Aimbinder and G.B. Furman, Sov. Phys. (JETP), 58, 575 (1983).
- [21] N.E. Aimbinder, G.A. Volgina, A.N. Osipenko, E.B. Furman, and I.G. Shaposhnikov, J. Molec. Struct., 111, 65 (1983).
- [22] N.N. Bogolyubov and Yu. A. Mitropol'skii, "Analytic Methods in the theory of Non-linear Oscillations," Gordon and Breach (1964).
- [23] M. Matti Maricq, Phys. Rev., B33, 4501 (1986).
- [24] V.L. Ermakov and D. Ya. Osokin, Phys. Stat. Sol. (b) 116, 239 (1983).
- [25] D. Ya. Osokin, Molec. Phys., 48, 283 (1983).
- [26] A. Pines and J.S. Waugh, J. Magn. Reson., 8, 354 (1972).
- [27] U. Haeblerlen, J.D. Ellet and J.S. Waugh, J. Chem. Phys., 55, 53 (1971).
- [28] O.S. Zueva, Bull. Acad. Sci. USSR, Phys. Ser., 42, 100 (1978).
- [29] A.R. Kessel and O.S. Zueva, Phys. Lett., A68, 347 (1978).
- [30] O.S. Zueva and A.R. Kessel, Sov. Phys. Solid State, 21, 2032 (1979).
- [31] O.S. Zueva and A.R. Kessel, J. Molec. Struct., 83, 383 (1982).
- [32] O.S. Zueva, J. Molec. Struct., 83, 379 (1982).
- [33] W.K. Rhim, D.P. Burum and D.D. Elleman, Phys. Rev. Lett., 37, 1764 (1976).
- [34] M.J. Weber, J. Phys. Chem. Solids, 17, 267 (1961).

### SCOPE FOR FUTURE WORK

The present microprocessor-controlled pulsed NQR spectrometer can be upgraded by the following modifications. The r.f. power transmitter used in the present spectrometer system is capable of delivering a maximum r.f. power of  $\approx 800$  Watts. Enhancing r.f. power to KW range is advantageous because pulse duration would then be shortened. This is useful for a whole range of NQR experiments including multiple-pulse experiments. Also performing soft-pulse excitation experiment with hard  $\pi$ -pulse leads to better refocusing of the interactions prepared by soft-excitation pulse and yields reliable ZSEEM. Another modification of the spectrometer is in terms of A/D conversion rate of the signal analyzer. It will be useful to enhance the present A/D conversion rate of 400 KHz to MHz range. This will help in acquiring fast decaying signals and also multiple-pulse responses in short intervals.

Our investigations on soft-pulse excitation experiment showed an initial oscillatory behaviour in the ZSEEM spectrum. We have proposed that this behaviour is due to random orientation of efg tensors in the powder samples studied. Soft-pulse excitation experiments on single crystals may throw some light on this aspect.

We have observed spin-locking employing the sequence  $90_x - (\tau - \theta_{(x+\phi)} - \tau)_n$  for various values of  $\tau \leq T_2$ . However, the uncertainty in identifying the echo base-line in the presence of transmitter feed-through pulses in our spectrometer system (particularly for lower  $\tau$  values) has prevented us from obtaining a quantitative relation between  $T_{2\phi}$  and  $\tau$ . Suppressing transmitter feed-through pulses either by means of Q-damping of the probe or by means of better receiver gating schemes would help in obtaining quantitative accuracy and to come up with a functional relation between  $T_{2\phi}$  and  $\tau$ . Multiple-pulse experiments on single-crystal samples are also of interest.

We have observed spin-locking with arbitrary  $\phi$  values from powder samples containing  $^{35}\text{Cl}$  ( $I = 3/2$ ) nuclei using the spin-locking sequence. This observation cannot be explained on the basis of presently available theories. Development of a general theory of spin-locking in NQR for powder samples is therefore of enormous interest. It would also be interesting to design theoretically the pulse sequences which can cause selective averaging and implement them in NQR spectroscopy in analogy with WAHUHA-4 and MREV-8 pulse cycles used in high resolution NMR of solids.